ERDC/CHL TR-09-1

Coastal and Hydraulics Laboratory

US Army Corps
of Engineers®
Engineer Research and
Development Center

Surge and Wave Island Modeling Studies
Coastal Field Data Collection Program

Wave Transformation Over Reefs: Evaluation of One-Dimensional Numerical Models

Zeki Demirbilek, Okey G. Nwogu, Donald L. Ward,
and Alejandro Sánchez

January 2009

ERDC/CHL TR-09-1
January 2009

Wave Transformation Over Reefs: Evaluation of One-Dimensional Numerical Models

Zeki Demirbilek, Donald L. Ward, and Alejandro Sánchez

Coastal and Hydraulics Laboratory
U.S. Army Engineer Research and Development Center
3909 Halls Ferry Road
Vicksburg, MS 39180-3999

Okey G. Nwogu

University of Michigan
Department of Naval Architecture and Marine Engineering
2600 Draper Road
Ann Arbor, MI 48109-2145

Final report

Prepared for Headquarters, U.S. Army Corps of Engineers
Washington, DC 20314-1000

Abstract: Three one-dimensional (1D) numerical wave models are evaluated for wave transformation over reefs and estimates of wave setup, runup, and ponding levels in an island setting where the beach is fronted by fringing reef and lagoons. The numerical models are based on different governing equations. BOUSS-1D and RBREAK2 are phase-resolving models that respectively solve the time-dependent Boussinesq and shallow water equations. WAV1D solves the 1D wave-averaged energy conservation equation.

Laboratory data obtained from four physical modeling studies conducted by Seelig (1983), Gourlay (1994), Thompson (2005), and Demirbilek and Nwogu (2007) are used in the evaluation of numerical models. The numerical models produced reasonable correlation with the data. Overall BOUSS-1D representation of wave breaking and wave dissipation were realistic and compared well to data. The model's estimates are sensitive to values of input bottom friction and turbulence length scale coefficients. RBREAK2 is robust because it does not attempt to explicitly represent the wave breaking processes. However, the model is highly dissipative when applied to wide fringing reefs and is only applicable when the runup beach is reasonably close to the predominant wave breaking location. The model predictions were also found to be less sensitive to values of friction factor. The correlation with one of the data sets was good, but not as good for two other data sets. WAV1D is the simplest model evaluated in this study. This model is appropriate for preliminary and feasibility level estimates.

Contents

Figures and Tables

Figures

Tables

Preface

The investigations reported herein were conducted in the Coastal and Hydraulics Laboratory (CHL) of the U.S. Army Engineer Research and Development Center during the period of 2006-2008. These research studies were performed to assess predictive capability of numerical wave models for estimates of wave setup, ponding levels, and runup for the Surge and Wave Island Modeling Studies (SWIMS) of the Coastal Field Data Collection Program. This program was initiated by the U.S. Army Corps of Engineers in 2005 to develop improved methodologies for predicting coastal flooding associated with typhoons and hurricanes at the U.S. Pacific and Caribbean Islands. Dr. Jane M. Smith, CHL, is Principal Investigator of SWIMS and William Birkemeier is Coastal Field Data Collection Program Manager.

The research described in this report was conducted and the report was written by Dr. Zeki Demirbilek, CHL; Okey G. Nwogu, University of Michigan; Donald L. Ward, CHL, and Alejandro Sánchez, CHL. Edward F. Thompson (now retired) conducted a laboratory experiment and participated in the preliminary modeling simulations. Dr. Smith and Jose Sanchez, former Chief of Harbors, Entrances and Structures Branch, reviewed the first draft version of this report. J. Holley Messing, Coastal Engineering Branch, Navigation Division, CHL, format-edited the draft report. The work was conducted under the supervision of Jose Sanchez, Jackie S. Pettway, Chief, Harbors, Entrances, and Structures Branch; and Ty Wamsley, Chief, Coastal Processes Branch. Dr. Rose Kress was Chief, Navigation Division, and Bruce Ebersole was Chief, Flood and Storm Protection Division. Dr. William D. Martin was Deputy Director, CHL, and Thomas W. Richardson was Director of CHL.

COL Gary E. Johnston was Commander and Executive Director of ERDC. Dr. James R. Houston was Director.

1 Introduction

Background

Typhoon and hurricane storm surges and waves reaching the shores of the Pacific islands, Caribbean islands, and the mainland, USA, have caused significant damages in the coastal zone. On the U.S. Gulf Coast, for example, Hurricane Opal made landfall in 1995 near the time of low tide and still resulted in severe flooding by storm surges and waves. Waves riding on storm surge can penetrate miles inland from the coast, and the resulting wave runup and mean water level can cause significant damages. These effects are most intense near the landfall area, but are also affected by the typhoon and hurricane approach to the coastal areas.

Most Pacific islands are well-protected by natural fringing coral reefs. Waves undergo significant transformation as they shoal and break on fringing reefs before flooding the coastal areas. Reliable estimate of the maximum inundation caused by typhoon or hurricane waves is important for establishing flood risk and emergency management operations. For estimates of coastal flooding, it is useful to model coastal wave transformation along a cross-shore transect and neglect longshore (shore parallel) processes. This approach is particularly useful for a fringing reef environment, in that it allows powerful nonlinear models to be applied to large spatial regions with manageable computer run times. It will be shown later in this report that this horizontally one-dimensional (1D) approach can produce useful information, even along fairly irregular coasts. Preliminary tests of both 1D and two-dimensional (2D) Boussinesq models to Hurricane Iniki along an irregular section of coast in Kauai, Hawaii, found surprisingly similar maximum inundation limits (Demirbilek and Nwogu 2007). Numerical wave modeling described in this report is limited to evaluation of 1D wave models.

The U.S. Army Corps of Engineers (USACE) initiated the Surge and Wave Island Modeling Studies (SWIMS) program in 2005 to develop improved methodologies for predicting coastal flooding associated with typhoons and hurricanes in the U.S. Pacific and Caribbean islands. A comprehensive understanding of the physics of wave inundation over reef systems is required to develop reliable predictive models for typhoon-and hurricane-emergency planning, and calculation of flooding and erosion rates.

Modeling approaches

Modeling of offshore waves for typhoon and hurricane events requires reliable wind fields and track information of storms. Deepwater wave estimates are sensitive to the storm intensity and speed. The nearshore waves are obtained from offshore incident waves. A dynamically coupled 2D numerical model of coastal waves and storm surges is still evolving. For evaluation of the wave effects along the island coastlines, a set of deepwater 2D nested wave models coupled to ocean circulation models driven by nested typhoon and hurricane wind fields is necessary. Deepwater modeling results may be coupled to phase-averaged spectral wave models or phase-resolving nonlinear shallow-water wave models. The SWIMS program plans to implement this framework in an improved island flood prediction modeling system.

Storm waves over a reef are closely tied to storm surge. Storm surge elevates water level above the reefs and on mild beach slopes of the islands. This causes waves to break further inland and swash to runup further on islands' beaches. The interaction between surge and waves is nonlinear.

This report provides detailed information concerning evaluation of three 1D numerical wave models for investigating wave transformation processes over reefs and resulting runup estimates required for island flooding. The numerical wave models considered are BOUSS-1D and RBREAK2. The third model WAV1D uses the energy conservation equation to predict wave transformation over the reef and employs empirical formulas from the *Coastal Engineering Manual* (Headquarters (HQ) USACE 2002) for calculating wave runup. The empirical formulas implemented have been modified, as necessary, by calibration to data obtained from four reef applications. Four experimental data sets are used in this model evaluation study. The first data set is for wave transformation over coral reefs for Hayman Island from a laboratory study (Gourlay 1994). The second data set is from a laboratory study of wave breaking on a reef in Guam (Seelig 1983). The third and fourth data sets are from two recent physical model studies for waves passing over reefs of composite slopes, typical of those found in the Pacific Islands (Thompson 2005; Demirbilek and Nwogu 2007; Demirbilek et al. 2007b).

The layout of this report is as follows. Background and modeling approaches are discussed in this Introduction (Chapter 1). A review of reef

characteristics, including description of types and zones of reefs that determine how waves interact with reefs, is provided in Chapter 2. Chapter 3 is dedicated to the BOUSS-1D model evaluation, model description, a summary of the model's applicable governing equations, critical parameters affecting wave transformation over reefs, and comparison of model results to the four reef data sets. Chapter 4 describes evaluation of RBREAK2 and Chapter 5 gives the evaluation of WAV1D models. Results from three wave models are discussed in Chapter 6. Conclusions are provided in Chapter 7. Additional information from modeling is provided in Appendices A through E, including results from a sensitivity study conducted in 2005 on investigation of BOUSS-1D model parameters.

2 Reef Characteristics

Types of reefs

Coral reefs commonly develop and evolve into three distinct geometric shapes: platform, barrier, and fringing reefs (Gourlay 1994, 1996a and b). Platform reefs, also known as atolls, are flat-topped and typically look like islands with a reef ring around a central lagoon. The lagoon in a platform reef is not necessarily shallow, and some times can be deep. The Great Barrier Reef in Australia, which has a land mass, is a good example of barrier reefs, and its reef line starts a significant distance out in the sea, nearly 100 km offshore. In contrast, fringing reefs develop much closer to the shore around Pacific and Caribbean Islands, and they are characterized by narrower widths as compared to the barrier reefs. Figure 1 depicts the reef profile for the two most common types of reefs. The still water level (SWL) is not shown on these sketches, but usually is located below the reef platform. The time variation in the water level can be significant, and at times the entire reef may be covered by water, or parts of reef may be submerged while the other parts are exposed.

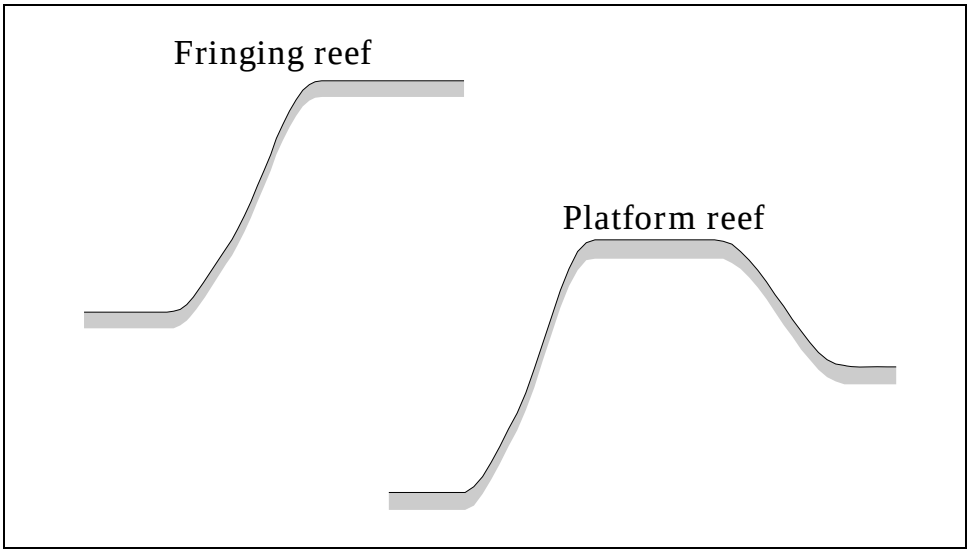

Figure 1. Typical sketch of reef profiles for fringing reefs (top) and platform reefs (bottom).

Generally speaking, reefs fronting a continental land mass may be denoted as “fringing reefs,” while reefs located in the open ocean are referred to as “platform reefs.” The coral reefs in the tropical regions of the Pacific,

Indian, and Atlantic Ocean may form either as fringing reefs around islands, or as barrier reefs or separate atolls and island reefs (Jensen 2001; Vernon 1986). The geometric shape (form) and structure (morphology) of coral reefs vary with the local conditions, and the wave climate is the most important factor in shaping a reef. Earlier research by Roberts (1975) and Ogg and Koslow (1978) found significant differences between the physical and ecological profiles of the reefs located in high- or low-wave energy environments. When the offshore reef face is subject to a high-energy wave climate, spurs and grooves commonly develop in the reef-face region. In the low wave energy environments, reef slopes are generally flatter, and spurs and grooves do not appear. These irregularities in the reef topology can influence wave energy loss as a result of wave breaking and bottom friction (Jensen 2001; Jaffe and Richmond 1993). The special effects of spurs and groove features are not considered in the present study of wave modeling over reefs.

Morphological reef zones

The geological structure of reefs can be divided into different morphological zones. Hardy et al. (1991), Gourlay (1994, 1996a, 1996b), and Massel and Gourlay (2000) have treated reefs with four morphological zones: face, crest, flat, and lagoon. An understanding of reef zones is important to numerical modeling of wave transformation processes that take place over distinct parts of a reef. The reef geometry consists of a steep slope, a reef crest, and a longer shallow reef plateau following the crest (Figure 2). The most seaward part of a reef is the reef face, also known as the reef slope, which may rise above the seabed abruptly, mildly, or nearly vertically. The reef face is also the region having a number of different sizes of irregularly-shaped coral grooves and spurs. Approximately 75 to 95 percent of the incident wave energy impinging on reefs is dissipated in this seaward zone called the reef slope or reef face.

Following the reef nomenclature as defined by Gourlay (1994, 1996a, 1996b), we define the top segment of the reef slope as the reef crest zone, sometimes referred to as the reef front. It is commonly covered by thick layers of corals and algae. This is the reef region where the most intense wave breaking takes place. The reef crest is often the highest frictional zone and has the highest elevation above the mean sea level (MSL). The reef flat is immediately landward of the reef crest and usually below the MSL, and exposed at low tide.

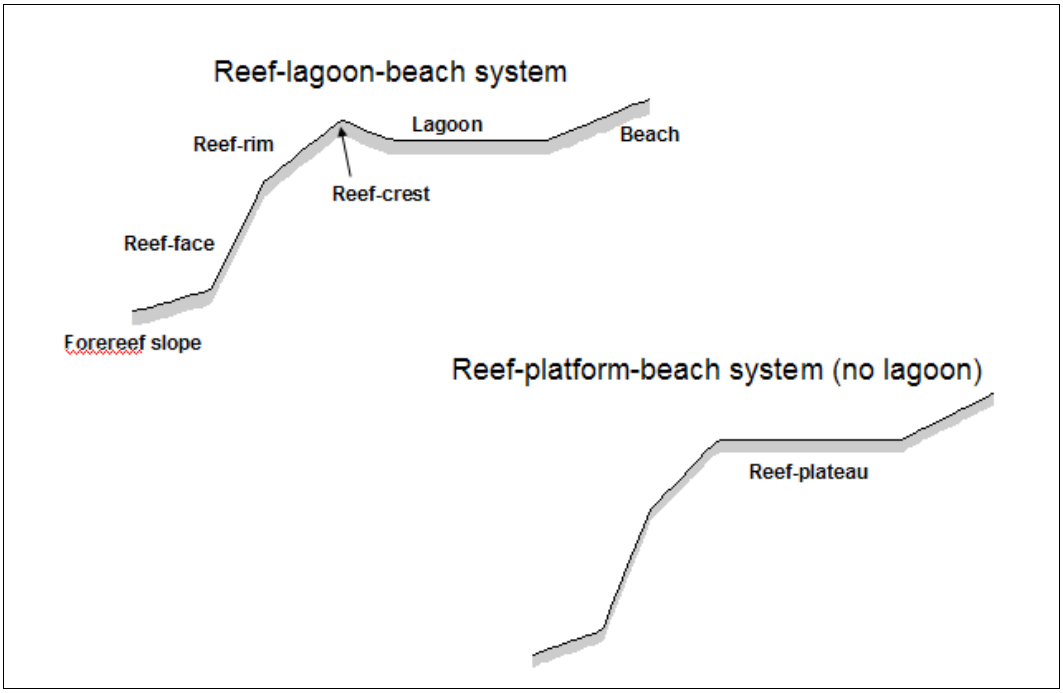

Figure 2. A reef-lagoon-beach system (top), and a reef-platform-beach system (bottom).

A coastal lagoon or a reef plateau is the landward end of the reef system. This section of reef may contain deeper channels known as gutters or drainage channels. Up to a 1 knot (0.5 m/sec) current can flow through these channels (Hardy et al. 1991; Gourlay 1994). The reef lagoon bottom is generally below MSL, and the depth may vary from a few centimeters to a few meters. Coral reefs typically grow to about mean low tide level and after maturing, are essentially horizontal. If waves break on the reef edge at low tide, not much wave energy is left to propagate across the reef top. At high tide or during passage of typhoons and hurricanes with storm surges, more wave energy can propagate across the reef top. Consequently, the maximum depth-limited wave parameters over the reef top should be considered in the calculation of island flooding estimates.

The topography of reefs in the Pacific and Atlantic oceans and Caribbean Sea are non-uniform, and the size, profile, and morphology of the reefs are not necessarily similar. Waves impinging on complex reef topography are influenced by a variety of hydrodynamic processes including the turbulence generated by waves and flow over the reef's specific structure. Because it is not easy to characterize the topography of reefs with certainty, numerical modeling of waves over reefs remains as one of the most difficult coastal engineering challenges. Earlier attempts have relied on simplified models, limiting the success of numerical wave modeling over

long reef widths with complex morphological zones. Empirical methods required site-specific in-situ data for model calibration and scaling of empirical parameters. With these challenges in mind, the capabilities of Boussinesq-type and shallow-water wave models are investigated for reef applications. The goal of this study is to identify strengths/weaknesses of numerical models, robustness, and ability to produce reliable wave estimates for island flooding and inundation. The models' performances are compared to experimental data sets obtained for different reefs. The numerical wave models are evaluated for incorporation into an island flooding predictive system for the Corps.

Earlier research studies have shown that the physical structure (morphology) of reef geometry determines the characteristics of wave transformation and resulting wave breaking and attenuation over reefs (Hardy et al. 1991; Gourlay 1994, 1996a, 1996b; Massel and Gourlay 2000). A large body of data and knowledge about reefs has emerged in the last 30 years. These site- and reef geometry-specific data may not be used for other reef geometries. For this reason, the SWIMS program aims to develop predictive modeling tools for generic reefs for coastal flooding caused by typhoons and hurricanes in the Pacific and Atlantic islands.

Wave modeling for reefs

The Pacific islands have rather complex coastal bathymetries, and some have shore-connected wide fringing reefs. The current design guidance for estimating wave setup and wave runup for island flooding estimates is based on empirical formulae derived from laboratory experiments for planar beaches and sloping structures (HQ USACE 2002). These guidelines are not valid to estimate wave setup and wave runup over complex reef topographies. It is generally recognized that nonlinear wave-wave interactions lead to strong low-frequency (infragravity) oscillations of the water level close to shorelines. The ultimate goal of this research is to improve the reliability of wave transformations over reefs for producing accurate estimates of wave setup and wave runup in engineering works.

Wave runup estimates associated with the low-frequency oscillations over reef-type topographies can be significantly higher than those for planar beaches (Demirbilek and Nwogu 2007; Nwogu and Demirbilek 2006). Seelig (1983), for example, conducted laboratory experiments with a reef topography representing several sites along the Guam coast. Significant differences exist between the runup characteristics of regular and irregular

waves. Regular waves produced a larger setup of the mean water level on the reef. Maximum runup values were comparatively higher in irregular sea states resulting from low-frequency oscillations. It is necessary for the predictive models to describe the overall physics of wave transformation across reefs as accurately as possible. Only then can models be relied upon to estimate wave setup and runup for inundation of the low-lying coastal areas of islands. Because the time-domain Boussinesq-type wave models are capable of representing low-frequency oscillations affecting wave setup and wave runup (Nakaza and Hino 1990; Demirbilek and Nwogu 2007), the BOUSS-1D model is considered in this evaluation.

The weakly-dispersive models based on Boussinesq-type water wave evolution equations (Nwogu and Demirbilek 2001) are often used to model wave transformation in intermediate and shallow water depths. Boussinesq models have also been extended to simulate wave runup and coastal flooding (e.g., Titov and Synolakis 1995; Demirbilek and Nwogu 2007; Demirbilek et al. 2007b; Nwogu and Demirbilek 2006; Kennedy et al. 2000; Li and Raichlen 2002). However, the effects of wave breaking and bottom friction are still parameterized in Boussinesq models. Since the parameterizations represent simplifications of complex turbulent nonlinear processes, Demirbilek and Nwogu (2007) recently evaluated different parameterizations of Boussinesq wave models necessary to describe the complex physics of wave energy dissipation, infragravity wave motions and wave runup across wide fringing reefs representative of the Pacific islands.

Time-domain models, such as RBREAK2 (Kobayashi et al. 1987), that solve the nonlinear shallow-water equations, may also be used to simulate long-wave runup. Shallow-water models typically employ either implicit numerical dissipation or explicit dissipative terms to handle wave breaking. Good agreement has been reported for a variety of applications of the shallow-water equations for runup problems. However, the shallow-water equations are restricted to non-dispersive long waves. For weakly-dispersive storm waves propagating from intermediate water depths to the shoreline, the shallow-water assumptions of hydrostatic pressure and depth-uniform horizontal velocities may become invalid.

Spectral wind-wave models such as, STWAVE (Smith et al. 2001), CMS-Wave (Demirbilek et al. 2007a), and SWAN (Booij et al. 1998) are commonly used to simulate wave propagation and transformation in

coastal areas. These models solve wave-averaged energy conservation-type equations with parameterization for wave energy dissipation caused by wave breaking, bottom friction, and nonlinear energy transfer resulting from triad wave interactions. Mean water level is calculated with a cross-shore momentum equation. Spectral models could potentially be used to simulate nonlinear wave energy transformation across reefs but cannot directly simulate the runup process. WAV1D is a one-dimensional version of a spectral wave model.

This report documents results from the evaluation of three types of wave models: a Boussinesq-type model (BOUSS-1D), a shallow-water wave equation type model (RBREAK2), and a wave-averaged energy flux model (WAV1D). The results from these models are compared to data sets to determine their suitability for typhoon- and hurricane-induced flooding applications along the reef-fringed islands. The numerical wave models are compared to data sets obtained from four laboratory experiments: a 1:36 laboratory model study conducted in 2005 at the U.S. Army Engineer Research and Development Center (ERDC) (Thompson 2005), a 1:80 laboratory model study performed in 2006 at the University of Michigan (Demirbilek et al. 2007b), a 1:20 laboratory study for Hayman Island reef (Gourlay 1994; Massel and Gourlay 2000), and a 1:64 scale laboratory study for a reef in Guam (Seelig 1983). Nonlinear wave transformation over fringing reef topographies was investigated in these experiments to determine the variation of regular and irregular wave height, wave setup, and wave runup over different reef geometries. Evaluation of BOUSS-1D is described in Chapter 3, where model predictions are compared to the four data sets. Results for RBREAK2 and WAV1D models are compared to these data sets in Chapters 4 and 5, respectively.

3 BOUSS-1D Model Evaluation

Model description

The BOUSS-1D numerical model evaluated in the present study is a one-dimensional version of BOUSS-2D model (Nwogu and Demirbilek 2001), which is based on a fully nonlinear variant of the Boussinesq equations derived by Nwogu (1993b). Additional information on Boussinesq wave models can be found in Demirbilek and Nwogu (2007), Nwogu and Demirbilek (2007), Nwogu and Demirbilek (2006), Asmar and Nwogu (2006), Demirbilek et al. (2005a, 2005b), and Nwogu (1996).

The depth-integrated mass and momentum equations of the Boussinesq model are formulated in terms of the free surface elevation $\eta(x,t)$, the depth-averaged horizontal velocities $\bar{\boldsymbol{u}}$, and the horizontal velocity at elevation $z = z_\alpha$ below the SWL, $u_\alpha(x,t)$, as

$$\eta_t + \nabla\cdot\left[(h+\eta)\bar{\boldsymbol{u}}\right] = 0 \tag{1}$$

$$\begin{aligned} \boldsymbol{u}_{\alpha,t} &+ g\nabla\eta + (\boldsymbol{u}_\eta\cdot\nabla)\boldsymbol{u}_\eta + w_\eta\nabla w_\eta \\ &+ (z_\alpha-\eta)\left[\nabla(\boldsymbol{u}_{\alpha,t}\cdot\nabla h) + (\nabla\cdot\boldsymbol{u}_{\alpha,t})\nabla h\right] \\ &+ \frac{1}{2}\left[(z_\alpha+h)^2-(h+\eta)^2\right]\nabla(\nabla\cdot\boldsymbol{u}_{\alpha,t}) \\ &- \left[(\boldsymbol{u}_{\alpha,t}\cdot\nabla h)+(h+\eta)\nabla\cdot\boldsymbol{u}_{\alpha,t}\right]\nabla\eta \\ &+ \frac{1}{h+\eta}\nabla\left[\upsilon(h+\eta)\nabla\cdot\boldsymbol{u}_\alpha\right] + \frac{f_w}{2(h+\mu)}\boldsymbol{u}_b|\boldsymbol{u}_b| = 0 \end{aligned} \tag{2}$$

where x denotes the two horizontal directions and t is time, g is the gravitational acceleration, h is the seabed elevation (defined as positive downwards from the SWL), f_w is a bottom friction coefficient, $\upsilon(x,t)$ is an eddy viscosity coefficient, u_η and w_η are the horizontal and vertical velocities at the free surface ($z = \eta$), u_b is the horizontal velocity at the seabed ($z = -h$), and the subscript t indicates a time derivative. The elevation of the velocity variable is chosen to be $z_\alpha = -0.535\,h$ (for $h > 0$) to minimize differences between the linear dispersion characteristics of the Boussinesq model and the exact dispersion relation for small amplitude waves (Demirbilek and Nwogu 2007).

Wave breaking and dissipation

Wave breaking is parameterized in the momentum equation (Equation 2) with an artificial eddy viscosity term, and is designed to reproduce the overall wave energy dissipation caused by wave breaking, but to not produce the details of the turbulent motion. A conceptual breaking model is still required to define the onset of breaking and the post-breaking evolution of the eddy viscosity in space and time. Demirbilek and Nwogu (2007) developed and tested two formulations for describing the spatial and temporal evolution of the eddy viscosity after the onset of breaking. The first is the default formulation for spilling breakers, and the second formulation is for plunging breakers that occur on the faces of reefs with steep slopes. Because details of these formulations are described elsewhere by Demirbilek and Nwogu (2007), only some salient features are summarized below, as frequent reference will be made in the model evaluation to some parameters used for the wave breaking and dissipation.

The plunging wave breaking formulation follows Smagorinsky's (1963) concept of localized energy dissipation at the front of a shock or discontinuity, in which the eddy viscosity is proportional to the velocity gradient at the wave front. In the model notation, this may be written as

$$\nu(\boldsymbol{x},t) \;=\; B(\boldsymbol{x},t) l^2 \left[u_{s,x}^2 + v_{s,y}^2 \right]^{1/2} \tag{3}$$

where l is a characteristic length scale that is related to the wave height, $B(x,t)$ is a breaking wave factor that ranges from 0 to 1, and u_s is the tangential velocity at the free surface and is obtained from the horizontal velocity u_η at the free surface ($z = \eta$). An advection-diffusion equation is solved for the spatial and temporal evolution of the wave breaking factor. For the simulations in this report, unless otherwise noted, $l = H_s$.

Numerical solution

The wave model equations are solved by integrating in time and using a finite-difference method. The computational domain is discretized as a rectangular grid with the prognostic variables η and u_α defined at the grid points in a staggered manner. The surface elevation is defined at the grid nodes, and the velocities are defined half a grid point on either side of the elevation grid points. A modified third-order accurate Crank-Nicholson scheme is used to integrate the equations (Nwogu and Demirbilek 2001).

A simple but robust scheme (Nwogu and Demirbilek 2007) is used to simulate the flooding and drying of computational cells. The Smagorinsky-type artificial viscosity term effectively smoothes out spurious numerical oscillations at the moving boundaries. For additional information, see Demirbilek and Nwogu (2007).

Critical modeling parameters for reef applications

Three parameters that govern wave energy dissipation in the Boussinesq model play an important role in the estimates of wave setup, wave runup, and wave height variation along the reef and lagoon. These are the Smagorinsky-type eddy viscosity coefficient, wave breaking turbulent length scale, and bottom friction coefficient. The role of these parameters in wave transformation over reefs is discussed next.

The Smagorinsky-type eddy viscosity coefficient (C_v) is used to stabilize wave runup computations. Care should be exercised because, if the value of this coefficient is too large, it can cause excessive numerical dissipation. The typical value of this parameter ranges from 0 to 1, with a default value $C_v = 0.2$.

The wave-breaking turbulent length scale (l) is the eddy length scale parameter that controls the rate of wave energy dissipation for breaking waves. The greater the value of this parameter, the stronger is the rate of wave energy dissipation. The default value of this parameter is the offshore significant wave height, i.e., $l = H_s$ for irregular waves moving over nearly flat (non-sloping) surfaces. For sloping reef surfaces, the turbulent length scale is also dependent on the slope.

The bottom friction coefficient (f_w) controls wave energy dissipation resulting from the turbulent boundary at the seabed. In wave applications, the bottom friction is usually parameterized as a quadratic drag term with a wave friction factor f_w or Chezy coefficient ($C_f = \sqrt{2g / f_w}$), where g = 9.81 m/sec^2. The friction factor can vary over a large range (0.001 to 1.0), and depends on the Reynolds number and relative roughness of the seabed.

Model evaluation objectives

The objectives of the BOUSS-1D model evaluation were:

1. Evaluate the model against four laboratory data sets to determine its general suitability for different types of reef applications.
2. Investigate the sensitivity of model predictions to parameterized wave processes (breaking and dissipation).
3. Determine appropriate values of the adjustable model parameters for each experimental data set. These include wave friction factor, wave breaking dissipation parameter (turbulent-length scale) and Smagorinsky eddy-viscosity coefficient (sub-grid processes).
4. Assess the validity of the universal parameterization developed by Demirbilek and Nwogu (2007) for plunging and spilling breakers.
5. Investigate the generation of nonlinear waves in shallow depths, and how these affect the evolution of wave spectra along the reef profile at different water depths.
6. Study wave height variation over different zones of fringing reefs with different slopes.
7. Study changes in wave setup in the reef lagoon caused by low-frequency nonlinear waves.
8. Study wave runup on beach faces with different slopes.

A description of four laboratory reef data sets is provided in this chapter. The four data sets used in the model evaluation are Hayman Island reef experiments (Gourlay 1994), and three Guam reef experiments (Seelig 1983; Thompson 2005; Demirbilek et al. 2007b). Each experiment and evaluation of the BOUSS-1D is described next. This is followed by two chapters that describe evaluations of RBREAK2 and WAV1D models.

Hayman Island reef experiments

Gourlay (1994) conducted laboratory experiments for a fringing reef located on the southern side of Hayman Island in North Queensland, Australia, to investigate the stability of a proposed reef-top structure located 270 m from the reef edge. The structure was submerged when the tide was above mean sea level, during which it had negligible influence upon the breaking and transformation of waves.

Dimensions of the reef profile used in these experiments are provided in Figure 3. The overall prototype width of reef is approximately 800 m. The reef face starts at about 15 m depth, rising with a slope of 1:4.5 to reach a crest elevation of 1.9 m. The reef ends with an initially sloping reef top that becomes horizontal about 170 m from the reef edge. Figure 3 shows geometric dimensions of the reef profile in model scale and experimental

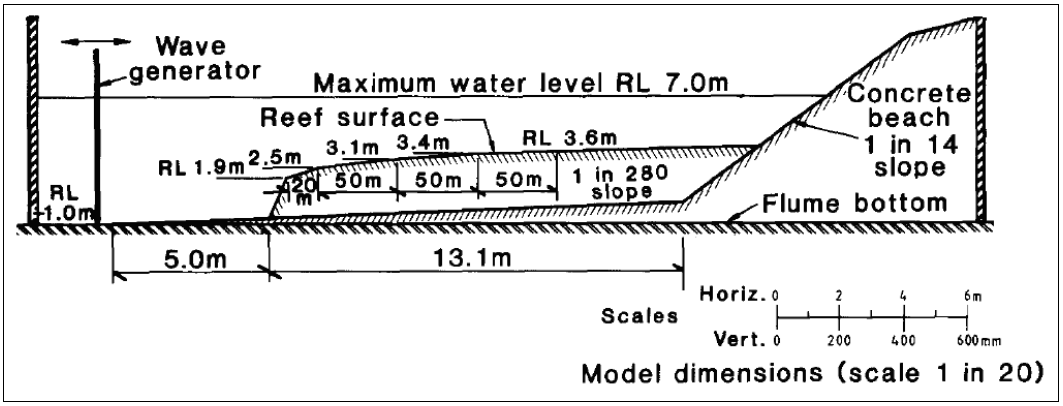

Figure 3. Hayman Island reef profile and experimental layout (modified from Gourlay 1994).

layout. Tides and storm surge were considered with waves in these 1:20 scale experiments. Laboratory tests were conducted in a wave flume that was 30 m long and 0.9 m wide, and had a 0.4 m maximum water depth. A mild (1:280) offshore bottom slope was present in front of the model reef. The numerical modeling domain for Hayman Island reef is shown in Figure 4.

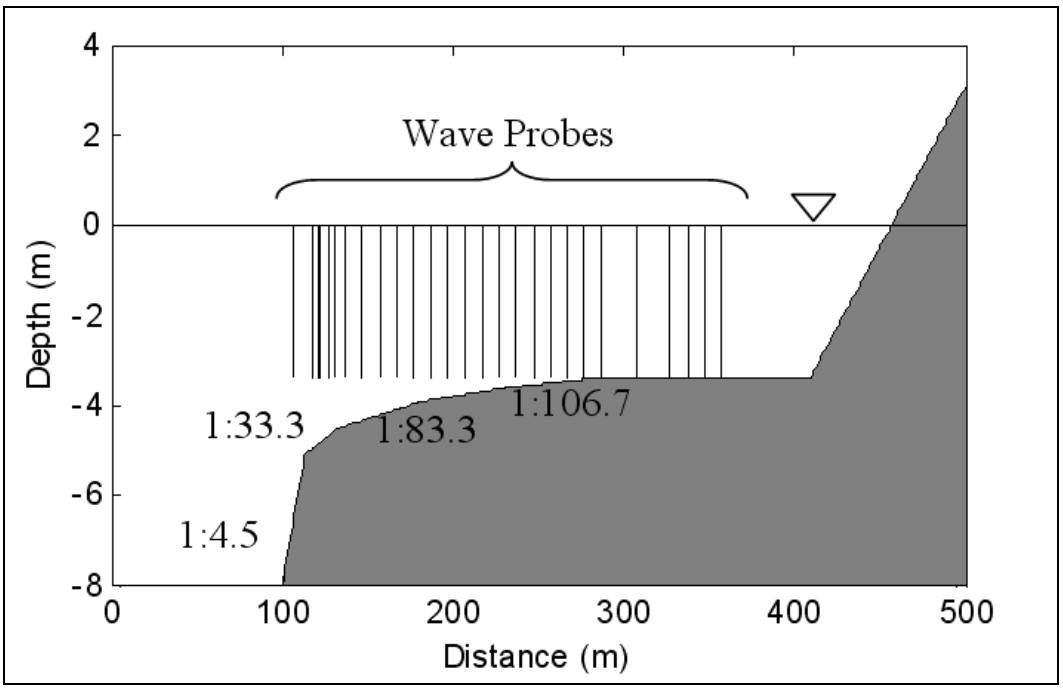

Figure 4. Numerical modeling domain for Hayman Island reef.

Three sets of experiments were performed (Test Series 1-3), each corresponding to a different tidal water level. These test series had six wave conditions with constant steepness (H_0/L_0 = 0.048). A paddle wavemaker was used in these experiments to generate regular (monochromatic)

waves. Measured wave height data based on zero crossing represented the average value of twenty individual wave trains. The data were collected at about a dozen of equally spaced capacitance type wave gauges placed at an interval of $1/12^{th}$ of the incident wavelength. Waves on the reef top were measured at different locations for each experiment, and gauge locations were determined based on visual observation of where the waves broke at the plunge point in the surf zone. Analyzed results were presented at prototype scale using Froude scaling laws (Gourlay 1994). The range of wave parameters and water levels for test conditions are listed in Table 1. The position of wave measurements is not listed in Table 1 for these experiments because wave gauges were placed at different locations for varying water levels.

Table 1. Wave and water levels for Hayman Island experiments.

Test Series 1			Test Series 2			Test Series 3		
T (sec)	*H* (m)	SWL (m)	*T* (sec)	*H* (m)	SWL (m)	*T* (sec)	*H* (m)	SWL (m)
6.8	3.61	3.4	6.75	3.39	1.4	6.7	3.57	2.1
6.62	3.45		6.66	3.35		6.62	3.25	
5.9	2.63		5.81	3.03		5.9	2.84	
5.41	2.19		5.36	2.07		5.4	2.11	
4.69	1.66		4.69	1.6		4.69	1.6	
3.84	1.05		3.8	1.02		3.84	1.05	

A nonlinear wave shape parameter (see Equations 3 and 4 in Gourlay 1994) similar to the shallow-water form of the Ursell number was used for classifying wave transformation over reefs to analyze and interpret experimental results. The shape parameter distinguished between deep, intermediate, and shallow water conditions, and helped to characterize wave transformation processes over reefs, including types of wave breakers, wave setup, wave height variation, and wave runup. Assuming that waves breaking on the reef were not deepwater waves, Gourlay (1994) showed that wave processes occurring on reefs were mainly controlled by the water depth and wave conditions present at the reef edge. For increasing values of wave height and decreasing water depths at the reef edge, wave breaking in these experiments was observed further seaward of the reef face. A greater percent of the wave energy dissipation was reported from these experiments for increasing water depth over the reef edge for large wave heights. Less wave dissipation occurred for waves with smaller heights and steepness.

These experiments showed that the height of plunging breaking waves on the reef face and edge usually decreased with decreasing water depth at the reef edge. The height of waves passing over the reef edge increased until waves started to break on the reef top by spilling. The amount of wave energy for spilling breakers was found to be comparatively less than that for plunging breakers, and reforming waves with higher height were observed in the landward end of the surf zone. For wave height, H, and water depth over reef crest, d, the plungers generally broke at larger H/d ratios than spillers. The height of waves passing over the reef edge without breaking were nearly constant to the point where waves became unstable and broke further inshore on the reef top. Waves traveling over the more gentle or constant slope of the reef top did not always break. These results indicate that the wave breaking type occurring on reefs is not determined by the incident wave conditions, and that the water depth above the reef crest becomes the controlling factor. These observations differ from the wave height variation typically observed on planar beaches, but are strikingly similar to the type of wave breaking occurring on offshore bars. Gourlay (1994) has characterized wave breaking in terms of the surf-similarity parameter (Irribaren number), defined as

$$\zeta_0 = \frac{\tan\alpha}{\sqrt{H_0 / L_0}} \tag{4}$$

where $\tan\alpha$ is the bottom slope, and H_0/L_0 is the deepwater wave steepness. For reef face slope = 1:4, reef edge slope = 1:30, and $H_0/L_0 = 0.048$, spilling wave breaking occurred for $\zeta_0 = 0.14$, and plunging type breaking for $\zeta_0 = 1.15$. The extent of the surf zone and rate of wave energy dissipation were dependent on the wave breaking type occurring over the reef (Gourlay 1994, 1996a, 1996b).

For the Hayman Island reef experiments, BOUSS-1D simulations were performed for water levels of 3.4, 2.1, and 1.4 m using the same geometry and wave conditions as given by Gourlay (1994). No assumptions were made concerning spatial and temporal variation of waves or breaking types along the reef zones. For the six larger wave heights, results are provided in this Chapter, and for the remaining test conditions, model results are compared to data in Appendix A.

The variation in the calculated wave height for the two largest incident wave heights is compared to data in Figures 5-10. Default values of model parameters were used, and no attempt was made to calibrate the model parameters with data. A good agreement is obtained between model results and data by using BOUSS-1D in a "blind mode" (un-calibrated), showing that the model is able to reproduce measured wave height variation and wave setup (Figures 5-10) for the two largest waves at three water levels. The largest difference between calculated and measured wave heights and water levels occurs for the lowest water level (1.4 m). BOUSS-1D simulation results for experimental Tests 11, 12, 21, 22, 31, and 32 are shown in Figures 5-10. Results for other test conditions are provided in Appendix A.

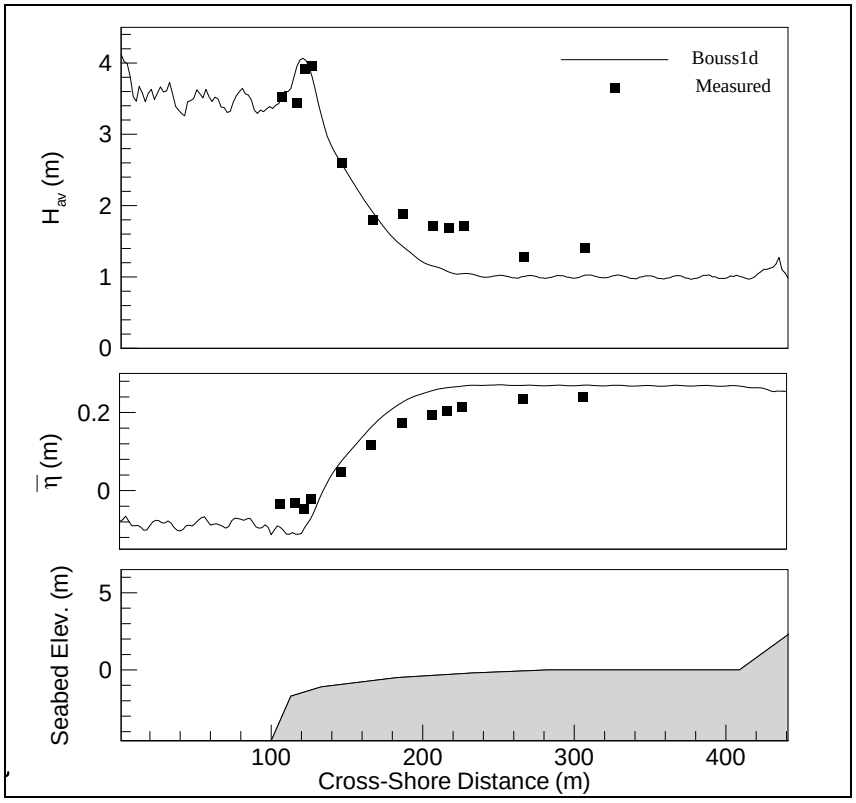

Figure 5. Test 11 (SWL = 3.4 m, H = 3.61 m, T = 6.8 sec).

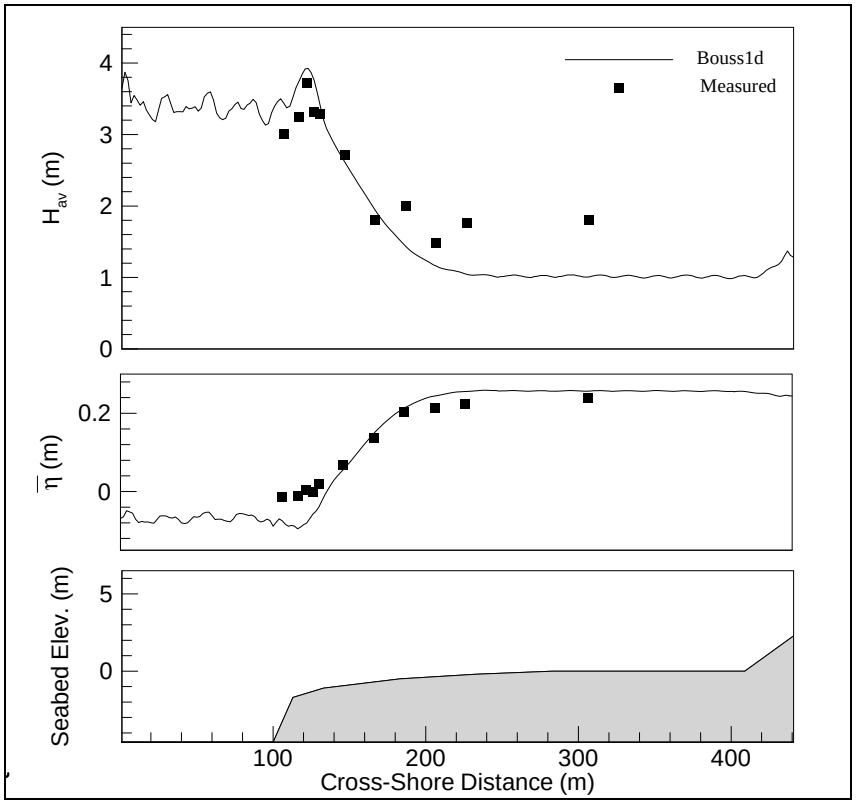

Figure 6. Test 12 (SWL = 3.4 m, *H* = 3.4 m, *T* = 6.6 sec).

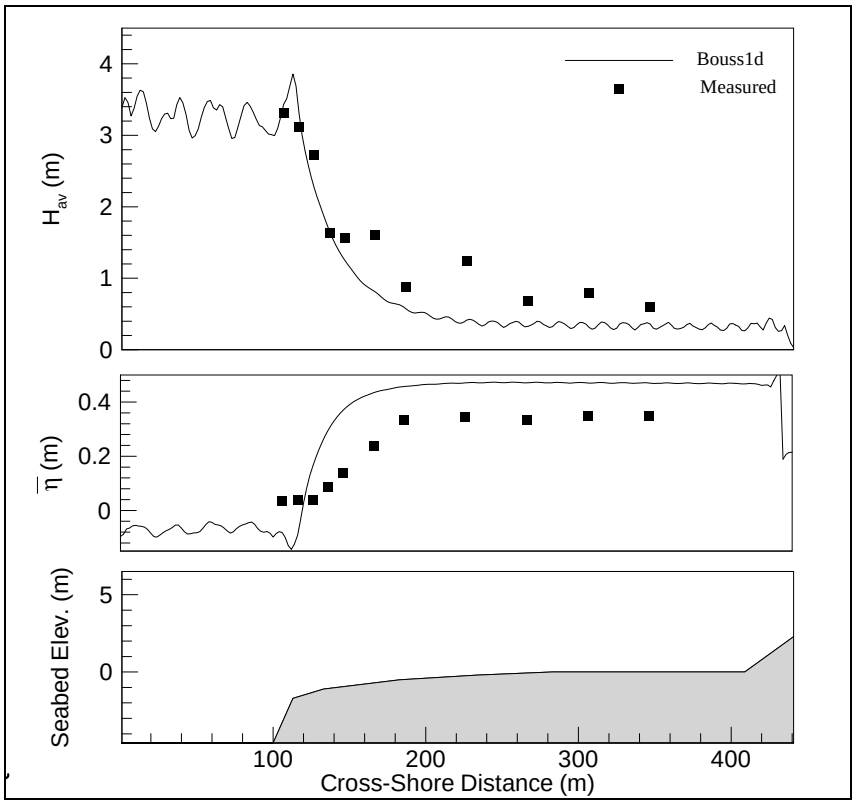

Figure 7. Test 21 (SWL = 1.4 m, *H* = 3.39 m, *T* = 6.8 sec).

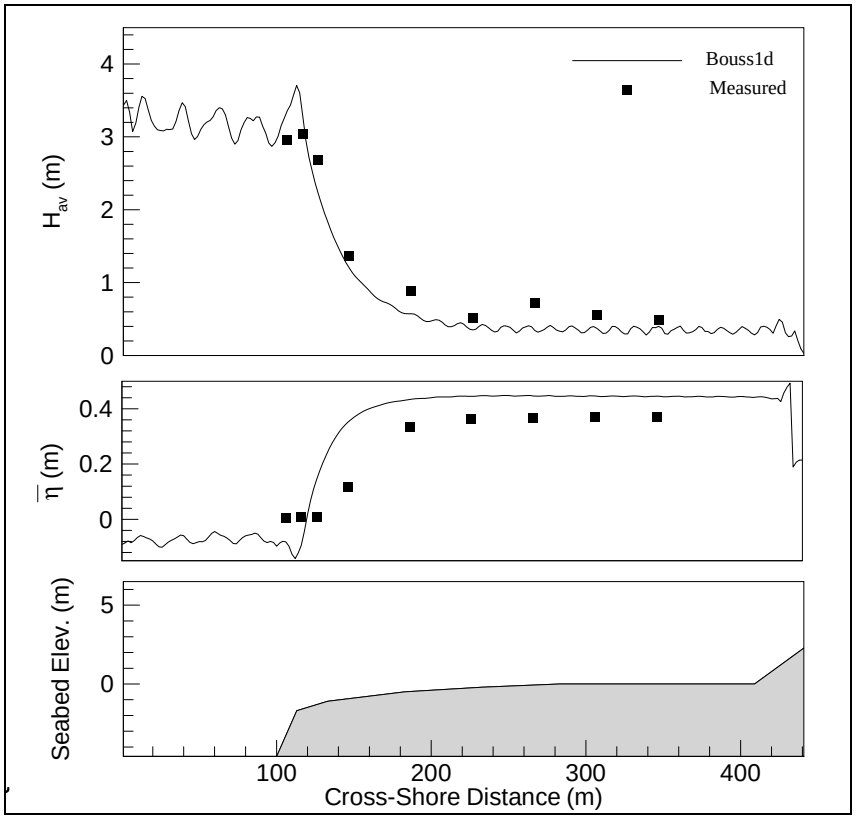

Figure 8. Test 22 (SWL = 1.4 m, *H* = 3.35 m, *T* = 6.7 sec).

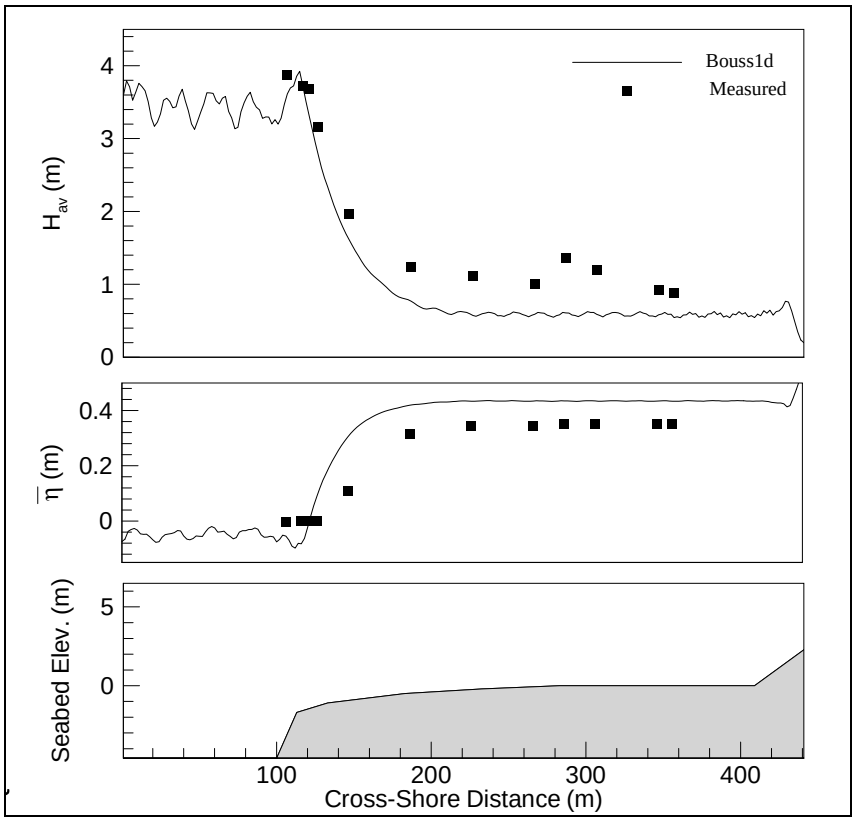

Figure 9. Test 31 (SWL = 2.1 m, *H* = 3.57 m, *T* = 6.7 sec).

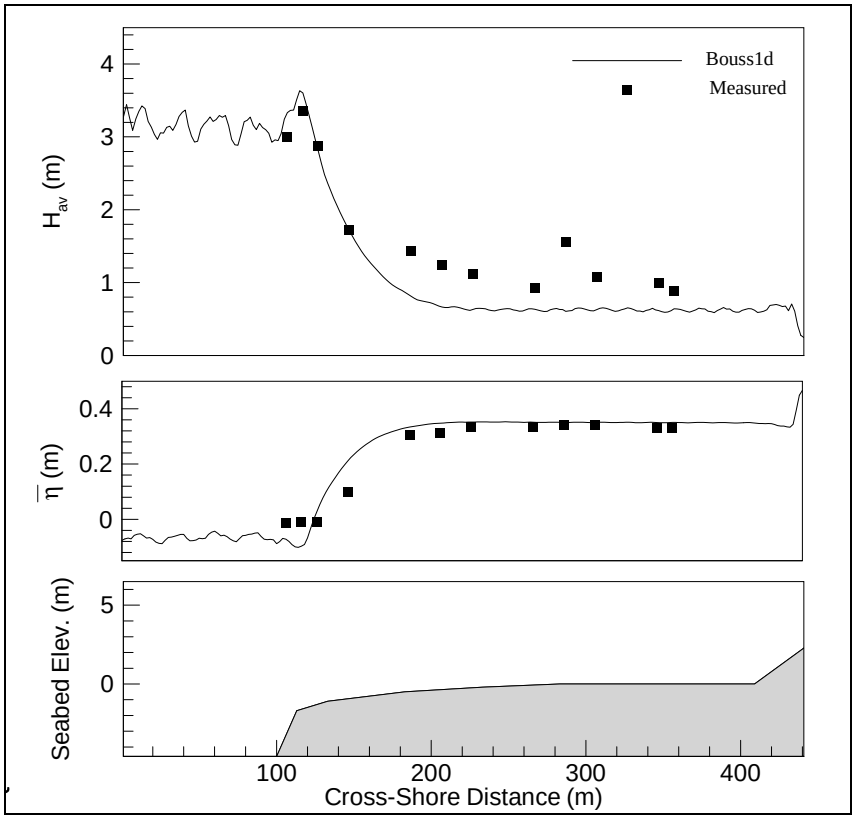

Figure 10. Test 32 (SWL = 2.1 m, H = 3.26 m, T = 6.6 sec).

Calculated wave height and water level variations along the reef profile from BOUSS-1D model simulations were obtained by using default parameters (C_f = 20, $l = H_s$, $\delta_{min} = H_s/1{,}000$, C_v = 0.2). Default values were used for the critical model parameters. The numerical model captures the data trend, and the largest differences occur on the reef top. A more favorable comparison could have been obtained if model parameters were calibrated using the experimental data. By employing default parameters for all wave conditions simulated, the location of wave breaking is determined accurately by the BOUSS-1D model. Overall, calculated wave heights are slightly less than data, and water level is underestimated near the point of wave breaking. The agreement between model calculated wave heights and data is not as good as that of wave setup on the reef top. This difference may be related to the method used in the calculation of wave heights. Zero-crossing was used for laboratory measurements and spectral analysis for BOUSS-1D. Calculated and measured water levels and wave heights for all test conditions are compared in the scatter plots in Figures 11 and 12.

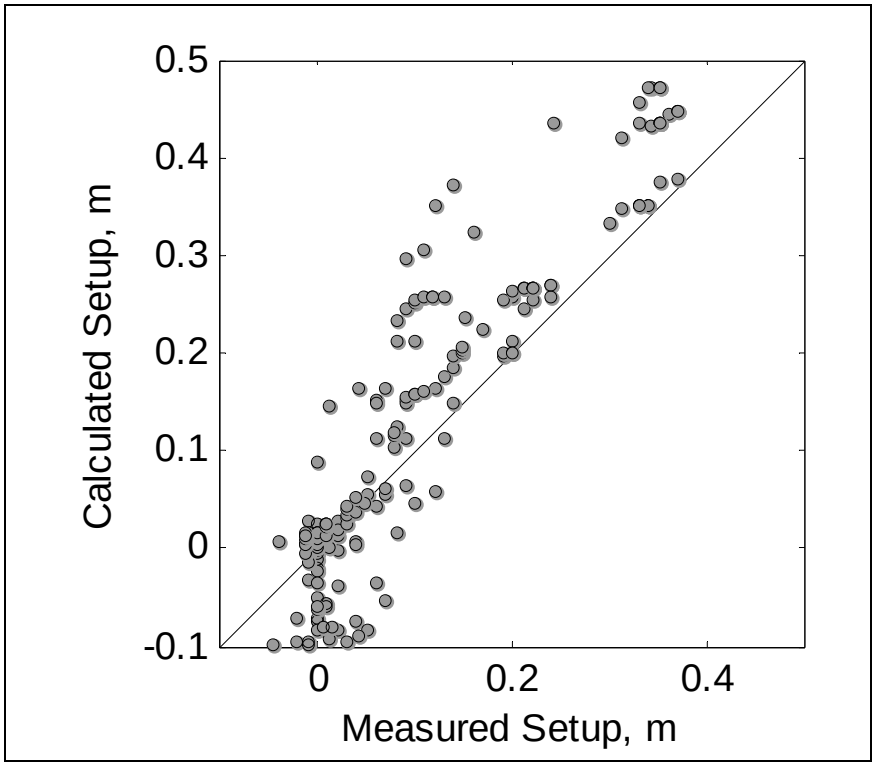

Figure 11. Comparison of BOUSS-1D calculated and measured wave setup for Hayman Island reef (all test conditions).

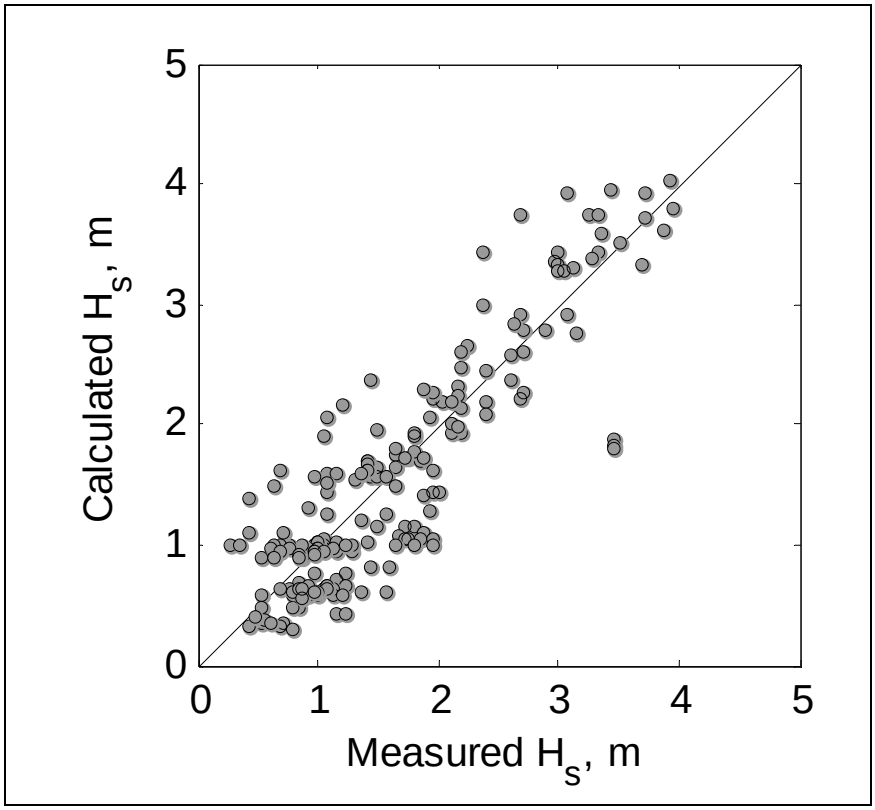

Figure 12. Comparison of BOUSS-1D calculated and measured wave height for Hayman Island reef (all test conditions).

Guam reef experiments

Seelig (1983) conducted physical model flume tests to investigate wave transformation and water level variation across a reef profile common to the island of Guam. An idealized reef profile representative of typical fringing reefs in Guam was used in these experiments. The fringing reef profile shown in Figure 13 starts with a slope in relatively deep water, and has a distinct reef crest region connected to a lagoon and a beach. The reef profile used in these experiments consisted of three sloping regions, with slopes of 1:5, 1:18.8, and 1:10.6, starting from the deepest end landward. The corresponding prototype scale horizontal lengths of these regions are 82.9, 136.8, and 86.6 m. The length and depth of the lagoon are 150 m and 2.1 m, respectively, and beach slope is 1:12. The reef dimensions for these experiments are given in Figure 13. The physical model was built at a 1:64 Froude scale.

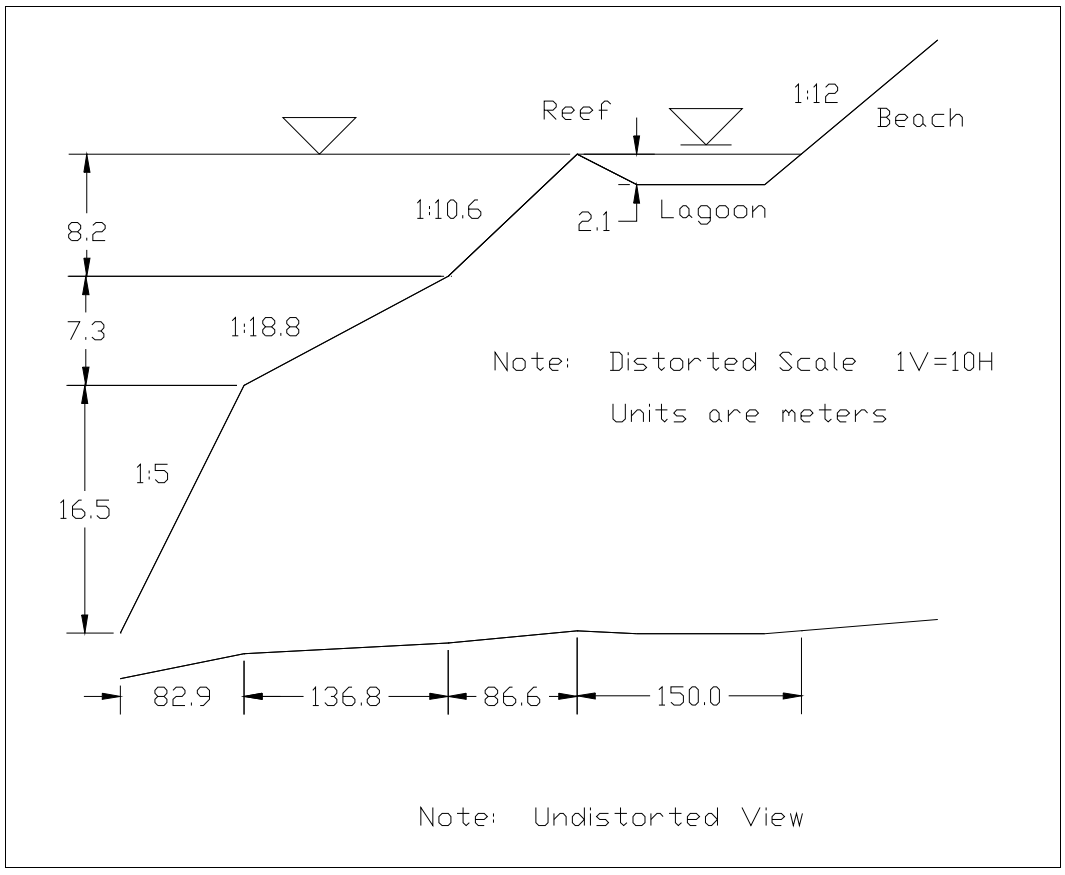

Figure 13. Reef structure used in physical model study by Seelig (1983). Dimensions are in prototype scale.

This laboratory study was conducted to determine the influence of wind waves on the ponding level, surf beat, transmitted wave characteristics, and wave runup on a sloping beach shoreward of the reef lagoon. Both monochromatic and irregular waves were considered to compare differences in the wave runup for regular and irregular seas. Data analysis was performed for wave height variation along the entire reef, water level variation in the lagoon, and wave runup estimate on the beach. Experimental results were reported in the prototype units using Froude scaling laws.

The input wave parameters for each test condition in these experiments were not reported. In addition, all experimental results were presented in the form of best-fit curves to data. The lack of information about incident wave conditions for each test run of these experiments presents a great uncertainty to numerical modelers. Modelers can use different combinations of incident wave parameters (H and T) to obtain the same value of the wave energy flux parameter in the best-fit curves of Seelig (1983).

Experimental results revealed that both deepwater wave characteristics and wave nonlinearities (i.e., wave grouping effects) in shallow-water depths affected the spatial and temporal wave transformation processes observed over the reef profile. Measured time series of wave height variation across the reef length, water level change (ponding), and surf beat processes in the lagoon zone of this reef were sensitive to the deepwater wave parameters and nearshore wave nonlinearities (Seelig 1983). The wave setup and wave runup on the beach face were also affected.

These laboratory experiments were conducted for two water depths and two lagoon widths. Tests were performed with a zero depth (water level even with the top of the fringing reef), 2 m depth (above the fringing reef crest), and lagoon widths of 150 m (shown in Figure 13) and 525 m. Although Seelig (1983) did not provide incident wave parameters for each individual experimental run, he indicated that values of wave periods ranged from 8 to 16 sec, and deepwater significant wave heights ranged from 2.5 to 10.7 m. Table 2 shows the prototype range of input parameters for these experiments used in the BOUSS-1D simulations.

A detailed BOUSS-1D sensitivity study was performed in 2005 and 2006 and recorded in an unpublished report by Drs. Edward F. Thompson (now retired) and Donald L. Ward. The main findings of the earlier research

study are provided in Appendix B of this report. These shed some insight about the role of various model parameters, how each parameter affects wave transformation over the reef, wave setup and wave evolution in the lagoon, and wave runup on the beach face. Additional information about Seelig's experiments and earlier sensitivity study is provided in Chapter 4 through Chapter 7 of this report.

In the earlier study, an indexing scheme was used for identifying parameters similar to those listed in Table 2. In the indexing scheme, the first digit of the test number was either 1 or 2, indicating a water level over the reef of 0 or 2 m, respectively. The second digit (1 or 2) corresponded to the lagoon width of 150 or 525 m, respectively. The third digit (1, 2, or 3) represented values of T_p = 8.0, 12.0, or 16.0 sec, respectively, where T_p is the peak wave period. The fourth digit (1, 2, 3, or 4) was assigned to the value of H_s = 2.5, 5.0, 7.5, or 10.55 m, respectively, where H_s is the significant wave height in the offshore section of the wave model domain. As an example, the index 1133 corresponded to zero depth over the reef crest, 150-m-wide lagoon, 16.0-sec wave period, and 7.5-m wave height. See Appendix B for details.

Table 2. Range of parameters for Seelig experiments (prototype units).

Depth over reef crest, d_r (m)	Lagoon width, (m)	Wave period, T_p (sec)	Wave height, H_s (m)
0	150	8 to 16	2.5 to 11
2	150	8 to 16	2.5 to 11
0	525	8 to 16	1 to 11
2	525	8 to 16	1 to 11

Experimental results were presented by Seelig (1983) using an energy flux parameter (wave power) defined as $H_0^2\ T_p$, where H_0 and T_p are deepwater significant wave height and peak period, respectively. Because values of H_0 and T_p for experimental test conditions were not specified, Table 3 provides the values of wave height, wave period, and corresponding energy flux parameter ($H_0^2\ T_p$) that have been used in the present BOUSS-1D simulations for the case of depth of water over reef = 0 m and lagoon width = 150 m. The input conditions used in BOUSS-1D simulations for the 2-m lagoon water depth and 150-m lagoon width, and for a 525-m-wide lagoon with 0 and 2 m water depths are provided in Appendix C.

Table 3. Wave parameters used in BOUSS-1D simulations for Seelig experiments (lagoon width = 150 m, depth = 0 m).

Test ID	H_s (m)	T_p (sec)	$H_s^2 T_p$ (m²*sec)
101	2.85	8.00	65
102	4.36	8.00	152
103	4.97	8.00	197
104	3.77	10.00	142
105	5.92	10.00	350
106	9.30	10.00	864
107	5.05	12.00	306
108	7.76	12.00	722
109	9.15	12.00	1,006
110	5.44	14.00	414
111	8.28	14.00	960
112	10.68	14.00	1,597
113	5.36	16.00	459
114	8.23	16.00	1,084
115	10.55	16.00	1,781

Seelig (1983) obtained two short-wave parameters from the analysis of measured laboratory surface elevation and runup time series. These were the significant wave height transmitted over the reef normalized by local water depth ($\frac{(H_s)_t}{d}$), and the value of highest runup level ($R_{\max}$) in a 34-min time series, defined as the maximum vertical distance above the SWL. The long-wave parameters were derived from a moving average of the surface elevation time series (averaging time of twice the peak period). The mean value of the measured water surface elevations was defined as $\bar{\eta}(i) = \frac{1}{2NP}\sum_{j=-NP}^{NP-1} \eta(i+j)$, where $NP = \frac{T_p}{\Delta t}$, η is the instantaneous water surface elevation, Δt the sampling interval, and $\bar{\eta}$ the time varying long-wave component of the water surface elevation. Statistical parameters derived from the long-wave time series included the mean value of $\bar{\eta}(i)$ measured in the middle of the lagoon, referred to as lagoon ponding level ($\bar{\eta}_{mean}$) and its standard deviation (σ), and values of the $\bar{\eta}(i)$ above SWL percent of the time ($\bar{\eta}_{1\%}$).

For a test condition with H_{m0} = 8 m, T_p = 16 sec and d_r = 0 m, a sample plot of significant wave height and mean water level variation across the reef is shown in Figure 14. For the Seelig fringing reef topography, the calculated values of wave runup from BOUSS-1D are compared to data in Figure 15. Seelig (1983) developed an empirical best-fit curve for the mean water level in the lagoon (ponding) from the analysis of experimental data, and expressed it as

$$\bar{\eta} = a_1 + a_2 \ln(H_{m0}^2 T_p) \tag{5}$$

where a_1 and a_2 are dimensional empirical constants that depended on the SWL in the lagoon in these experiments. Analyzed data from these experiments were plotted by Seelig as a function of the wave energy flux parameter $(H_{m0}^2 T_p)$. The values of significant wave height H_{m0} (wave height calculated from the zero-moment of the wave spectrum) and T_p (spectral peak wave period) corresponding to each data point were not provided. For the range of wave periods in Table 2 (see also Seelig 1983), numerical simulations were performed for three spectral peak periods (T_p = 8, 12, and 16 sec). For simulations made with T_p = 12 sec, significant wave height (H_{m0}) values were varied from 3 to 8 m. For simulations made with T_p = 16 sec, wave heights were varied from 3 to 10 m. Two lagoon water levels (d_r = 0, 2 m) were used in simulations, with other BOUSS-1D inputs as follows: Δx = 5 m, Δt = 0.2 sec, C_f = 20, $l = H_s$, $\delta_{min} = H_s/1{,}000$, and C_v = 0.3. Default values were used for the critical model parameters.

Because there were no spatial measurements of waves along the reef profile from these experiments, only BOUSS-1D estimates are shown in Figure 14. Results show that the wave heights increase as waves move over the reef face, becoming the largest at the reef crest, and wave breaking causes wave heights to decrease over the reef lagoon. This represents a typical spatial evolution of the wave transformation over fringing-type reefs.

The predicted wave setup in the lagoon is compared with the empirical curve of Seelig (1983) in Figure 15. The simulation results for T_p = 16 sec fit the empirical curve better than results of T_p = 12 sec. Figure 16 shows a comparison of the predicted maximum runup height obtained from analysis of a 34-min record with the best-fit line of Seelig (1983).

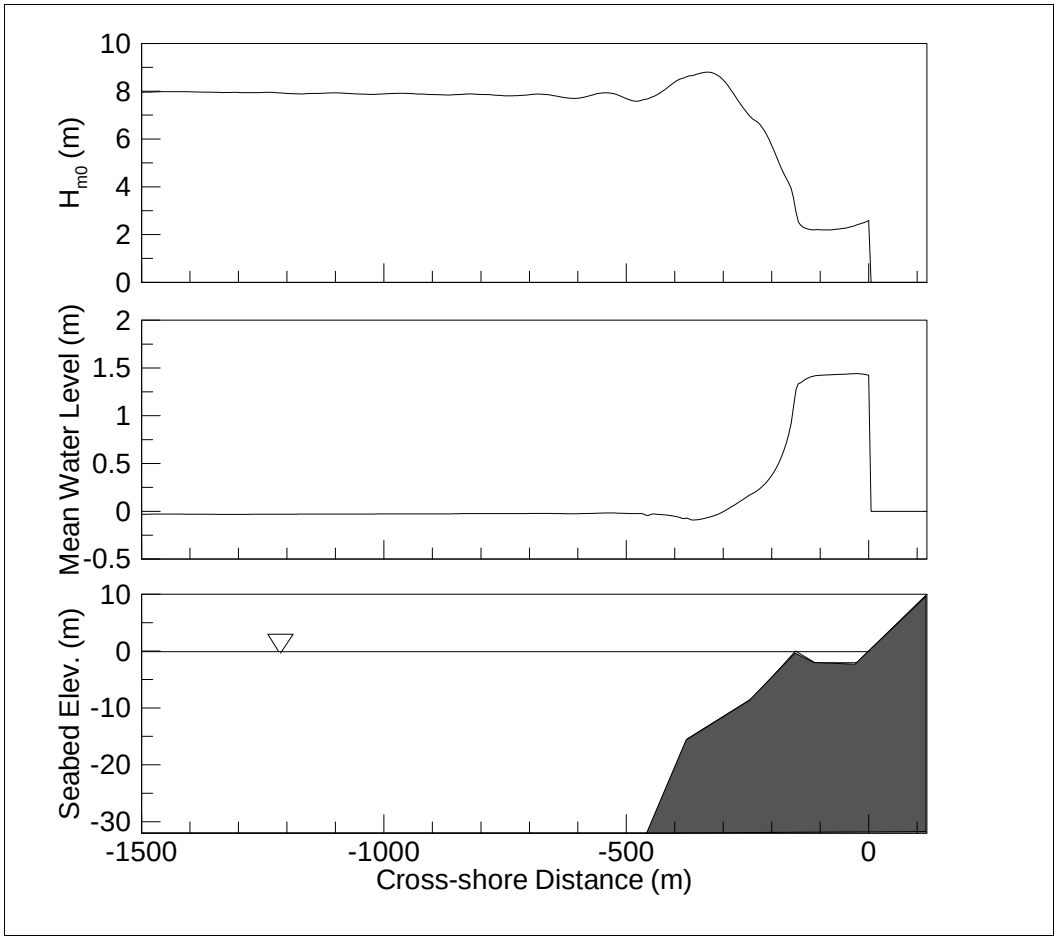

Figure 14. Variation of significant wave height and mean water level over a reef-lagoon topography (H_{m0} = 8 m, T_p = 16 sec).

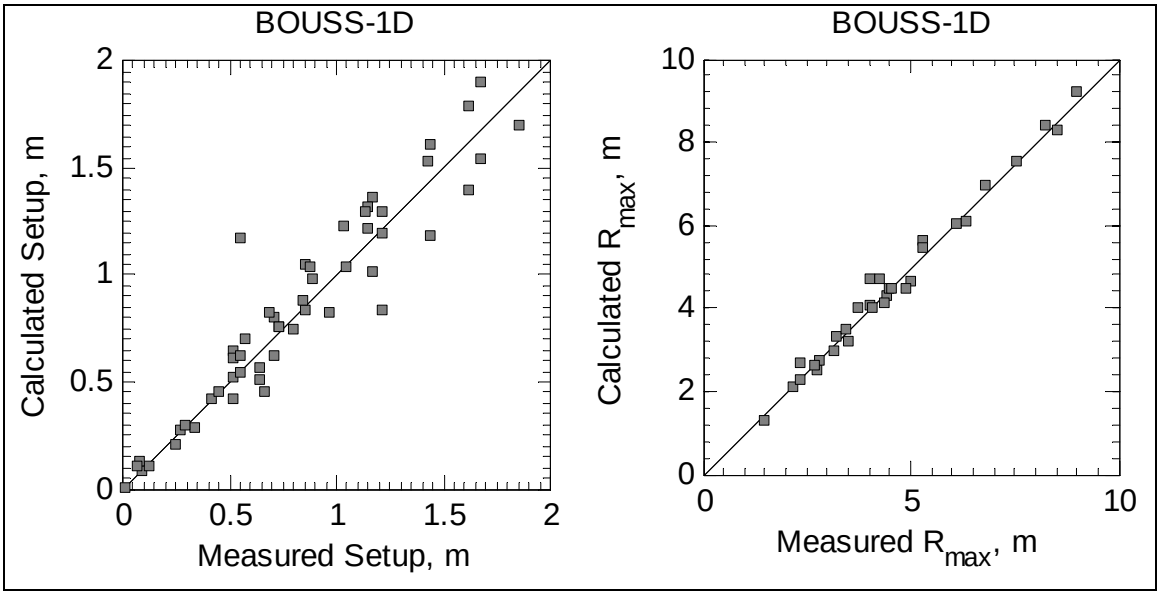

Figure 15. Comparison of BOUSS-1D calculated wave setup and maximum runup with data.

The BOUSS-1D slightly underestimates the maximum runup height for the largest and longest waves. To show the robustness of BOUSS-1D and its ability to replicate these experiments, no attempt was made to improve the model-data match by adjusting the values of critical model parameters (e.g., bottom friction coefficient, turbulent length scale, etc).

The BOUSS-1D results from the present evaluation study are summarized in Figures 16 and 17. Calculated model ponding levels at the middle of the lagoon are compared to the best-fit empirical formula of Seelig (1983) in Figure 16. Ponding levels are plotted against the wave power for wave periods of 12 and 16 sec and two water depths (0 and 2 m) over the reef crest for the lagoon width of 150 m. Overall, a reasonable agreement is obtained between calculated ponding levels from BOUSS-1D and data for the range of parameters considered. Calculated maximum wave runup values are compared to experimental results (the best-fit empirical formula) in Figure 17. Results are plotted using the wave power parameter for the same conditions and geometry as in Figure 16. A sensitivity study revealed that the best agreement between the model and data was obtained for the Chezy coefficient of 20 (the default is 30).

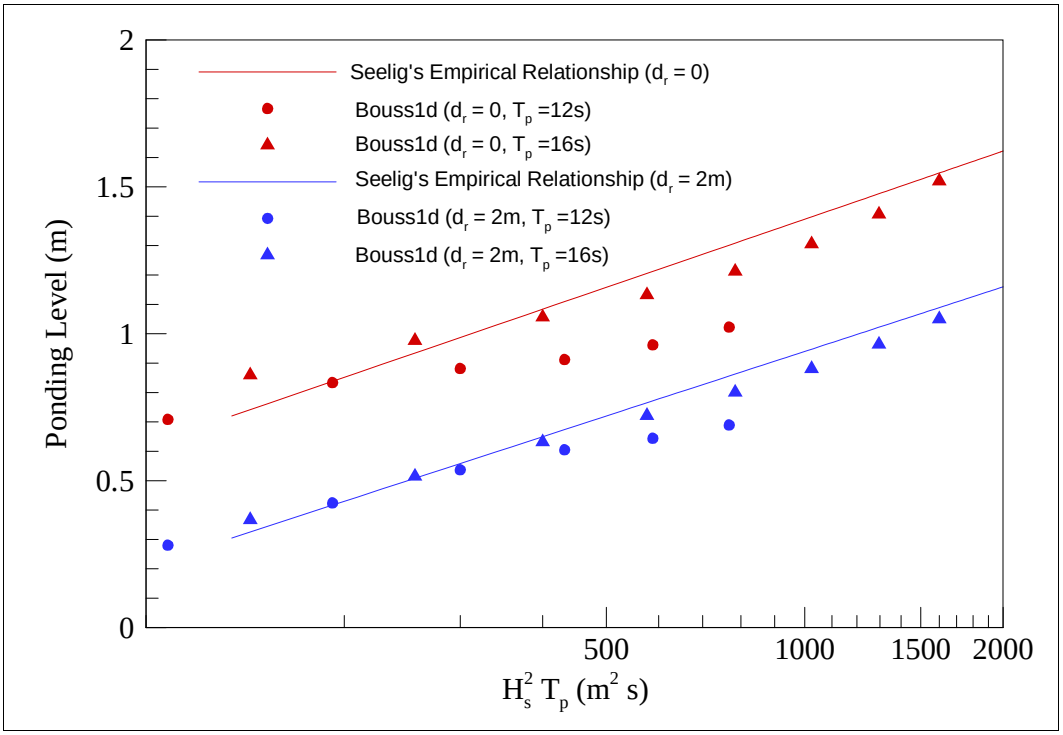

Figure 16. Comparison of BOUSS-1D lagoon ponding level with best-fit empirical formula of Seelig (1983).

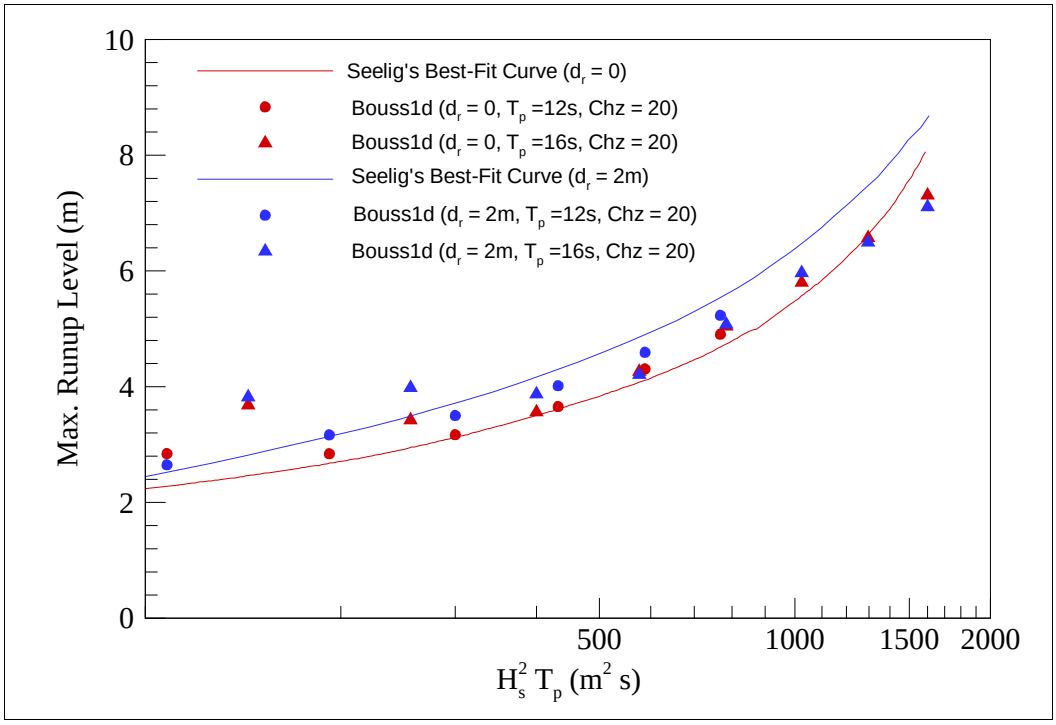

Figure 17. Comparison of maximum wave runup height with the best-fit line by Seelig (1983).

CHL reef experiments

Thompson (2005) conducted laboratory experiments to investigate wave transformation across fringing reefs, where the shoreline runup was strongly influenced by low-frequency oscillations on the reef. The experiments were carried out in the directional wave basin of the Coastal and Hydraulics Laboratory (CHL), ERDC. Information about these experiments, including layout and reef geometry tested in this study, test conditions, instrumentation, and analyses of data, is provided by Thompson (2005).

These 2D laboratory experiments were conducted in the 29-m-wide by 52-m-long directional wave basin of CHL to investigate wave transformation across fringing reefs. An 18-m-long by 2.44-m-wide sloping reef bathymetry was built in the middle of the basin, as shown in Figure 18. The cross-sectional profile of the reef face was similar to the one used in previous hydraulic model tests by Seelig (1983). The fringing reef configuration in these experiments had a flat reef top instead of the barrier reef configuration with a lagoon, as used by Seelig (1983). The flat reef top is more typical of conditions along the southeast coast of Guam. These experiments were conducted at a much larger model scale (1:36), as

compared to the Seelig experiments (1:64). The experimental layout is depicted in Figure 18. These measurements are all given in model scale.

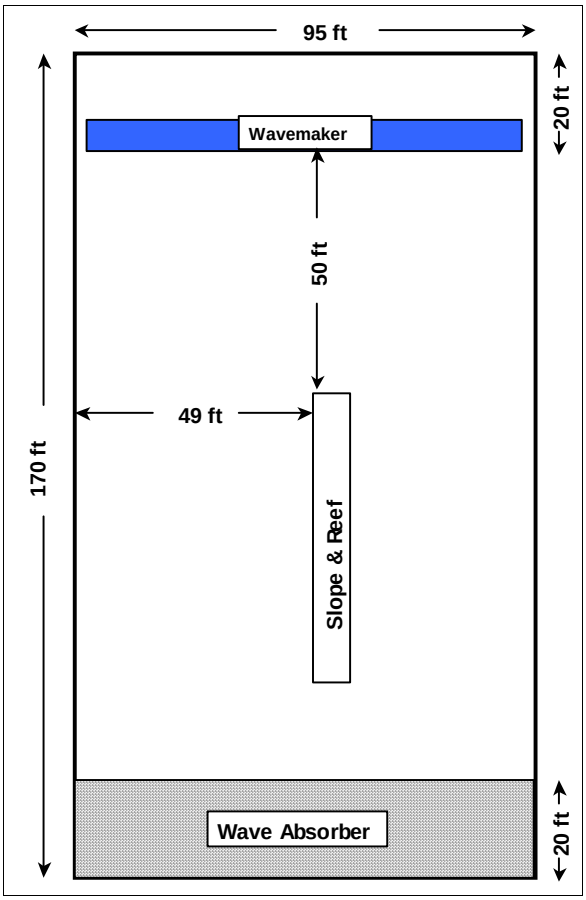

Figure 18. Basin layout for CHL laboratory experiments.

Nine wave gauges were used to measure the water surface elevation at different locations in the wave basin (Figure 19). The elevation where the reef flat meets the sloping beach is 0.0 m. The wave gauges were deployed at distances of -21.4, -21.08, -20.49, -9.13, -6.09, -4.59, -2.45, and -1.84 m relative to the shoreline, where end of the reef flat joins with the beach. Two water levels (elevation = 0.0 and 0.056 m) were used in these experiments, corresponding to still water depths of 0.744 and 0.8 m in the constant-depth offshore section of the basin. The still-water depth of 0.744 m corresponds to an initially dry reef top. Nineteen different tests were conducted with different combinations of significant wave height, peak wave period, and water level. The test conditions are summarized in Table 4.

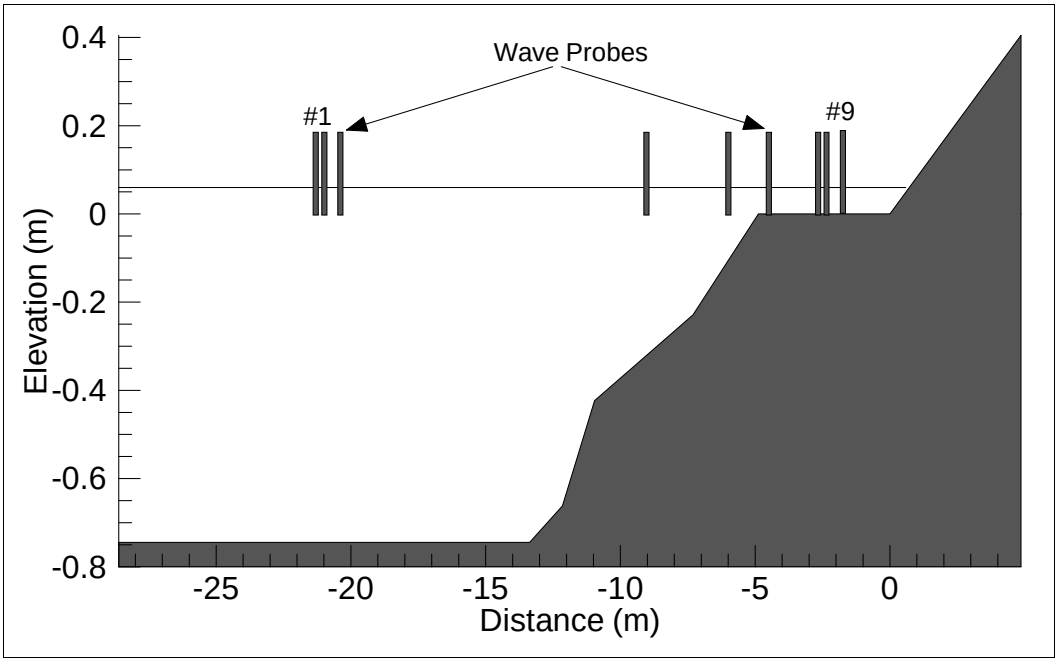

Figure 19. Cross-sectional view of CHL laboratory experimental setup.

Table 4. Test conditions for CHL laboratory experiments.

Test ID	Water Level (m)	H_s @ Gauge #1 (m)	Target, T_p (sec)
GUAM01	0.056	0.094	1.67
GUAM02	0.056	0.101	2.5
GUAM03	0.056	0.094	1.67
GUAM04	0.056	0.125	1.67
GUAM05	0.056	0.16	2.5
GUAM06	0.056	0.125	1.67
GUAM07	0.056	0.176	2.5
GUAM08	0.0	0.21	1.67
GUAM09	0.0	0.166	1.67
GUAM10	0.0	0.187	2.5
GUAM11	0.0	0.221	2.5
GUAM12	0.0	0.104	1.67
GUAM13	0.0	0.094	2.5
GUAM14	0.0	0.185	1.67
GUAM15	0.0	0.116	1.67
GUAM16	0.056	0.179	1.67
GUAM17	0.056	0.197	1.67
GUAM18	0.056	0.168	2.5
GUAM19	0.056	0.217	2.5

Nineteen test conditions were used in these experiments (Table 4). These runs consisted of different combinations of significant wave height, peak period, and water level. Incident waves are represented by wave parameters at Gauge 1 (Figure 19). The test conditions included two spectral peak periods (1.67 and 2.5 sec), two water levels (0.0 and 0.056 m), and a range of incident wave heights (from 0.094 to 0.217 m).

Four tests were selected for the evaluation of BOUSS-1D. The selected test conditions include sea states with two different peak periods, two water levels, and an incident wave height of $H_s \approx 0.1$ m. The corresponding prototype sea states in the GUAM01 and GUAM02 tests had peak periods of 10 and 15 sec, respectively, wave height of approximately 3.6 m, and water level of 2 m on the reef. The GUAM12 and GUAM13 tests used similar conditions with an initially dry reef.

The time series data available from each gauge of these experiments allow for a detailed investigation of wave evolution on the reef, starting from deepwater to the shallow ends of the reef profile. The reef profile used in the BOUSS-1D simulations is shown in Figure 19. The incident wave input to the model was the measured water surface elevation time series at Gauge 1. The simulations were performed at prototype scale with $\Delta x = 0.1$ m, $\Delta t = 0.02$ sec and default values for other parameters ($l = H_s$, $C_f = 20$, $\delta_{min} = H_s/1{,}000$, $C_v = 0.2$). The water depth in the offshore section was set to 0.6 m to minimize the amount of wave energy that is truncated in the numerical model resulting from the deepwater (high-frequency) cutoff limit of the Boussinesq equations (Nwogu and Demirbilek 2001; Demirbilek et al. 2005a, 2005b).

The measured and predicted significant wave height variations across the reef slope topography are compared in Figures 20 to 23. The waves shoal slightly before breaking just offshore of the reef for the GUAM01 test (Figure 20). The simulations with the default model parameters capture the overall wave height variation with slight discrepancies at Gauge #4 on the slope, and Gauges 7 and 8 on the reef. BOUSS-1D reproduces the measured wave evolution on the reef in these experiments without calibrating the model. Given the shallowness of water depth on the reef, the parameterized bottom friction term was expected to play an important role in the wave energy dissipated on the reef flat. Consequently, a few simulations were repeated with a lower value of the friction coefficient ($f_w = 0.004$ or $C_f = 50$) as opposed to the default values ($f_w = 0.01$ or $C_f = 30$).

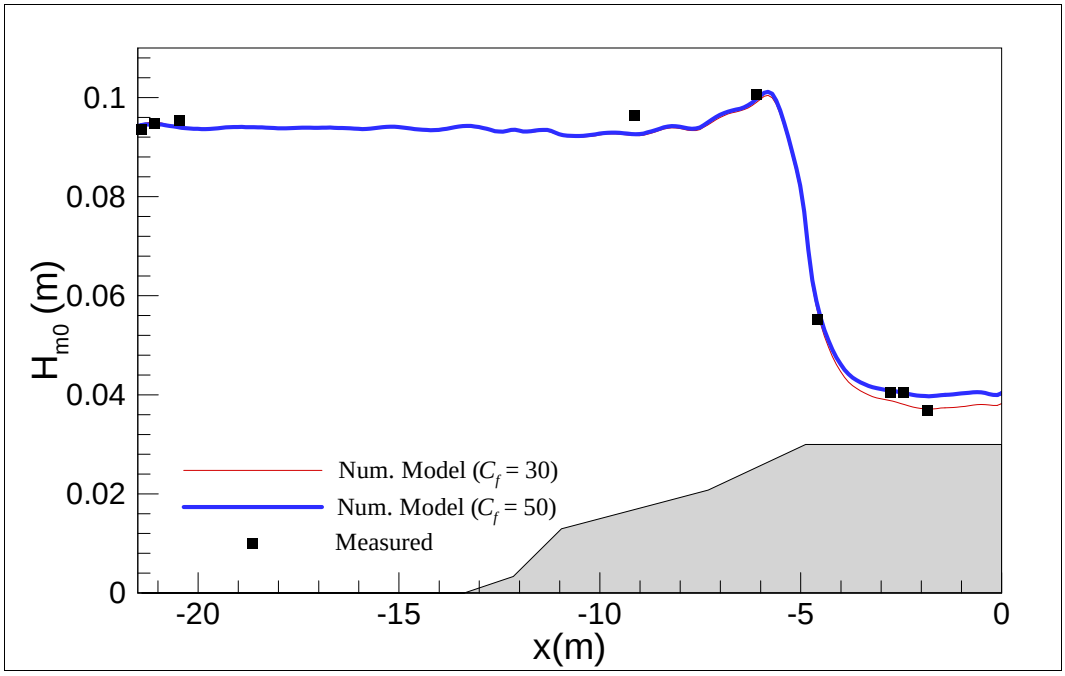

Figure 20. Measured and calculated significant wave height distribution for GUAM01 test.

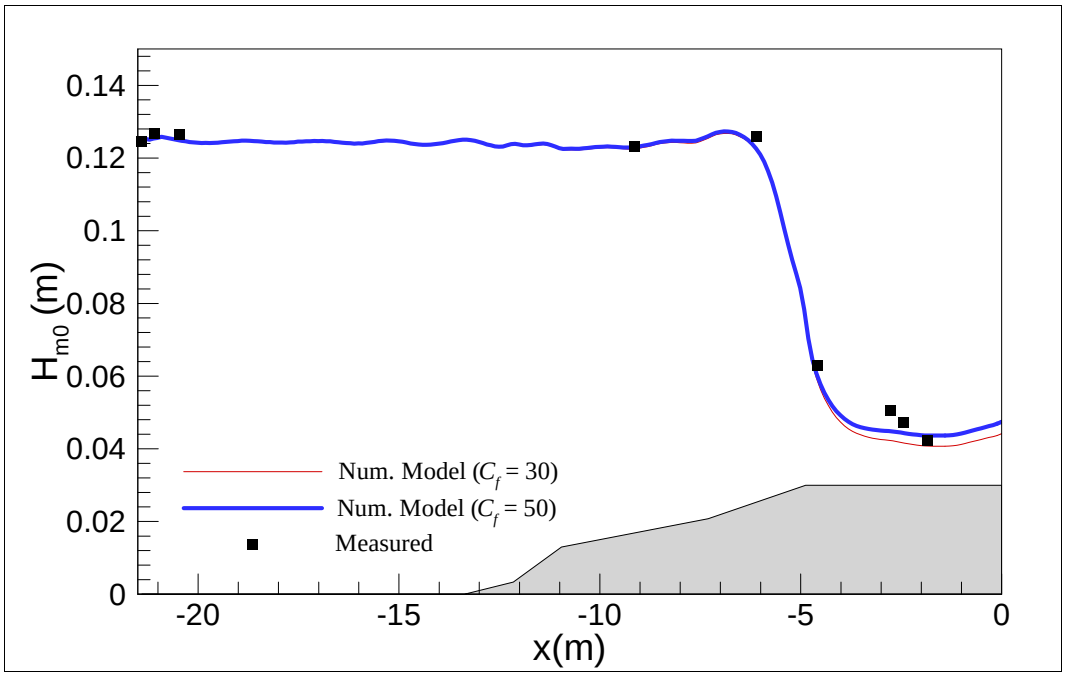

Figure 21. Measured and calculated significant wave height distribution for GUAM02 test.

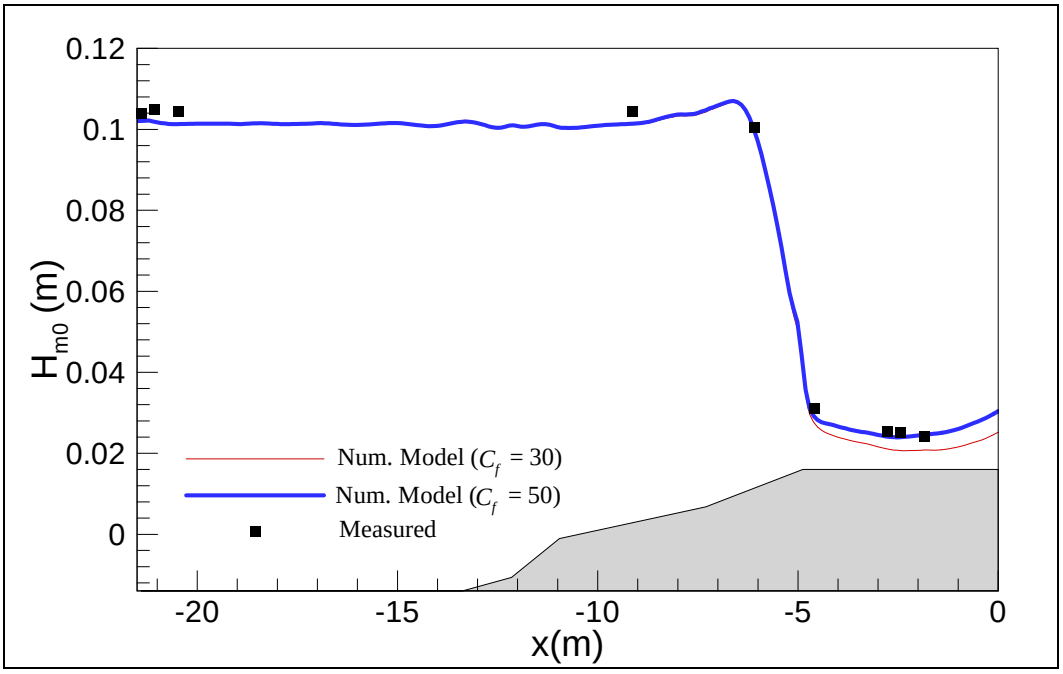

Figure 22. Measured and calculated significant wave height distribution for GUAM12 test.

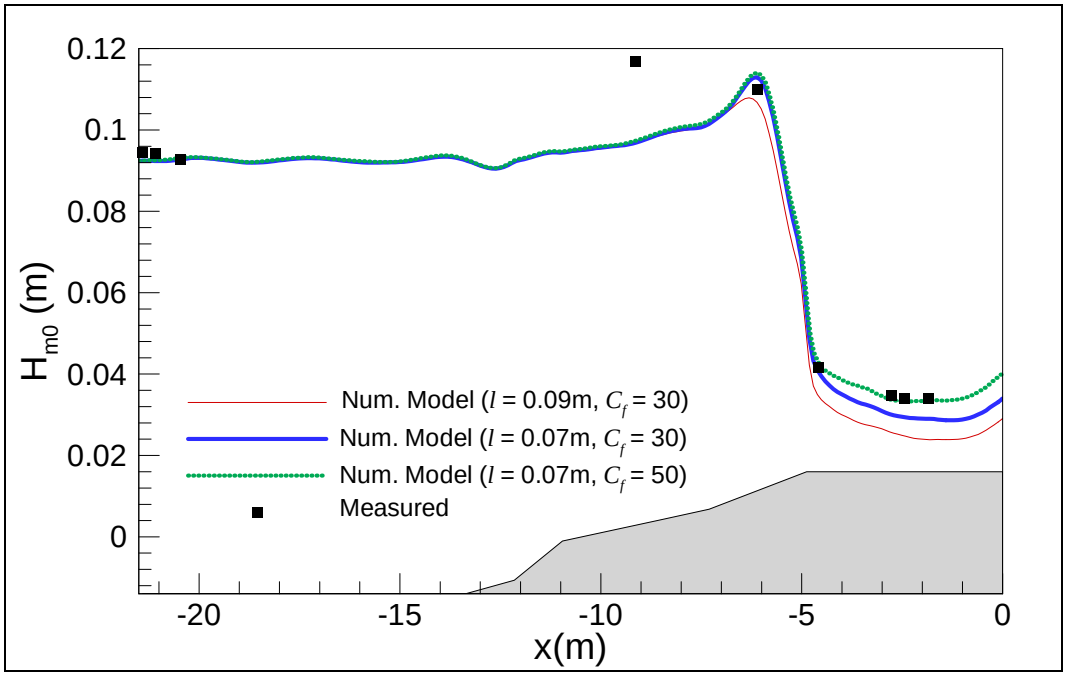

Figure 23. Measured and calculated significant wave height distribution for GUAM13 test.

The different friction coefficient value did not affect the wave height in the deeper sections seaward of the reef, but it increased wave height on the reef by approximately 8 percent. This improved the match at Gauges 7 and 8 but worsened the match at Gauge 9. The use of a Chezy friction coefficient $C_f = 50$ did significantly improve the model-data match on the reef for the GUAM12 test (Figure 22).

For the GUAM13 test with longer-period waves, BOUSS-1D slightly underestimated the wave height at Gauge 5 just seaward of the reef where waves started to break (Figure 23). Decreasing the turbulent length scale l from the default value of 0.094 to 0.07 m improved the match at Gauge 5, although this still underestimated the wave height on the reef. Overall, in terms of wave heights on the reef, the best match between model and data was obtained with the bottom friction coefficient $C_f = 50$.

The significant wave height distribution represents only an overall view of the wave energy transformation across the reef (Figures 20 to 23). The variation seen in the wave height does not describe how the wave energy is redistributed in the frequency domain as a result of nonlinear wave-wave interactions. Thus, it is also necessary to compare the spectral densities of the measured and predicted surface elevation time-histories. Spectral densities are obtained with a Fourier transform technique. Figures 24 to 27 show comparison of the measured and predicted wave spectra at Gauges 3, 5, 7, and 9 for the GUAM01, GUAM02, GUAM12, and GUAM13 tests. The corresponding time series are plotted in Figures 28 to 31.

Because of nonlinear wave-wave interactions occurring in the shallow water depth (Nwogu 1993a and b), the wave spectra on the reef at Gauges 7 and 9 consist entirely of low-frequency motions. In addition, the existing wave energy at the incident wave frequencies is dissipated at these gauges. The BOUSS-1D reproduces the nonlinear energy transfer to the low frequency modes, but there are some salient differences between the measured and predicted wave spectra in Figures 24 to 27.

There is a distinct low-frequency peak at $f \approx 0.064$ Hz in the measured spectra at Gauge 5 just offshore of the reef. The model did not predict this peak, which is also present in the measured spectra at Gauges 4 and 6 (not shown), but this peak does not appear at the other gauge locations. It might result from a local phenomenon (either numerical or physical)

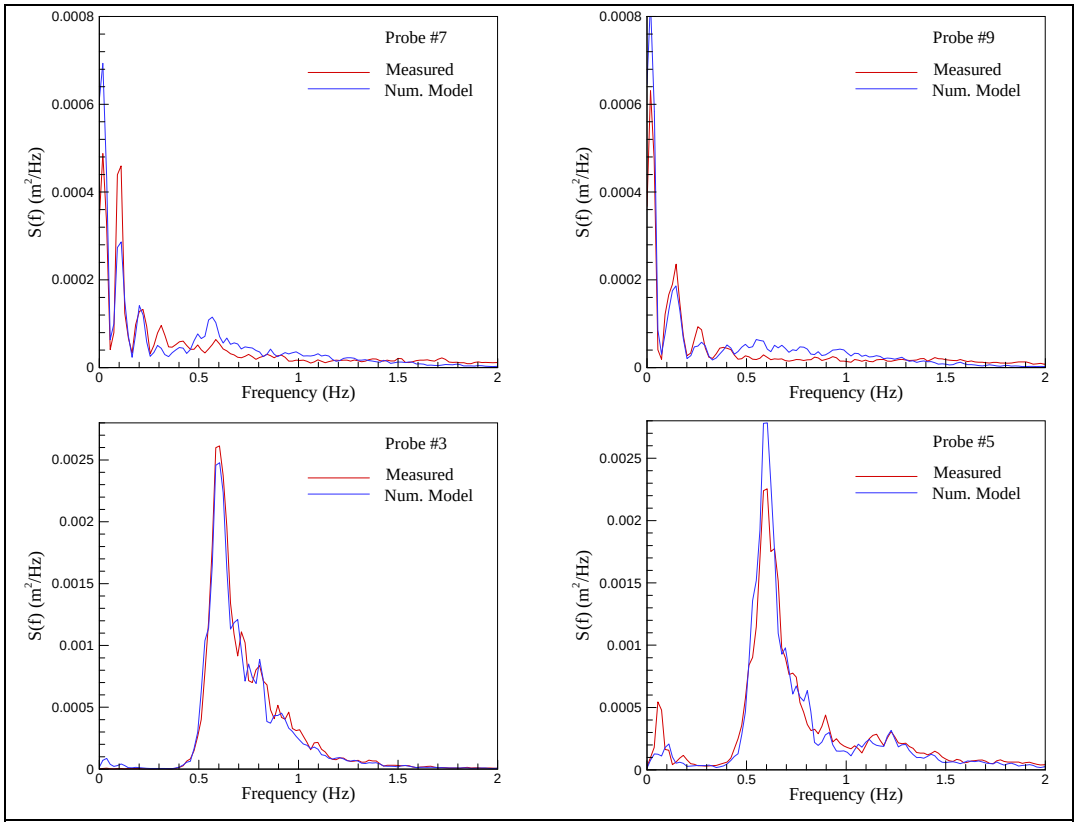

Figure 24. Measured and calculated wave spectra for GUAM01 test.

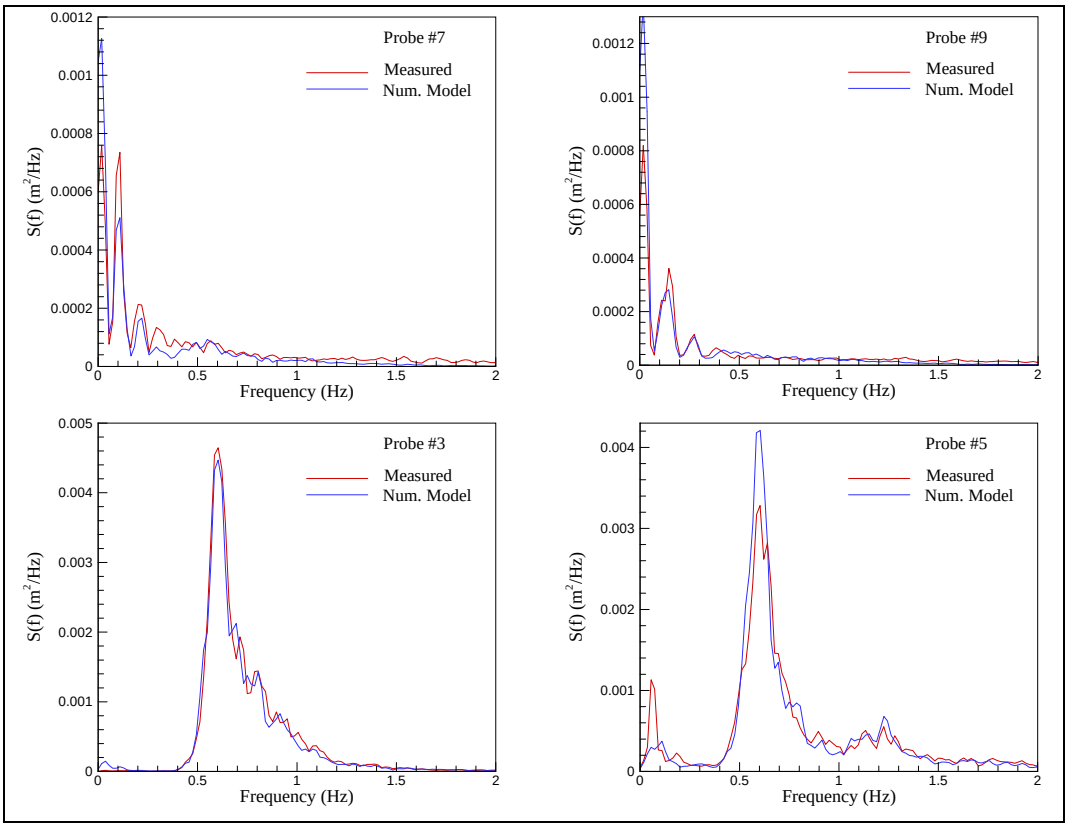

Figure 25. Measured and calculated wave spectra for GUAM02 test.

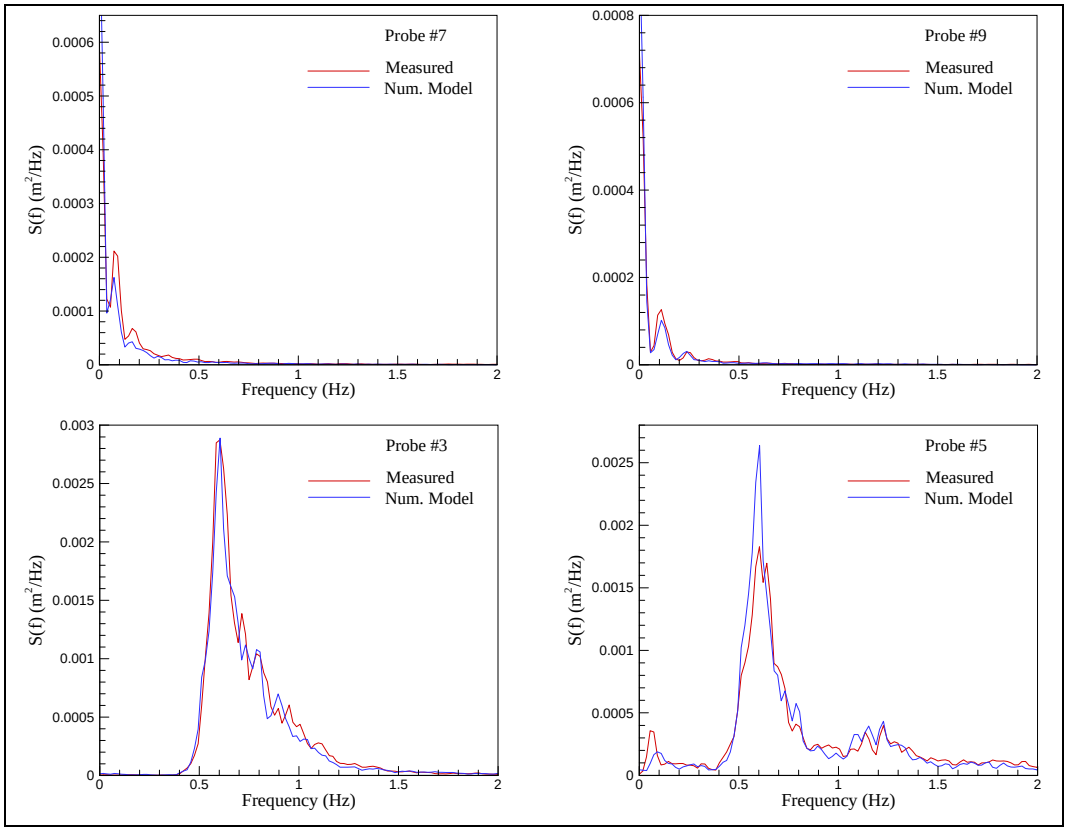

Figure 26. Measured and calculated wave spectra for GUAM12 test.

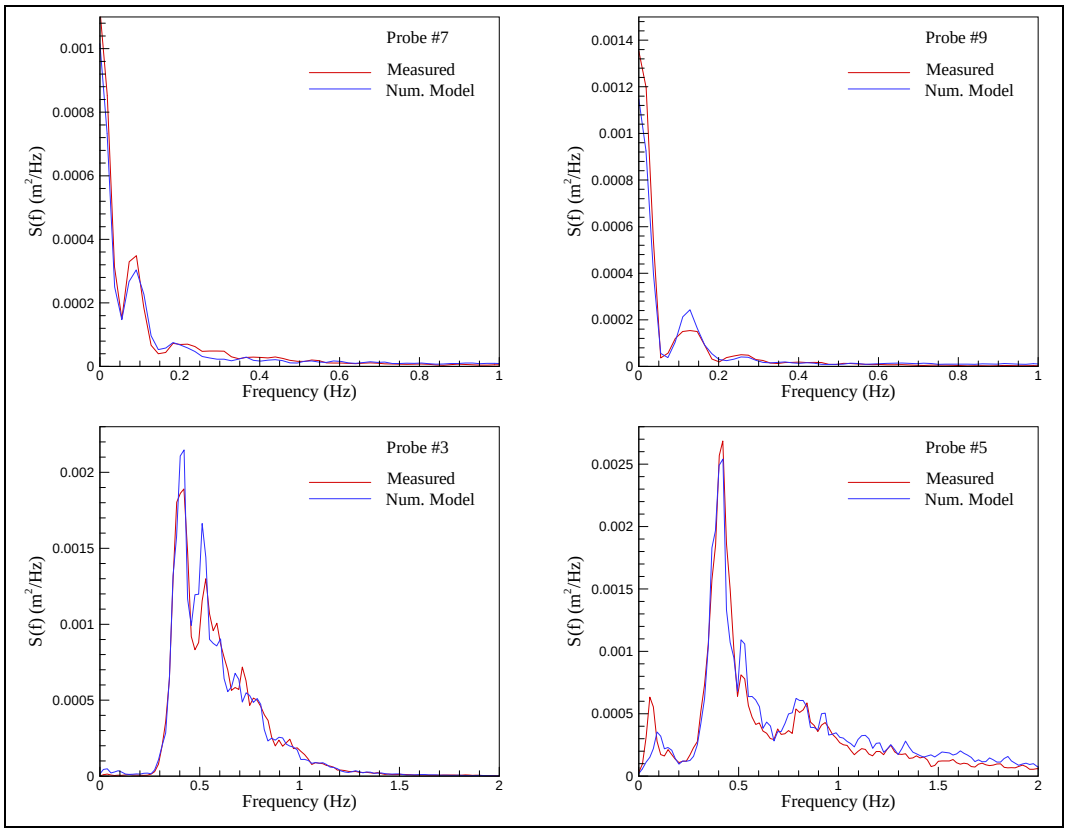

Figure 27. Measured and calculated wave spectra for GUAM13 test.

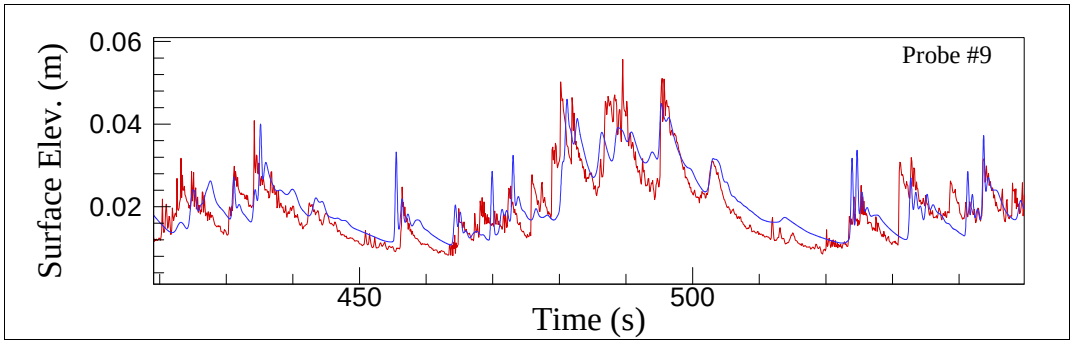

Figure 28. Close-up view of measured and calculated surface elevation time series at Gauge 9 for GUAM12 test; measured (red), numerical model output (blue).

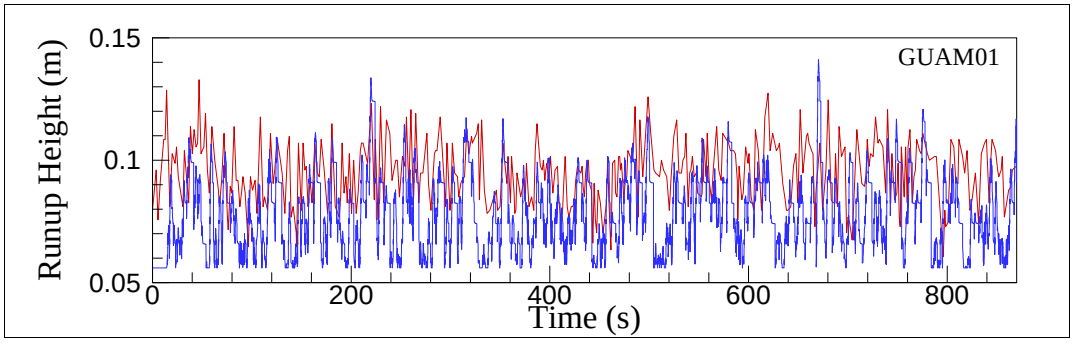

Figure 29. Comparison of measured (red) and predicted (blue) runup height for GUAM01 test.

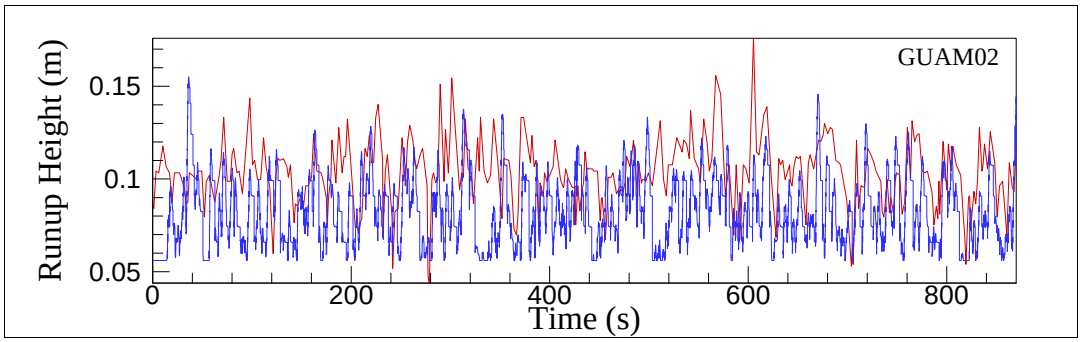

Figure 30. Comparison of measured (red) and predicted (blue) runup height for GUAM02 test.

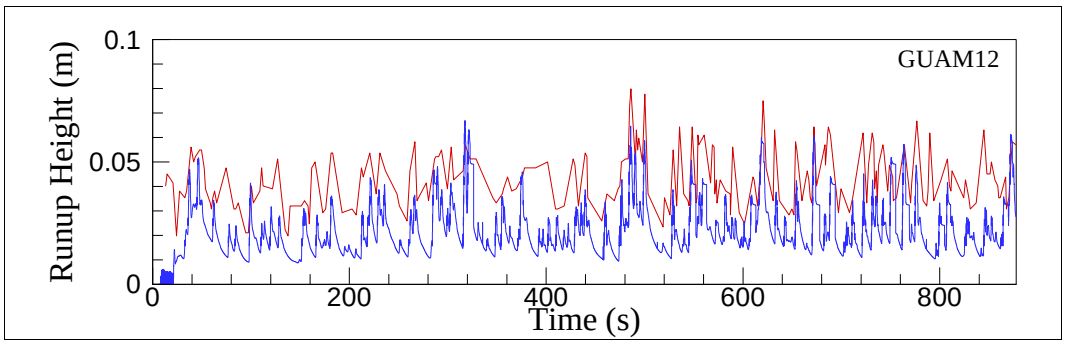

Figure 31. Comparison of measured (red) and predicted (blue) runup height for GUAM12 test.

associated with the discontinuity in slope between the sloping and flat-reef sections, or perhaps a local standing wave created by the steep slope on the reef face, which was not simulated in the Boussinesq model. The origin of the peak at $f \approx 0.064$ Hz in the measured spectra cannot be conclusively identified at this time. Calculated wave spectra from BOUSS-1D on the reef (Gauges 7 and 9) had several distinct low-frequency oscillation peaks as in the measured spectra. The numerical model tended to overestimate the lowest peak and underestimate the second peak. Overall, comparisons are quite good.

The measured and calculated water surface elevation time series are shown in Figure 28 for Gauge 9 for the GUAM12 test. The low-frequency (infragravity) waves are evident in the close-up view of the measured and predicted surface elevation time series. Numerical model results (in blue) provide further evidence that the BOUSS-1D is able to reproduce the overall trends in the data including the phasing of the low-frequency motions on the reef.

The low-frequency motions are more visible for the lower water level tests (GUAM12 and GUAM13) where the flat reef section was initially dry. Clearly, the numerical model is able to describe the nonlinear steepening and highly asymmetric profile of post-breaking waves on the shallow reef. However, there are some discrepancies in the detailed time-domain characteristics between the measurements and model results. Given that the wave breaking process is parameterized in the Boussinesq model, the model may not capture fine details of post-breaking waves on a wave-by-wave basis. The BOUSS-1D breaking criterion is based on the ratio of the water particle velocity at the crest to the phase velocity. The phase velocity is computed using linear theory and the average zero-crossing period of the incident wave train. This might lead to an early or later initiation of breaking for individual waves, depending on the individual wave frequencies and amplitudes.

Finally, it is also necessary to consider a comparison between measured and calculated wave runup time series. The runup heights in these experiments were measured with capacitance-wire wave gauges. Unfortunately, the output from the gauges could not be directly compared to the numerical model predictions because unexplained jumps appeared in the data. Runup peak elevations were alternatively obtained by digitizing video recordings of the runup process. For four tests (GUAM01, GUAM02,

GUAM12 and GUAM13), the time histories of the runup peaks obtained from the video data are compared in Figures 29 to 32 to the model-predicted runup elevations (relative to reef).

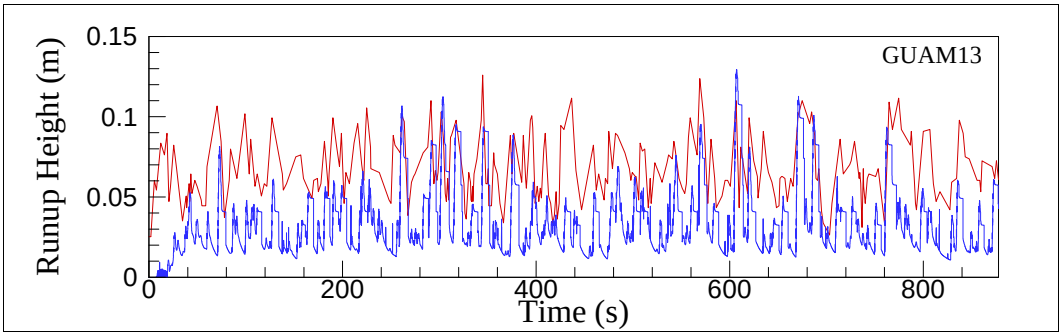

Figure 32. Comparison of measured (red) and predicted (blue) runup height for GUAM13 test.

The digitized video data in Figures 29 to 32 provide an envelope of the runup peaks while the numerical model predicts a detailed time history of the runup elevation during both the runup and rundown. In general, the magnitudes of the model-predicted runup peaks are similar to the observed peaks (Figures 29 to 32), although there are discrepancies in the details of the fluctuations. Samples of maximum runup heights are given in Table 5 only for four test conditions for illustration purposes. BOUSS-1D calculated runup values are in good agreement with data.

Table 5. Summary of measured and calculated maximum runup heights.

Test ID	Maximum Runup Height (m)		% Difference
	Measured	Calculated	
GUAM01	0.13	0.14	8
GUAM02	0.18	0.16	11
GUAM12	0.08	0.07	13
GUAM13	0.13	0.13	0

University of Michigan reef experiments

Demirbilek and Nwogu (2007) and Demirbilek et al. (2007b) describe details of laboratory experiments conducted in the 35-m-long by 0.7-m-wide wind-wave flume at the University of Michigan (UM). The cross section of the reef face is identical to that used by Seelig (1983) and Thompson (2005), but has two different features. First, the fringing reef profile in the UM study has a flat reef top instead of the barrier reef profile with a lagoon used by Seelig (1983). Second, the reef top used in the UM

experiments is wider (~384-m-wide prototype scale) than that used in the Thompson experiments (~175-m-wide prototype scale). The 1:64 scale model of a 2D fringing reef with the reef profile connecting to a sloping beach is shown in Figure 33. The reef-beach system consists of a 1:12 sloping beach preceded by a 4.8-m-wide reef flat and a composite slope reef face. The experiments were designed to provide insight into the physics of nonlinear wave transformation and runup on fringing reef profiles with known bottom friction properties.

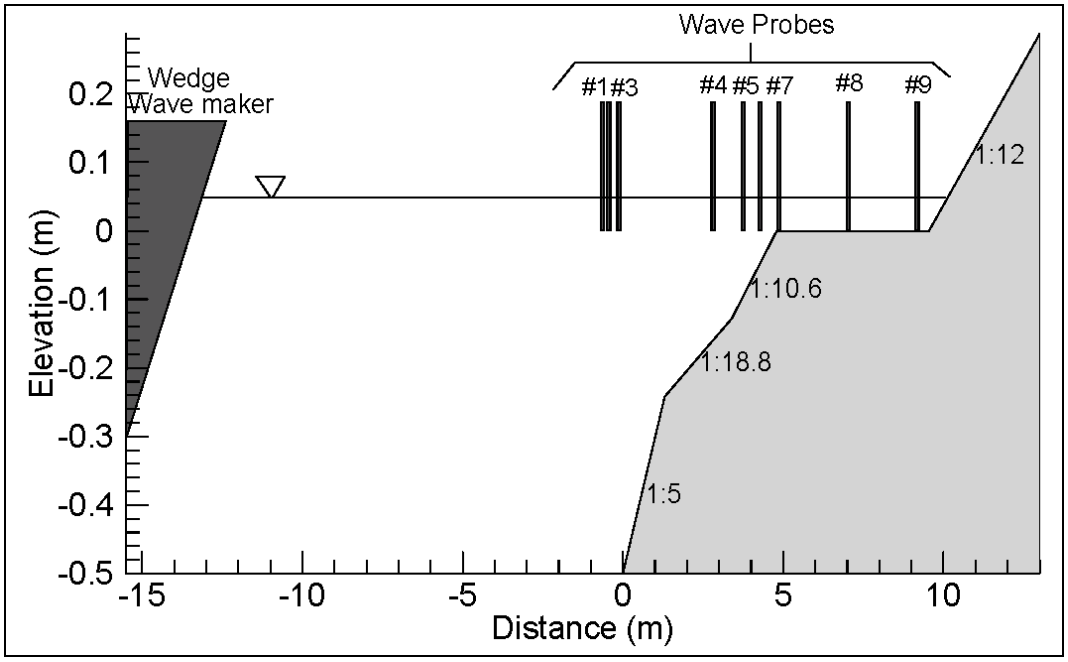

Figure 33. Experimental setup for UM fringing reef experiments.

Three capacitance-wire wave gauges were installed in the constant-depth section of the flume to quantify the amount of wave reflection, and six additional capacitance-wire wave gauges measured the wave conditions across the reef profile (Figure 33). Wave runup on the beach was recorded by a 1-m-long capacitance-wire runup gauge installed on the beach face. The wave gauge locations in Table 6 are relative to the toe of the reef slope. The reef-top gauges were designed to provide accurate measurements of wave setup over the reef flat.

Table 6. Wave gauge coordinates for UM experiments.

Sensor	*X* (cm)
Gauge 1	-0.69
Gauge 2	-0.49
Gauge 3	-0.18
Gauge 4	2.75
Gauge 5	3.68
Gauge 6	4.23
Gauge 7	4.84
Gauge 8	6.99
Gauge 9	9.13

The laboratory scale test conditions summarized in Table 7 consisted of irregular sea states, with significant wave heights ranging from 3 to 8.5 cm, spectral peak periods from 1 to 2.5 sec, water levels (h_r) above the reef flat from 0 to 5.1 cm (or 50 to 55 cm above the flume floor), and no wind. The 50-cm water depth (h_r = 0 cm) corresponds to an initially dry reef flat, similar to conditions when a reef flat is exposed at low tide. Additional information about these experiments is provided by Demirbilek and Nwogu (2007) and Demirbilek et al. (2007b).

Table 7. Summary of test conditions for UM experiments.

Test ID	H_s (cm)	T_p (sec)	h_r (cm)
Test 20	6.1	1.25	5.1
Test 17	7.8	1.50	5.1
Test 21	8.2	1.75	5.1
Test 18	8.5	2.00	5.1
Test 46	5.9	1.25	3.1
Test 48	7.5	1.50	3.1
Test 57	7.7	1.75	3.1
Test 58	8.5	2.00	3.1
Test 27	5.5	1.25	1.6
Test 29	7.1	1.50	1.6
Test 30	7.6	1.75	1.6
Test 31	8.5	2.00	1.6
Test 36	6.8	1.50	0.0
Test 37	7.6	1.75	0.0
Test 38	8.4	2.00	0.0

A majority of the waves in these experiments broke on the reef face in a plunging manner. After breaking, waves reformed as bores and propagated across the reef flats to the beach. Undular and fully turbulent bores were observed over the flat reef section. The sensitivity of the BOUSS-1D predictions to the parameterization of the wave breaking process was investigated for one of the test conditions (Test 29) with H_s = 7.1 cm, T_p = 1.5 sec, and h_r = 1.6 cm. The measured water surface elevation time series at Gauge 1 was used to derive velocity boundary conditions for the numerical model. The simulations were performed with Δx = 5 cm, Δt = 0.01 sec, and default values for other parameters ($l = H_s$, C_f = 30, $\delta_{min} = H_s/1000$, C_v = 0.2). Based on the conclusions from an earlier sensitivity study in 2005 and 2006 by Thompson and Ward (see Appendix B), three wave breaking formulations have since been implemented in the BOUSS-1D and these were investigated: the Spilling Breaking Formulation (SBF), the Plunging Breaking Formulation (PBF)-1, and a modified plunging breaking formulation using the phase velocity instead of the orbital velocity at the wave crest (PBF-2). Demirbilek and Nwogu (2007) provide details of these formulations and a comparison of model results to data. Only a summary of the results is given here.

To illustrate how sensitive the wave setup over the reef is to the spatial distribution of the eddy viscosity, Figure 34 shows the comparison of the measured and calculated significant wave height and mean water level variation across the reef for the different wave breaking formulations. In this case, the SBF and the new PBF-1 predicted fairly similar post-breaking wave heights. The SBF formulation slightly underestimates the wave setup over the reef flat, and the PBF-2 formulation, in which the breaking factor is advected with the wave celerity, overpredicts the wave height near the break point and thus produces a higher setup over the reef. The decrease seen in the mean water level offshore of the reef in the measurements was caused by the use of a closed laboratory flume for the experiments with no replenishment of water pumped onto the reef.

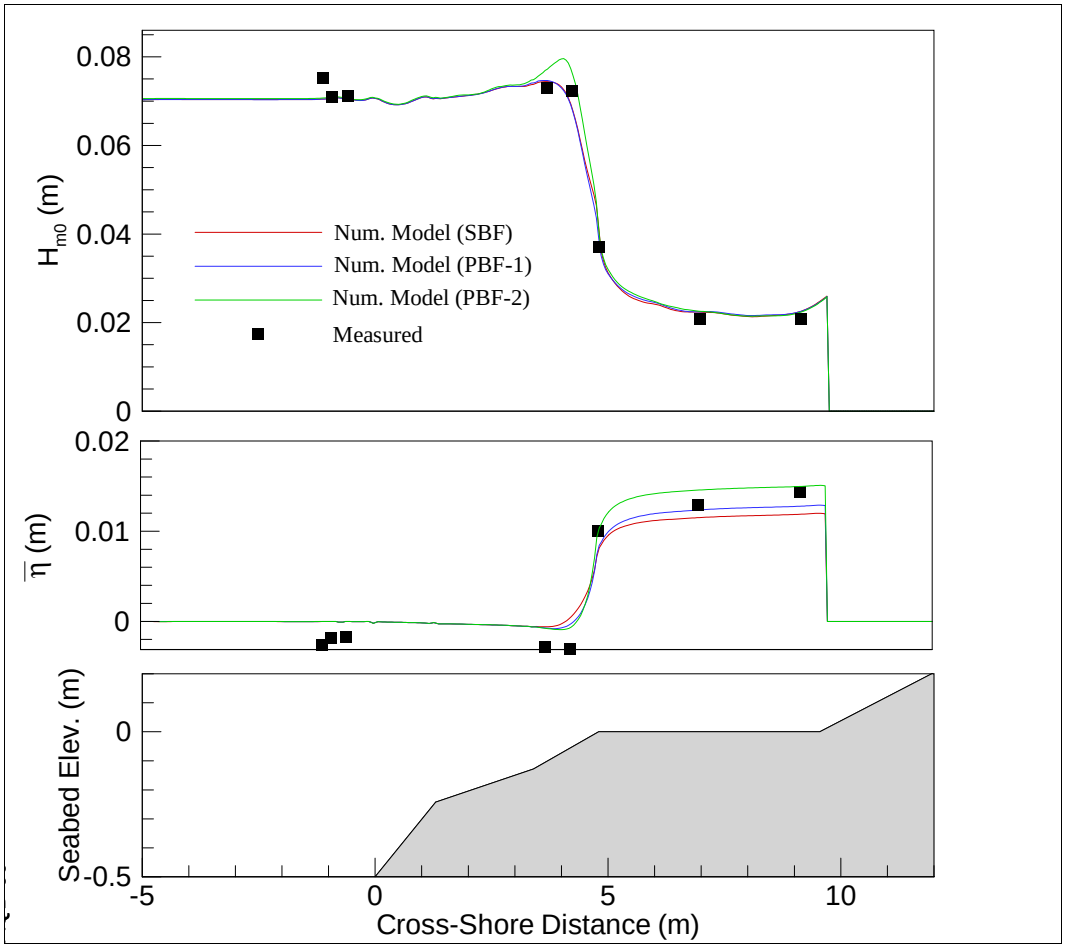

Figure 34. Measured and predicted significant wave height and mean water level variation for different wave breaking formulations for Test 29.

The sensitivity of the model predictions to the parameterized bottom friction coefficient is further investigated in the present study. Four tests with $H_s \approx 0.07$ m, $T_p = 1.5$ sec are performed for this purpose at different

water levels: h_r = 0.0 cm (Test 36), h_r = 1.6 cm (Test 29), h_r = 3.1 cm (Test 48), and h_r = 5.1 m (Test 17). Figures 35 to 38 are plots of the measured and predicted significant wave height and mean water level variations across the reef for two friction coefficients (C_f = 30 and C_f = 24). Good comparison between model-data is obtained for wave height and water level change over the reef.

Figures 35 to 38 also show that the use of C_f = 24 led to better matches of the post-breaking wave height for the lower water level cases (h_r = 0.0 and 1.6 cm) but not the higher water cases (h_r = 3.1 and 5.1 cm). This suggests the need to use a depth-dependent value of the bottom friction coefficient (e.g., Manning's type) for waves propagating over shallow reefs. Over shallow reef flats, larger water depths (h_r) support larger wave heights which produce larger bottom velocities, and therefore, C_f should be larger for higher water levels. One simple way to incorporate a depth-dependent bottom friction coefficient in the Boussinesq model is to use the Manning formulation where the friction coefficient varies as the sixth root of the water depth. A spatially-varying friction coefficient feature will be available in the next version of the Boussinesq model.

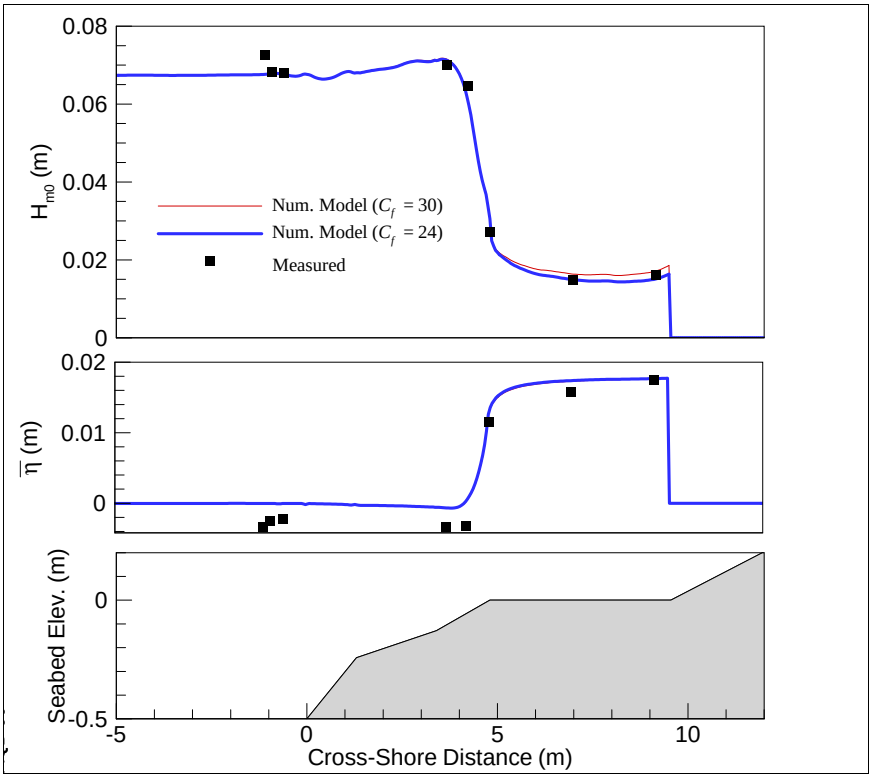

Figure 35. Measured and predicted significant wave height and mean water level variation for Test 36 (H_s = 0.07 m, T_p = 1.5 sec, h_r = 0.0 cm).

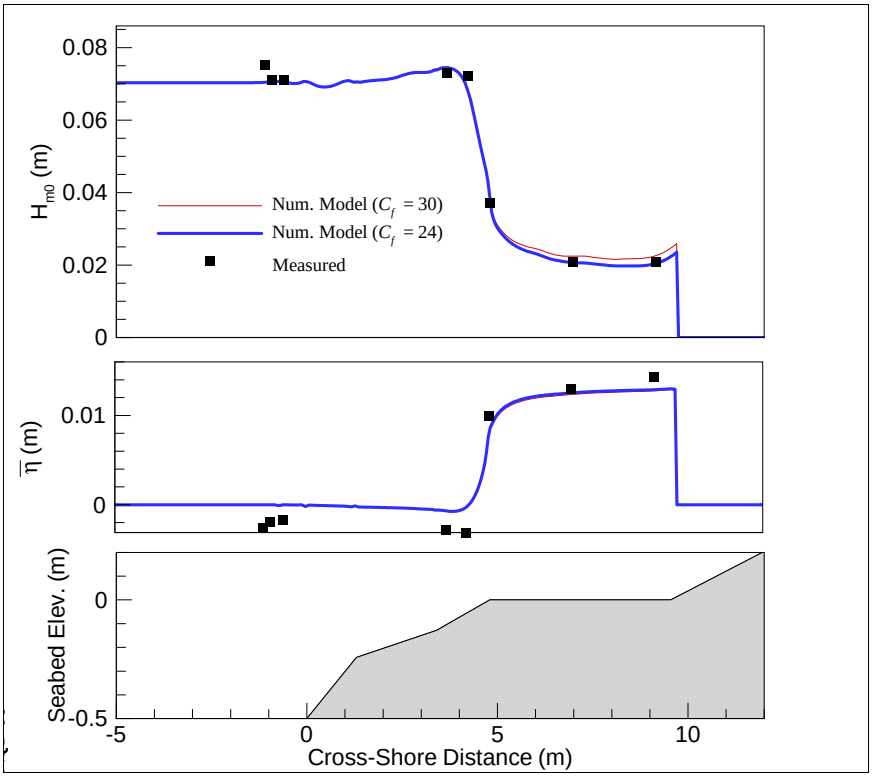

Figure 36. Measured and predicted significant wave height and mean water level variation for Test 29 (H_s = 0.07 m, T_p = 1.5 sec, h_r = 1.6 cm).

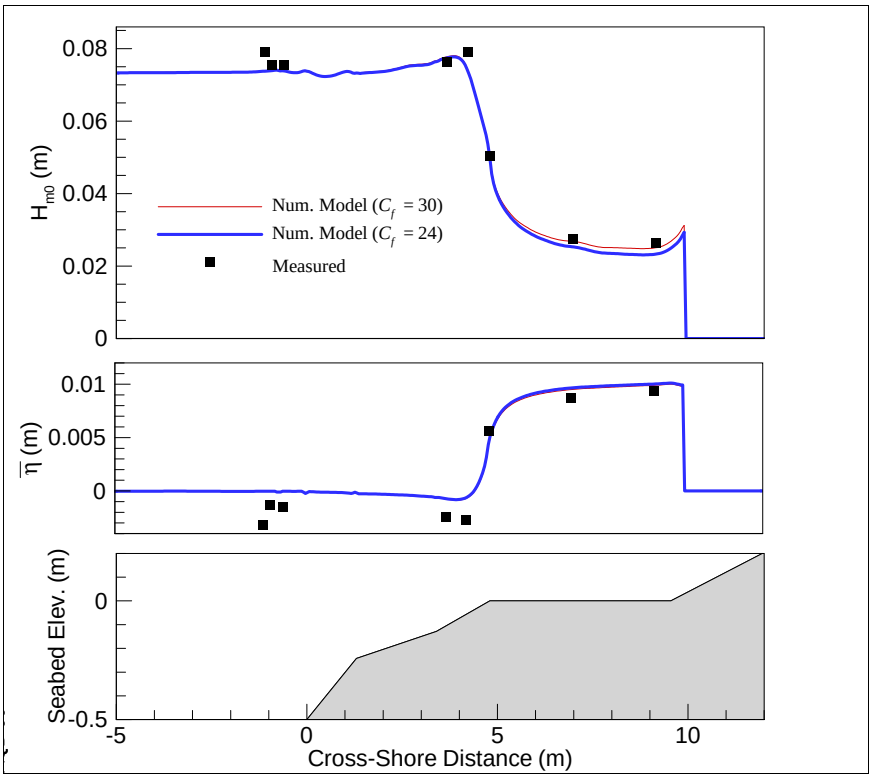

Figure 37. Measured and predicted significant wave height and mean water level variation for Test 48 (H_s = 0.075 m, T_p = 1.5 sec, h_r = 3.1 cm).

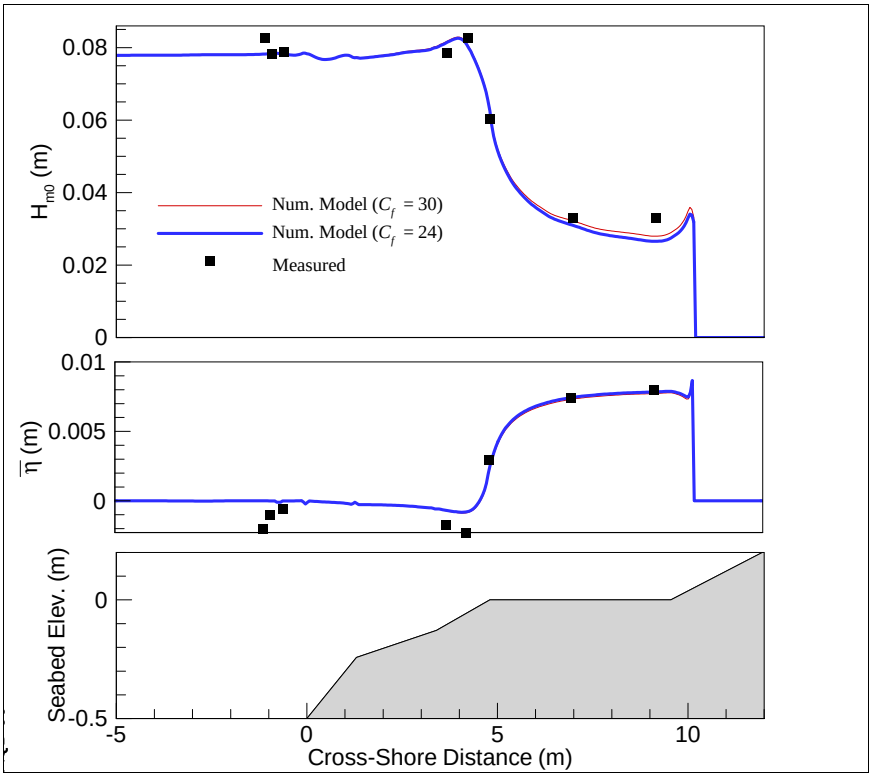

Figure 38. Measured and predicted significant wave height and mean water level variation for Test 17 (H_s = 0.08 m, T_p = 1.5 sec, h_r = 5.1 cm).

Because of the extensive set of the time series measurements (including runup on the beach) available from the UM experiments, it is possible to investigate the wave spectra evolution over the reef-beach system. By Fourier transforming an 800-sec segment of the measured/predicted time series from t = 100 sec to t = 900 sec, Demirbilek and Nwogu (2007) obtained the spectral densities of the water surface elevation time histories. Figures 39-42 show plots of the measured, and predicted wave spectra at an offshore gauge (Gauge 3), a reef-face gauge (Gauge 6), the mid-reef flat gauge (Gauge 8), and the nearshore gauge (Gauge 9) for Test 36 (h_r = 0.0 cm), Test 29 (h_r = 1.6 cm), Test 48 (h_r = 3.1 cm), and Test 17 (h_r = 5.1 cm), respectively. The corresponding time series are plotted in Figures 43-46.

The nonlinear transformation of the wave energy spectra from incident-wave frequencies in deep water to infragravity (low-frequency) motions over the reef flat is evident from the wave spectra plots in Figures 39-42. Overall, BOUSS-1D reproduces the nonlinear energy transfer to the low-frequency modes, with some cases slightly underpredicted while a few others are overpredicted. For example, while the wave spectra at the

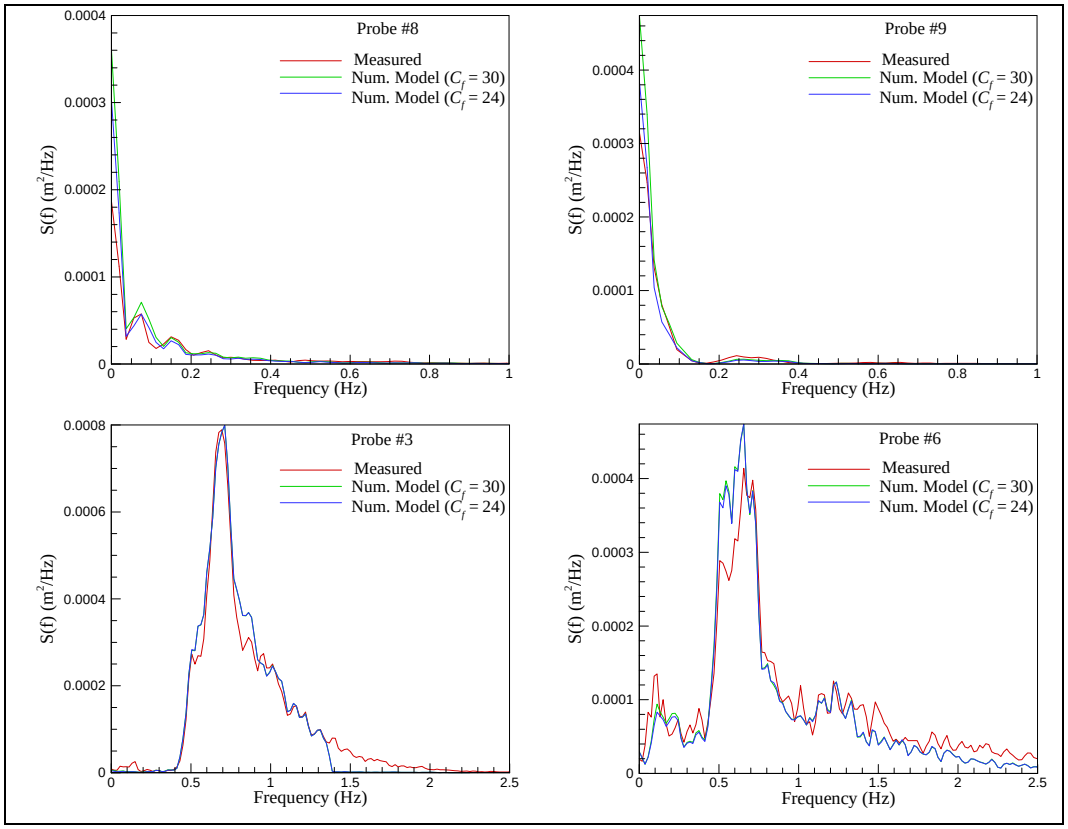

Figure 39. Measured and predicted wave spectra for Test 36.

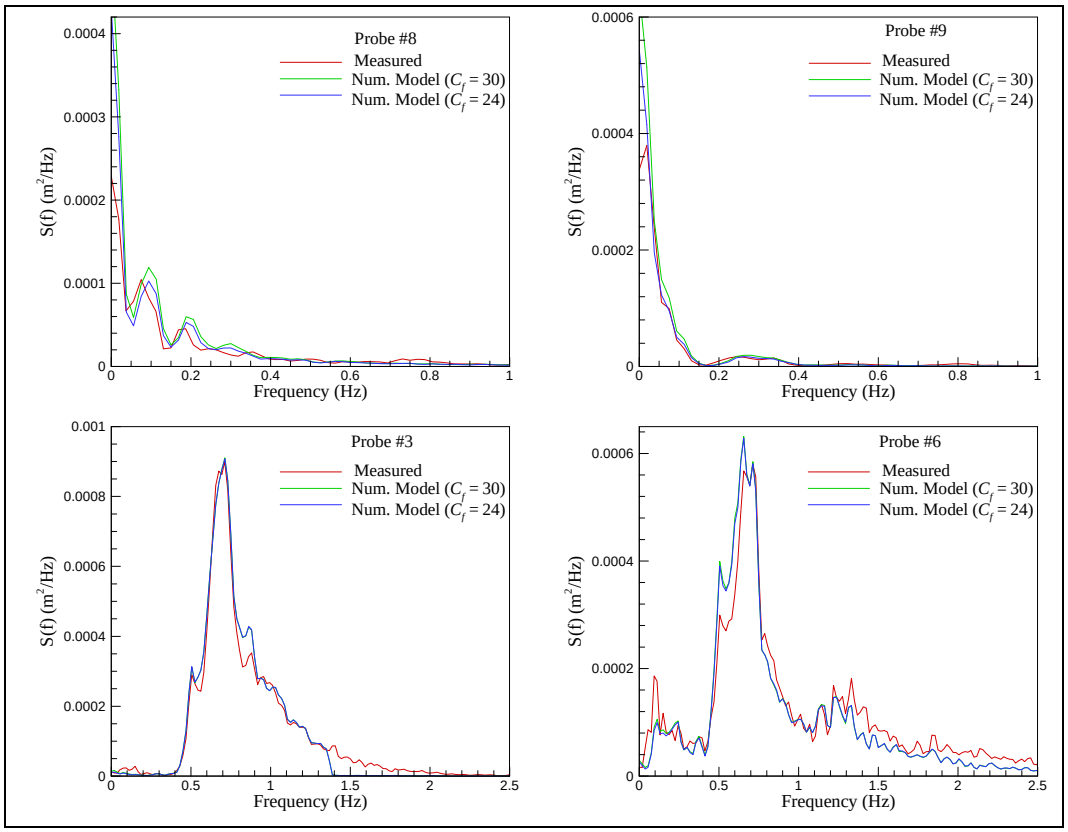

Figure 40. Measured and predicted wave spectra for Test 29.

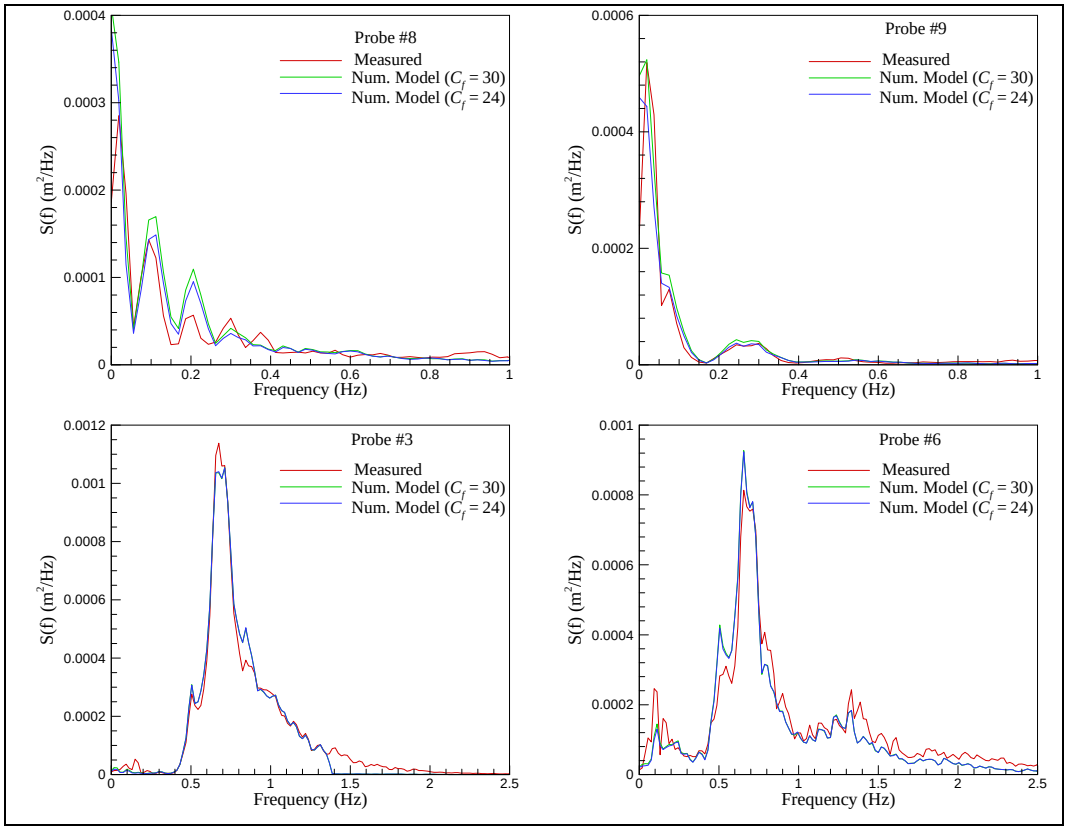

Figure 41. Measured and predicted wave spectra for Test 48.

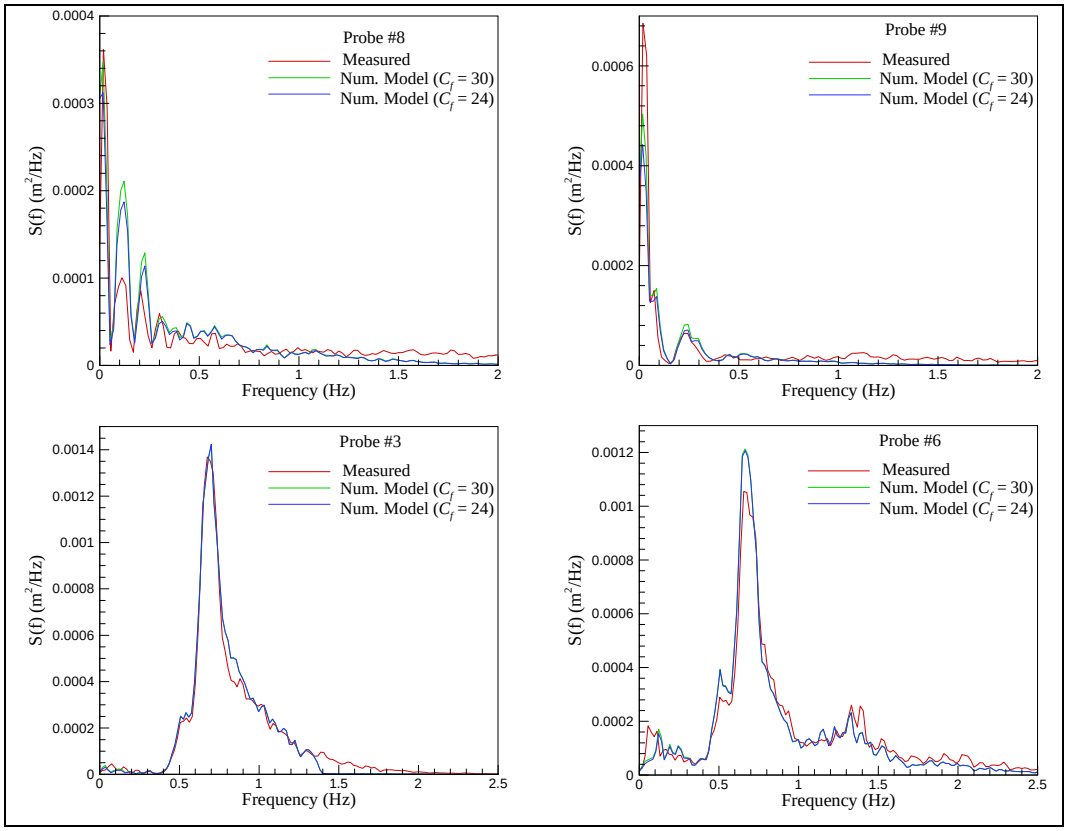

Figure 42. Measured and predicted wave spectra for Test 17.

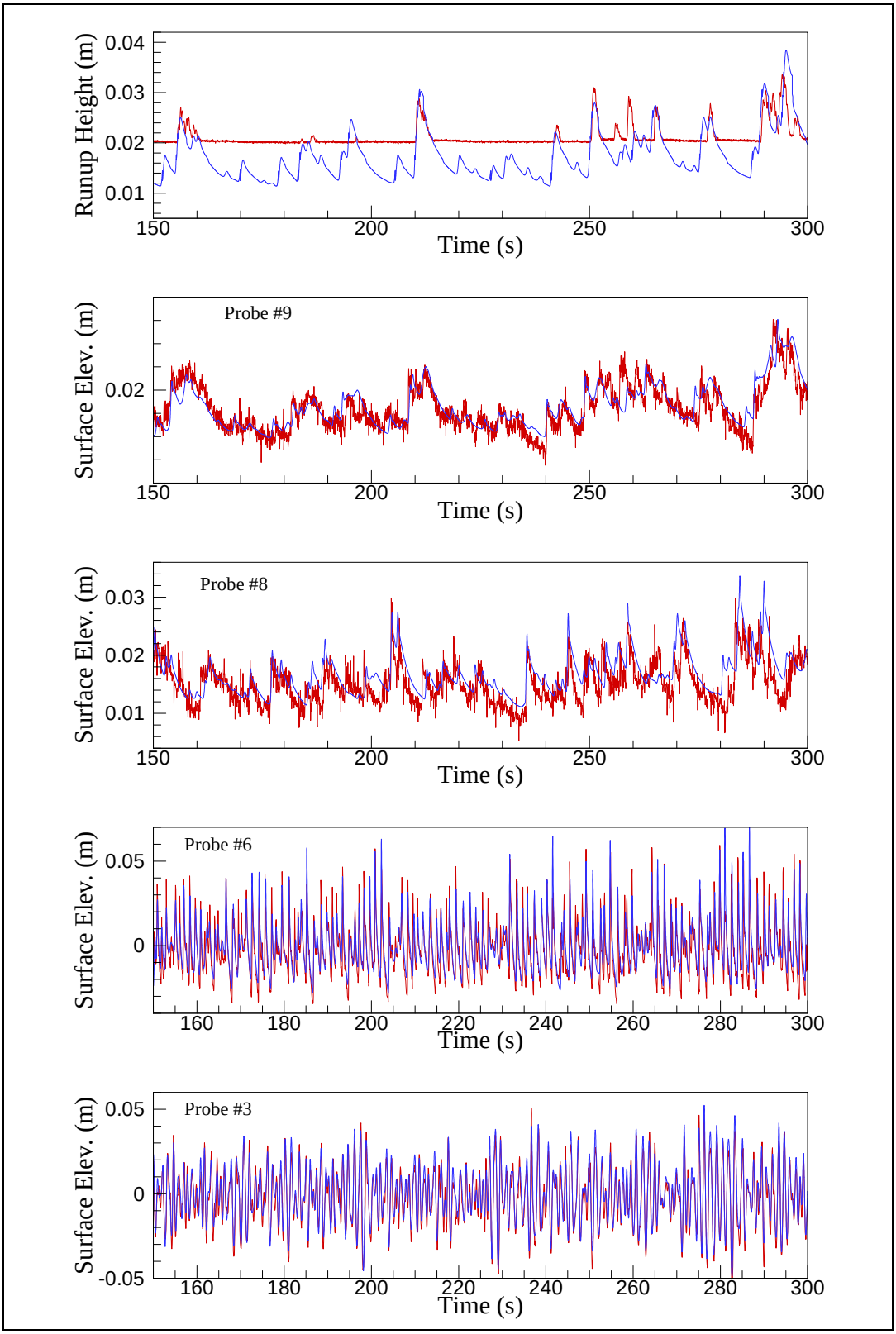

Figure 43. Measured and predicted surface elevation time series for Test 36; measured (red), numerical model prediction (blue).

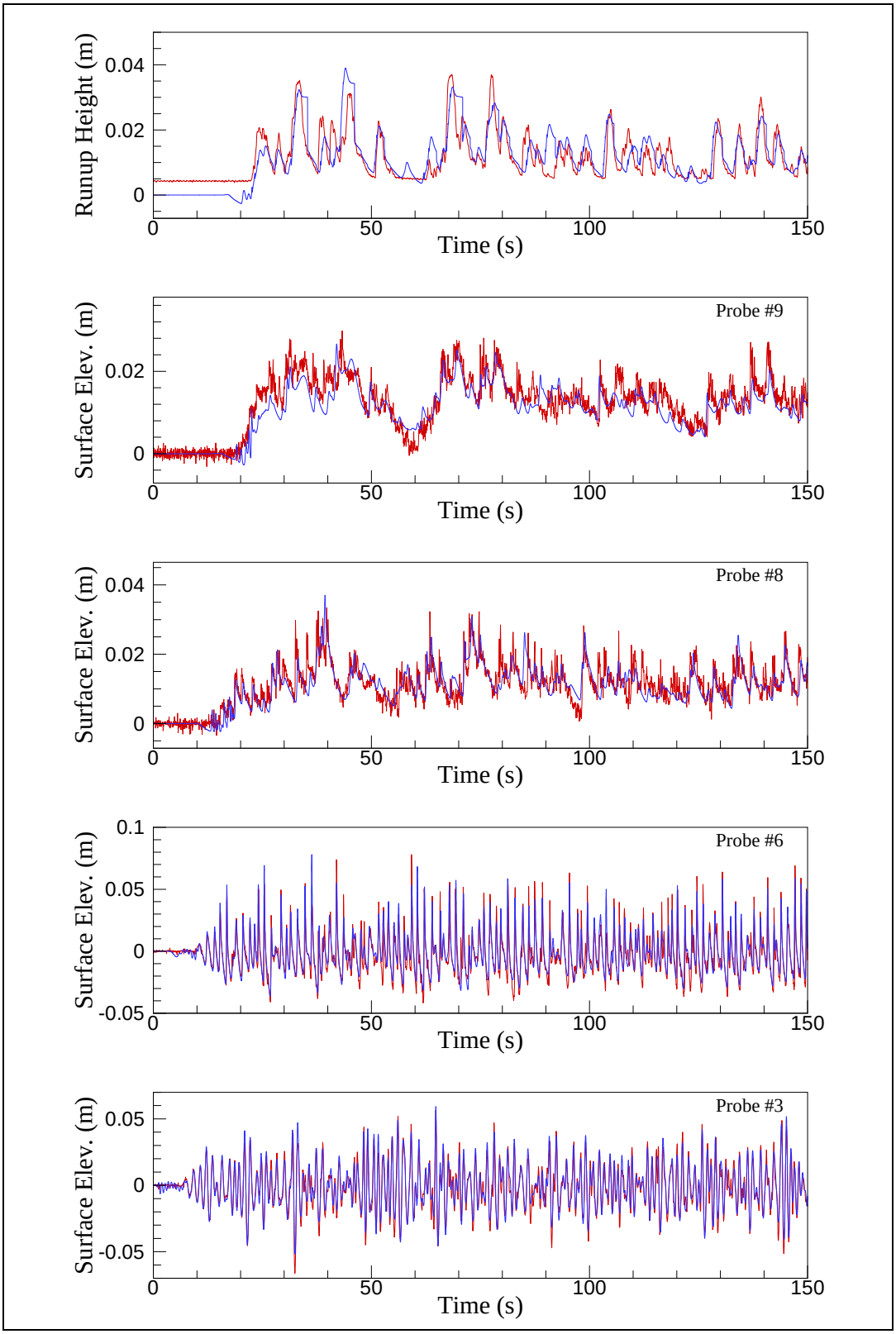

Figure 44. Measured and predicted surface elevation time series for Test 29; measured (red), numerical model prediction (blue).

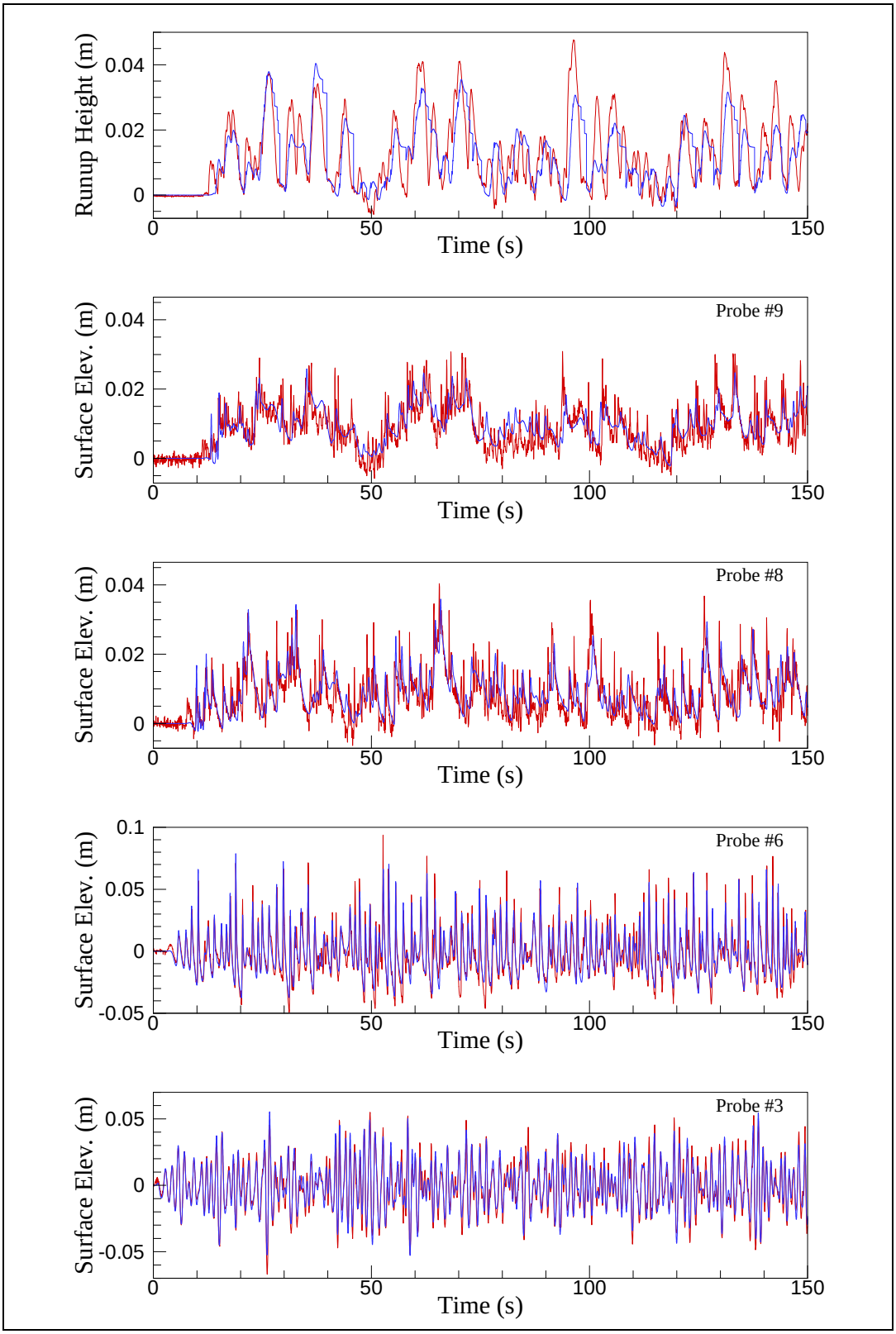

Figure 45. Measured and predicted surface elevation time series for Test 48; measured (red), numerical model prediction (blue).

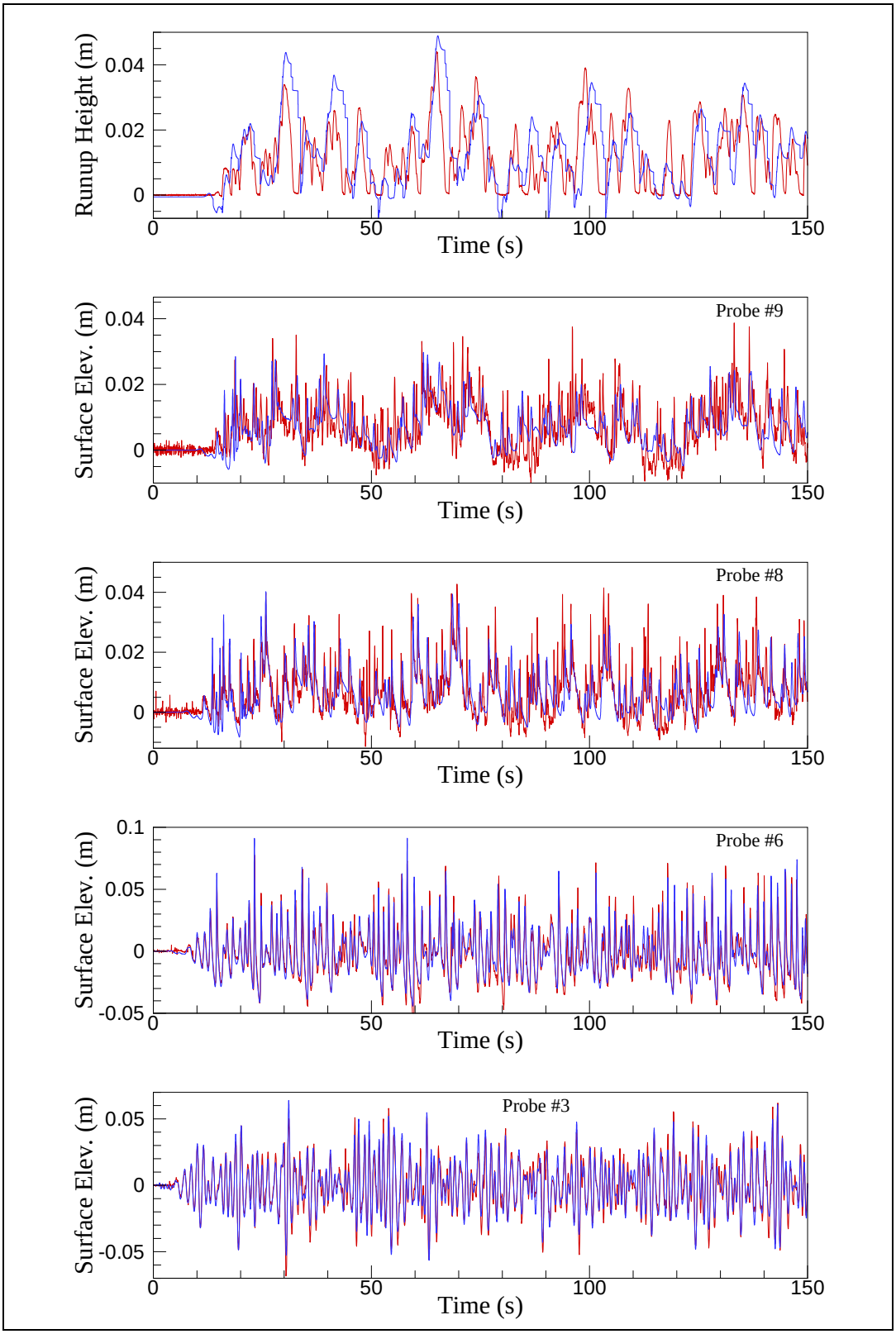

Figure 46. Measured and predicted surface elevation time series for Test 17; measured (red), numerical model prediction (blue).

nearshore gauge (Gauge 9) have a predominant low-frequency peak, the wave spectra at the mid-reef flat gauge (Gauge 8) has multiple low-frequency peaks. The nonlinear evolution of the spectrum over the reef flat at a finer frequency resolution (0.0025 Hz) is depicted in Figure 47. This shows a detailed view of the spectra for Test 48 at Gauges 7, 8, and 9, in the low-frequency region (0-0.25 Hz). At Gauges 8 and 9, located at the middle and end of the reef flat, respectively, the spectral peak periods are approximately 35 sec. However, there is very little energy at the 35-sec period (0.029 Hz) at the reef crest gauge (Gauge 7). This peak period corresponds to the first reef oscillation mode of a trapped wave with a wavelength approximately equal to four times the width of the reef flat (Demirbilek and Nwogu 2007). Because the first mode would have a node at the reef crest and an antinode at the shoreline, the trapped waves are amplified at the shoreline relative to the incident energy at the reef crest. For further discussion of this topic, see Demirbilek and Nwogu (2007).

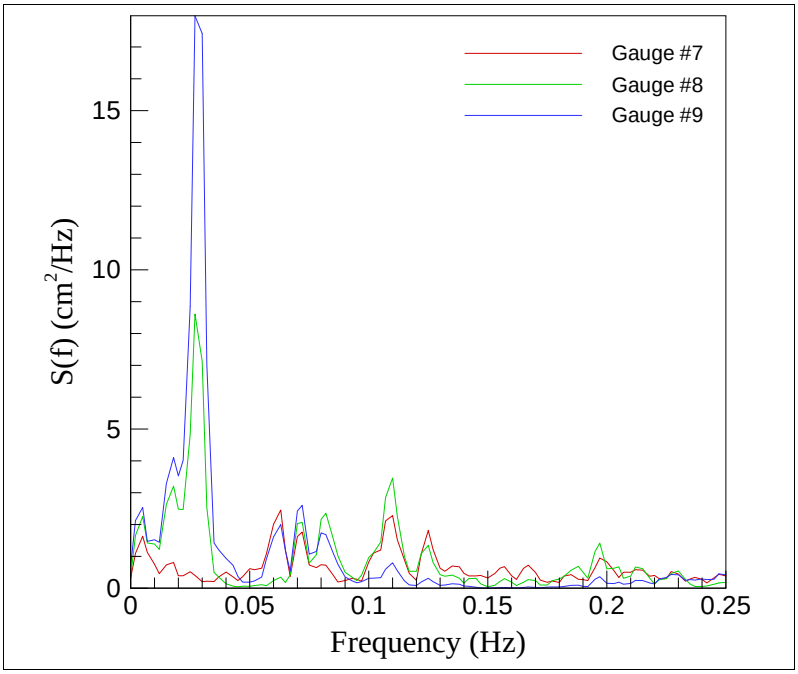

Figure 47. Low-frequency wave energy spectra for Test 48 at Gauges 7-9.

Combined with the results shown for wave spectra evolution plots, the water surface elevation time-series plots in Figures 43 to 46 lend more support to the fact that the BOUSS-1D model reproduces the overall trends of the nonlinear wave transformation in the UM experiments. Capabilities of the Boussinesq-type wave model have been highlighted by Demirbilek and Nwogu (2007) for representing both time- and frequency-domain nonlinear wave transformations over the reefs. They demonstrated the

model's ability to represent wave profile steepening, highly asymmetric wave profiles developing for post-breaking waves in relatively shallow depths, amplitude and phasing of the low-frequency motions on the reef flats, etc. Figures 39 through 47 show clearly that the low-frequency motions are stronger at the lower water level tests. The model wave runup predictions are also reasonable. As has been pointed out by Demirbilek and Nwogu (2007), the model cannot capture the fine details of post-breaking waves on a wave-by-wave basis because the wave breaking process is parameterized in the Boussinesq model.

The variations in the measured and predicted wave setup results are shown in Figure 48. A good comparison between the BOUSS-1D predictions and data is obtained at the reef top gauges, in the zone of primary interest. The 50-percent difference lines are shown to bracket the range of variability in the results. Measured and calculated wave setup at Gauges 4, 5, and 6 are essentially zero, and the model underpredicts wave setup at Gauge 7 for some tests. The best agreement is obtained for Gauges 8 and 9, the last two gauges which are closest to the sloping beach. The differences between the model and data for Gauges 8 and 9 are generally less than 15 percent.

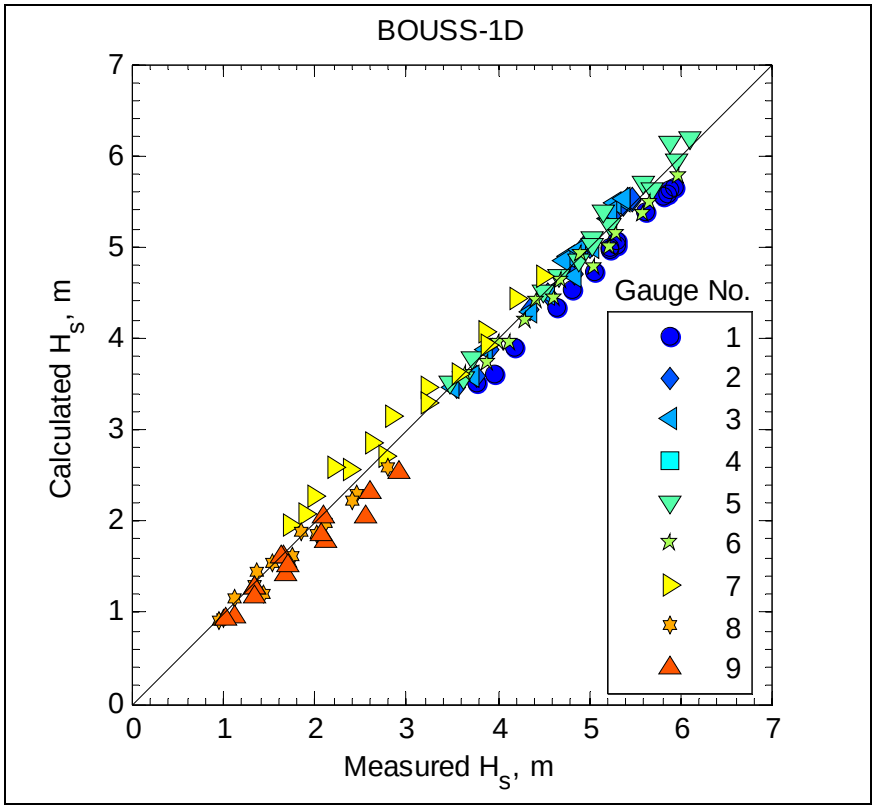

Figure 48. Comparison of calculated and measured wave setup for UM experiments.

For the UM experiments, the measured and predicted maximum runup heights are summarized in Table 8. Overall, magnitudes of the model-predicted runup peaks are similar to observed peaks, with an average difference on the order of 10 percent. The measured and predicted wave runup ($R_{2\%}$) values are compared in Figure 49. Agreement between the BOUSS-1D predictions and data is good, with differences less than 10 percent. Demirbilek et al. (2007b) describe the UM experiments, and provide both raw and analyzed data. Demirbilek and Nwogu (2007) provide an in-depth comparison of measured and calculated wave parameters. Interested readers should consult these previous reports for additional information about the UM experiments.

Table 8. Summary of measured and calculated maximum runup heights.

Test ID	Maximum Runup Height (m)		% Difference
	Measured	Predicted	
Test 17	0.055	0.062	13
Test 18	0.084	0.090	6
Test 20	0.032	0.036	13
Test 21	0.072	0.075	4
Test 27	0.030	0.025	-16
Test 29	0.045	0.049	9
Test 30	0.060	0.064	7
Test 31	0.094	0.110	16
Test 36	0.040	0.042	6
Test 37	0.061	0.048	-21
Test 38	0.075	0.071	-5
Test 46	0.043	0.031	-29
Test 48	0.048	0.058	21
Test 57	0.075	0.066	-13
Test 58	0.083	0.083	0

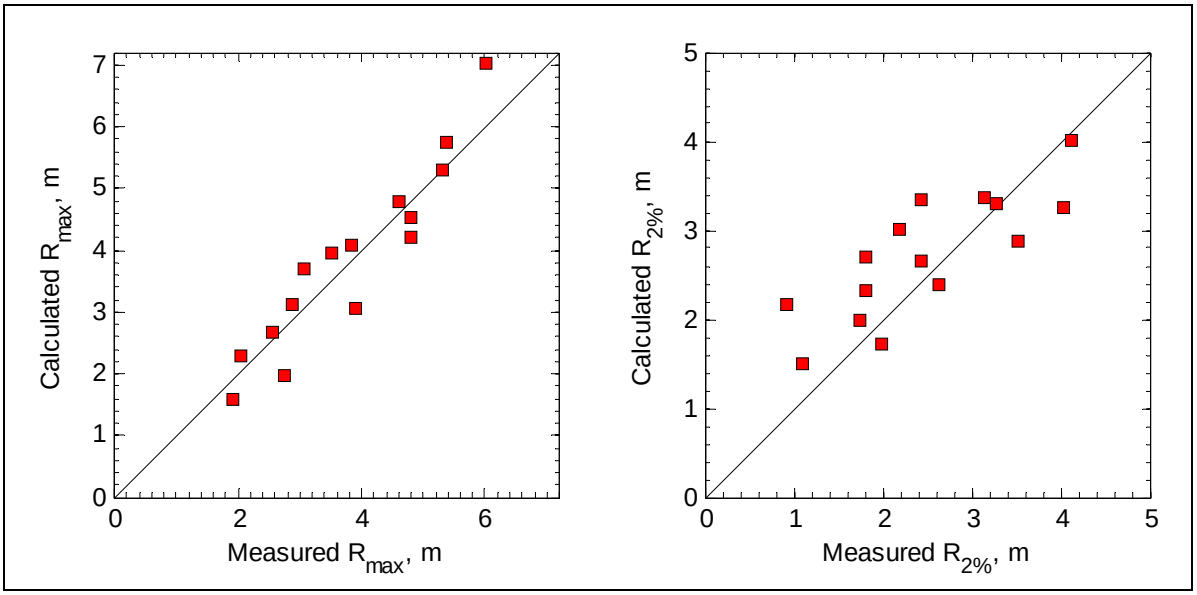

Figure 49. Comparison of calculated and measured wave runup (R_{mas} and $R_{2\%}$) for UM experiments.

4 RBREAK2 Evaluation

Model description

RBREAK2 is a 1D vertically-averaged numerical model for wave runup and overtopping on permeable and impermeable slopes of irregular shape. It is one of a series of numerical models developed by Dr. Nobuhisa Kobayashi and his students at University of Delaware. The original model, IBREAK, was for monochromatic waves; RBREAK was developed for random waves. IBREAK and RBREAK allowed the use of only one friction factor along the bottom. To use the model for cases such as an irregular sandy bottom fronting a riprap revetment, RBREAK was modified to allow the use of multiple friction factors for different reaches of the bathymetry. The modified RBREAK was called RBREAK2. Other models in the series included PBREAK for porous slopes and SBREAK for solitary waves. RBREAK2 is fully described in Kobayashi and Poff (1994).

RBREAK2 allows for the input of multiple slopes defining the bathymetry of both submerged and exposed structures. For exposed structures, the program calculates the oscillating waterline as runup/rundown on the slope, or computes overtopping if the elevation of runup exceeds the height of the slope. Because the model allows spatially-varying bottom friction factors, the model is suitable for both permeable and impermeable slopes, as well as slopes that transition between permeable and impermeable.

The computer program IBREAK, for monochromatic waves, is capable of simulating any incident wave train at the seaward boundary of the computational domain. With irregular waves, however, the irregular waterline oscillations on the slope caused numerical instabilities unless the constant time step was reduced, greatly increasing the computation time. RBREAK included an automated adjustment of the time step so that smaller time steps would be used only where necessary to avoid numerical instabilities. RBREAK2 expands on the automated time step adjustment by requiring a separate program called BEFORR2 to be run before RBREAK2. BEFORR2 determines the appropriate values of the time step size and also adjusts the small water depths used to define the location of the computational waterline if necessary. By running BEFORR2 prior to running RBREAK2, computational instabilities are generally avoided. In the tests described

herein, with the computational domains divided into a grid of between 350 and 1,000 cross-shore grid cells and 150 normalized wave periods, total runtime on a 3.40 GHz Pentium 4 personal computer (PC) was less than 1 min for both BEFORR2 and RBREAK2.

RBREAK2 solves the vertically-integrated equations for mass and cross-shore momentum over a permeable or impermeable slope. A friction factor f is used for a simplified representation of the shear stresses acting on the slope. The governing equations are given (Kobayshi and Poff 1994) as

$$\frac{\partial h}{\partial t} + \frac{\partial}{\partial x}(hu) = 0 \tag{6}$$

$$\frac{\partial}{\partial t}(hu) + \frac{\partial}{\partial x}\left(hu^2\right) = -gh\frac{\partial \eta}{\partial x} - \frac{1}{2}f|u|u \tag{7}$$

where:

h = water depth above impermeable slope
t = time
x = cross-shore coordinate taken to be positive landward with x = 0 at the seaward boundary of the computational domain
u = depth averaged horizontal velocity
g = gravitational acceleration
η = free surface water elevation above SWL.

The numerical model does not explicitly model wave breaking but instead dissipates energy numerically in the flow field. The nonlinear shallow water equations (NLSWE) in conservative form are appropriate for steep waves propagating in a shallow environment. At some point wave breaking occurs and dissipates energy. In the nonlinear shallow water equations, characteristics converge making a shock, like a bore, in the surf. The converging characteristics are, in effect, a computational prediction of the onset of breaking. This convergence is difficult for numerical schemes to resolve and a dissipative shock-capturing scheme is necessary. RBREAK uses an explicit dissipative Lax-Wendroff finite-difference method which uses limited up-winding to dissipate this excess energy. In essence, the method predicts the breaking and then dissipates energy, like breaking.

This equation set and solution scheme are only appropriate for shallow water (such as water depth less than 0.05 times the wavelength). This shallow-water condition typically is met in the surf zone but is violated outside of the surf zone for wind waves. For the case of a wave traveling over a long distance in a water depth deeper than required for depth-limited breaking, unrealistically large dissipation in H_s with travel distance will be predicted.

One advantage of using time-dependent modeling of nearshore wave transformation with the NLSW equations for the island fringing reef application is that nonlinear infragravity wave development over the reef is inherently included. Thus, the time-varying ponding level over the reef and its consequences for setup and runup at shore can be directly extracted from the model.

RBREAK2 is not suited for vertical slopes, but is computationally capable of handling reasonably steep slopes (order of 1:1) by using reduced horizontal spacing in the computational domain. It has the capability of generating monochromatic incident wave trains internally. The waves are generated using the Stokes second-order wave theory (*Shore Protection Manual* 1984) if the Ursell parameter U_r is less than 26, or cnoidal wave theory (Svendsen and Brink-Kjaer 1972) if $U_r \geq 26$. The Ursell parameter is defined as

$$U_r = \frac{HL^2}{d_t} \tag{8}$$

where:

H = wave height at the seaward boundary
L = wavelength determined by linear wave theory
d_t = water depth below SWL at the seaward boundary.

For irregular waves, the incident wave train is generated externally and read into RBREAK2.

Comparison to physical models

RBREAK2 output was compared to data collected from physical models using the same data sets described in Chapter 3 for the BOUSS-1D model.

Because RBREAK2 was developed for beaches and coastal structures in shallow water, the model is not suitable for the deep water off the reefs tested in the physical models. In the application to the four experiments described below, the seaward boundary of the RBREAK2 computational domain in all cases was therefore set at the toe of the reef.

RBREAK2 calculates runup and rundown shoreward of the sea/land interface (shoreline). If the SWL is equal to the elevation of the reef, RBREAK2 assumes the seaward edge of the reef is the shoreline. Therefore, for tests where the SWL was the same as the reef, the water depth was increased for the RBREAK2 runs by 0.1 m prototype. This small increase in depth proved sufficient to ensure the shoreline was established at the shoreward edge of the lagoon.

An option in RBREAK2 stores the variations in the computational depth, defined as elevation of the water surface above the impermeable bottom at a given point, at user-specified nodal points. The collected time series at each nodal point was analyzed in the time domain for significant wave height and mean depth, among other parameters. Subtracting bottom elevation from the mean depth at each nodal point gave the elevation of the mean water surface. Setup and setdown were defined as the positive or negative difference between the mean water surface elevation and the SWL, respectively. In the following sections, significant wave height, setup/setdown, and height of maximum wave runup determined by RBEAK2 are compared to data collected from physical model experiments.

For tests with irregular waves, a wave generation program developed in-house at CHL was used to generate the incident wave train using a Joint North Sea Wave Project (JONSWAP) spectrum. For the monochromatic runs in the experiments by Gourlay (1994), these waves were generated within RBREAK2.

For all runs in RBREAK2 reported herein, the friction factor f in each segment was set at 0.05. All cases were run for 150 waves, defined as a time length of 150 T_p for irregular waves or 150 T for regular waves (Ahrens and Heimbaugh 1988). In all cases, the length of the beach was adjusted if necessary to prevent overtopping.

All runs in RBREAK2 were set at the same scale as the physical models. Results were converted to prototype scale for this report. Details on each

of the physical model experiments were given in Chapter 3. Additional RBREAK2 results are presented in Appendices A through D. For each experiment, a few selected results from RBREAK2 are included in the sections below to describe the model's performance and to compare the numerical model and physical model results.

Hayman Island reef experiments

A cross-section of the Hayman Island experiments conducted by Gourlay (1994) was shown in Figures 3 and 4 in Chapter 3. The experiment included a flat reef in front of a beach with a 1:14 slope, and variable slopes from the seaward face of the reef flat down to the flume bottom. Three water levels were tested, with depths over the reef flat of 3.4, 1.4, and 2.1 m (in prototype). Experiments were conducted with monochromatic waves at a scale of 1:20. The experiments were used to test the stability of a structure on the reef flat; the RBREAK2 runs did not include the structure.

RBREAK2 has the capability of generating its own monochromatic wave trains. The generated waves are either cnoidal or Stokes second-order wave theory. For the test cases used in this study (Table 1 in Chapter 3), RBREAK2 generated cnoidal waves for Test Series 2 with wave periods of 6.75 and 6.66 sec, and for Test Series 3 with wave period of 6.7 sec. RBREAK2 generated Stokes second order waves for the remaining test cases.

The physical model domain was broken into cross-shore grid cells of 0.5 m (0.025 m model), which required 714 grid cells for the water depth of 3.4 m over the reef, 658 grid cells for the depth of 1.4 m over the reef, and 676 grid cells for the depth of 2.1 m over the reef. The number of grid cells varied with water depth because the model uses the shoreline at SWL for the landward edge of the computational domain, and as SWL increases the shoreline moves further back on the beach.

RBREAK2 provides output of water surface elevations at specific nodal points, similar to placing a wave gauge in a physical model. For the RBREAK2 runs reported herein, data were collected at nodes spaced every 10 m (0.5 m model) between x = 0 and the reef flat, and every 5 m (0.25 m model) across the reef flat, for a total of 22 nodes.

Figures 50-52 show results from RBREAK2 compared to the physical model data for three runs with wave periods from 6.7 to 6.8 sec, and

depths over the reef flat of 1.4, 2.1, and 3.4 m, respectively. The apparent trend in the RBREAK2 calculations at lower water levels is a decreasing significant wave height and increasing setup for waves approaching the reef flat. Predicted wave heights are reasonable (within 50 percent of measurements), but the wave setup is overestimated, especially at the higher water levels.

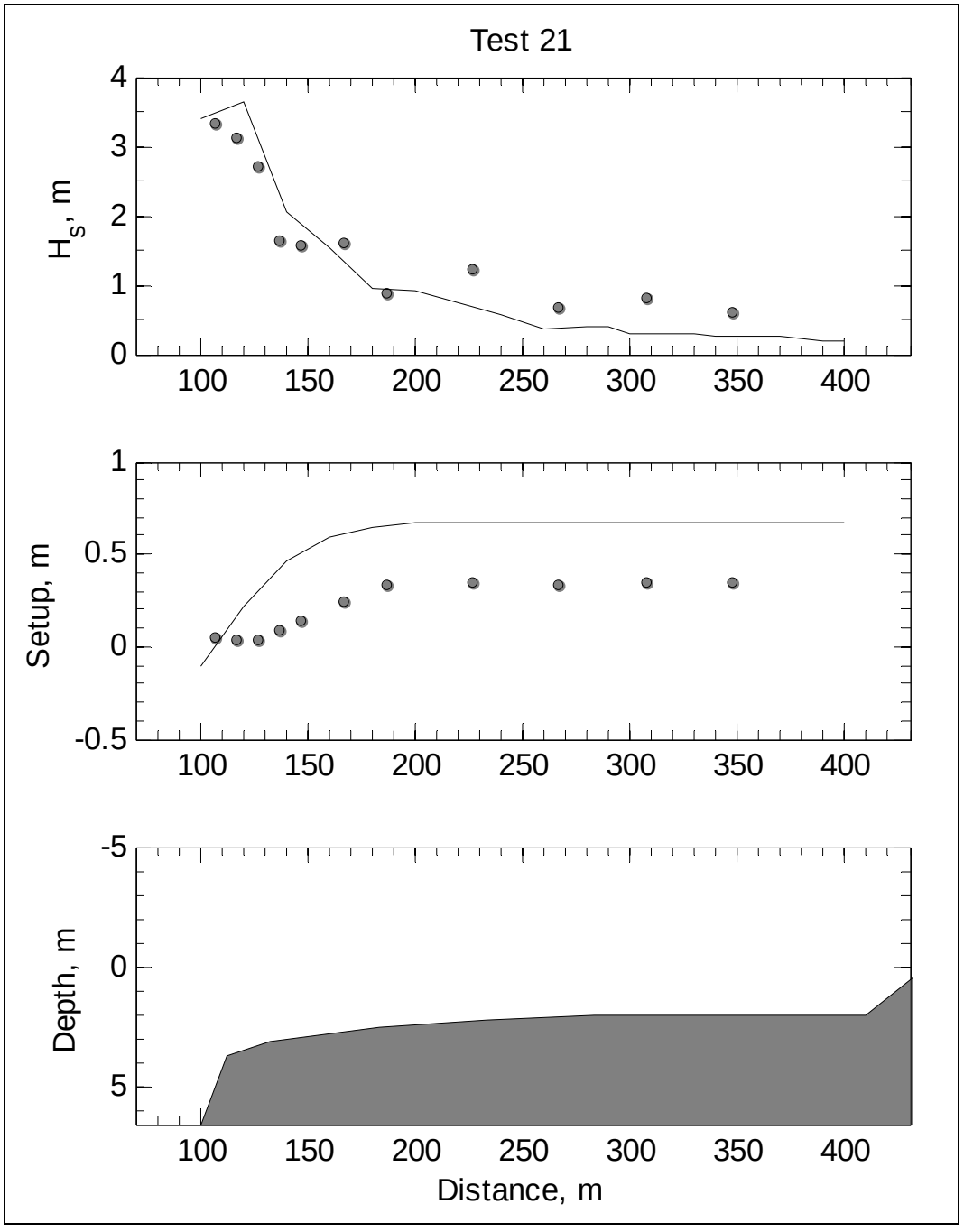

Figure 50. Results from Hayman Island experiments (T = 6.75 sec, SWL = +1.4 m).

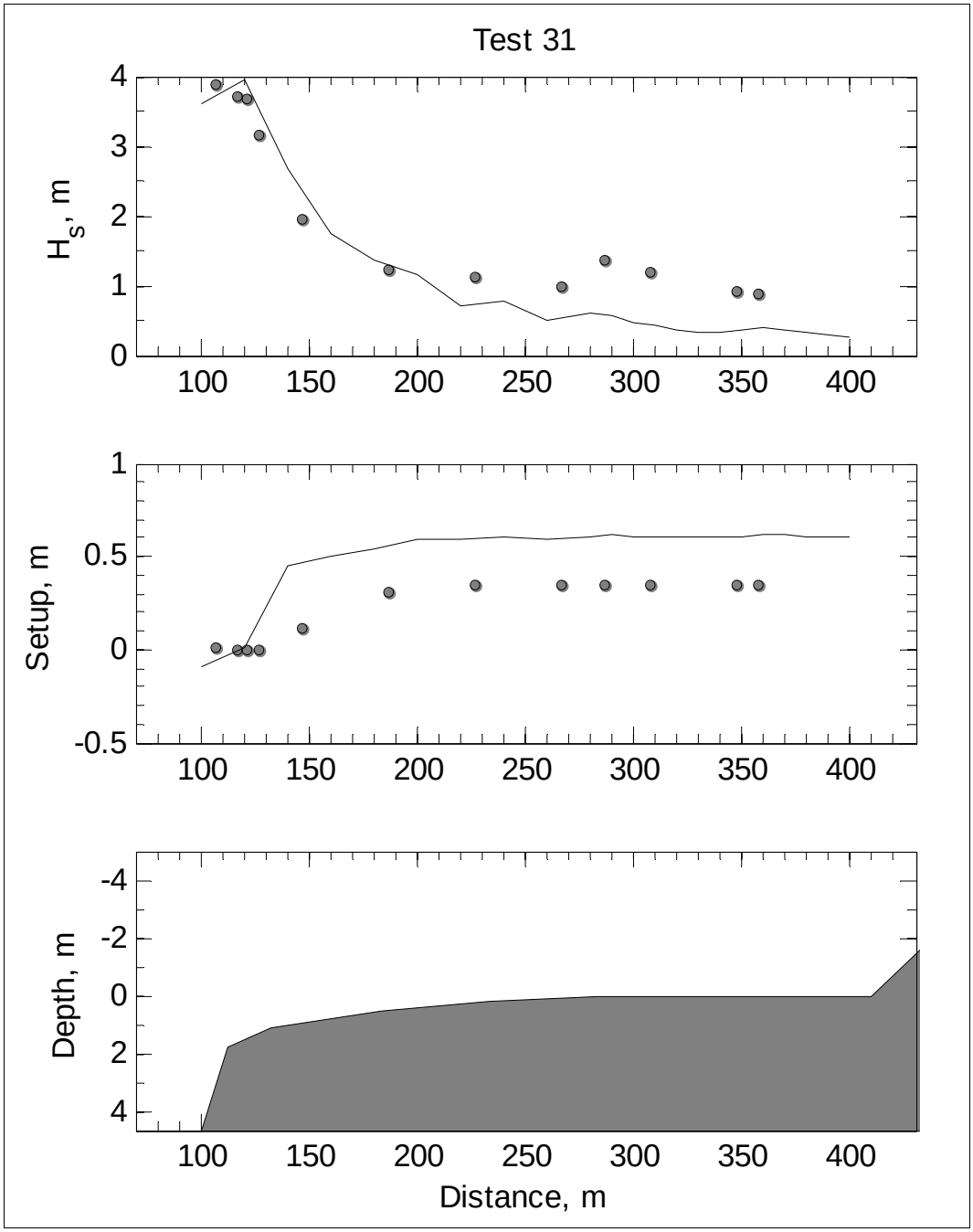

Figure 51. Results from Hayman Island experiments (T = 6.7 sec, SWL = +2.1 m).

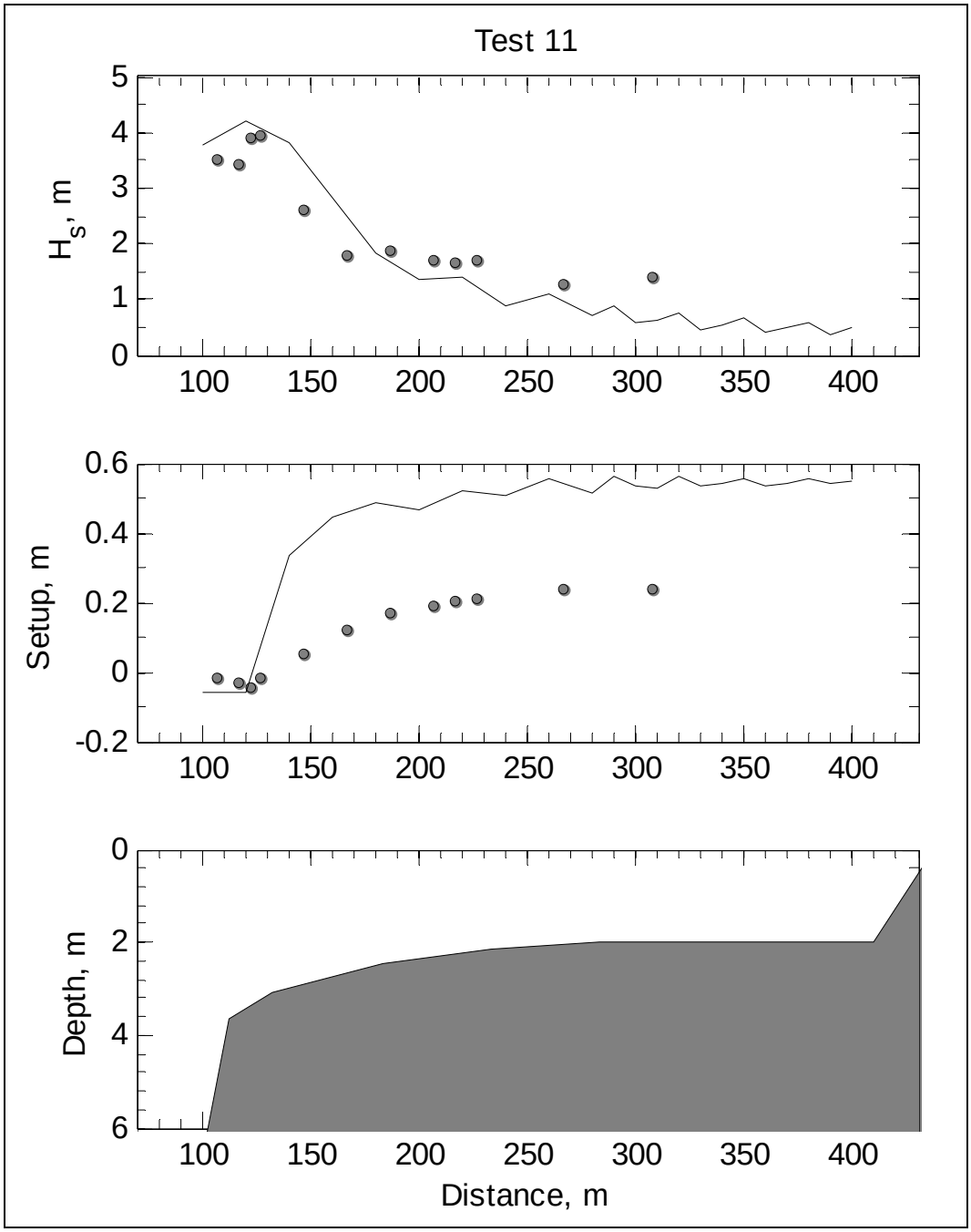

Figure 52. Results from Hayman Island experiments (T = 6.8 sec, SWL = +3.4 m).

Wave periods at each water level ranged from about 3.8 sec to about 6.8 sec. Figure 53 shows results from the lowest water level (+1.4 m) with the shortest wave period (3.8 sec). Comparing Figure 53 with Figure 50 (the lowest water level for the longest wave period), it appears that the heights of the longer wave periods are better predicted as these waves are shoaling across the reef, but wave setup is better predicted for the shorter wave periods. Results for the full set of test cases, presented in

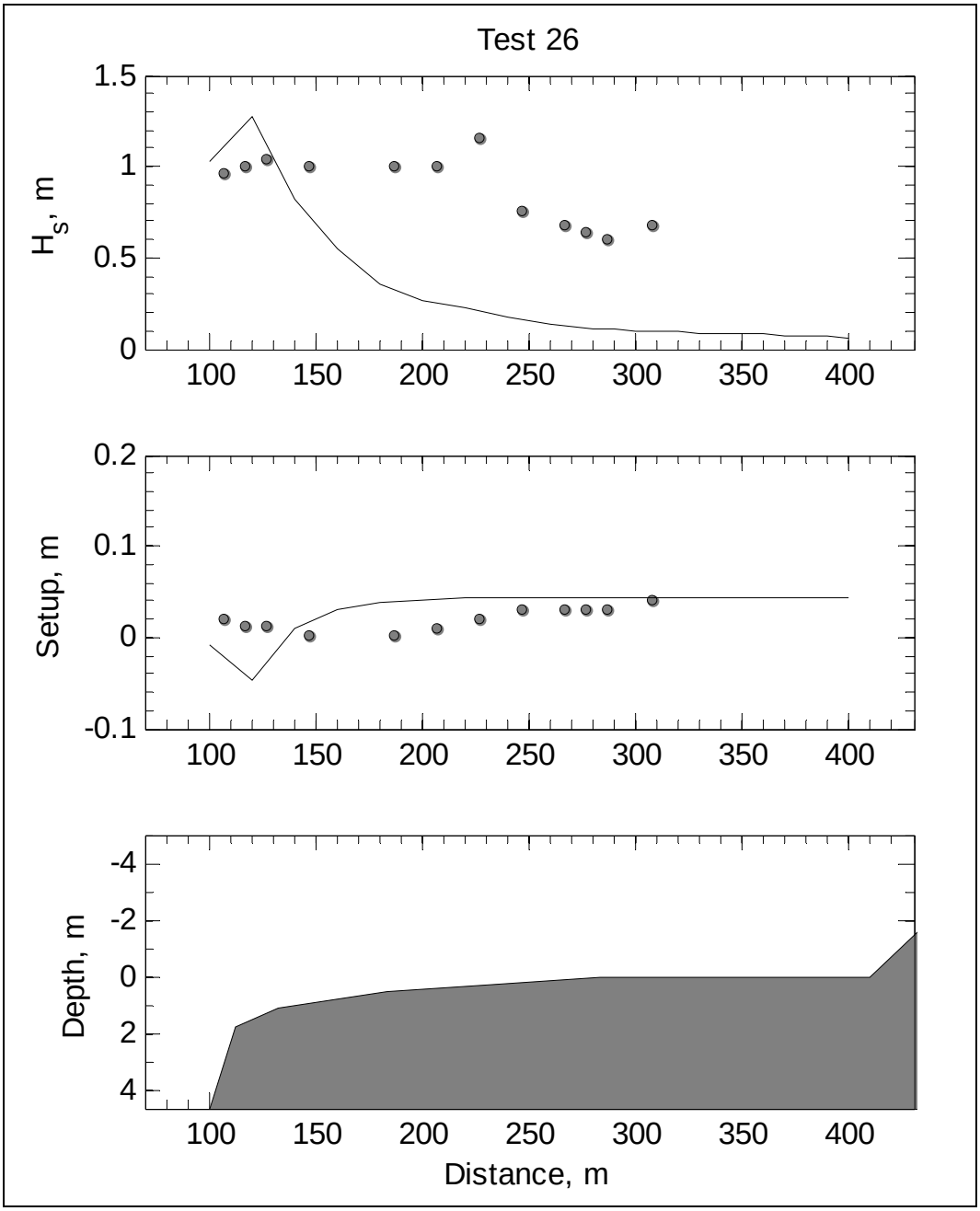

Figure 53. Results from Hayman Island experiments (T = 3.8 sec, SWL = +1.4 m).

Appendix A, show that wave heights are increasingly underpredicted as the wave period becomes shorter. Average wave heights and setup values at each RBREAK2 nodal points are provided in Tables A1 and A2. Table A3 provides the maximum vertical runup calculated from RBREAK2 for the Hayman Island tests.

Seelig reef experiments

The RBREAK2 model was used to simulate the results obtained from physical model experiments of Seelig (1983) for a fringing reef. As noted in Chapter 3, the reef used in these experiments included a fringing reef seaward of a lagoon. Two water levels were tested, with the water level even at the top of reef crest and a 2-m water level above it (prototype). Tests were conducted both for a narrow (150-m wide) and a wide (525-m wide) lagoon. The lagoon bottom was 2.1 m below the top of the fringing reef. These experiments were conducted at an undistorted linear scale of 1:64. The RBREAK2 model inputs were similarly defined for the 1:64 scaled model dimensions. A cross-section of the reef is shown in Figure 13 of Chapter 3. The range for the test conditions are provided in Table 2 of Chapter 3, and Tables C1, C2 and C3 in Appendix C of this report provide values of parameters used in this numerical modeling study.

A minimal depth over the reef of the 10 cm prototype (d_r = 0.1 m) was required in RBREAK2 so that the model would consider the reef as a submerged structure instead of being exposed. This was necessary for RBREAK2 to treat the slope on the shoreward side of the lagoon as the shoreline. If the depth over the reef were set to 0.0 m, the reef would not be submerged, RBREAK2 would assume the reef as an exposed shoreline, and the lagoon would be dry at the start of numerical runs.

The experimental structure was constructed of roughened concrete and did not include the irregularities and channels typical of natural reef formations. The natural reef is expected to be more permeable as compared to the reef used in these experiments, and would permit some seaward flow from the lagoon, which will reduce ponding levels. The RBREAK2 model input was adapted to represent the layout of the Seelig experiments. The value of bottom friction factor, $f_{wp,}$ was assumed to be 0.05 for the concrete slope, and the permeability at the reef crest was neglected.

Seelig (1983) used two wave gauges at 0.5 m (laboratory scale) spacing within the lagoon to estimate ponding levels during these experiments. In the RBREAK2 runs, model results were saved at nodal points spaced 16 m apart in prototype (0.25 m in the experiments) for the narrow lagoon, and 32 m apart (0.5 m in the experiments) for the wide lagoon. RBREAK2 results were saved in front of the fringing reef at 17 nodes for the narrow lagoon, and at 26 nodes for the wide lagoon.

The RBREAK2 computational domain was divided into grids cells of 0.36 m (0.01 m at laboratory scale) for the narrow reef runs, with 714 grid cells at low water and 752 grid cells at high water. For the wide reef, grid cells were 0.72 m (0.02 m at laboratory scale), and there were 649 grid cells at low water and 668 grid cells at high water.

At higher water levels (d_r > 0.0 m), the reef restricts less flow out from the lagoon back into the open ocean. Ponding levels are less for higher depths over the reef. This is evident both from the data (Seelig 1983) and from the results of RBREAK2.

Figure 54 compares calculated ponding levels in the lagoon from RBREAK2 to measured values. The measured setup data were averaged from two gauges that were positioned 0.5 m apart in the laboratory close to the seaward reef edge of the flat portion of lagoon. Calculated RBREAK2 results in Figure 54 are averages of the setup from two nodal points situated 0.5 m apart at the seaward edge of the lagoon. Wave setup values are relative to SWL for each water level. Agreement with data is good for 16-sec period waves (red symbols). RBREAK2 underestimates the ponding levels by approximately 25 percent for the 12-sec waves (blue symbols). Surprisingly, model results for the low (solid symbols) and high water (open symbols) levels are essentially the same.

Significant wave heights saved at the nodal points for the narrow and wide reefs are given in Tables C4 and C5, respectively. Tables C6 and C7 provide wave setup (setdown) at each nodal point for these reefs. Table C8 provides the vertical elevation of maximum runup computed by RBREAK2.

The runup data in Table C8 for the narrow lagoon is compared to the measured runup in Figure 55. The calculated runup values are less than the measured values for nearly all cases. This is expected because the RBREAK2 computational scheme is highly dissipative, and greater losses occur resulting from wave breaking as the waves travel over the flat reach of the reef. For this reason, irrespective of incident wave heights, there is practically no difference in the model results for the low (solid symbols) and high water (open symbols) levels.

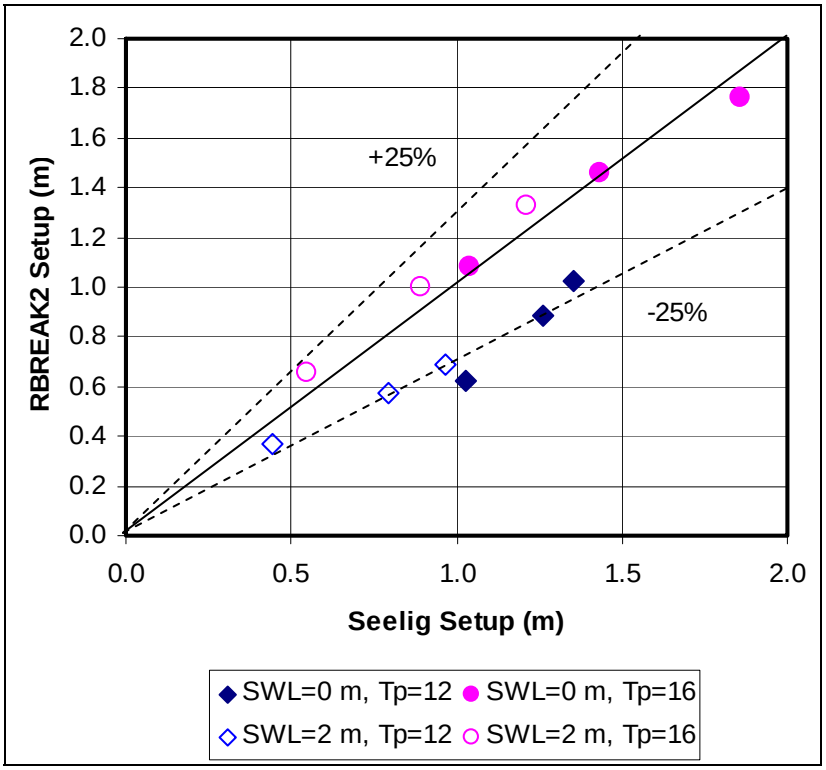

Figure 54. Comparison of calculated and measured lagoon setup for Seelig experiments.

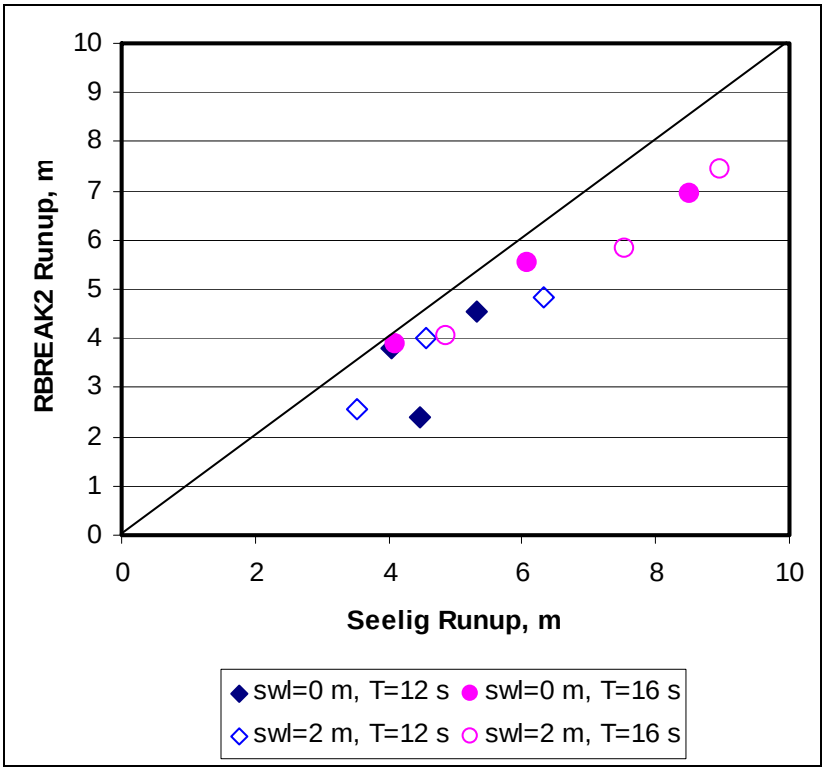

Figure 55. Comparison of calculated and measured maximum runup for Seelig experiments.

CHL reef experiments

Thompson (2005) conducted a series of physical model experiments replicating a reef found off the island of Guam. Bathymetry of the reef is shown in Figures 18 and 19 of Chapter 3. The tests were conducted at a scale of 1:36 with a flat reef in front of a 1:12 beach slope, with the reef extending offshore with variable slopes from the reef top down to the basin bottom. Two water levels were tested; one was set even with the flat reef, and the other was at an elevation of 2.0 m (prototype) above the reef flat. For RBREAK2 simulations, 0.1 m (prototype) was added to the depth when the water level was at the reef flat elevation. This was necessary to force the shoreline to the landward side of the reef. Test conditions for the CHL experiments are listed in Table 4 of Chapter 3.

RBREAK2 results for the CHL experiments and data are included in Appendix D. Of the 19 simulations performed, the runs for test conditions 1-7 and 16-19 were run for the high water level (2 m above the reef), and for test conditions 8-15 for the low water level at the reef crest elevation. In the RBREAK2 simulations, the reef was divided into grid cells of 0.9 m (0.025 m laboratory scale), with 536 grid cells for the low water runs and 562 grid cells for the high water level tests.

Of the nine wave gauges used in the CHL experiments, Gauges 1-3 were located seaward of the reef, and Gauges 4-9 were located on the reef. Nodal points along the reef were selected to correspond to the location of the wave gauges for direct comparison of the numerical model results with the physical model data. In addition to nodal points at the wave gauge locations, RBREAK2 results were also saved at 20 nodal points 40 m apart (0.5 m laboratory scale) along the reef.

The comparison of RBREAK2 results to data for the long period waves and water level at the reef crest is depicted in Figure 56 (T_p = 10 sec, h_r = 0 m) and Figure 57 (wave period, T_p = 15 sec, h_r = 0 m). Calculated and measured significant wave height and setup are shown for GUAM01 and GUAM02 of the CHL experiments. For low period waves, the agreement between the model and data is not as good for high water over a reef flat top as compared to low water level. Figures 58 and 59 (T_p = 15 sec, h_r = 2 m) show results for a 2-m depth over the reef top. These figures show calculated and measured significant wave height and setup for GUAM12 and GUAM13 of the CHL experiments. For the GUAM01 (10-sec wave

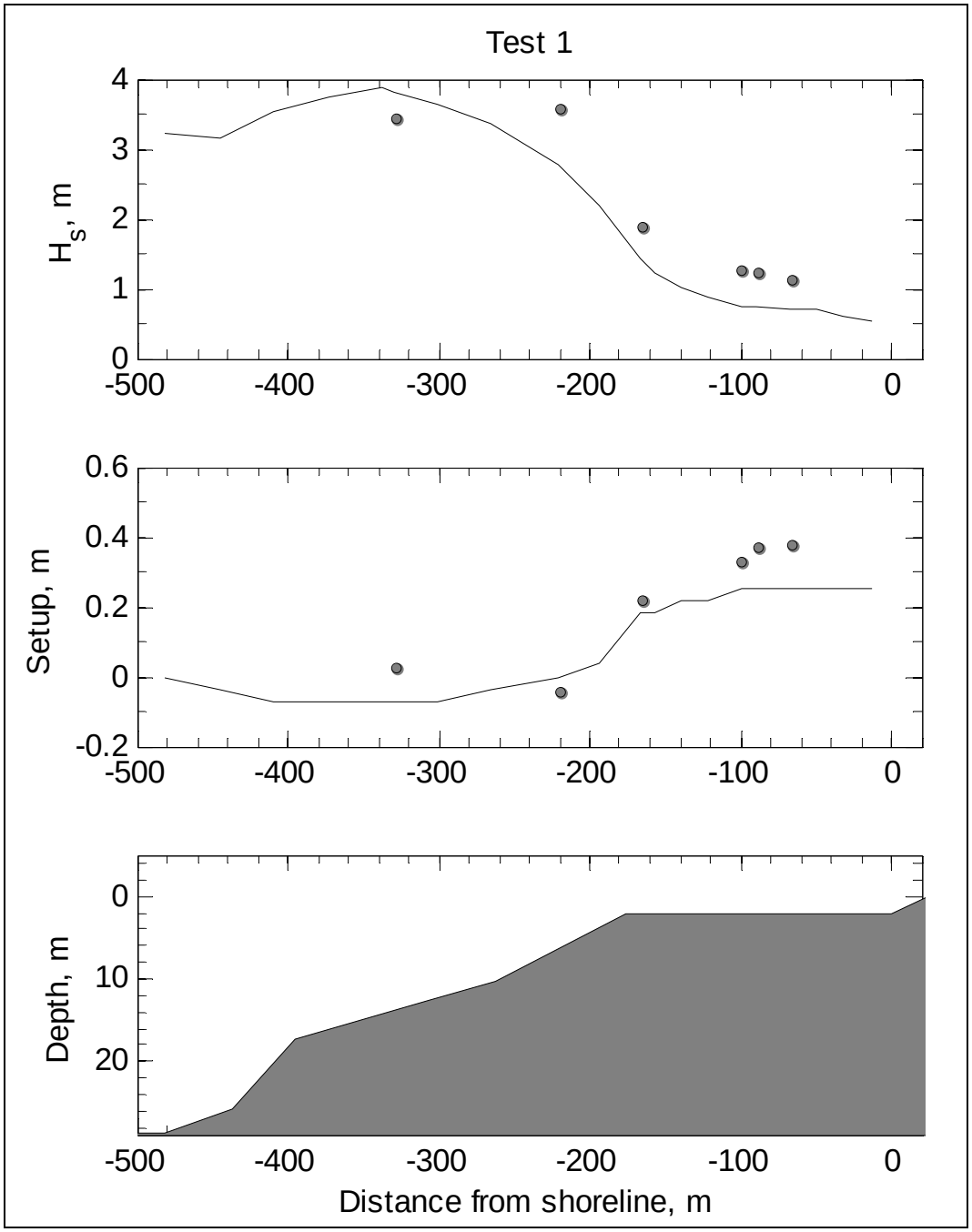

Figure 56. Calculated and measured significant wave height and setup for Test 1 of CHL.

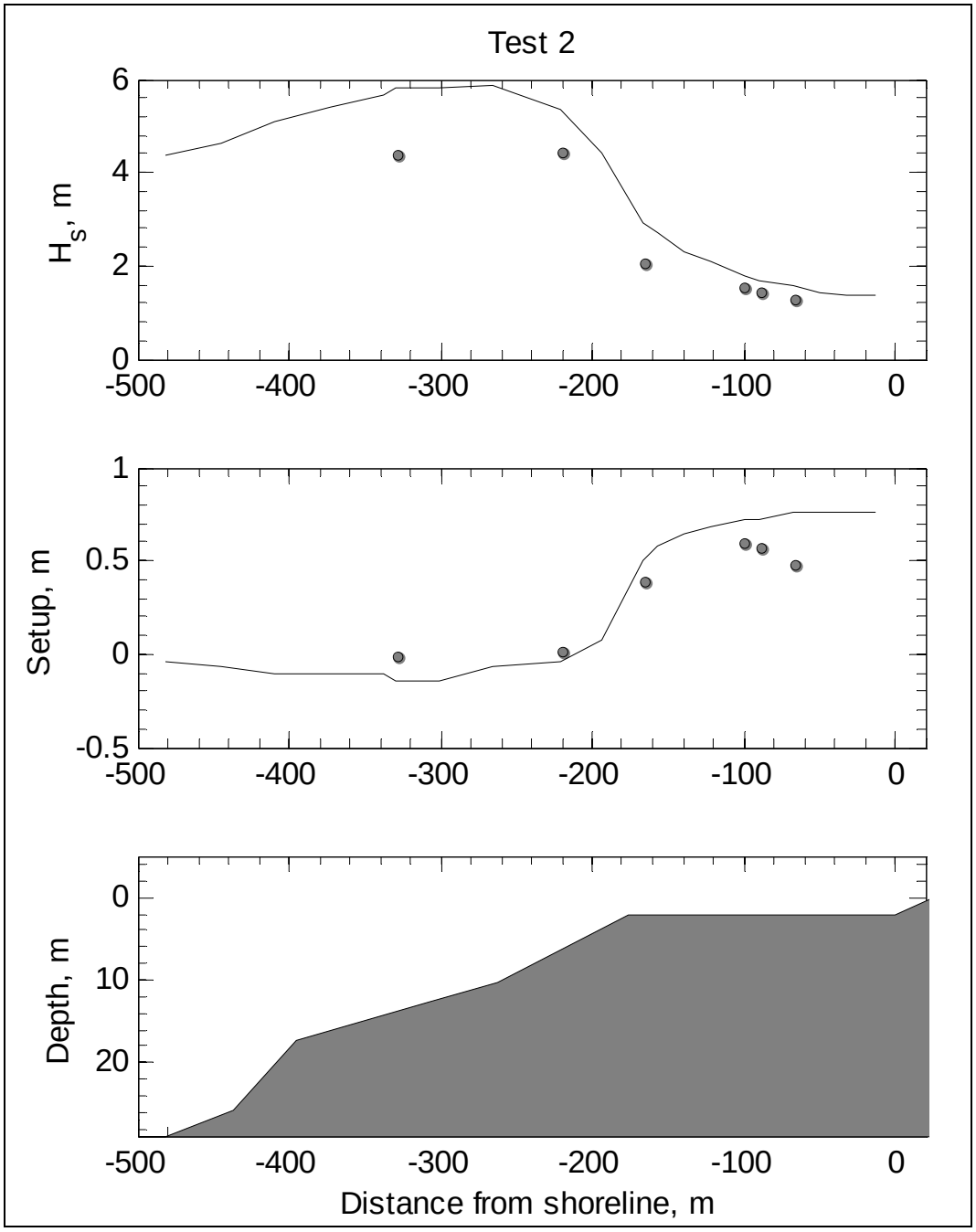

Figure 57. Calculated and measured significant wave height and setup for Test 2 of CHL.

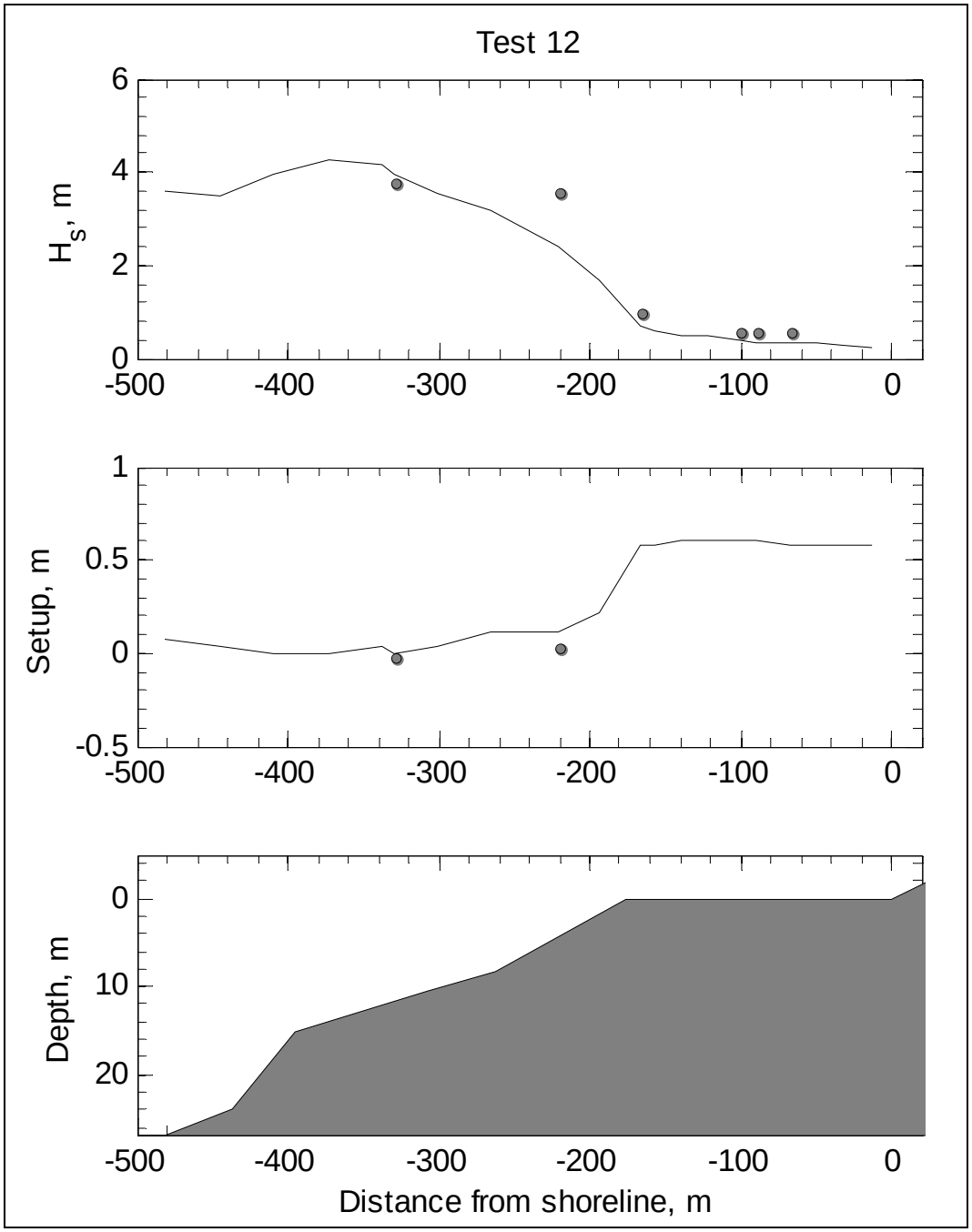

Figure 58. Calculated and measured significant wave height and setup for Test 12 of CHL.

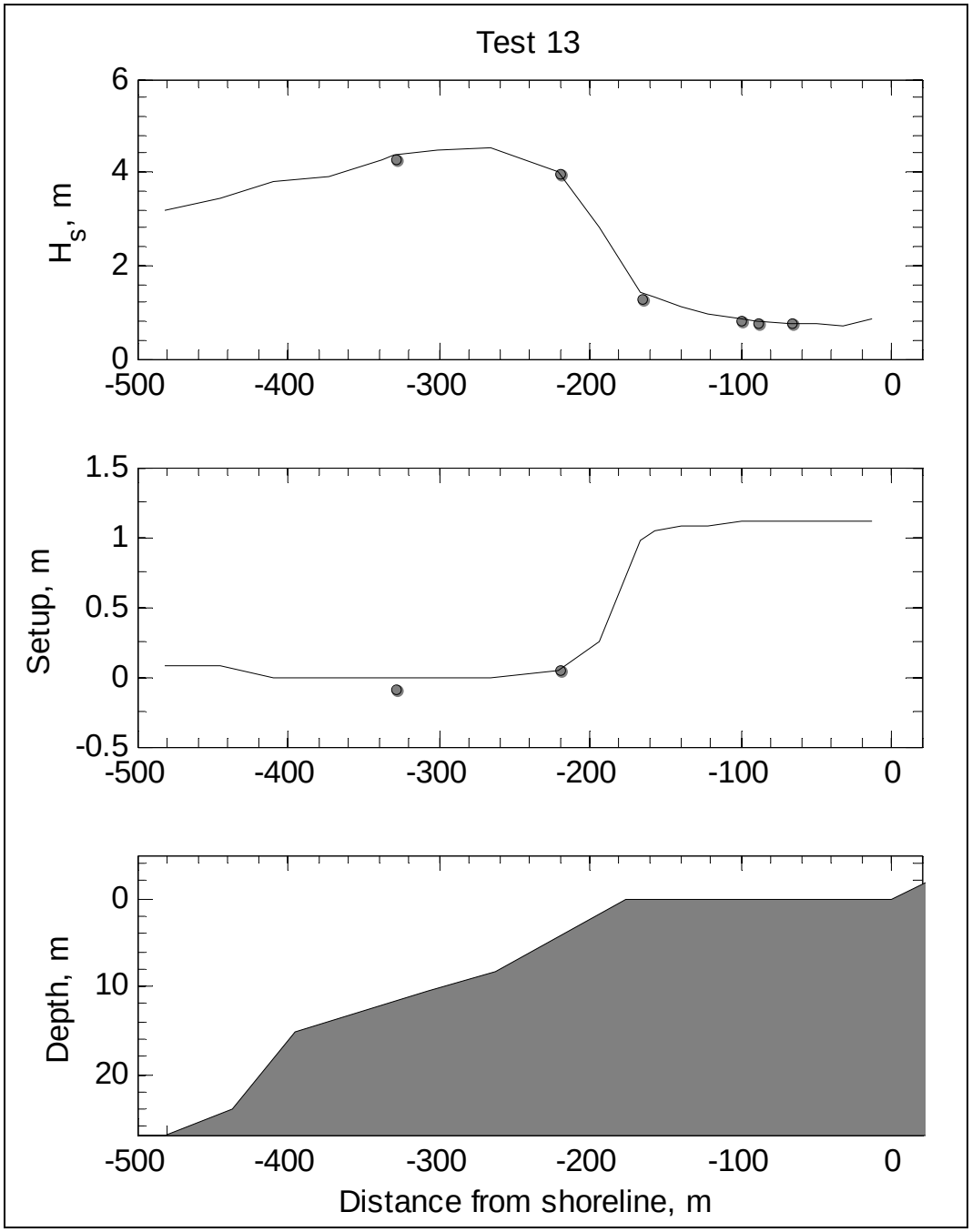

Figure 59. Calculated and measured significant wave height and setup for Test 13 of CHL.

period), the calculated significant wave height first increases over the reef face, then it starts to decrease before reaching the reef crest and without reaching a height to depth ratio representative of incipient breaking, and continues to underpredict the data on the reef flat. For longer period (15-sec) waves, RBREAK2 overpredicts wave heights on the reef face, while comparison to data on the reef flat is slightly improved.

Figure 60 shows the measured setup from CHL experiments for the higher water level (2.0 m). The figure includes data from Gauge 4, near the seaward edge of the reef flat (diamond symbols), Gauge 6, near the middle of the reef flat (square symbols), and Gauge 9, near the landward edge of the reef flat (triangle symbols). The setup calculated by RBREAK2 compares favorably with data for a longer wave period (T_p = 15 sec, open symbols), but the model underpredicts data by about 50 percent for the shorter wave period (T_p = 10 sec, solid symbols). This difference occurs for all gauges, and there is no obvious correlation with the location of gauges. This underprediction appears to be a factor of wave energy being dissipated at too deep of water depth (setup is inversely proportional to water depth). Significant wave height, wave setup, and maximum runup calculated at the nodal points from RBREAK2 for these runs are provided in Tables D9, D10, and D11, respectively.

University of Michigan experiments

Demirbilek et al. (2007a) conducted a comprehensive set of laboratory experiments in a wind-wave flume at the University of Michigan (UM). The combined effect of waves and winds on wave setup and runup was investigated through extensive test conditions which included a series of wave-only, wind-only and waves-plus-wind experiments. Demirbilek and Nwogu (2007) describe analyses of the unique dataset obtained from these experiments, and provide results from numerical modeling with a Boussinesq model. In the present study, wave-only test conditions are further examined with three different numerical models. The experimental setup is shown in Figure 33 and a list of selected test conditions is given in Table 7 of Chapter 3. The reef had a flat area in front of the beach, and multiple slopes extending from the reef top down to the bottom of the flume. These experiments were conducted at a scale of 1:64.

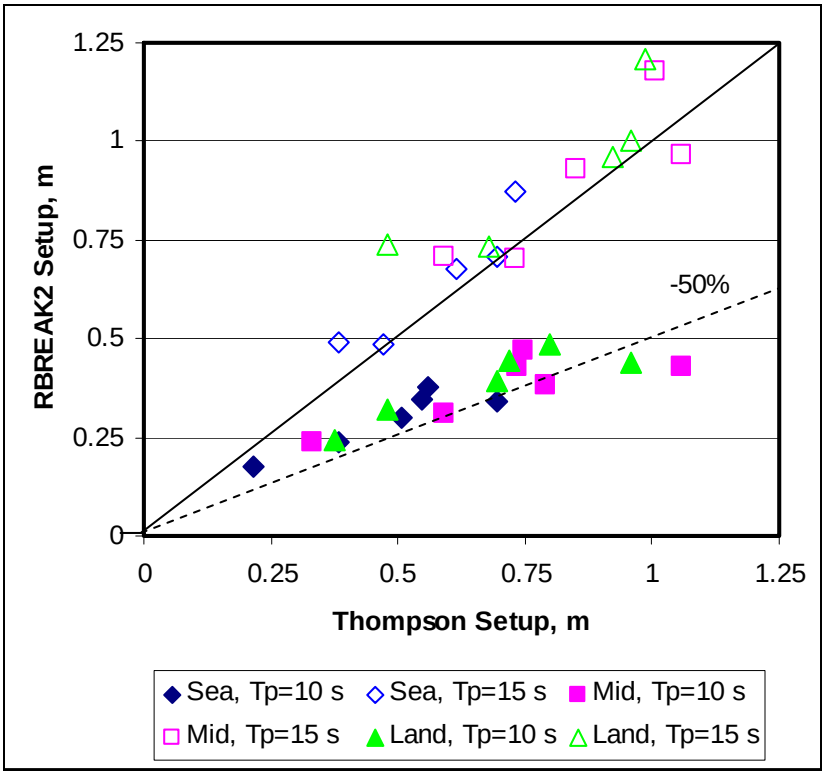

Figure 60. Comparison of calculated and measured wave setup (SWL = 2.0 m).

Four water levels were investigated in the UM experiments, as shown in Table 7 of Chapter 3. For the lowest water level, even with the top of the reef, the water depth was increased by 0.1 m (prototype scale) to force the landward boundary of the RBREAK2 computational domain to the landward side of the reef. The computational domain was divided into grid cells of 2 m width (0.025 m laboratory scale), with 383 to 406 grid cells, depending on the water level.

Of the nine wave gauges used in the UM experiments (Table 6 in Chapter 3), Gauges 1-3 were located seaward of the reef, and Gauges 4-9 were located on the reef. Nodal points along the reef were selected to correspond to the location of the wave gauges for a direct comparison of numerical model results with physical model data. In addition to nodal points at the wave gauge locations, RBREAK2 results were saved at nodal points 40 m apart (0.5 m laboratory scale) along the reef.

It was noted during the comparison to the CHL experiments that RBREAK2 results agreed better with data for longer waves when the water level was even with the reef flat. The effect of wave period on RBREAK2 is urther examined here, and results are shown in Figures 61-63.

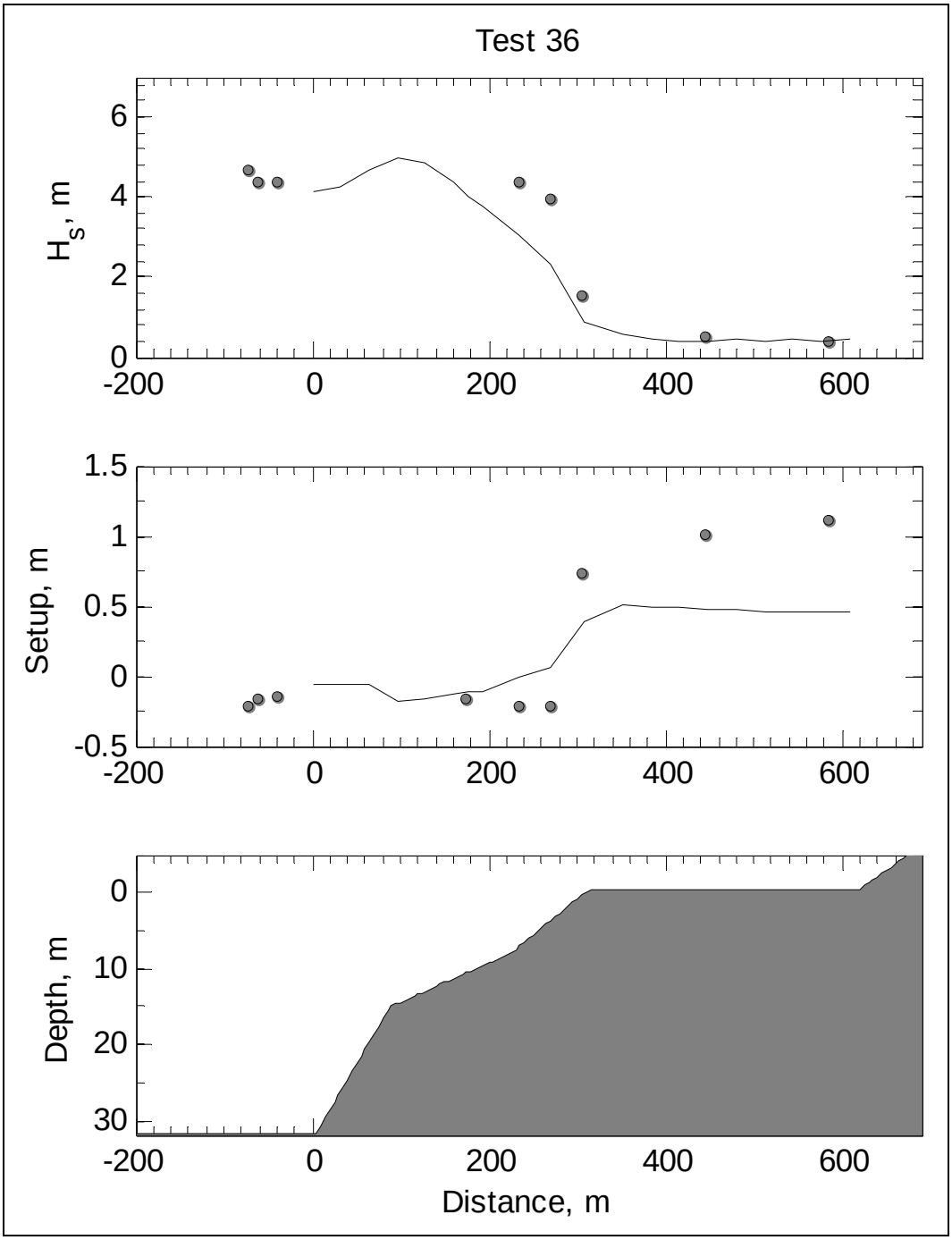

Figure 61. Results for UM Test 36 (T_p = 12 sec, SWL = 0.0 m).

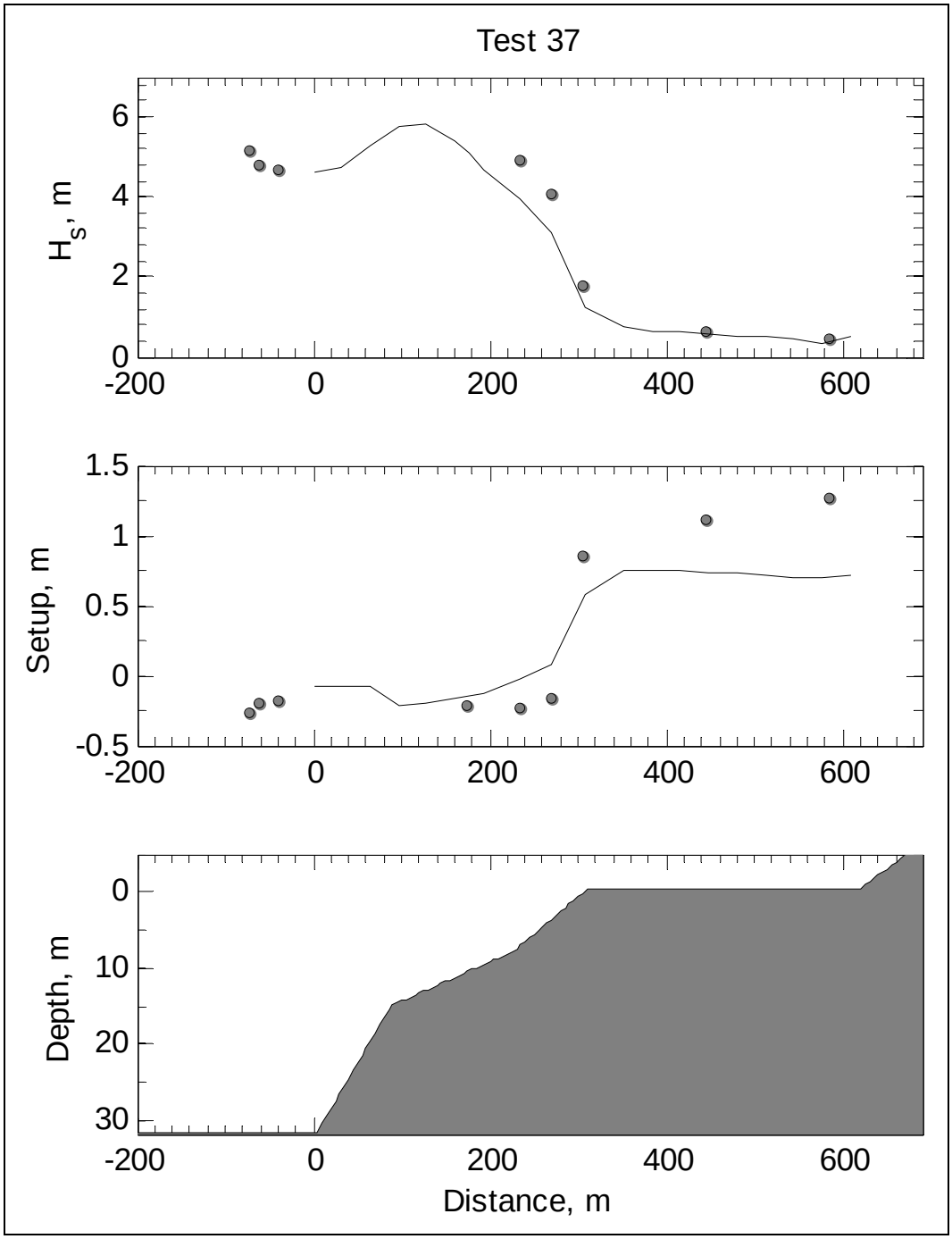

Figure 62. Results for UM Test 37 (T_p = 14 sec, SWL = 0.0 m).

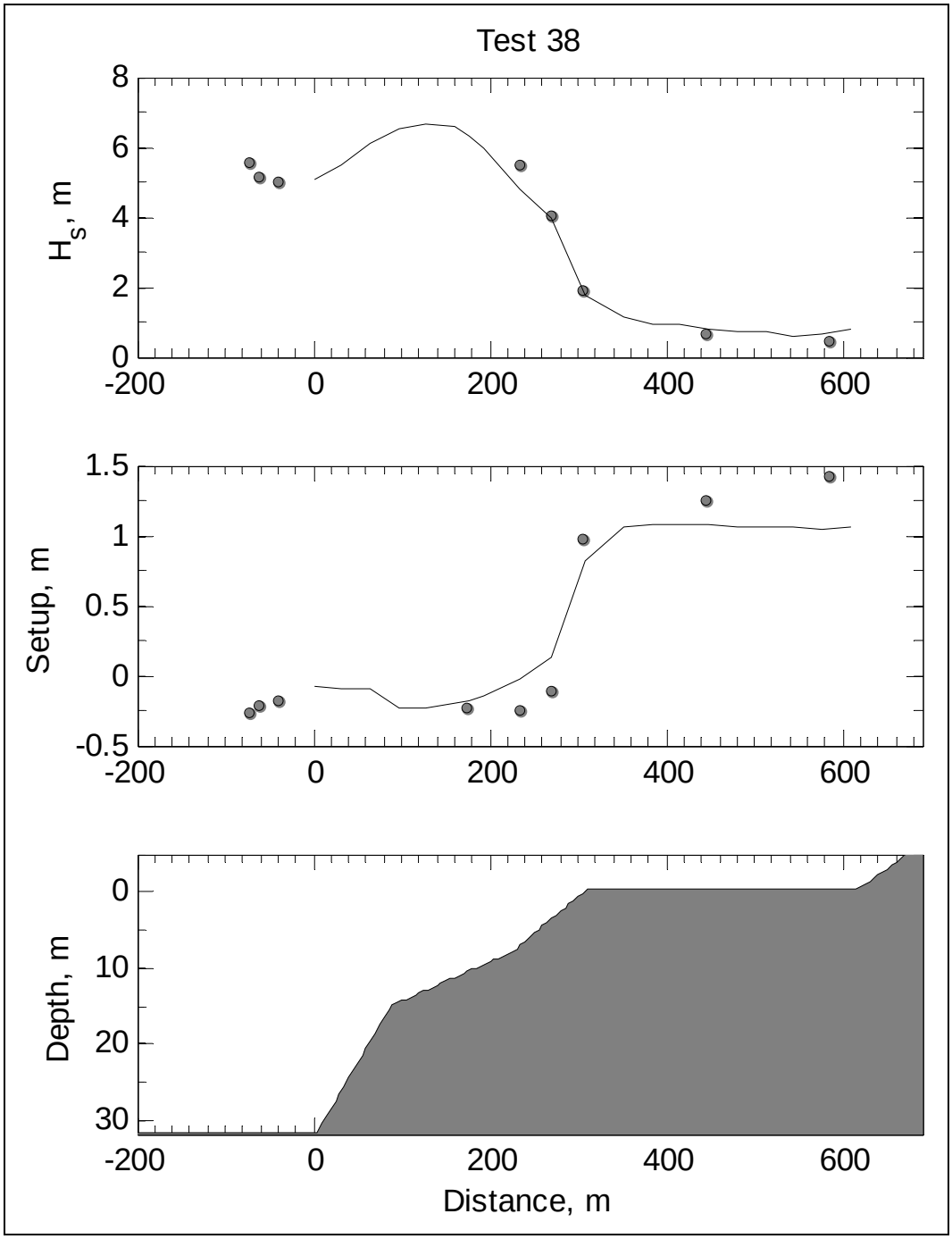

Figure 63. Results for UM Test 38 (T_p = 16 sec, SWL = 0.0 m).

The water level is even with the reef flat in Figures 64-66. Results for wave periods of 12, 14, and 16 sec, respectively, are shown in Figures 61-63. Calculated significant wave heights for these wave periods compare favorably with data, but as shown in the CHL tests, waves decay too far offshore for the shorter wave periods. Calculated wave setup values agree with data along the reef face and are underestimated along the reef flat for shorter wave periods. Calculated wave setup values from RBREAK2 along the UM reef flat improve with increasing wave periods.

RBREAK2 results compare well to data for longer wave periods but not for shorter wave periods. For example, the 16-sec (longest) wave period in the UM experiments, Figure 64, shows model results at high water level (3.25 m over the reef flat). Results for the 12-sec wave period at 1 and 2 m water levels in Figures 65-67 show poorer agreement with the data. Compared with the 0.0 m water level shown in Figure 61, both significant wave height and wave setup from RBREAK2 for short wave periods compare less favorably with data with increasing water level. Surprisingly, RBREAK2 predicted wave setup better for a 12-sec wave period at the highest water level 3.25 m (Figure 67).

Results of significant wave height, wave setup, and maximum runup calculated from RBREAK2 are provided in Tables E1, E2, and E3, respectively.

Runup estimates from RBREAK2 are plotted against the measured data from UM in Figures 68 and 69. Data are presented in Figure 68 for four water levels. The data for the lowest water level (SWL = 0.0 m) are in blue diamonds. RBREAK2 underestimates wave runup by approximately 50 percent at 1-m (pink square) and 2-m (green triangle) water levels. Model results improve slightly at the highest 3.25 m water level (orange circles). The runup data are plotted in Figure 69 for different wave periods. Surprisingly, model accuracy is not sensitive to wave period as there is no correlation apparent between model estimates for different values of wave periods.

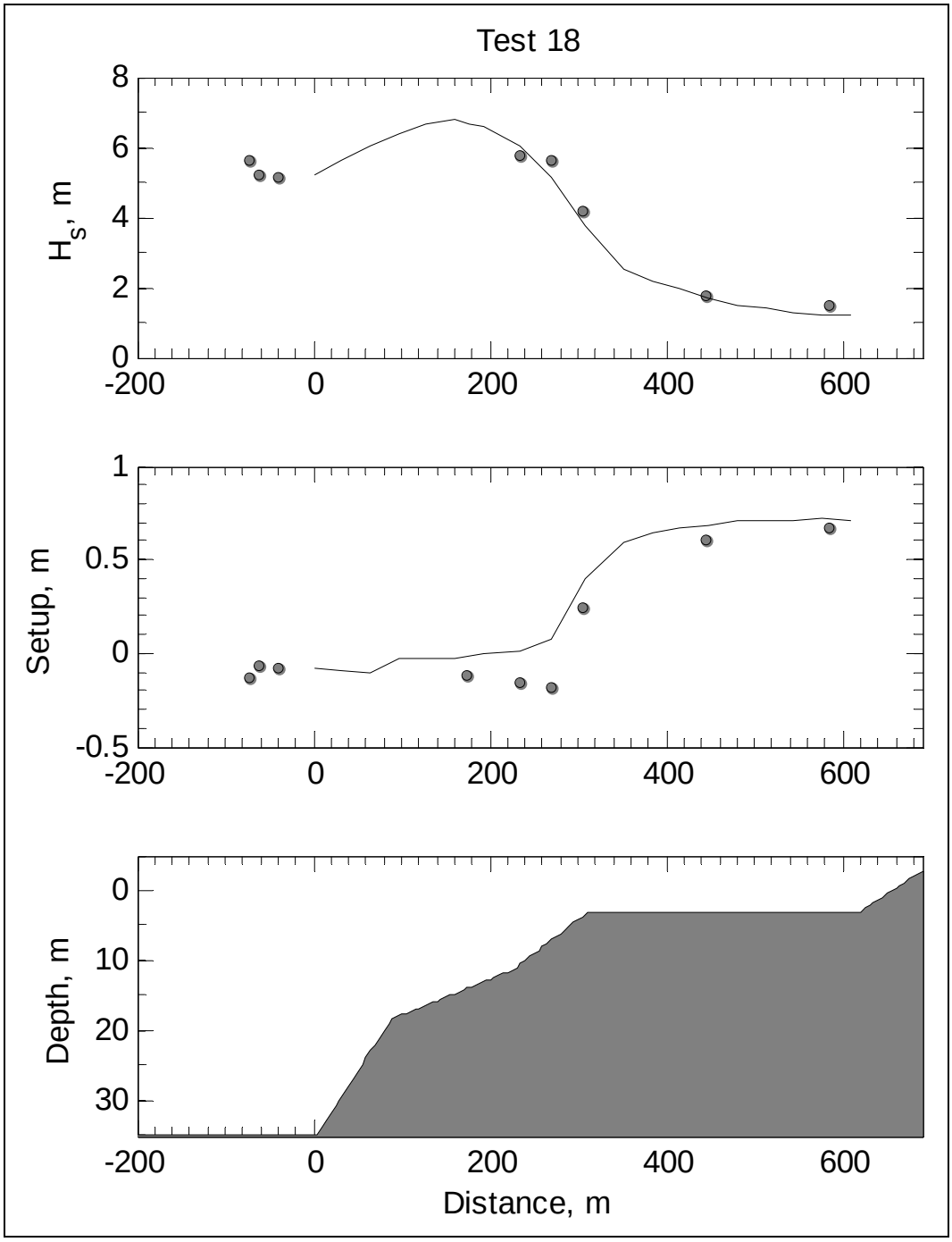

Figure 64. Results for UM Test 18 (T_p = 16 sec, SWL = 3.25 m).

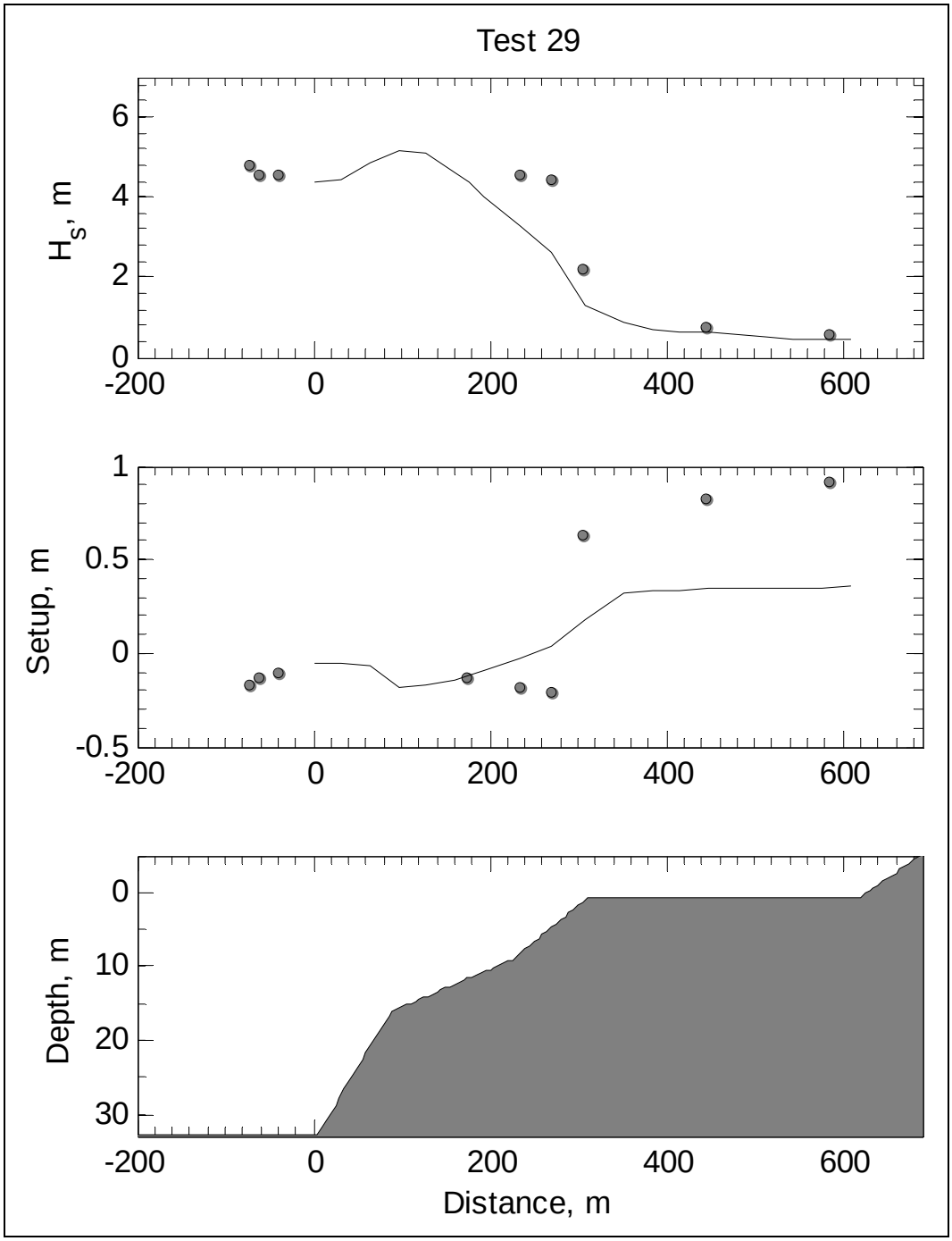

Figure 65. Results for UM Test 29 (T_p = 12 sec, SWL = 1.0 m).

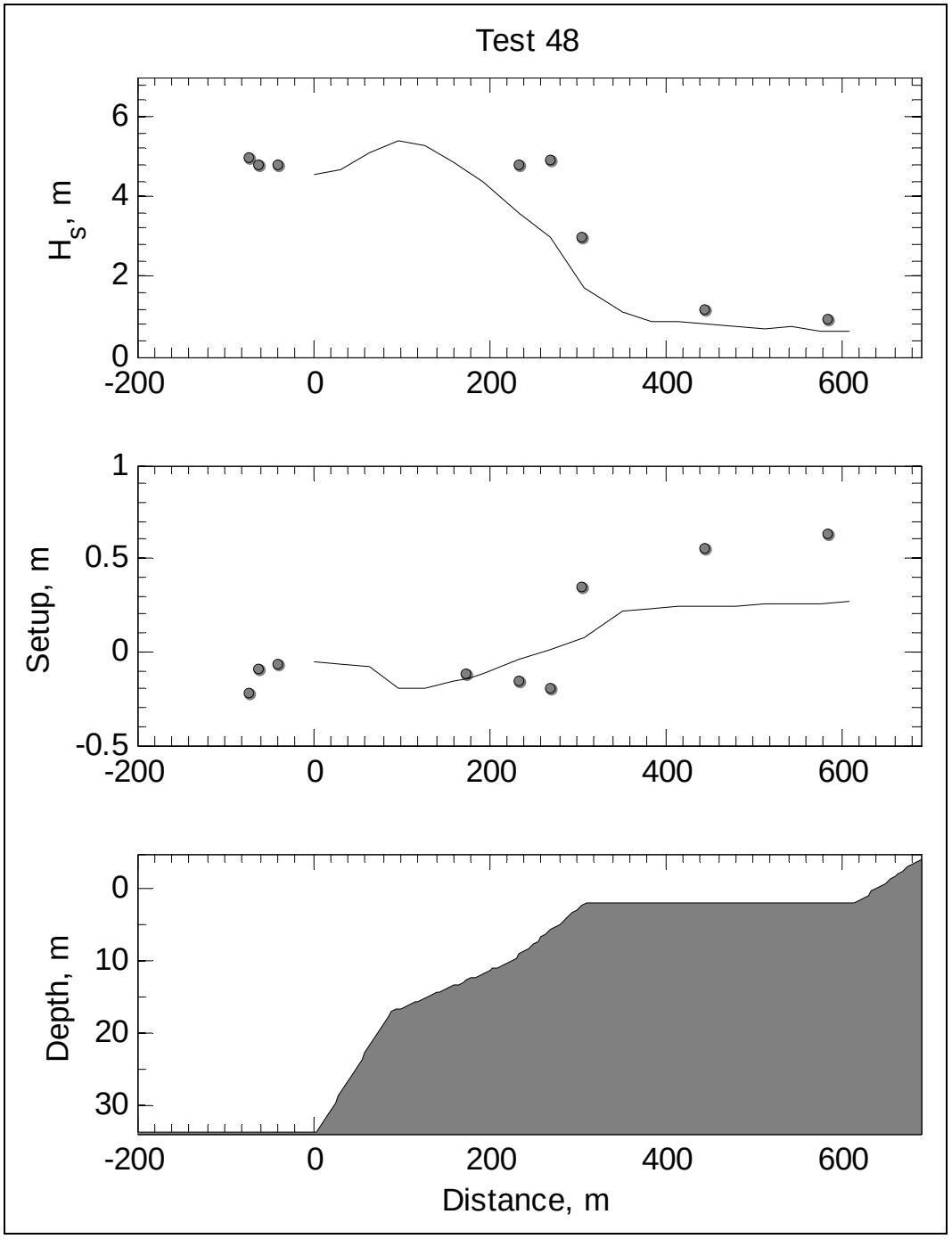

Figure 66. Results for UM Test 48 (T_p = 12 sec, SWL = 2.0 m).

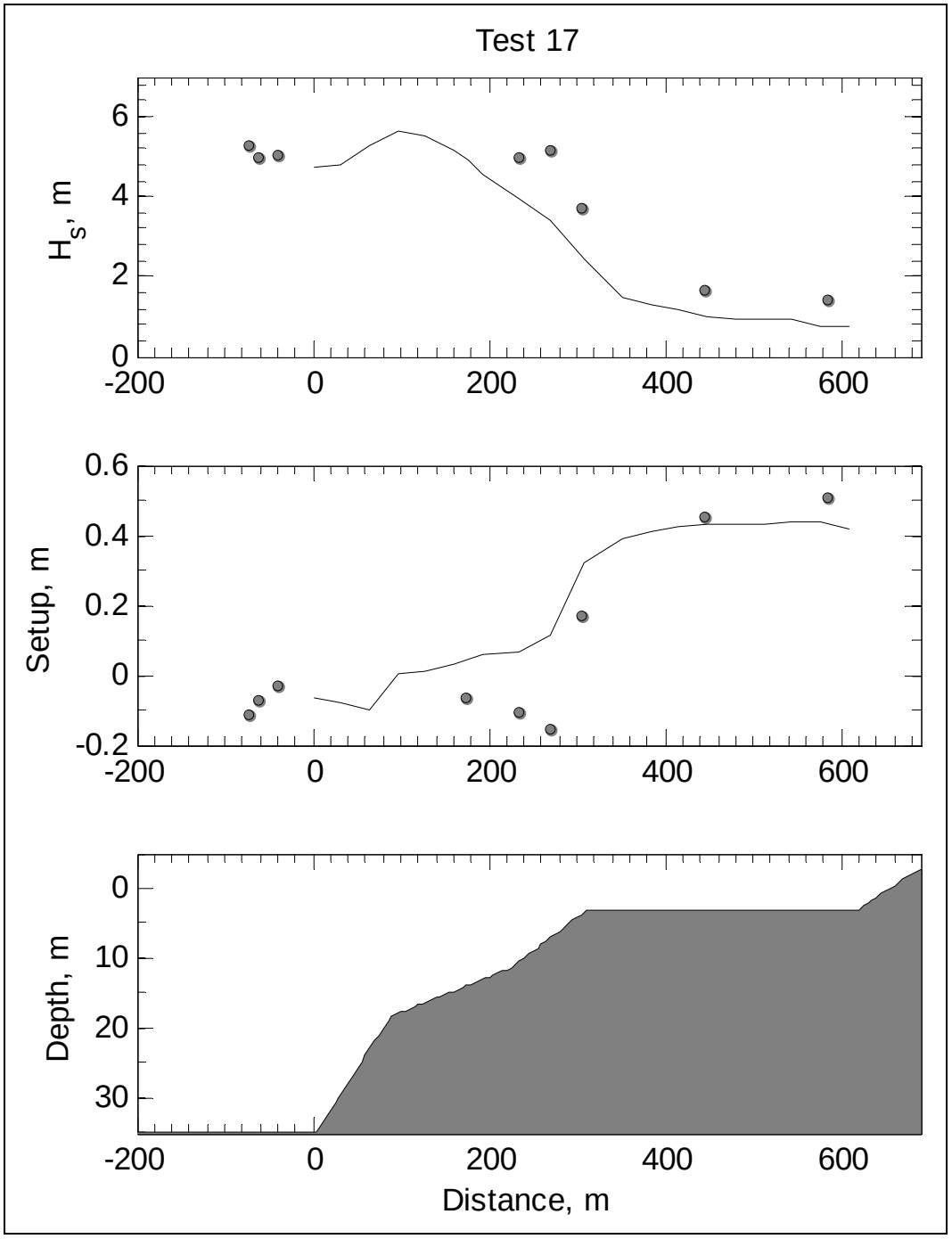

Figure 67. Results for UM Test 17 (T_p = 12 sec, SWL = 3.25 m).

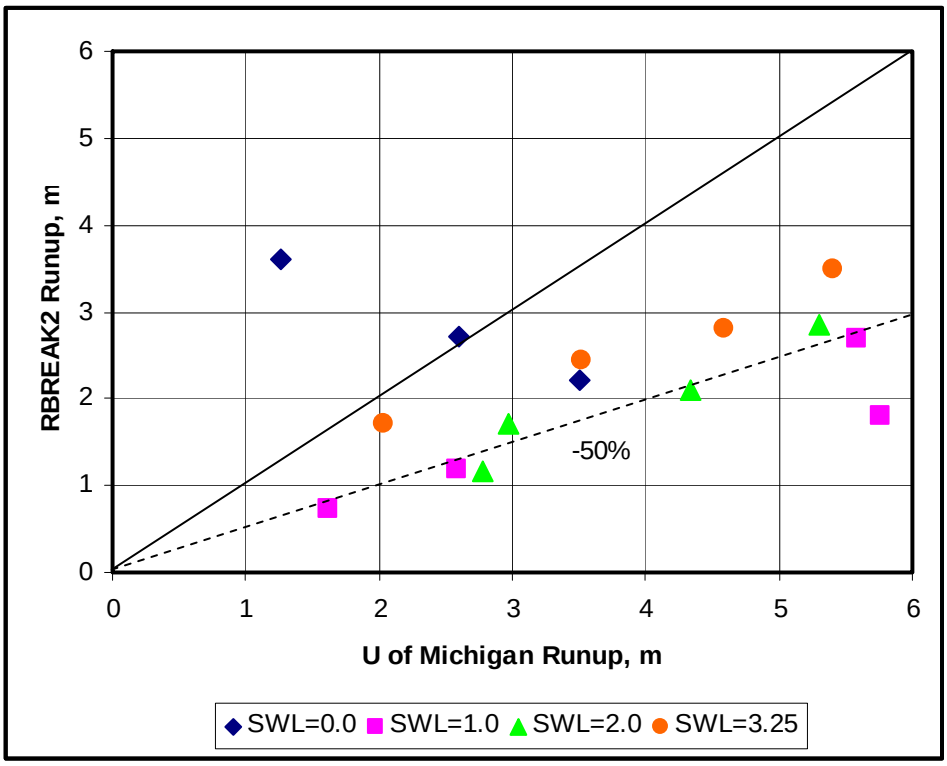

Figure 68. Comparison of calculated and measured runup for three water levels.

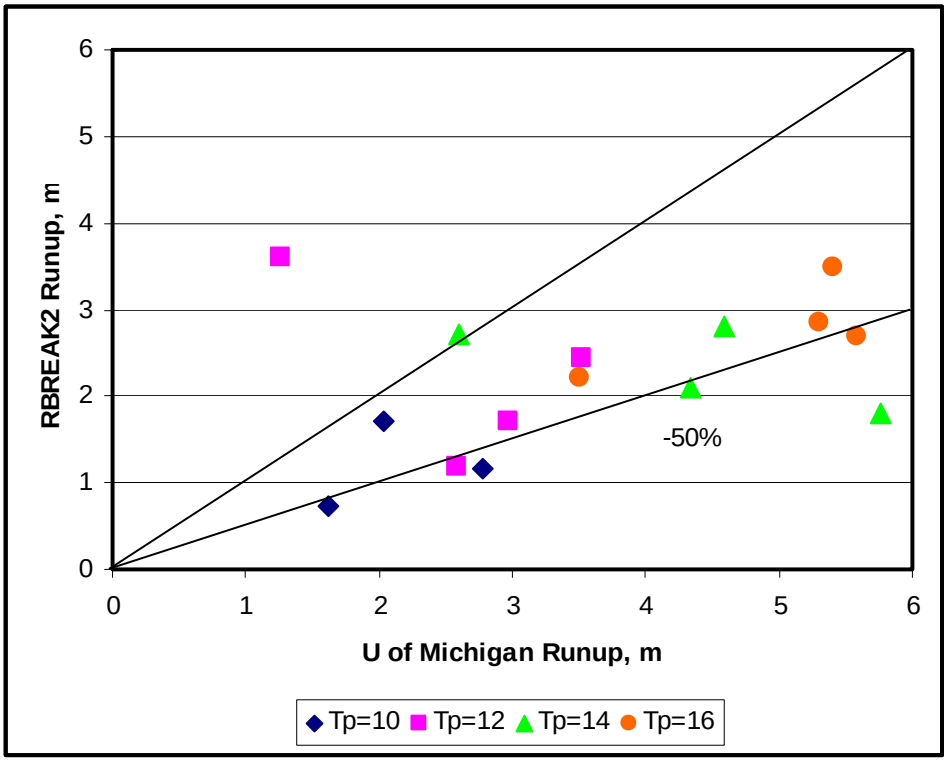

Figure 69. Comparison of calculated and measured runup for different peak wave periods.

5 WAV1D Model Evaluation

Model description

Different types of 1D models, based on the conservation of wave energy flux and momentum, have been used successfully in calculation of wave transformation and water levels in the surf zone (Gerritsen 1980; Thornton and Guza 1983; Dally et al. 1985; Dally 1992; Larson and Kraus 1991; Smith 1993; Massel and Brinkman 2001; Grasmeijer and Ruessink 2003). There are two approaches that can be used in 1D energy flux models. Single wave models (e.g., Dally et al. 1985) simulate the wave transformation of a representative or characteristic wave height, wave period and direction, while probabilistic models simulate wave transformation based on a discrete number of wave classes (e.g., Larson and Kraus 1991). Grasmeijer and Ruessink (2003) found that single wave models performed better and were considerably simpler and faster than probabilistic models. A single wave approach is used in WAV1D.

In a 1D approach, assuming alongshore uniformity in the bathymetry, the time-averaged wave energy flux equation is written as

$$\frac{\partial}{\partial x}(EC_g \cos\theta) = D_b + D_f \tag{9}$$

where E is the wave energy density per unit area, C_g is the wave group velocity, θ is the incident wave angle relative to shore normal, and D_b and D_f are the wave energy dissipation resulting from breaking and bottom friction, respectively. By assuming that the individual wave heights follow a Rayleigh distribution (HQ USACE 2002), we have

$$p(H) = \frac{2H}{H_{rms}} \exp\left[-\left(\frac{H}{H_{rms}}\right)^2\right] \tag{10}$$

In the case of irregular waves, the root-mean-squared (rms) wave height H_{ms} can be obtained by

$$E = \frac{1}{8}\rho g \int_0^\infty H^2 p(H) dH = \frac{1}{8}\rho g H_{rms}^2 \tag{11}$$

where the significant wave height is estimated as $H_s = \sqrt{2}H_{rms}$, and in the case of regular waves, $E = \frac{1}{8}\rho g H^2$.

The time-averaged and depth-integrated 1D momentum equation, assuming uniformity in the alongshore direction (y-direction) and ignoring mixing and cross-shore currents, may be written (Dally et al. 1985) as

$$\rho g(h+\bar{\eta})\frac{\partial \bar{\eta}}{\partial x} + \frac{\partial S_{xx}}{\partial x} = \tau_{wx} \tag{12}$$

where $\bar{\eta}$ is the mean water level (or wave setup) relative to SWL, h is the still-water depth relative to a specific vertical datum, and S_{xx} is the wave radiation stress in the cross-shore direction. The wave radiation stress is approximated using linear wave theory for an arbitrary wave angle (Longuet-Higgins and Stewart 1964) as

$$S_{xx} = E(n(\cos^2\theta + 1) - 0.5) \tag{13}$$

where θ is the incident wave angle relative to shore normal and $n = 0.5\left[1 + 2kd / \sinh(2kd)\right]$. The wave energy flux and momentum equations (Equations 9 and 12) are solved simultaneously from deep to shallow water using a forward stepping scheme. Note that because of nearshore wave setup, it is possible to calculate wave heights over an initially dry land.

The WAV1D model includes wave shoaling, refraction, breaking, and bottom friction. Although the WAV1D model cannot represent the nonlinear transfer of energy in the wave spectrum, it can describe the average wave energy dissipation and wave setup over the reefs. The WAV1D model is efficient, robust, and works for extreme wave conditions. This makes the energy flux model a useful engineering tool for nearshore wave transformation and water levels along cross-shore transects.

Wave breaking and bottom friction

Because the wave breaking term in Equation 9 is the dominant term in the surf zone, the estimated wave results are sensitive to the type of wave breaking formulation used. Two formulations are used to estimate the breaking wave dissipation.

The first formulation adopted for wave breaking dissipation is based on the work of Battjes and Janssen (1978). Recently, Alsina and Baldock (2007) and Janssen and Battjes (2007) reported the following expression for wave breaking dissipation as

$$D_b = \frac{3\sqrt{\pi}}{16}\rho g B \frac{1}{T}\frac{H_{rms}^3}{d}Q_b \tag{14}$$

where B is the wave breaking intensity factor (set to 1.0), and the fraction of broken waves Q_b is estimated as

$$Q_b = 1 + \frac{4}{3\sqrt{\pi}}\left(R^3 + \frac{3}{2}R\right)\exp\left(-R^2\right) - \mathrm{erf}(R) \tag{15}$$

where erf is the error function, and $R = H_b/H_{rms}$. The value of 1.0 was used for the wave breaking intensity factor for four experiments and no calibration was performed. The breaking wave height is obtained by $H_b = 0.88 \tanh(\gamma kd/0.88)/k$, where k is the wave number *and* the breaker index γ is calculated using the following expression (Battjes and Stive 1985): $\gamma = H_b/d = 0.5 + 0.4 \tanh(33\, H_o/L_o)$. Nearly 75 to 95 percent of wave energy is attenuated over reefs (e.g., Lugo-Fernandez et al. 1998). The parameter B was assumed to be 1.0 in the present study. This parameter controls wave breaking dissipation and breaking intensity in the Alsina and Baldock (2007) formulation.

Equation 14 was obtained by following a similar approach as in Battjes and Janssen (1978), except that a complete Rayleigh distribution has been assumed for the breaking waves, instead of assuming a truncated Rayleigh distribution. Alsina and Baldock (2007) compared Equation 14 to the breaking formulations of Thornton and Guza (1983), Baldock et al. (1998) and Grasmeijer and Ruessink et al. (2003), and found that Equation 15 produced the smallest errors for steep slopes. The energy flux model (WAV1D) with the wave breaking formulation of Alsina and Baldock (2007) is subsequently referred to as ABJB07.

The second breaking formulation tested is the empirical model of Dally et al. (1985) expressed as

$$D_b = \frac{\kappa}{d}\left[E - \min(E, E_s)\right]C_g \tag{16}$$

where κ is an empirical decay coefficient, C_g is the wave group velocity, and E_s is the stable wave height energy defined as

$$E_s = \frac{1}{8}\rho g(\Gamma d)^2 \tag{17}$$

where Γ is the stable wave height as a fraction of the water depth. Following Dally et al. (1985), Demirbilek and Panchang (1998), and Zhao et al. (2001), 0.15 and 0.4 for values of κ and Γ, respectively, were used in WAV1D for four experiments and no calibration was performed. This wave breaking formulation has been applied successfully in modeling wave transformation over irregular bathymetry including reefs (Gerritsen 1980; Dally 1992). For mild and flat slopes, this method is conservative because the wave height does not decrease once it reaches a stable wave height value. Subsequently, the wave energy flux model (WAV1D) with the wave breaking formulation of Dally et al. (1985) is referred to as DDD85.

Equation 16 does not depend on the wave period and wave height distribution chosen. The wave height distribution is used only to obtain a characteristic wave height from the wave energy. Equation 16 works best for monochromatic waves because it was developed from laboratory studies. Another important feature of Equation 16 is that it is not wave period dependent, but the parameter κ is indeed a function of the wave period (Dally et al. 1985; Demirbilek and Panchang 1988; Zhao et al.2001).

The wave dissipation resulting from bottom friction is calculated as

$$D_f = \frac{\rho f_w}{12\pi}\left(\frac{2\pi H_{rms}}{T\sinh(kd)}\right)^3 \tag{18}$$

where f_w is the wave-related friction coefficient given by

$$f_w = \min\left\{0.3, \exp\left[-6.0 + 5.2\left(A_b / k_w\right)^{-0.19}\right]\right\} \tag{19}$$

where A_b is the near-bed orbital excursion calculated from linear wave theory, and k_w is a hydraulic roughness length assumed here to be the same as the physical reef roughness. Lowe et al. (2005) investigated the hydraulic reef roughness along several transects of coral reefs in Hawaii and recommended k_w = 0.16 ± 0.03. Previously, Gerritsen (1980) studied

wave breaking and suggested values between 0.025-0.125. Demirbilek and Nwogu (2007) considered reef roughness in terms of the Chezy friction factor, and their equivalent values to the f_w friction coefficient ranged from 0.01 to 0.15.

Estimation of wave parameters

In comparing phase-averaged and time-dependent models with laboratory measurements, it is important to be clear on how the statistics are calculated from the time series. In phase-averaged models, the zeroth moment significant wave height is calculated as

$$H_{mo} = 4\sqrt{\int_0^\infty S(f)df} \tag{20}$$

where $S(f)$ is the energy density spectrum. This statistic can be obtained accurately from time-dependent models such as BOUSS-1D which includes the entire frequency range including both gravity and infragravity waves. For the phase-averaged model, a more appropriate statistic is the significant wave height, defined as

$$H_s = 4\sqrt{\int_{f_c}^{f} S(f)df} \tag{21}$$

where f_c is the cut-off frequency for excluding infragravity wave frequencies. In general, the cutoff may be set to $2T_p$ or $f_p/2$, but here it is set to f_c = 0.0167 Hz or T_c = 60 sec (prototype scale), where $f_c = 1/T_c$. Phase-averaged models such as WAV1D cannot capture the infragravity wave energy because they cannot simulate nonlinear wave-wave interactions that produce these low-frequency oscillations.

Wave runup statistics

A modified version of the empirical wave runup relations developed by Mase (1989) for smooth, impermeable, and gentle beach slopes is used in the WAV1D to calculate wave runup statistics using the following general expression:

$$\frac{R}{H_r} = a\xi_r^{\ b} \tag{22}$$

where R is the runup statistic, a and b are two empirical coefficients, H_r is the reef top significant wave height, and ξ_r is the surf similarity parameter defined as $\xi_r = \tan\alpha / \sqrt{H_r / L_o}$, where α is the beach slope and L_o is the deepwater wavelength. For the maximum runup ($R_{max} = R$ in Equation 22), values of the empirical coefficients selected were a = 2.32 and b = 0.77. For the two-percent runup ($R_{2\%} = R$ in Equation 22), these coefficients were selected as a = 1.86 and b = 0.71. On fringing reefs, waves usually break near the reef edge, and may reform over the reef top if the geometry of the reef permits. Thus, it is appropriate to use the wave height over the reef top H_r in Equation 22 instead of the deepwater wave height. The wavelength used in the surf similarity parameter is based on the peak period of deepwater waves.

The objectives of the WAV1D model evaluation were:

1. Evaluate the model against four laboratory experiments and compare the results with measurements and BOUSS-1D results to determine its general suitability for different types of reef applications.
2. Determine if default wave breaking dissipation parameters are sufficient to produce reliable and consistent estimates of nearshore wave height and wave setup as compared to measured laboratory data for fringing reefs.
3. Evaluate WAV1D runup statistics with laboratory measurements.

Hayman Island reef experiments

In this section, estimates from the wave energy conservation model WAV1D, using wave breaking formulas of ABJB07 and DDD07, are compared to the Hayman Island laboratory experiments (Gourlay 1994). Unless otherwise stated, the parameters used in these wave breaking formulations were as follows: B = 1.0 in the ABJB07, κ = 0.15, and Γ = 0.4 in the DDD85. See Chapter 3 for information about these experiments. Measured and calculated wave heights and mean water levels (wave setup) across the fringing reef are depicted in Figures 70-72. The estimates of wave heights over the reef from WAV1D agree with data, although there is a considerable scatter in the measurements. Both ABJB07 and DDD85 formulas overestimate wave setup for Tests-11 and 21 (Figure 70), and the comparison for Test 24 is shown in Figure 71. Seelig (1983) found that random waves of a given offshore significant wave height and period produce less setup as compared to monochromatic waves of the same wave height and period. He attributed the difference in the wave setup to irregular

waves containing about half the energy of equivalent monochromatic waves. Consistent with this reasoning, the WAV1D model with the ABJB07 formula appears to underestimate wave setup, as shown in Figures 70 to 72.

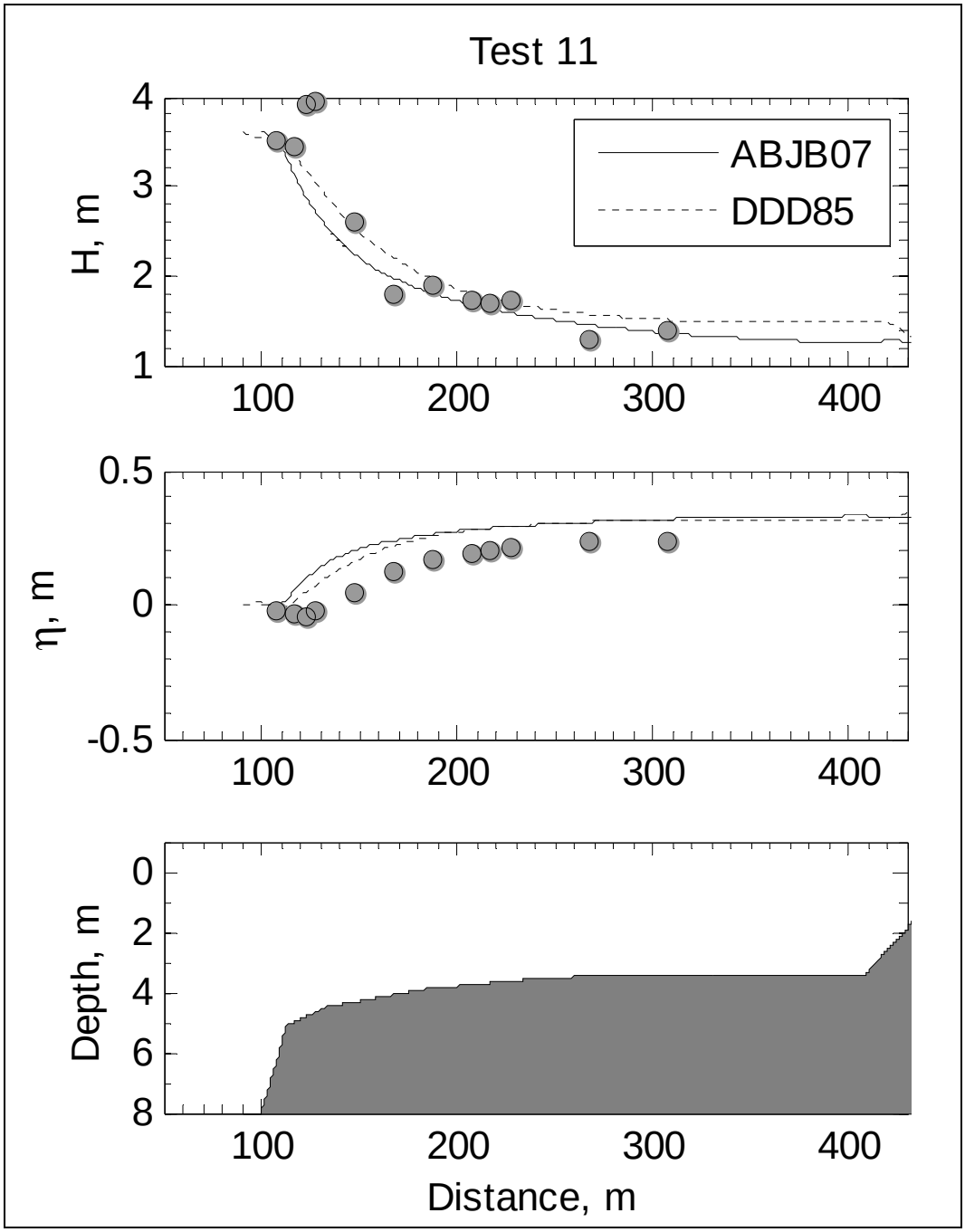

Figure 70. Comparison between measured and computed wave heights and mean water levels for Test 11 (H_i = 3.44 m, T = 6.8 sec, h_r = 3.4 m).

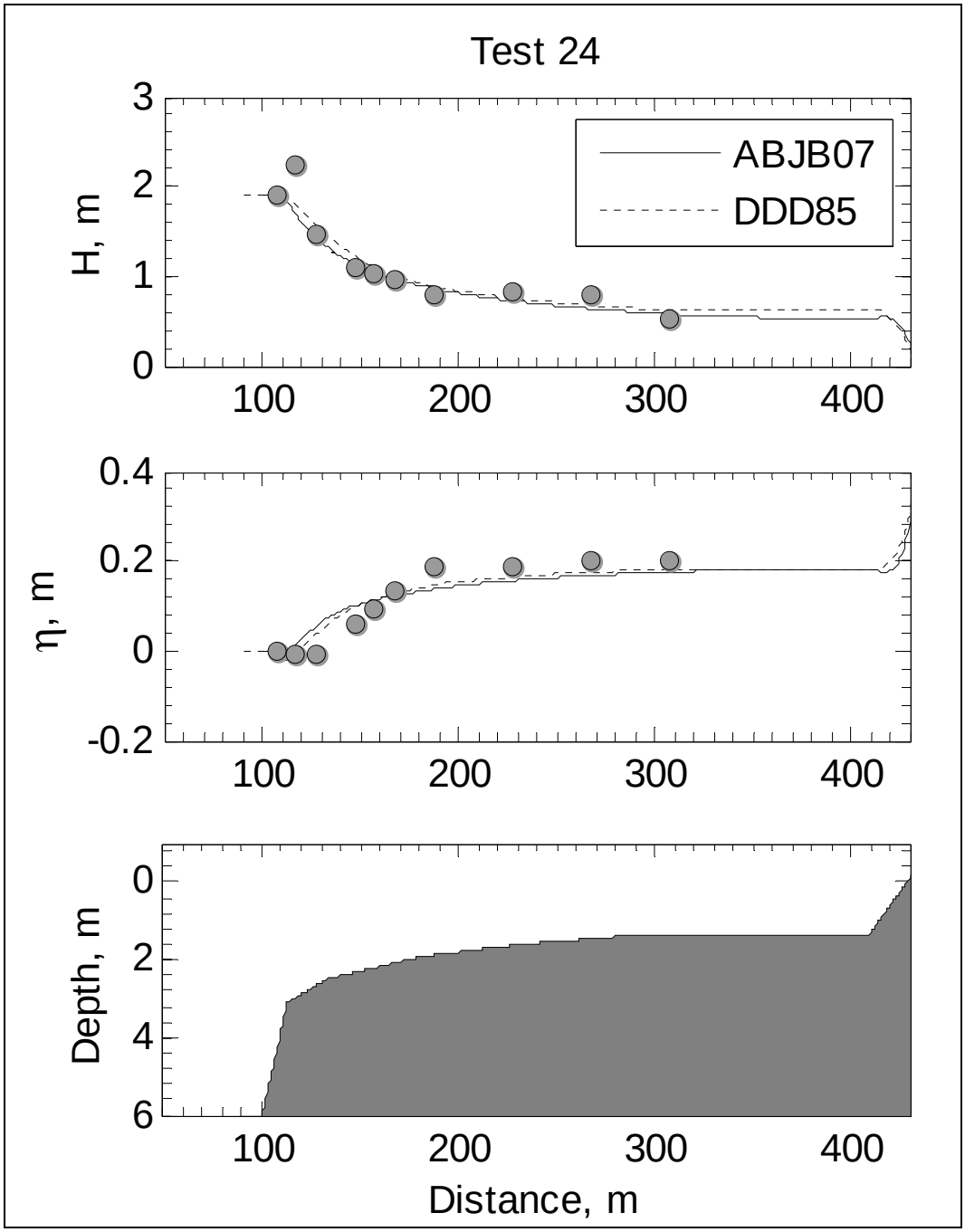

Figure 71. Comparison between measured and computed wave heights and mean water levels for Test 24 (H_I = 1.90 m, T = 5.4 sec, h_r = 1.4 m).

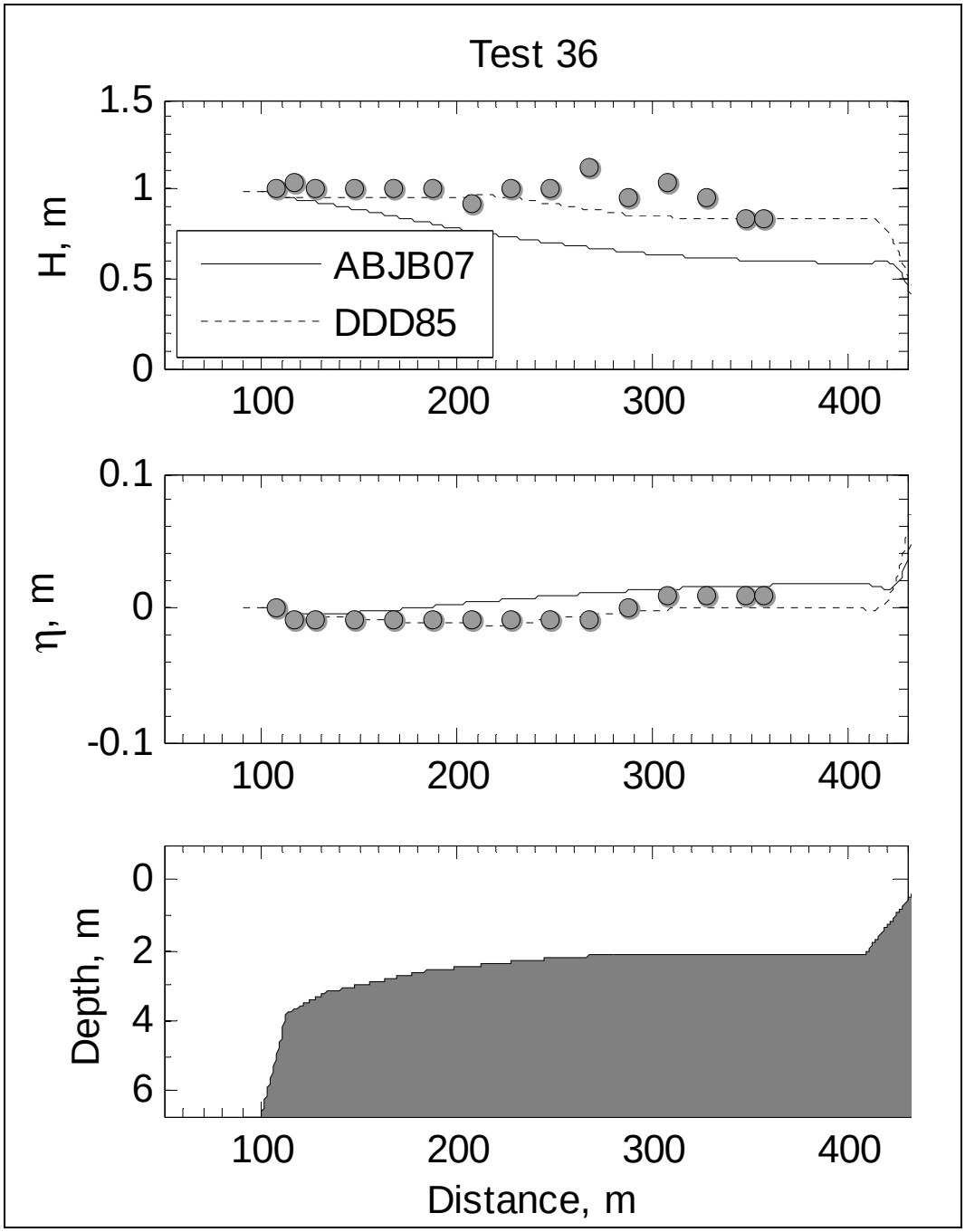

Figure 72. Comparison between measured and computed wave heights and mean water levels for Test 36 (H_I = 0.99 m, T = 3.8 sec, h_r = 2.1 m).

Measured and computed wave heights and mean water levels obtained with the WAV1D model using the ABJB07 and DDD85 formulas are compared in Figures 73 and 74. The model results agree better with data for wave heights and mean water levels obtained with the DDD85 formula for these monochromatic waves. The RMSE values (rms errors) for wave heights and mean water levels over the reef top obtained with the ABJB07 formula are 0.33 and 0.5 m, respectively. For the DDD85 formula, the rms errors for wave heights and wave setup over the reef top are 0.25 and 0.05 m, respectively.

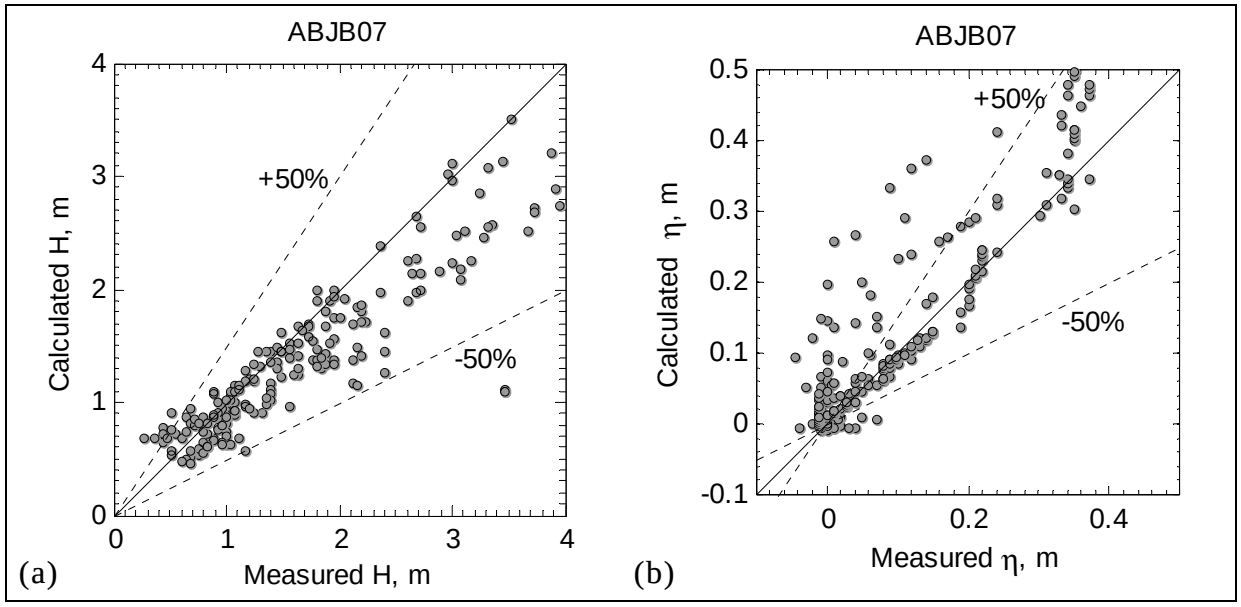

Figure 73. Comparison between measured and computed wave heights (a) and mean water levels (b) for BJB07.

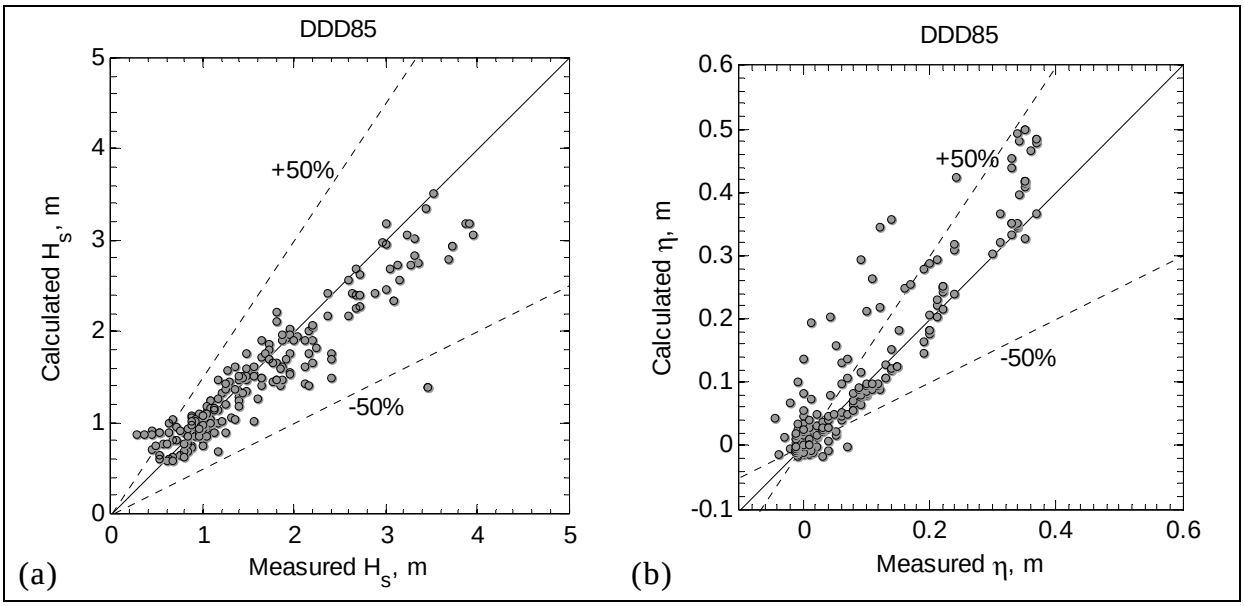

Figure 74. Comparison between measured and computed wave heights (a) and mean water levels (b) for DDD85.

Seelig reef experiments

For the laboratory experiments of Seelig (1983), only the wave setup over the reef top and maximum wave runup data were available for comparison with numerical model results. Figure 75 shows a comparison of measured and calculated wave setup on the reef top obtained from the ABJB07 and DDD85 wave breaking formulas. Both formulas were applied with default parameters and no data fitting was performed. These formulas produced similar wave setup estimates for lower setup values (less than 0.8 m). For wave setup values greater than 0.8 m, the ABJB07 formula overpredicted wave setup on the reef. The largest differences between ABJB07 and DDD85 are for the laboratory cases with measured setup values greater than 0.8 m.

Numerical tests were performed to investigate the sensitivity of results obtained with the ABJB07 wave breaking formula for different values of the breaking intensity factor B. The best fit to laboratory measurements (Figure 75) was obtained by using a value of the wave breaking parameter $B = 1.3$. Therefore, the wave breaking formulations for the Seelig experiments were performed with ABJB07 ($B = 1.3$) and DDD85 ($\kappa = 0.15$ and $\Gamma = 0.4$). The wave height on the reef top, beach slope, and deepwater wavelength were used in the calculation of maximum wave runup with the empirical relation of Mase (1989). Figure 76 shows a comparison of calculated and measured maximum wave runup for Seelig's laboratory experiments. ABJB07 and DDD85 produced similar maximum runup values in agreement with measurements. Using the overpredicted wave setup from the ABJB07 formula, the maximum runup estimates (greater than 5 m) were slightly improved. For runup less than 5 m, both formulations produced similar runup estimates, and results were within the 50 percent error bands. The percent differences between model results with two wave breaking formulas and data yielded similar errors because, for random waves, the maximum runup strongly depends on the input waves. The runup values greater than 6 m were all underestimated (negative bias).

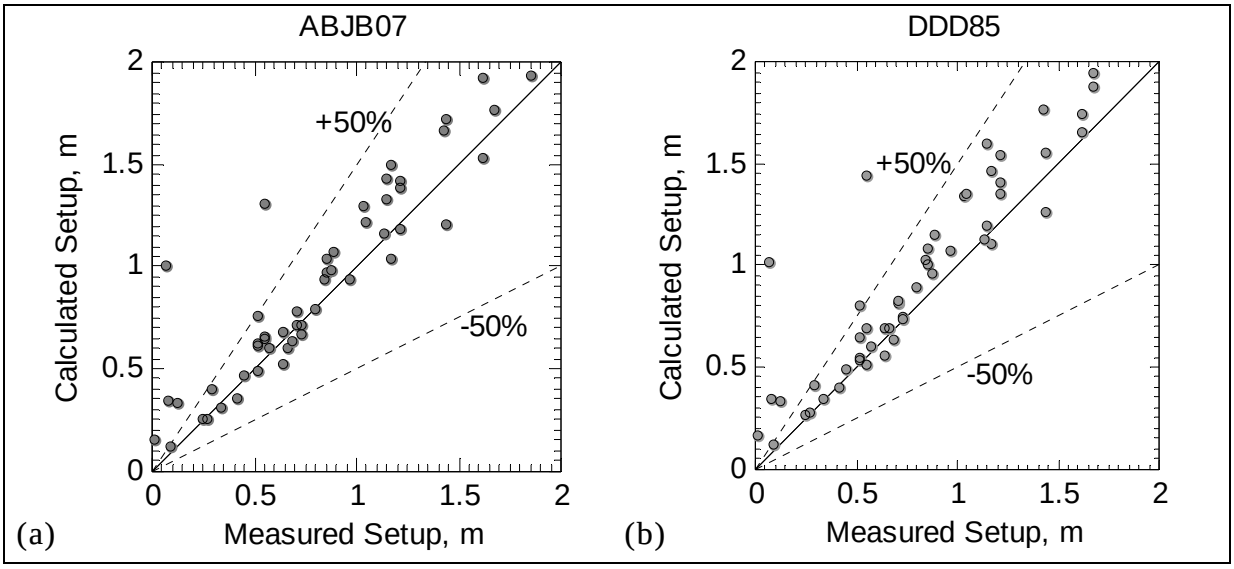

Figure 75. Comparison between measured and calculated (WAV1D) wave setup for Seelig experiments.

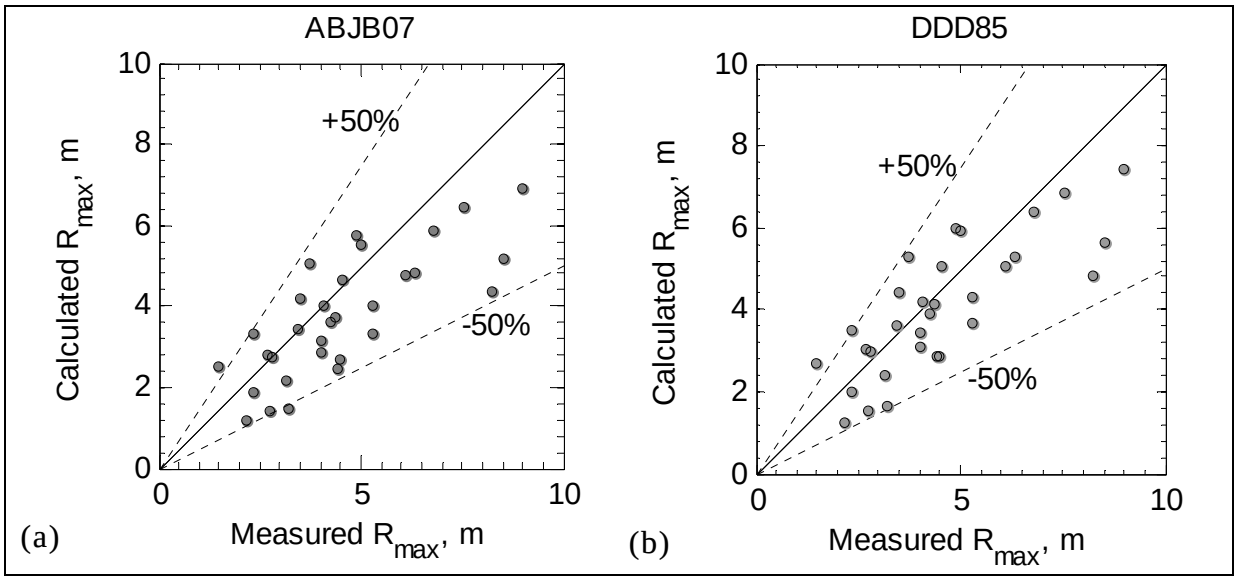

Figure 76. Comparison between measured and calculated (WAV1D) R_{max} for Seelig experiments.

CHL reef experiments

In this section, the ABJB07 and DD85 formulations implemented in the WAV1D model are compared to data from the CHL laboratory experiments (Thompson 2005). Calculated cross-shore variation and point measurements of wave height and mean water level are shown in Figures 77 for Test 5, which had a 2 m initial water depth over the reef top. Both wave height and wave setup estimates were within the 50 percent of measurements after the model was calibrated with data, which provided values of $B = 1.0$, $\kappa = 0.15$, and $\Gamma = 0.4$ in the ABJB07 and DDD85 wave breaking formulations, respectively.

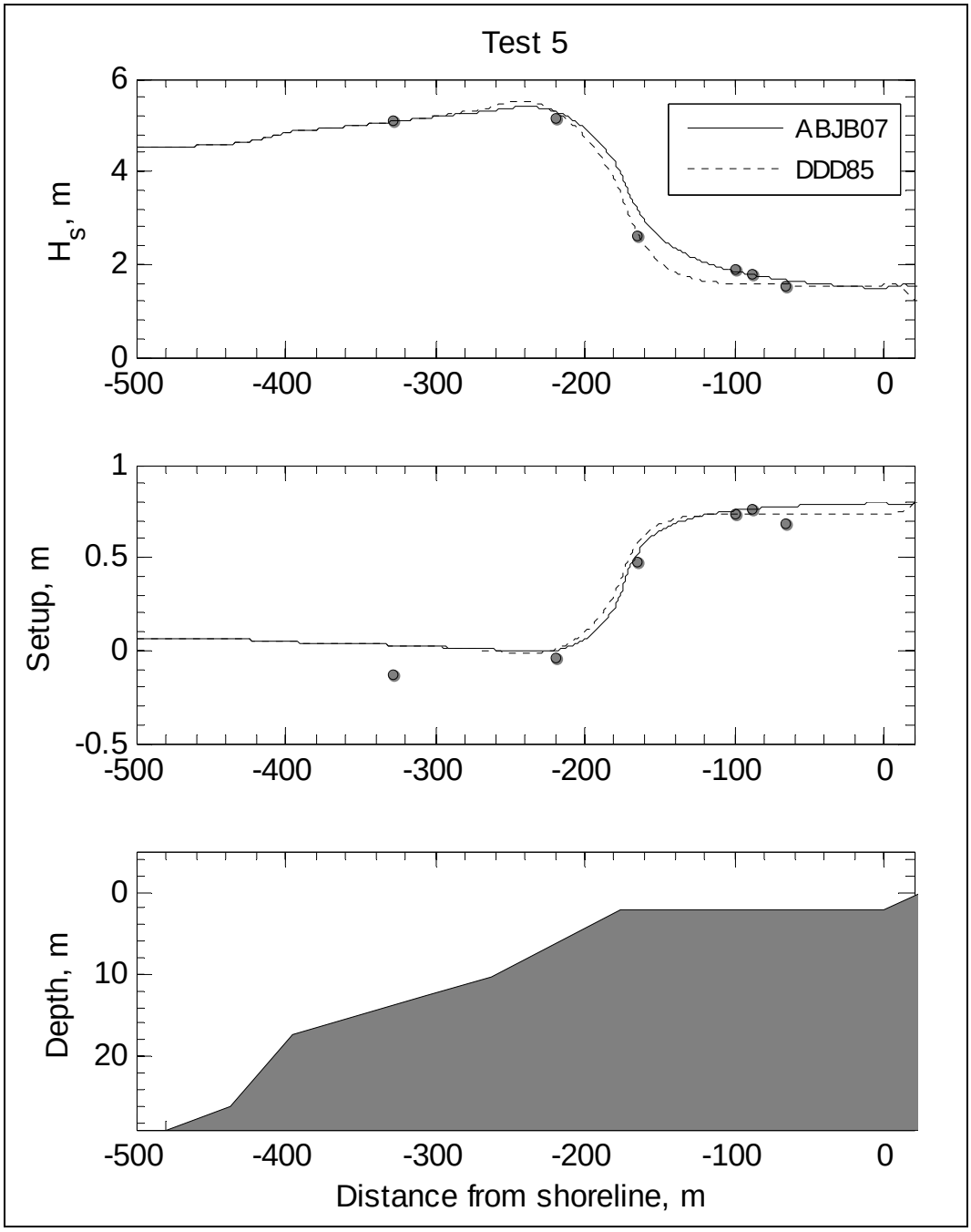

Figure 77. Comparison between measured and calculated (WAV1D) wave heights and mean water levels for Test 5 (H_s = 6.28 m, T_p = 15.0 sec, d_r = 2.01 m) of CHL experiments.

Figure 78 shows the comparison of the calculated cross-shore variation of wave heights and mean water level, and point measurements for Test 11, which had a 0 m initial water depth on the reef. Wave height estimates from WAV1D on the reef top are reasonable. However, mean water level measurements were not available for the 0 m initial water depth on the reef top, and only the model results are plotted.

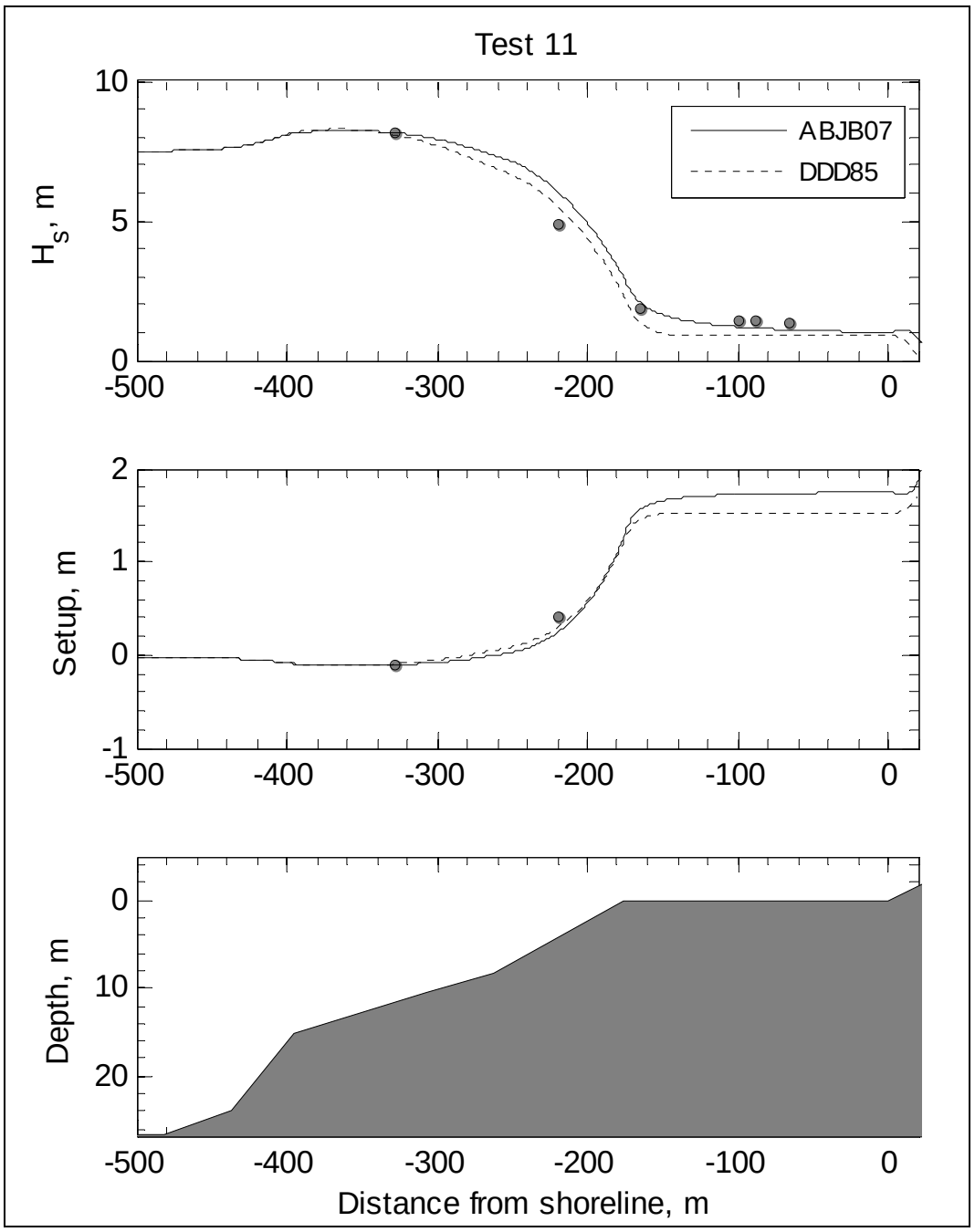

Figure 78. Comparison between measured and calculated (WAV1D) wave heights and mean water levels for Test 11 (H_s = 7.49 m, T_p = 15.0 sec, d_r = 0.0 m) of CHL experiments.

Scatter plots of the measured and predicted wave heights and mean water levels for all of the Test 11 CHL experiments are shown in Figures 79 to 82. Similar to the results for the Seelig reef experiments, the ABJB07 formula provides a comparatively better estimate of wave heights on the reef top than the DDD85 formula for the CHL experiments. This may be because DDD85 reaches a constant stable wave height over the reef top, and this

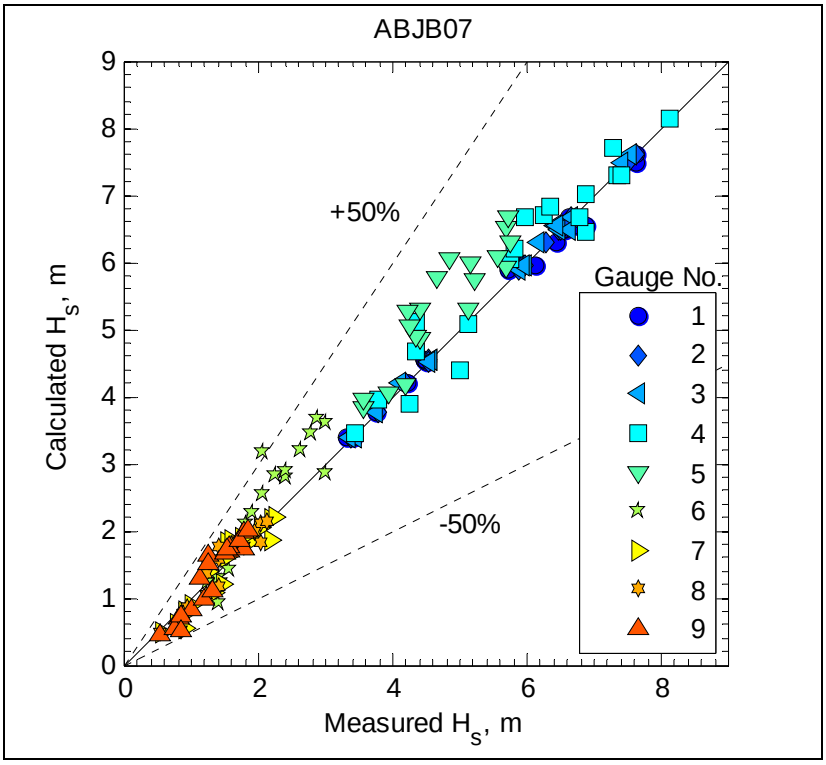

Figure 79. Comparison between measured and calculated (WAV1D) significant wave heights for CHL experiments.

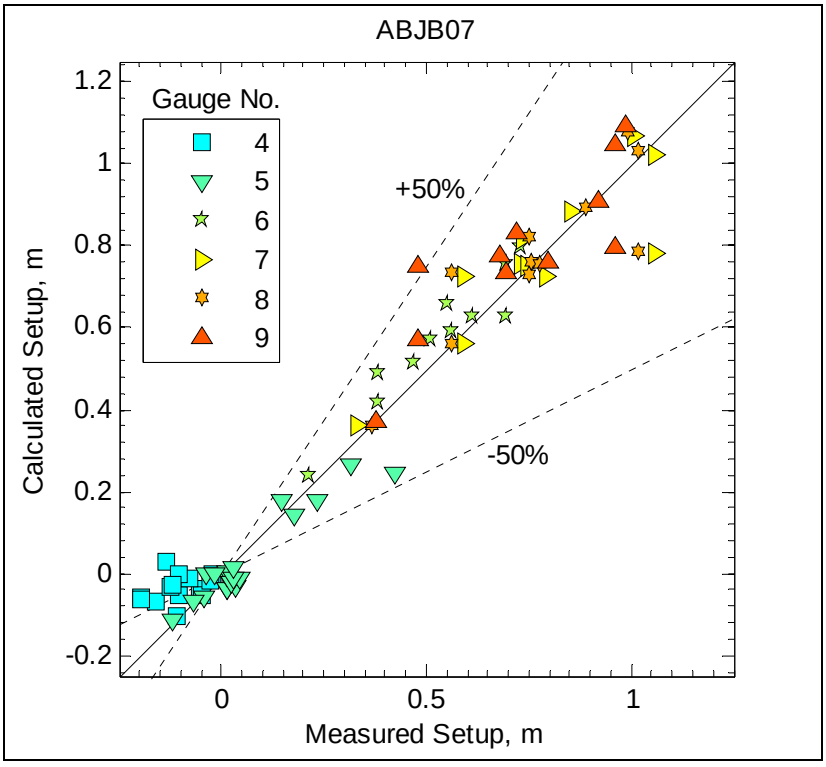

Figure 80. Comparison between measured and calculated (WAV1D) mean water levels for CHL experiments.

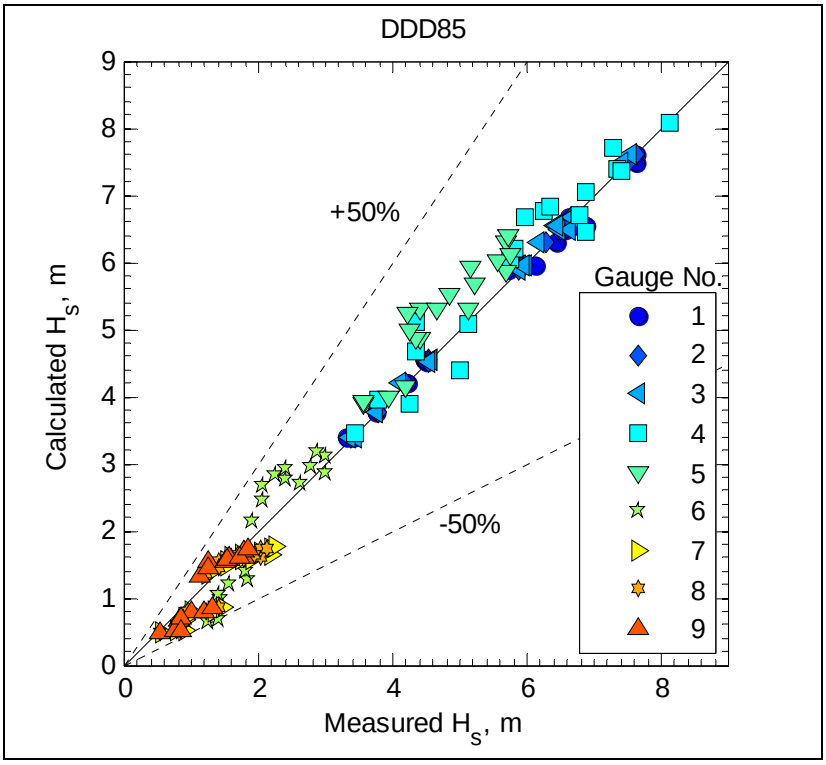

Figure 81. Comparison between measured and calculated (WAV1D) significant wave heights for CHL experiments.

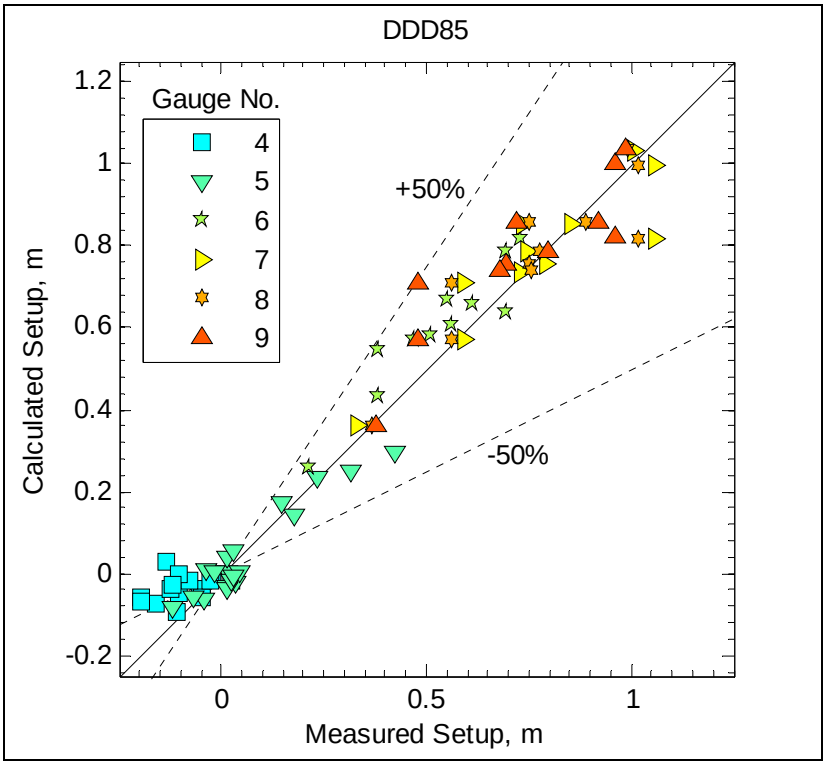

Figure 82. Comparison between measured and calculated (WAV1D) mean water levels for CHL experiments.

could be partially circumvented by decreasing the stable wave height parameter in DDD85 from its initial value of 0.42. Both of the ABJB07 and DDD85 formulas produced results that were in reasonable agreement with the measured mean water levels (wave setup) when the initial water depth over the reef was not zero. For the zero water depth, the measured setup values from these experiments were much less as compared to predicted values. Additional studies are needed to further investigate possible causes of these observed differences.

The wave setup generally increases as the water depth over the reef top decreases. This is expected from the cross-shore momentum equation (Equation 12). However, previous studies (Gourlay 1994) have found that there may be a threshold below which wave setup may not occur.

University of Michigan reef experiments

The laboratory experiments conducted for an in-depth study of wave transformation processes over a fringing reef profile at the University Michigan (UM) are simulated with the WAV1D model. Results for a selected set of test conditions are presented in this section. These experiments considered effects of both wind and waves, wave setup and wave runup on a fringing reef (Demirbilek et al. 2007a).In this numerical study, the simulations are performed for wave-only test conditions, and compared to the laboratory measurements. Effects of wind and other additional information concerning analysis of the data, and detailed numerical simulations, can be found in Demirbilek and Nwogu (2007). Comparisons between calculated and measured wave heights, mean water levels, and wave height variation for wave-only test conditions are provided here.

Twenty nine wave-only test conditions were performed in the UM experiments. Two examples of the wave transformation and setup (mean water level) are shown in Figures 83 and 84. The predicted and measured significant wave heights and mean water levels generally compare well. Calculated wave heights at Gauges 4 and 5 (forth and fifth from the left) have a negative bias. As waves propagate over the reef face, they shoal and break near the reef edge. ABJB07 predicts less energy dissipation over the reef face and consequently, a larger wave height is obtained near the reef edge. Over the reef top, the DDD85 formula overestimates wave heights because waves have attained a stable wave height. In contrast, a fraction of the waves continues in the ABJB07 formula to break over the reef top and more dissipation occurs. Overall, the ABJB07 and DDD85 formulas

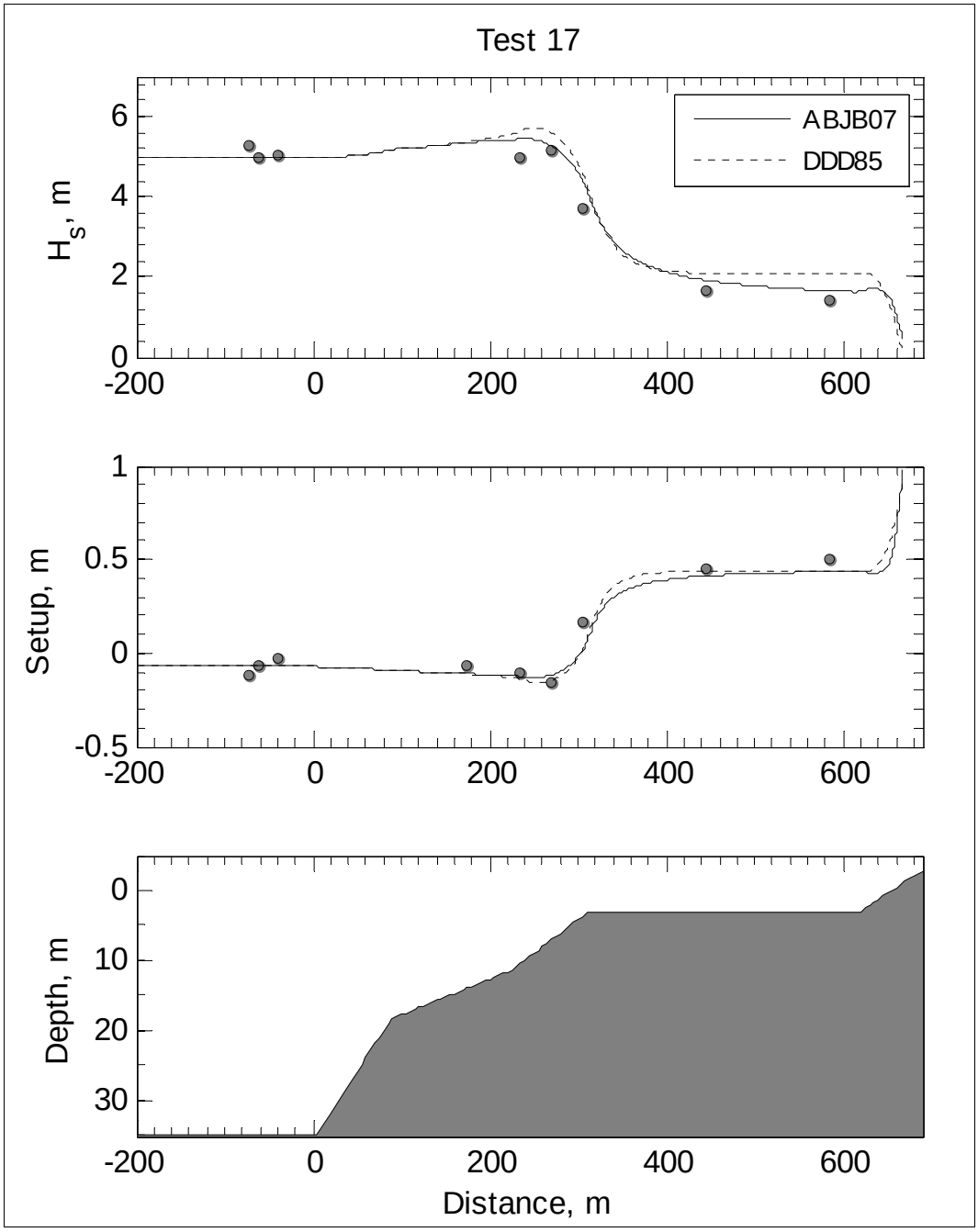

Figure 83. Comparison between measured and calculated (WAV1D) significant wave heights and mean water levels for Test 17 of UM experiments.

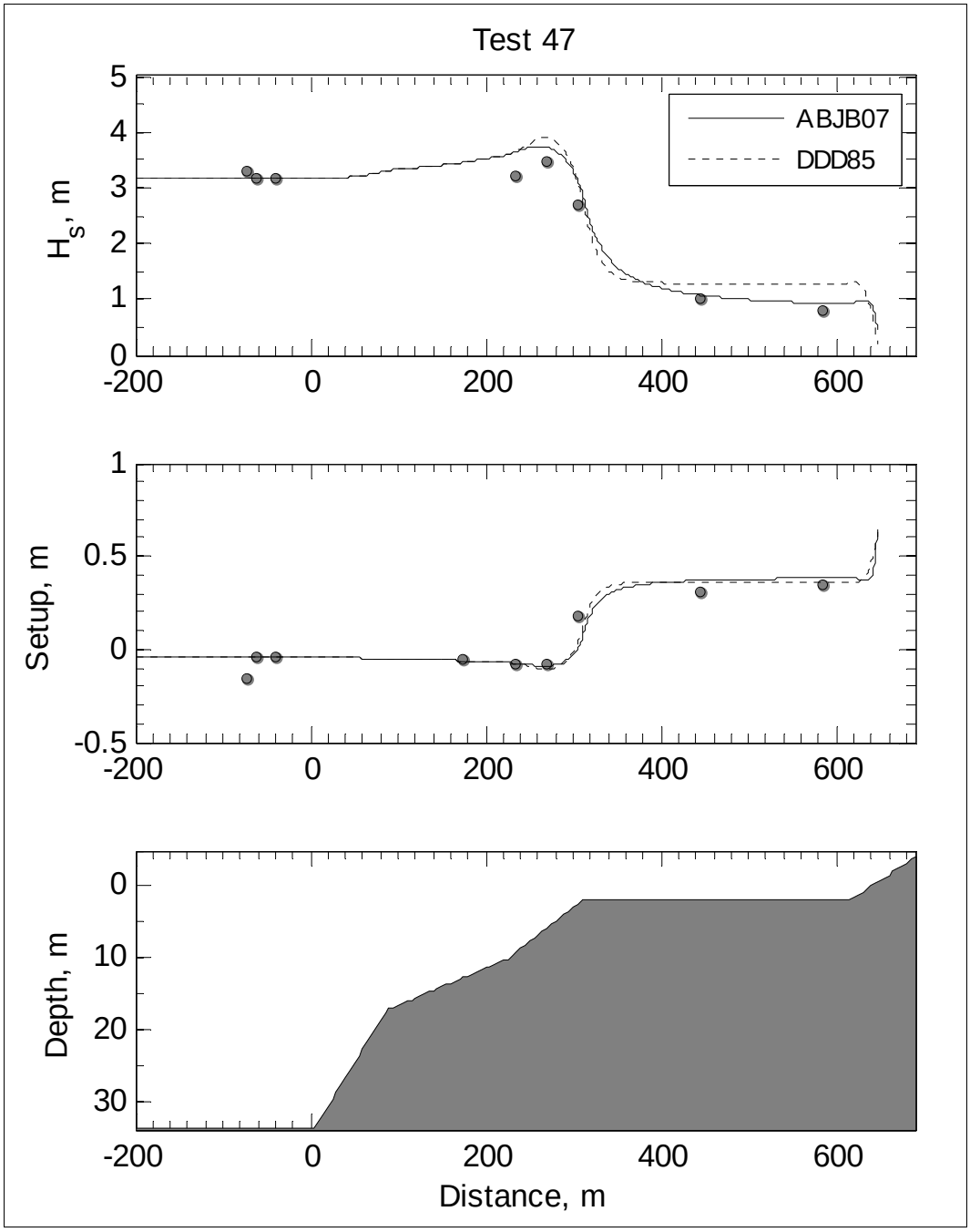

Figure 84. Comparison between measured and calculated (WAV1D) significant wave heights and mean water levels for Test 47 of UM experiments.

predicted similar water levels over the reef top. Since wave setup is directly proportional to the gradient in wave height squared, and inversely proportional to the local water depth (Equation 12), most of the wave setup is generated in a narrow region near the reef edge, where wave heights dissipate rapidly over relatively shallow water depths. The ABJB07 and DDD85 formulas predict similar wave heights near the reef edge. Because the setup generated over the reef top is relatively small, the wave setup calculated with these formulas over the reef top is not much different.

A scatter plot of measured and predicted significant wave heights for the ABJB07 formulation is shown in Figure 85. Except for a few data points at Gauge 7, predictions are within the 50-percent of the measured values (dashed lines). Gauge 7 is located on the reef edge (surf zone), and has the largest scatter. This may be attributed to limitations of the two wave breaking formulas used in WAV1D or result from the fact that the gradients in wave height and setup are large in this area. Consequently, model errors in either of these contribute to errors in the other parameters caused by feedback. Small errors in the gauge position could also contribute to these errors. In addition, for the smooth UM and CHL reef experiments, values of the wave breaking intensity parameter $B = 1.26$ and $B = 1.3$ were determined by calibrating WAV1D with laboratory data. The equivalent parameter κ in the wave breaking formulation of Dally et al. (1985) was assumed to be 0.17 for reef applications reported here. In real world applications, values of parameters κ, Γ, and B can be based on model validation with site-specific field data because these parameters can vary with the geometry of the reef profile, reef surface roughness, water levels, type of wave breaking, and incident wave height and wave period.

The calculated water levels using the ABJB07 formula are compared to measured data for all 9 gauges in Figure 86. The calculated mean water levels over the reef top (Gauges 8 and 9) are compared to data, and the scatter is within 50 percent, indicative of the difference between the model and data. The largest scatter at Gauge 7 is probably caused by deficiencies in the ABJB07 wave breaking formulation.

Wave heights over the reef face predicted with the DDD85 formulation are also within 50 percent of the measured values (Figure 87). Wave heights at the reef edge (Gauge 7) are overestimated. Wave heights over the reef top (Gauges 8 and 9) are over-predicted in some cases by more than 50 percent. Similar to the ABJB07 formulation, the calculated wave setup results on the reef top from the DDD85 formulation were in reasonable agreement with data (Figure 88).

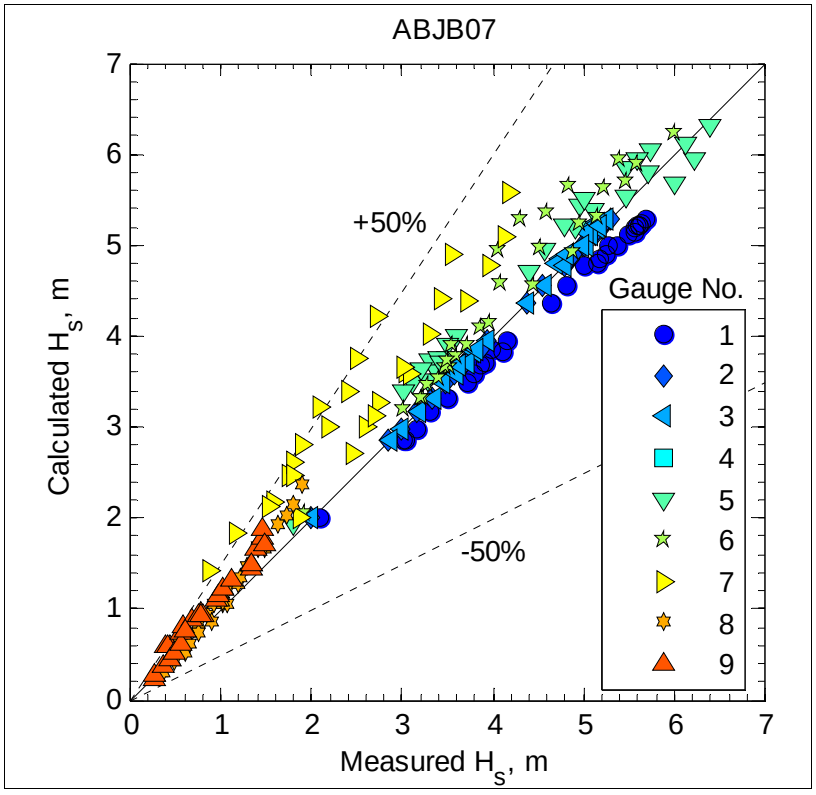

Figure 85. Comparison between measured (UM experiments) and calculated (WAV1D) significant wave with ABJB07 formulation.

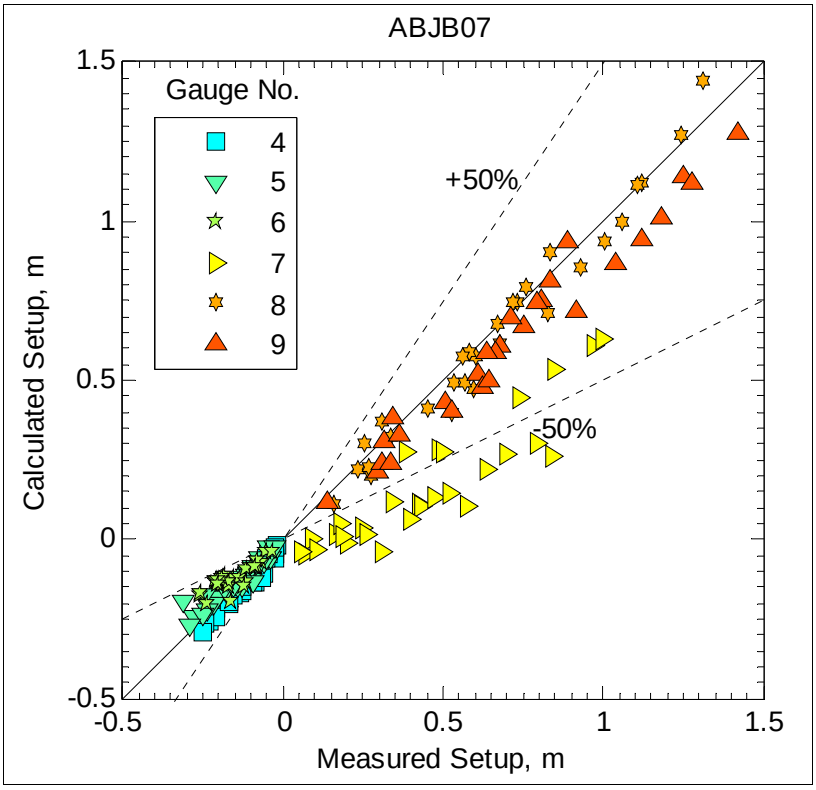

Figure 86. Comparison between measured (UM experiments) and calculated (WAV1D) significant wave with ABJB07 formula.

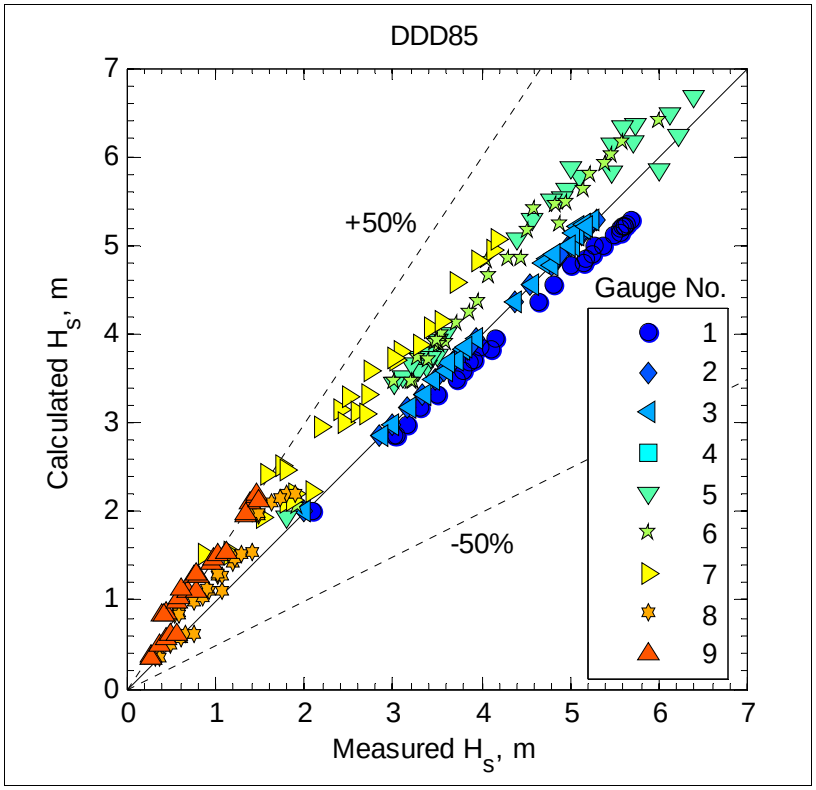

Figure 87. Comparison between measured (UM experiments) and calculated (WAV1D) significant wave using DDD85 wave breaking formula.

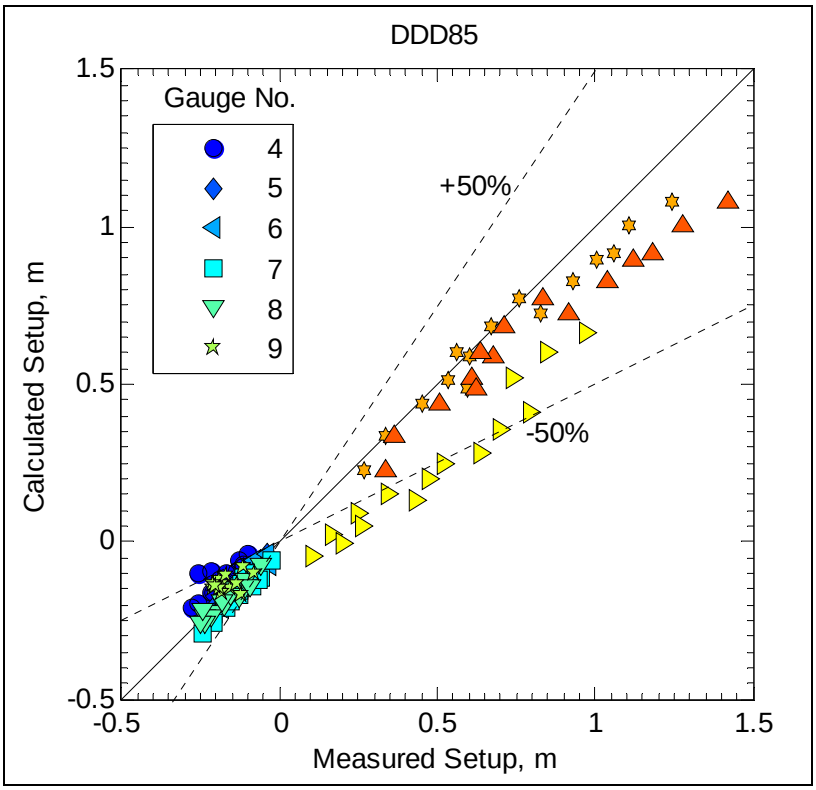

Figure 88. Wave setup comparison between measured (UM experiments) and calculated (WAV1D) using ABJB07 wave breaking formula.

Figure 89 shows the comparison between the measured and calculated wave runup obtained from Equation (22) using the ABJB07 and DDD85 models for wave height. Maximum runup and 2-percent runup estimates were defined with respect to the SWL. The calculated and measured wave runup values were in good agreement, and calculated values are over-estimated at lower runup values ($R_{2\%} < 1.5$ m). The WAV1D model with the ABJB07 formulation underestimates the largest runup values because of excessive wave dissipation on the reef top. In contrast, the DDD85 formula overestimates the largest runup values because wave dissipation over the reef top cannot be accurately modeled with this formula. In general, the WAV1D model with the ABJB07 formulation does a slightly better job of predicting the wave runup than the DDD85 formula. The difference in calculated runup values for the two breaking formulations is mainly caused by the difference in wave heights estimated on the reef top. The DDD85 formula consistently predicts larger wave heights on the reef top and larger runup values than the ABJB08 formula.

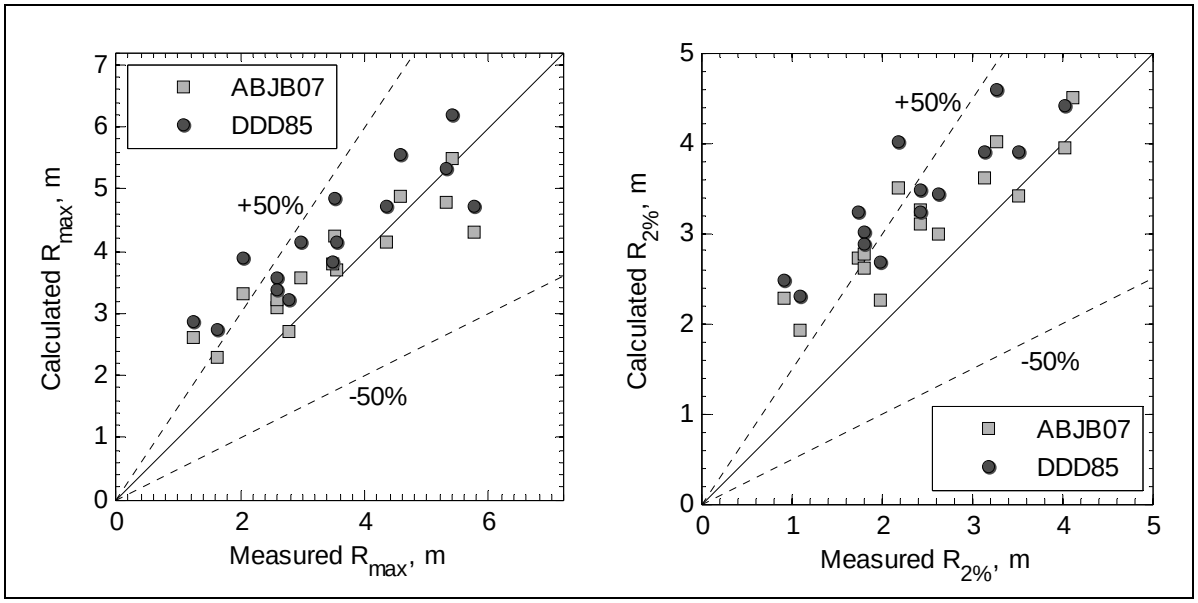

Figure 89. Maximum runup and 2-percent runup comparison between measured (UM experiments) and calculated (WAV1D with ABJB07 and DDD85).

6 Discussion of Results

BOUSS-1D was run essentially in a “blind mode” without attempting to calibrate the model parameters with data for simulations in this report. There were no assumptions made a priori about characteristics of wave transformation and type of waves breaking along the reef zones. The motivation was to objectively evaluate the BOUSS-1D model capabilities using data from four laboratory experiments. Calculated wave heights from deepwater to the toe of beaches located at the end of reef profiles, wave setup/setdown on top of reefs, and resulting wave runup estimates on shorelines are provided in Chapter 3 and Appendices A-E.

Overall, the BOUSS-1D model predicted wave height, wave setup, and runup using default values of model parameters for bottom friction and turbulence, and compared well with data. The model was able to reproduce measured cross-shore wave height variation, wave setup and wave runup for a wide range of conditions tested in these four laboratory experiments. It was determined that the largest difference, varying from 10 to 50 percent for different experiments between model estimates and data, occurred at the lowest water level. The range for the average difference varied from 10 to 20 percent for different water levels in the four laboratory experiments. BOUSS-1D determined the position of wave breaking accurately by employing default parameters for 95 percent of the wave conditions simulated. In general, the calculated wave heights were slightly underestimated. The mean water level was also slightly underestimated near the point of wave breaking for test conditions with low water above the reef crest. The agreement with data for wave setup on the reef was better than that for the calculated wave heights. It is possible that this could caused by the type of methods that were used in the calculation of the wave heights (i.e., zero-crossing, spectral, averaging, and also setup is an integral process in the wave height calculation). For the Hayman Island reef, a summary of the calculated and measured water levels and wave heights for all test conditions is provided in the scatter plots (Figures 11 and 12 in Chapter 3).

For the Guam fringing reef experiments of Seelig, the wave runup estimates from BOUSS-1D were compared to data for two lagoon widths (150 and 525 m), and two water levels (0 and 2 m). The data analyzed from

these experiments were presented (Seelig 1983) as a function of a dimensional parameter ($H_{m0}^2 T_p$), similar to the wave energy flux parameter. Because the values of significant wave height H_{m0} and T_p corresponding to each experimental data point were not provided, BOUSS-1D simulations were performed for three spectral peak periods (T_p = 8, 12, and 16 sec), and the significant wave height (H_{m0}) values from 3 to 10 m. The default values of bottom friction and turbulence coefficients and other critical BOUSS-1D model parameters were used (C_f = 20, $l = H_s$, $\delta_{min} = H_s/1{,}000$, C_v = 0.2). There were no spatial measurements of waves available from these experiments along the reef profile. Calculated results showed that wave heights increase as waves move over the reef face, the largest height occurred at the reef crest, and subsequently waves broke and wave height decreased over the reef lagoon. This was a common trend for typical spatial evolution of wave transformation occurring over the four fringing-type reefs investigated in this study.

For the Seelig reef experiments, BOUSS-1D slightly underestimated the maximum runup height for the largest and longest waves. No attempt was made to improve model-data match by adjusting values of critical model parameters (e.g., bottom friction coefficient, turbulent length scale, etc.). The BOUSS-1D results for these experiments are summarized in Figures 16 and 17 in Chapter 3. Comparison of the calculated ponding levels (water level change in the reef lagoons) to the best-fit empirical formula of Seelig at the middle of lagoon is provided in Figure 16. For the range of parameters considered, a good agreement was obtained between the calculated ponding levels from BOUSS-1D and the data. Using default parameters, a good agreement was also obtained (Figure 17) between the calculated maximum wave runup values and the best-fit empirical formula to experimental results.

For the CHL reef experiments, nineteen test conditions (Table 4 in Chapter 3) were simulated with BOUSS-1D using different values of significant wave height, peak period, and water level. Input conditions included two spectral peak periods, two water levels, and a range of incident wave heights. These experiments had time series data available, allowing a detailed investigation of wave evolution on the reef starting from deepwater to the shallower end of the reef profile. The simulations performed using default model parameters captured the physical processes well, including variation of wave height on the reef slope, reef crest and on the reef flat. BOUSS-1D was able to reproduce the measured

wave evolution on the reef in these experiments without a model calibration. Additional simulations were performed to investigate the role of water depth on the reef flat in the parameterized bottom friction term that was expected to play a significant role on wave energy dissipation occurring on the reef flat. Simulations were made using a lower value of the friction coefficient (f_w = 0.004 or C_f = 50) as opposed to the default values (f_w = 0.01 or C_f = 30). Results indicated that a lower friction coefficient value did not affect wave height seaward of the reef, but this increased wave heights on the reef (5 to 10 percent). Using a lower friction coefficient improved the model-data match on the reef for some tests (Figure 22).

The significant wave height variation over the reef profiles presents only a small piece of information about wave energy transformation across reefs, because it fails to describe how wave energy is being redistributed in the frequency domain resulting from nonlinear wave-wave interactions. The same value of significant wave height can be obtained with ten different spectra shapes having a different distribution of wave energy spectral densities over the frequencies. This makes it necessary to compare the spectral densities of the measured and predicted surface elevation time-histories in order to assess the appropriateness of numerical models for wave transformation processes over reefs. The Fourier transforms were used to calculate the spectral densities of the water surface elevation time-histories from BOUSS-1D.

Comparison of the measured and predicted wave spectra at several gauges were shown (Figures 24-27) in tandem with the corresponding time series comparisons, as shown in Figures 28-31. These comparisons revealed the importance of nonlinear wave-wave interactions occurring in the shallow water depth, showing that the wave energy at the incident wave frequencies has completely dissipated at the gauges closest to the beach. For this reef application, BOUSS-1D has successfully reproduced the nonlinear energy transfer to the low frequency modes, but some differences exist between the measured and predicted wave spectra (Figures 24-27). Calculated wave spectra from BOUSS-1D on the reef (Gauges 7 and 9) had several distinct low-frequency oscillation peaks, as in the measured spectra. The numerical model overestimated the lowest peak and underestimated the second peak, but overall comparison was good.

Results indicate that the low-frequency motions over the reef flat become increasingly dominant at lower water level tests when the flat reef section is initially dry. BOUSS-1D shows the nonlinear steepening and highly asymmetric profile of post-breaking wave evolution on this shallow section of the reef. At the same time, there are differences in the detailed time-domain characteristics of measurements and model results. This is expected because the wave breaking process is parameterized in the Boussinesq model, and consequently the model may not capture the fine details of post-breaking waves on a wave-by-wave basis. Because the BOUSS-1D breaking criterion (ratio of the water particle velocity at the crest to the phase velocity) is computed with the linear theory, and uses the average zero-crossing period of the incident wave train, this can lead to an early (later) initiation of the breaking of individual waves depending on their frequencies and amplitudes.

For the CHL experiments, measured and calculated wave runup time series were also compared. In these experiments, wave runup heights were measured with capacitance-wire wave gauges, and data were too noisy with unexplained jumps that did not permit a one-to-one comparison with the numerical model predictions. The envelope of peak runup elevations were deduced from the digitized videos, and time-histories of runup peaks obtained were then compared to the calculated runup peaks by BOUSS-1D. The numerical model predicts a detailed time history of both runup/rundown elevation processes. The magnitudes of runup peaks from BOUSS-1D were similar to observed peaks (Figures 29-32). While a statistical analysis of wave runup gauge data was not necessary, because BOUSS-1D performed remarkably well in these experiments, such an analysis may be helpful in field applications for selecting appropriate values of Boussinesq model parameters to minimize differences between field data and calculated runup peaks. For the CHL experiments, a good agreement with data was obtained for the maximum runup heights (Table 5).

For the UM experiments, Demirbilek and Nwogu (2007) and Demirbilek et al. (2007b) provide detailed information about these laboratory experiments conducted in a wind-wave flume at UM. A comparatively wider flat reef top was used in the UM experiments as compared to those used in the Seelig and CHL experiments. This adjustment was made to accurately represent the width of the prototype reef profile in Guam. The UM experiments were designed to provide insight into the physics of nonlinear wave

transformation and runup on fringing reef profiles with known bottom friction properties as opposed to exact model scale reproduction of hydrodynamic processes over natural coral reefs. Both wind and wave effects on reefs were investigated.

Steep and highly nonlinear waves used in the UM experiments generally broke on the reef face in a plunging manner, after breaking waves reformed as bores that propagated across the reef flat toward the beach. Both undular and fully turbulent type bores were observed on the flat reef section. The ability of BOUSS-1D for simulating these bores was studied through parameterization of the wave breaking process using three different wave breaking formulations. These include a SBF, a PBF-1, and a modified plunging breaking formulation based on phase velocity instead of the orbital velocity at the wave crest (PBF-2). Details of these formulations are provided by Demirbilek and Nwogu (2007).

The SBF and PBF-1 both predicted similar post-breaking wave heights, with SBF slightly underestimating wave setup over the reef flat. On the other hand, the PBF-2 in which the bores were advected with the wave celerity overpredicted the wave height near the break point and yielded higher wave setup over the reef. This would suggest that the spatial distribution of eddy viscosity controls the wave setup over the reef, and calculated significant wave height, mean water level variation across the reef flat and wave runup on the beach are dependent on the type of wave breaking formulations used in the numerical models (Figures 33 and 37). The results further suggest that without accounting for wave turbulence, present numerical models cannot describe the complex physics of highly nonlinear wave processes taking place over the reef flat section starting from the onset of wave breaking location to the beach. Comparison of time-histories of measured and predicted water surface elevation (Figures 43-46) reveal the strength of BOUSS-1D in reproducing the time evolution of the sea surface at different gauge locations along the reef profile.

The sensitivity of model predictions to the parameterized bottom friction coefficient was investigated in the UM experiments for two values of friction coefficients (C_f = 30 and 24). Measured and predicted significant wave height and mean water level variations across the reef compared favorably for the higher friction (C_f = 24), which also led to a better match of the post-breaking wave height estimates at low water levels (h_r = 0.0

and 1.6 cm). But, an increased friction at higher water levels (h_r = 3.1 and 5.1 cm) did not improve model estimates. From these results, it was concluded that a depth-dependent value of bottom friction coefficient (e.g., Manning's type) would be necessary for waves propagating over very shallow reefs. On the shallow reef flats, greater water depths support larger wave heights that can produce stronger bottom velocities, suggesting larger values of C_f at higher water levels. A depth-dependent bottom friction coefficient can be incorporated by using the Manning formulation (i.e., friction coefficient to vary as the 6th root of the water depth). A spatially-varying friction coefficient feature will be available in the next version of Boussinesq model.

The UM experiments provide the most extensive set of time series measurements of waves over the reef and runup on the beach. Demirbilek and Nwogu (2007) obtained the spectral densities of the water surface elevation time-histories to investigate the evolution of wave spectra over the reef-beach system. The nonlinear transformation of the wave energy spectra in deep water from incident-wave frequencies to infragravity (low-frequency) motions over the reef flat is evident from the wave spectra shown in Figures 39-42 and 49. These results show that BOUSS-1D accurately reproduces the nonlinear energy transfer to the low-frequency modes with an underprediction in some cases, and overprediction for other cases. Results shown in Figures 34-49 demonstrate the model's suitability for nonlinear wave transformation processes over reefs, including wave profile steepening, highly asymmetric wave profiles developing following post-breaking waves in relatively shallow depths, and the emergence of amplitude and phasing of the low-frequency motions over the reef flat sections. Model results show that low-frequency motions totally dominate at the lower water levels on reef flats, and these control estimates of wave setup and wave runup over reefs and adjoining beaches. The model cannot capture fine details of the post-breaking waves on a wave-by-wave basis because the wave breaking process is parameterized in the Boussinesq model (Demirbilek and Nwogu 2007).

The second model evaluated is RBREAK2, which is based on shallow-water wave equations. RBREAK2 is not suitable for calculating waves in the deep water off the four reefs investigated in this study. The model was developed for beaches and coastal structures located in shallow water. In reef applications, the seaward boundary of the RBREAK2 computational domain was chosen to be the toe of reefs. Additionally, in all applications

with test conditions where the reef flat was initially dry, RBREAK2 would treat the reef crest as the shoreline (beach). For these cases, it was further necessary to add 0.1 m to the water depth for such test conditions to force the beach to be correctly situated. With these two constraints and even though RBREAK2 could not explicitly model wave breaking, the model was applied to four experiments as used in the evaluation of BOUSS-1D. An explicit dissipative Lax-Wendroff method with a limited upwinding scheme used in the RBREAK2 is excessively dissipative. For waves traveling over long distances, severe numerical wave energy dissipation caused by this numerical scheme renders the calculated wave heights to be unrealistically low. Therefore, the model should not be used over long distances or as a wave transformation model in applications.

In the four experiments, the friction factor f was used to tune the RBREAK2 model. A default friction of 0.05 was used and this value was adjusted to calibrate the model with laboratory data. To prevent overtopping, the length of the beach was also adjusted when necessary. RBREAK2 calculations at lower water levels produced decreasing significant wave heights and increasing setup on the reef flats. Generally, predicted wave heights were within 50 percent of measurements, and the model overestimated wave setup at higher water levels (Figures 52-55).

For the Hayman Island reef, RBREAK2 provided better estimates of wave heights for longer period waves shoaling over the reefs, and wave setup estimates for shorter wave periods. Wave heights were significantly underpredicted for shorter period waves. The maximum vertical runup elevations calculated from RBREAK2 were generally less than laboratory measurements. For the Seelig reef experiments, ponding levels were underestimated for higher depths over the reef. Model results for low and high water levels were similar (Figure 54). The calculated runup values were less than the measured values for nearly all cases. For the CHL experiments, the agreement between modeled and measured significant wave height and setup was good at low water levels as compared to high water levels over reef flats (Figures 53-58). For the UM experiments, calculated wave setup values for low wave periods agreed better with data along the reef face and were underestimated along the reef flat, but comparison showed improvement with increasing wave periods (Figures 61-66). Significant wave height and wave setup estimates from RBREAK2 for short wave periods compared less favorably with data at increasing water levels on reef flats. RBREAK2 underestimated wave runup by approximately

50 percent at 1 and 2 m water levels (Figures 68 and 69). Model results improved at the highest water level (3.25 m), but were surprisingly insensitive to the values of wave period.

The third model evaluated is WAV1D, based on a cross-shore energy flux and cross-shore momentum change. Two breaking relations are included as options. WAV1D was also evaluated with the four laboratory experiments used for the other numerical models. For the fringing reef geometries tested, the calculated wave heights and wave setups from the WAV1D model were generally in good agreement with measurements. Additional testing is required using field measurements and different reef profiles with high roughness to determine the model's suitability for prototype applications. This is necessary because WAV1D employs empirical wave breaking relations developed primarily for the planar beaches and smooth sloping structures, and thus care should be exercised in using the model for reef applications. As described in Chapters 3 through 5, wave breaking processes over fringing reefs are different from those on sandy beaches.

The breaking intensity used in the two empirical wave breaking formulas of WAV1D is a free parameter that must be carefully selected for fringing reefs because of their steep faces, high roughness and shallow depths. The parameter B was assumed to be 1.0 in the present study, which controls wave breaking dissipation and breaking intensity in the Alsina and Baldock (2007) formulation. The equivalent parameter κ in the wave breaking formulation of Dally et al. (1985) was assumed to be 0.15 for reef applications reported here. Values of these free parameters may be different for other reefs. For the smooth UM and CHL reef experiments, values of B = 1.26 and B = 1.3 were determined by calibrating WAV1D with laboratory data. In real world applications, values of parameters κ, Γ, and B can be based on model validation with site-specific field data because these parameters can vary with geometry of reef profile, reef surface roughness, water levels, type of wave breaking, and incident wave height and wave period.

The calculated wave setup from WAV1D was found to increase as a function of offshore wave height and water depth over the reefs. This trend was consistent with Equation 12. As waves started to break further offshore, model predicted wave setup values decreased substantially, suggesting that the accuracy of the model estimates depends on wave parameters offshore and over the reef zones in deeper water. Increasing the breaking

intensity factor B caused more wave energy loss in deepwater regions of reefs, and this in turn produced smaller values of wave setup on the reef flat. The calculated values of wave setup increased according to the cross-shore momentum equation (Equation 12) with decreasing water depth on the reef flat.

The rate of energy dissipation in WAV1D caused by wave breaking was found to be inversely proportional to the incident wave period. The energy decay coefficient may need to be parameterized as a function of wave period to consider this dependence. The wave energy decay coefficient is also expected to vary with the breaker type, and wave energy decay for plunging breakers more common for reefs may be greater than that for spilling breakers occurring on smooth planar beaches. Other free parameters in these empirical wave breaking formulations may also require calibration with data. These include the breaking wave height H_b in Alsina and Baldock (2007) and the stable wave height parameter Γ in Dally et al. (1985) used in these formulas. Because these parameters control the initiation and cessation of wave breaking, they determine the saturated wave height limit over reefs. Laboratory measurements used in this research suggest that the stable wave height parameter ($\Gamma = 0.42$) used in the saturated surf zone for sandy beaches is too high for the inner reef zones. Likewise, the breaking wave height based on Miche's criterion produced very low wave heights in the fringing reef applications studied. Additional research is needed to quantify and select appropriate parameters for the empirical wave breaking formulas that would account for different breaker types, wave dissipation, and reformation of broken waves over different reef geometries. The present study shows that reasonable estimates of wave height and water levels can be obtained over fringing reefs by calibrating WAV1D empirical coefficients with laboratory or field data.

For the Hayman Island experiments, WAV1D produced reasonable results as compared to laboratory data. There was a consistent offset between computed and measured wave setup/setdown. One could consider using a roller type wave breaking (e.g., Stive and De Vriend 1994) for this reef application to determine if the offset is related to types of wave breaking formulas. The model calculated wave heights and water elevations were within 50-percent of the data from the four laboratory datasets. A greater challenge remains in identifying appropriate values of several free parameters that would be best for field applications of WAV1D. This would

require a set of field data from several reef sites obtained for a range of wave conditions and water levels.

A number of comparative statistics for calculated wave height, wave setup, and wave runup from three numerical models are discussed next. The statistics are given for each reef experiment separately, and calculated (Equations 23-26) for the last gauge or model output nodal point closest to the toe of beach. The statistics given at a single point do not represent a full measure of the numerical model performances, and they do not represent the model's abilities to properly represent different wave processes over reefs. The most important statistics are those near the beach, which is typically the primary area of interest in terms of island flooding. The statistics at other locations along the reef can be different from these single-point statistics close to the beach. Nonetheless, the statistics presented are informative, and provide useful insight into each model performance.

The commonly used engineering statistics provided are the root-mean-square-error (RMSE), bias (defined as difference between calculated and measured), percent difference, and r^2 (coefficient of determination) where r is the correlation coefficient defined as

$$r = \frac{N\sum P_i O_i - \sum P_i \sum O_i}{\sqrt{N\sum P_i^2 - \left(\sum P_i\right)^2}\sqrt{N\sum O_i^2 - \left(\sum O_i\right)^2}} \tag{23}$$

where P_i and O_i represent respectively the values of the i-th prediction and observation (data). The mean percent difference is calculated as

$$MPD = \frac{100}{N}\sum_{1}^{N}\frac{P_i - O_i}{O_i} \tag{24}$$

The root mean square error (RMSE) is defined as

$$RMSE = \sqrt{\frac{1}{N}\sum_{1}^{N}(P_i - O_i)^2} \tag{25}$$

The bias is defined as

$$MBE = \frac{1}{N}\sum_{1}^{N}(P_i - O_i) \tag{26}$$

Summary statistics for the Hayman Island, Seelig, CHL, and UM reef experiments are provided in Tables 9-12, respectively, for wave height, wave setup, and maximum runup estimates. In general, the BOUSS-1D and WAV1D models performed quite well, with rms errors in wave height of 0.2 to 0.4 m, in wave setup of 0.1 to 0.2 m, and maximum runup of 1 to 1.5 m. RBREAK2 errors were generally larger for all parameters. Chapters 3 through 5 and Appendices A through E provide additional results and information about each numerical model performance.

Table 9. Statistics for Hayman Island reef experiments.

		H_s	$\bar{\eta}$
BOUSS-1D	RMSE	0.37	0.06
	Bias	-0.15	0.04
	% diff	-8	14
	r^2	0.52	0.94
RBREAK2	RMSE	0.77	0.20
	Bias	-0.67	0.16
	% diff	-64	30
	r^2	0.48	0.94
WAV1D	RMSE	0.33	0.05
	Bias	-0.15	-0.02
	% diff	-6	-13
	r^2	0.67	0.93

Table 10. Statistics for Seelig reef experiments.

		$\bar{\eta}$	R_{max}
BOUSS-1D	RMSE	0.15	0.25
	Bias	0.02	-0.01
	% diff	4	0
	r^2	0.90	0.98
RBREAK2	RMSE	0.24	1.18
	Bias	0.03	0.94
	% diff	26	-16
	r^2	0.69	0.86
WAV1D	RMSE	0.20	1.47
	Bias	0.08	0.81
	% diff	64	-14
	r^2	0.85	0.59

Table 11. Statistics for CHL reef experiments.

		H_s	$\bar{\eta}$
BOUSS-1D	RMSE	0.30	0.14
	Bias	-0.16	-0.12
	% diff	-9	-14
	r^2	0.81	0.96
RBREAK2	RMSE	0.33	0.27
	Bias	-0.13	-0.11
	% diff	-13	-15
	r^2	0.67	0.37
WAV1D	RMSE	0.20	0.12
	Bias	0.04	0.05
	% diff	10	10
	r^2	0.91	0.75

Table 12. Statistics for UM reef experiments.

		H_s	$\bar{\eta}$	R_{max}
BOUSS-1D	RMSE	0.23	0.06	0.95
	Bias	0.18	-0.02	-0.24
	% diff	9	-1	-21
	r^2	0.96	0.98	0.62
RBREAK2	RMSE	0.33	0.38	1.68
	Bias	0.19	-0.32	-1.27
	% diff	15	-39	-29
	r^2	0.52	0.57	0.44
WAV1D	RMSE	0.19	0.12	0.94
	Bias	-0.17	0.11	-0.44
	% diff	-20	13	-28
	r^2	0.98	0.97	0.73

7 Conclusions

Three different types of 1D numerical wave models (BOUSS-1D, RBREAK2, and WAV1D) were evaluated in this study with the four reef data sets obtained from physical modeling studies. Different fringing reef geometries were tested in these experiments, including one with a complex reef-lagoon-beach system, in which the beach was fronted by a lagoon, and the fringing reef had a complex profile consisting of different sloping sections with rapidly changing bathymetry. Two of the wave models (BOUSS-1D and WAV1D) successfully transitioned the incident waves across these reef systems and through the lagoon, and onto the beach slope. Because RBREAK2 is strictly a wave runup model, it could not be used as a wave transformation model for reefs, the model had to be started at the toe of reefs. A reasonable comparison is obtained between calculated wave height, wave setup, maximum runup, and ponding levels from three wave models and data from four physical model experiments.

In an earlier sensitivity study performed for the BOUSS-1D model, it was found that model results were sensitive to certain input parameters, particularly the Chezy bottom friction coefficient C_f and difficulties were reported for modeling large (near breaking) waves offshore of the reef. The model was also evaluated for plane slope experiments (Mase 1989), and similar problems were encountered in the calculation of wave runup on steep slopes (1:10) and very steep slopes (1:5). New wave breaking formulations included in BOUSS-1D have resolved these issues (see Chapters 3 and 7 for additional information). Improved maximum runup and lagoon ponding levels are obtained for the reef bathymetry modeled by Seelig (1983).

Three different schemes implemented in the Boussinesq model for wave breaking and dissipation processes over reefs and sloping permeable and impermeable structures are summarized in Chapter 3 of this report and details are provided elsewhere (Demirbilek and Nwogu 2007). Chapter 3 of this report on model evaluation provides a systematic and comprehensive description of the BOUSS-1D model application to the four physical model datasets. Overall, the model performed well in each experiment, and the predicted wave heights and runup estimates were in good agreement with measurements. For the CHL and UM experiments, the

BOUSS-1D model reproduced not only the overall trends, but also represented accurately the temporal and spectral characteristics of nonlinear wave transformation over fringing reefs. The time series data available from these experiments were used to investigate details of the wave-reef interaction processes.

The BOUSS-1D model capabilities were demonstrated in Chapter 3 of this report for the four laboratory reef experiments. Comparison of model predictions with data showed that the model was able to represent both time- and frequency-domain nonlinear wave transformation processes occurring over reefs. Examples of these processes include spatial and temporal variation of wave height and water level over reefs and lagoon systems, nonlinear evolution of the incident wave spectra over reef-lagoon bathymetries, wave profile steepening and highly asymmetric wave profiles resulting from post-breaking waves in relatively shallow depths, generation of amplitude and phasing of the low-frequency motions over the reef flat zone, and the statistical progression and evolution of the wave runup process over a sloping beach face. The BOUSS-1D model showed the low-frequency motions were stronger at lower water levels, overwhelming the wind-wave spectral components. The model calculated wave runup predictions compared favorably to data, aside from some slight discrepancies in the details of fluctuations present in some of the measured time series records. For the four experiments, the magnitudes of predicted maximum runup heights were similar to observed peaks, and the differences between model estimates and data ranged from 10 to 30 percent. Because the wave breaking and dissipation processes were parameterized in the Boussinesq model, the model could not capture fine details of post-breaking waves on a wave-by-wave basis.

The RBREAK2 model results for the Seelig reef experiments showed that model estimates for maximum runup and ponding level correlated well to data. Because the actual test conditions were unknown, the model was run for a range of wave parameters, and calculated results were within the scatter of data plots (Seelig 1983). Additional runs showed that RBREAK2 output was sensitive to the friction factor f_{wp} for rough slopes, and less sensitivity for smooth slopes. RBREAK2 does not calculate the breaking wave process but dissipates the energy using an energy approximation algorithm in the surf zone. This modeling approach has limitations for non-breaking waves transforming over wide and deep reef systems. RBREAK2 may be used for calculation of wave runup, but not for wave

height and water level variation over reef profiles starting from deep water to toe of the beach. This is because the numerical scheme implemented in RBREAK2 is highly dissipative. Consequently, the model cannot be used for wave transformation along reefs. The input wave parameters to RBREAK2 are those at the toe of the structure or beach for estimate of wave runup heights.

WAV1D provided good qualitative results for the four datasets used in this evaluation. Model predictions were generally within 50 percent of data for the majority of test conditions. Although model estimated wave heights and wave setup did not match data on the reef face in some tests, the model calculated wave heights on the reef top were quite reasonable. This suggests that energy-balance based wave models can provide reasonable estimates of wave heights without representing details of wave processes and despite neglecting the infragravity wave energy that dominates wave energy spectra on top of reefs. The WAV1D model is intended for practical applications, and is appropriate for studies requiring wave estimates for reefs projects. The model may also be used in engineering projects provided that various coefficients used in the parametric wave breaking dissipation formulas can be judiciously selected by calibrating the model with field data. In fact, it is recommended that the three wave models (BOUSS-1D, RBREAK2, and WAV1D) should be tested in prototype field applications to determine their applicability in engineering works. The next SWIMS report in this series will address the application of numerical models and provide findings from several field applications.

References

Ahrens, J. P., and M. S. Heimbaugh. 1988. *Approximate upper limit of irregular wave runup on riprap*. Technical Report CERC-88-5. Vicksburg, MS: U.S. Army Engineer Coastal Engineering Research Center.

Alsina, J. M., and T. E. Baldock. 2007. Improved representation of breaking wave energy dissipation in parametric wave transformation models. *Coastal Engineering* 54:765-769.

Asmar, W. E., and O. G. Nwogu. 2006. Finite volume solution of Boussinesq-type equations on an unstructured grid. *Proceedings International Conference on Coastal Engineering '06* V1. San Diego, CA, 73-85.

Baldock, T. E., P. Holmes, S. Bunker, and P. Van Weert. 1998. Cross-shore hydrodyamics within an unsaturated surf zone. *Coastal Engineering* 34:173-196.

Battjes, J. A., and J. P. F. M. Janssen. 1978. Energy loss and setup due to breaking of random waves, *Proceedings Coastal Engineering*, ASCE, 569-587.

Battjes, J. A., and J. J. F. Stive. 1985. Calibration and verification of a dissipation model for random breaking waves. *Journal of Geophysical Research* 90(C5):9159-9167.

Booij, N., R. C. Ris, and L. H. Holthuijsen. 1998. A third generation wave model for coastal regions, Part 1: Model description and validation. *Journal Geophysical. Research* 104(C4), p. 7,649.

Dally, W. R. 1992. Random breaking waves: field verification of a wave-by-wave algorithm for engineering applications. *Coastal Engineering* 16:369-397.

Dally, W. R., R. G. Dean, and R. A. Dalrymple. 1985. Wave height variation across beaches of arbitrary profile. *Journal Geophysical Research* 90(C6):11,917-11,927.

Demirbilek, Z., and O. G. Nwogu. 2007. *Boussinesq modeling of wave propagation and runup over fringing coral reefs, model evaluation report*. ERDC/CHL-TR-07-12. Vicksburg, MS: U.S. Army Engineer Research and Development Center.

Demirbilek, Z., and V. Panchang. 1998. *CGWAVE: A coastal surface water wave model of the mild slope equation*. Technical Report CHL-98-26. Vicksburg, MS: U.S. Army Engineer Waterways Experiment Station.

Demirbilek, Z., O. G. Nwogu, and D. L. Ward. 2007a. *Laboratory study of wind effect on runup over fringing reefs, Report 1: Data report*. ERDC/CHL-TR-07-4. Vicksburg, MS: U.S. Army Engineer Research and Development Center.

Demirbilek, Z., L. Lin, and A. K. Zundel. 2007b. *WABED model in the SMS: Part 2. Graphical interface*. ERDC/CHL CHETN-I-74. Vicksburg, MS: U.S. Army Engineer Research and Development Center.

Demirbilek, Z., A. Zundel, and O. Nwogu. 2005a. *BOUSS-2D wave model in the SMS: I. Graphical interface*. ERDC/CHL CHETN-I-69. Vicksburg, MS: U.S. Army Engineer Research and Development Center.

_____. 2005b. *BOUSS-2D wave model in SMS: II. Tutorial with examples*. ERDC/CHL CHETN-I-70. Vicksburg, MS: U.S. Army Engineer Research and Development Center.

Gerritsen, F. 1980. Wave attenuation and wave setup on a coastal reef. *Proceedings 17th International Conference on Coastal Engineering*. Sydney, Australia: New York, ASCE, 444-461.

Gourlay, M. R. 1994. Wave transformation on a coral reef. *Coastal Engineering* 23:17-42.

_____. 1996a. Wave setup on coral reefs. 1. Setup and wave-generated flow on an idealized two dimensional horizontal reef. *Coastal Engineering* 27:161-193.

_____. 1996b. Wave setup on coral reefs. 2. Setup on reefs with various profiles. *Coastal Engineering* 28:17-55.

Grasmeijer, B. T. and B. G. Ruessink. 2003. Modeling of waves and currents in the nearshore: parametric vs. probabilistic approach. *Coastal Engineering* 49:185-207.

Hardy, T. A., I. R. Young, R. C. Nelson, and M. R. Gourlay. 1991. Wave attenuation on coral reefs. *Australian Civil Engineering Transactions* 33:17-22.

Headquarters, U.S. Army Corps of Engineers. 2002. *Coastal Engineering Manual*. EM 1110-2-1100. Washington, DC: U.S. Army Corps of Engineers (in 6 volumes).

Jaffe, B. E., and B. M. Richmond. 1993. Overwash variability on the shoreline of Guam during Typhoon Russ. *Proceedings Seventh International Coral Reef Symposium* V1. Guam, 257-264.

Janssen, T. T., and J. A. Battjes. 2007. A note on wave energy dissipation over steep beaches. *Coastal Engineering* 54:711-716.

Jensen, M. S. 2001. *A study of coastal zone problems related to coral-sand beaches in East Africa – with special attention to coastal erosion*. A report supported and published by Danish International Development Agency (DANIDA), p.56.

Kennedy, A. B., Q. Chen, J. T. Kirby, and R. A. Dalrymple. 2000. Boussinesq modeling of wave transformation, breaking and runup. *Journal of Waterway, Port, Coastal and Ocean Engineering* 126:39-47.

Kobayashi, N., and M. T. Poff. 1994. *Numerical model RBEAK2 for random waves on impermeable coastal structures and beaches*. Research Report No. CACR-94-12. Newark, DE: Center for Applied Coastal Research, Ocean Engineering Laboratory, University of Delaware.

Kobayashi, N., A. K. Otta, and I. Roy. 1987. Wave reflection and runup on rough slopes. *Journal of Waterway, Port, Coastal, and Ocean Engineering* 113(3):282–298.

Larson, M., and Kraus, N. C. 1991. Numerical model of longshore current for bar and trough beaches, *Journal of Waterway, Port, Coastal, and Ocean Engineering* 117(4):326-347.

Li, Y., and F. Raichlen. 2002. Non-breaking and breaking solitary wave runup. *Journal of Fluid Mechanics* 456:295-318.

Longuet-Higgins, M. S., and R. W. Stewart. 1964. Radiation stress in water waves: A physical discussion with applications. *Deep Sea Research* 11.

Lowe, R. J., J. L. Falter, M. D. Bandet, G. Pawlak, M. J. Atkinson, S. G. Monismith, and J. R. Koseff. 2005. Spectral wave dissipation over a barrier reef. *Journal of Geophysical Research* 110(C04):1-16.

Lugo-Fernandez, A., H. H. Roberts, and J. N. Suhayada. 1998. Wave transformation across a Caribbean fringing-barrier coral reef. *Continental Shelf Research* 18:1,099-1,124.

Mase, H. 1989. Random wave runup height on gentle slope. *Journal of Waterway, Port, Coastal and Ocean Engineering* 115(5):649-661.

Massel, S. R., and R. M. Brinkman. 2001. Wave-induced setup and flow over shoals and coral reefs. Part 1. A simplified bottom geometry case. *Oceanologia* 43:373-388.

Massel, S. R., and M. R. Gourlay. 2000. On the wave modeling of wave breaking and wave setup on coral reefs. *Coastal Engineering* 39:1-27.

Nakaza, E., and M. Hino. 1990. Bore-like surf beat in a reef zone caused by wave groups of incident short period waves. *Fluid Dynamics Research* 7:89-100.

Nwogu, O. 1993a. On the generation of infragravity waves by shoaling multi-directional waves. *Proceedings of the Second International Symposium on Ocean Wave Measurement and Analysis, WAVES '93*, New Orleans, LA, 1-14.

Nwogu, O. 1993b. Alternative form of Boussinesq equations for nearshore wave propagation. *Journal of Waterway, Port, Coastal and Ocean Engineering* 119(6):618-638, ASCE.

Nwogu, O. G. 1996. Numerical prediction of breaking waves and currents with a Boussinesq model. *Proceedings 25th International Conference on Coastal Engineering* 4:4,807-4,820.

Nwogu, O., and Z. Demirbilek. 2001. *BOUSS-2D: A Boussinesq wave model for coastal regions and harbors*. ERDC/CHL TR-01-25. Vicksburg, MS: U.S. Army Engineer Research and Development Center.

Nwogu, O. G., and Z. Demirbilek. 2006. Nonlinear wave interaction with submerged and surface-piercing porous structures. *Proceedings International Conference on Coastal Engineering '06* V1. San Diego, CA, 287-299.

_____. 2007. Numerical simulation of wave runup and overtopping with Boussinesq-type equations. (Accepted for publication in *Coastal Engineering*).

Ogg, J. G., and J. A. Koslow. 1978. The impact of typhoon Pamela, 1976, on Guam's coral reefs and beaches. *Pacific Science* 32:105-118.

Roberts, H. H. 1975. Physical processes in a fringing reef system. *Journal of Marine Research* 33:233–260.

Seelig, W. 1983. Laboratory study of reef-lagoon system hydraulics. *Journal of Waterway, Port, Coastal and Ocean Engineering* 109:380-391.

Smagorinsky, J. 1963. General circulation experiments with the primitive equations. *Monthly Weather Review* 91:99-164.

Smith, J. M, A. R. Sherlock, and D. T. Resio. 2001. *Steady state spectral wave model user's manual*. Coastal and Hydraulics Laboratory Technical Report ERDC/CHL-TR-01-12. Vicksburg, MS: U.S. Army Engineer Research and Development Center.

Shore Protection Manual. 1984. 4th ed., 2 Vol, U.S. Army Engineer Waterways Experiment Station. Washington, DC: U.S. Government Printing Office.

Stive, M. J. F., and H. J. De Vriend. 1994. Shear stress and mean flow in shoaling and breaking waves. *Proceedings 24th International Conference on Coastal Engineering*. Kobe, NY: ASCE, 594–608.

Svendsen I. A., and O. Brink-Kjaer. 1972. Shoaling of cnoidal waves. *Proceedings 13th International Conference on Coastal Engineering*. New York: ASCE, 365–383.

Thompson, E. F. 1980. *Energy spectra in U.S. coastal waters*. Technical Report CERC-80-2, Vicksburg, MS: U.S. Army Engineer Coastal Engineering Research Center.

_____. 2005. *A physical model study for investigation of wave processes over reefs*. Coastal and Hydraulics Laboratory unpublished letter report. Vicksburg, MS: U.S. Army Engineer Research and Development Center.

Thornton, E. B., and R. T. Guza. 1983. Transformation of Wave Height Distribution. *Journal of Geophysical Research* 88(C10):5,925-5,938.

Titov, V. V, and C. E. Synolakis. 1995. Modeling of breaking and non-breaking long-wave evolution and runup using VTCS-2. *Journal of Waterway, Port, Coastal and Ocean Engineering* 121:308-316.

Vernon, J. E. N. 1986. *Corals of Australia and the Indo-Pacific*. Honolulu, HI: University Hawaii Press, p. 644.

Zhao, L., V. Panchang, W. Chen, Z. Demirbilek, and N. Chhabbra. 2001. Simulation of wave breaking effects in two-dimensional elliptic harbor wave models. *Coastal Engineering* 42:359-373.

Appendix A: Additional Results for Hayman Island Reef Experiments

Results of BOUSS-1D simulations for Hayman Island reef are described in Chapter 3. Results for additional test conditions listed in Table 3 are provided in this section of the report. Comparison with other numerical models and data is described in Chapter 6.

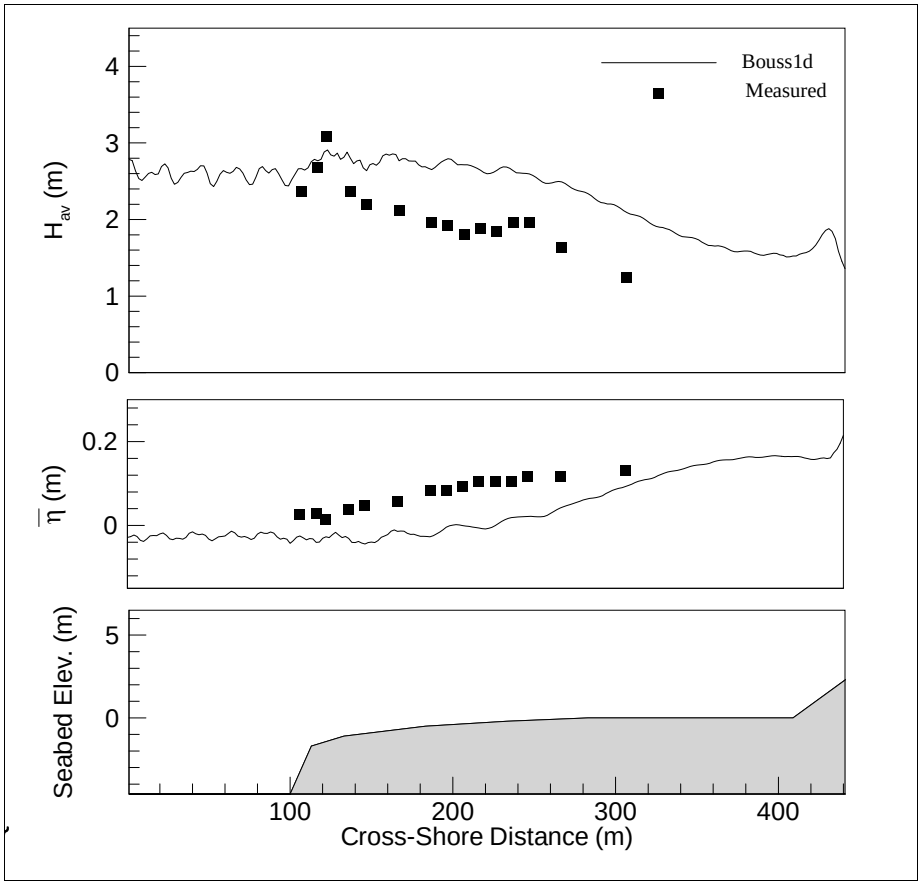

Figure A1. Test run 13 (SWL = 3.4 m, *H* = 2.63 m, *T* = 5.9 sec).

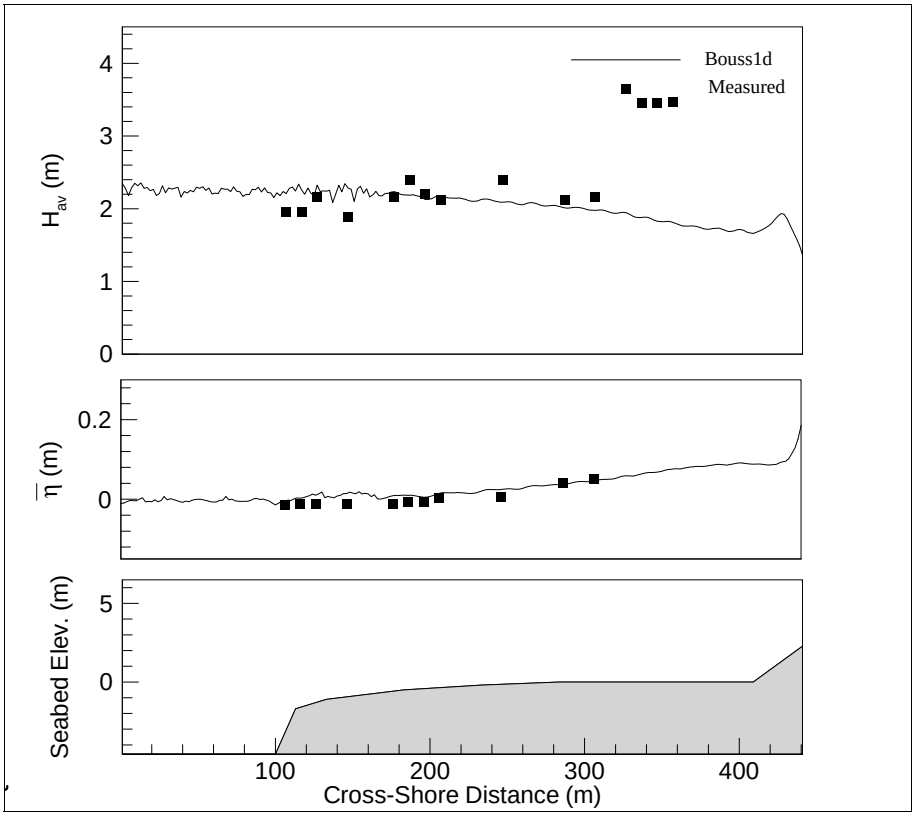

Figure A2. Test run 14 (SWL = 3.4 m, H = 2.19 m, T = 5.4 sec).

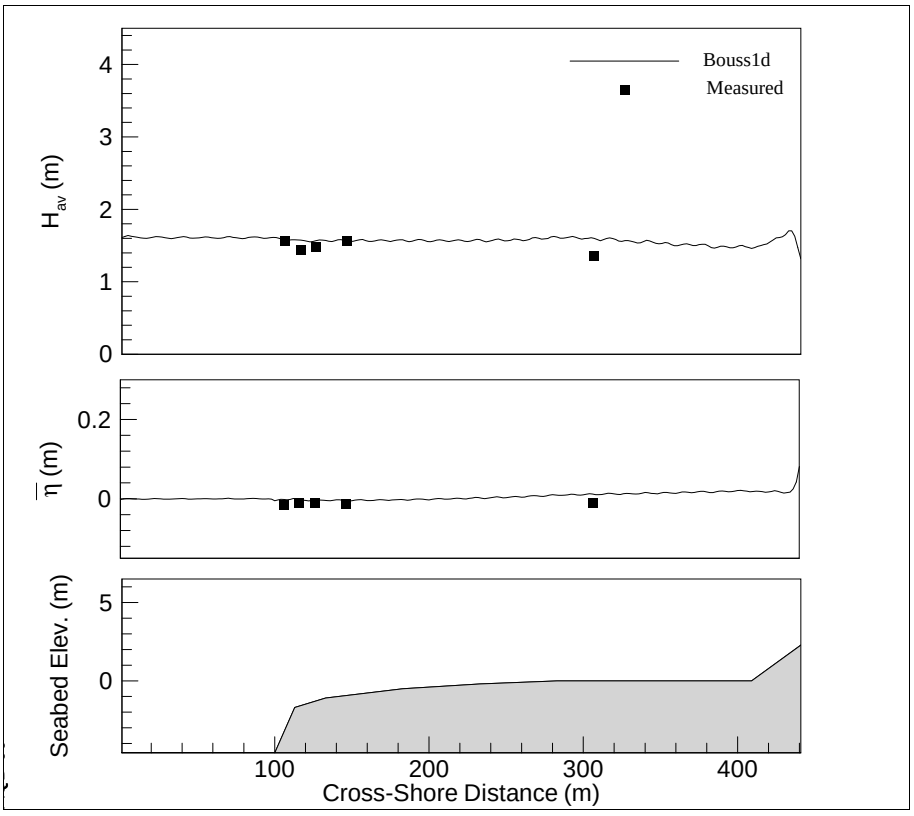

Figure A3. Test run 15 (SWL = 3.4 m, H = 1.6 m, T = 4.7 sec).

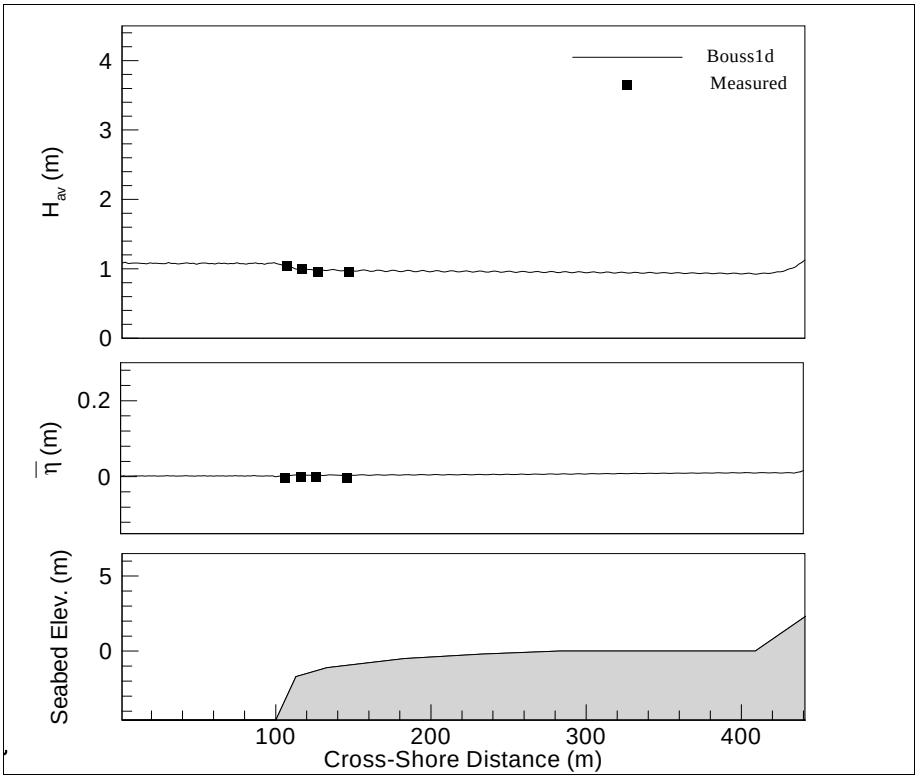

Figure A4. Test run 16 (SWL = 3.4 m, *H* = 1.05 m, *T* = 3.8 sec).

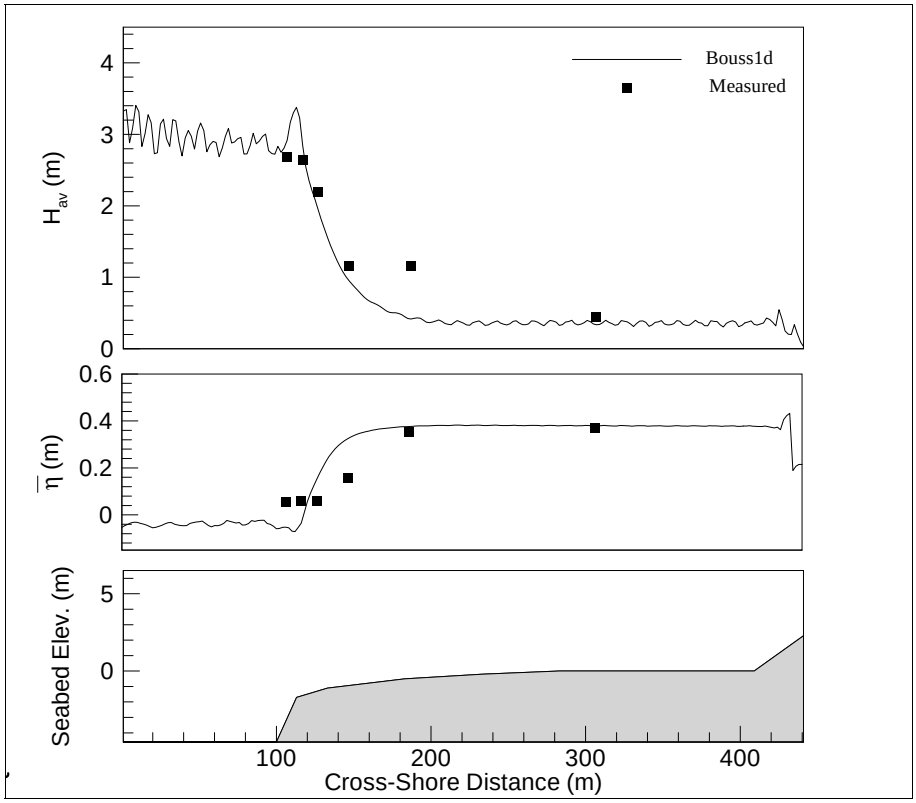

Figure A5. Test run 23 (SWL = 1.4 m, *H* = 3.03 m, *T* = 5.8 sec).

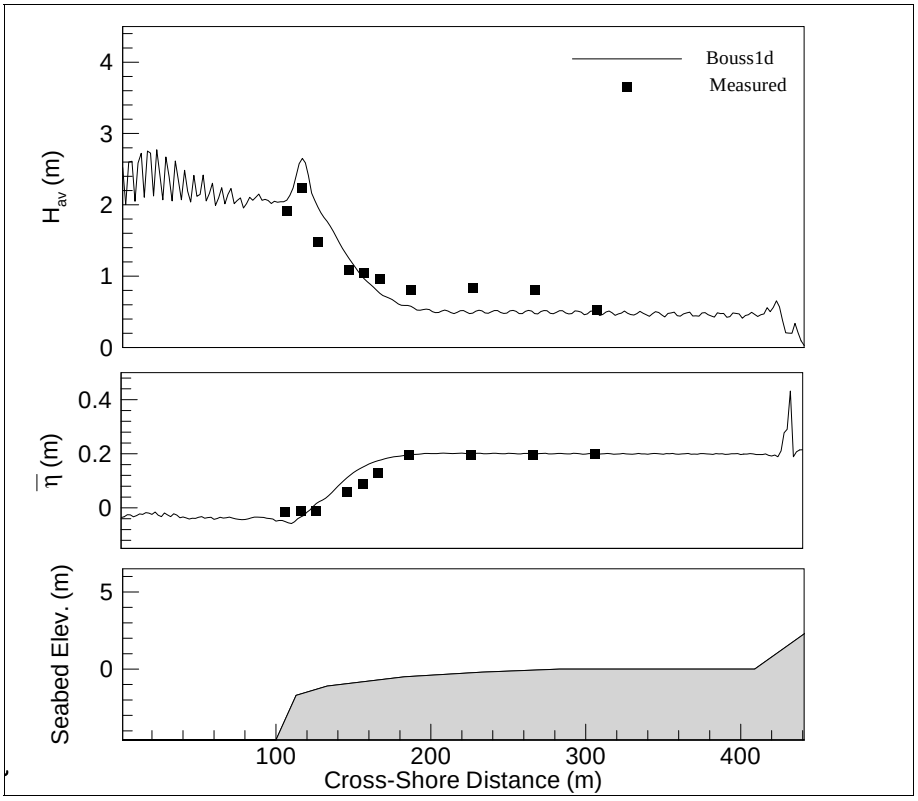

Figure A6. Test run 24 (SWL = 1.4 m, *H* = 2.07 m, *T* = 5.4 sec).

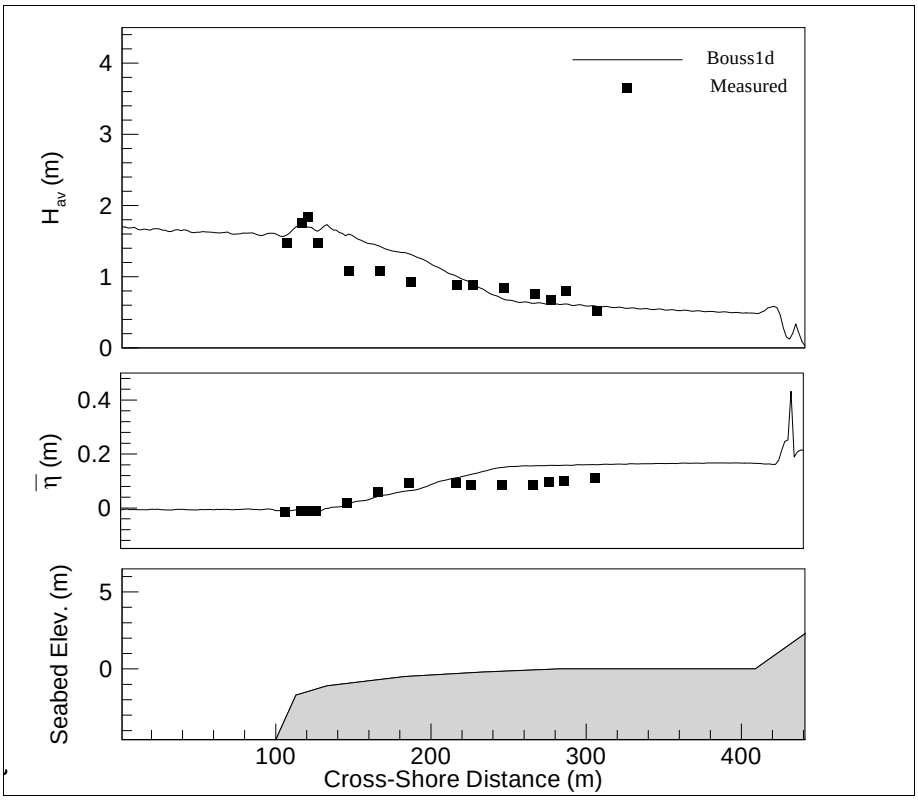

Figure A7. Test run 25 (SWL = 1.4 m, *H* = 1.6 m, *T* = 4.7 sec).

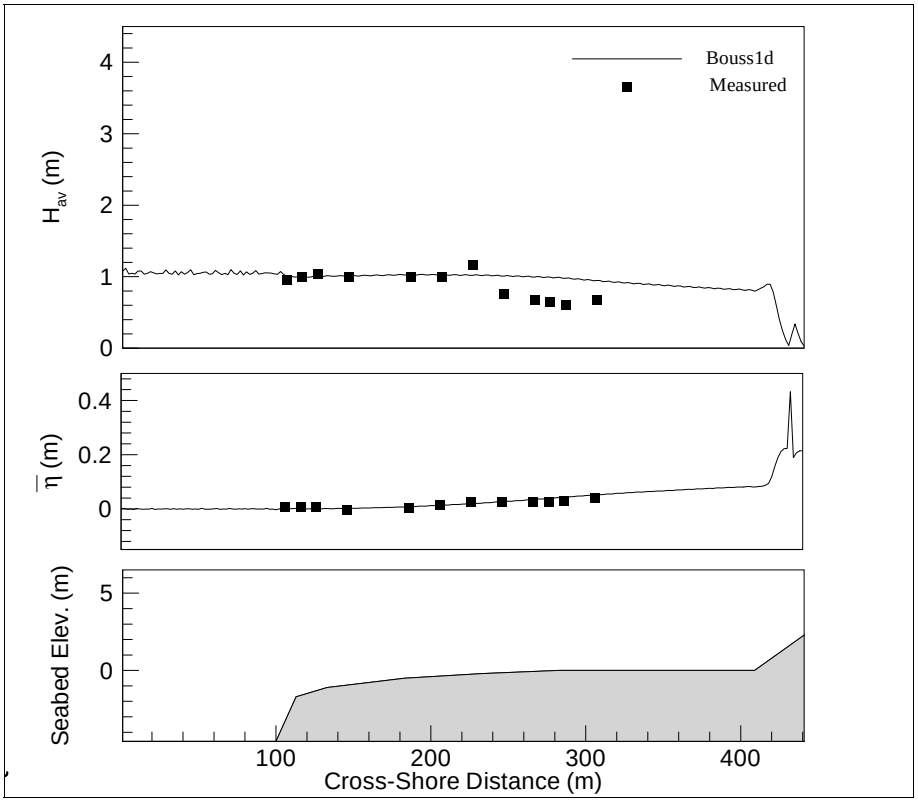

Figure A8. Test run 26 (SWL = 1.4 m, *H* = 1.02 m, *T* = 3.8 sec).

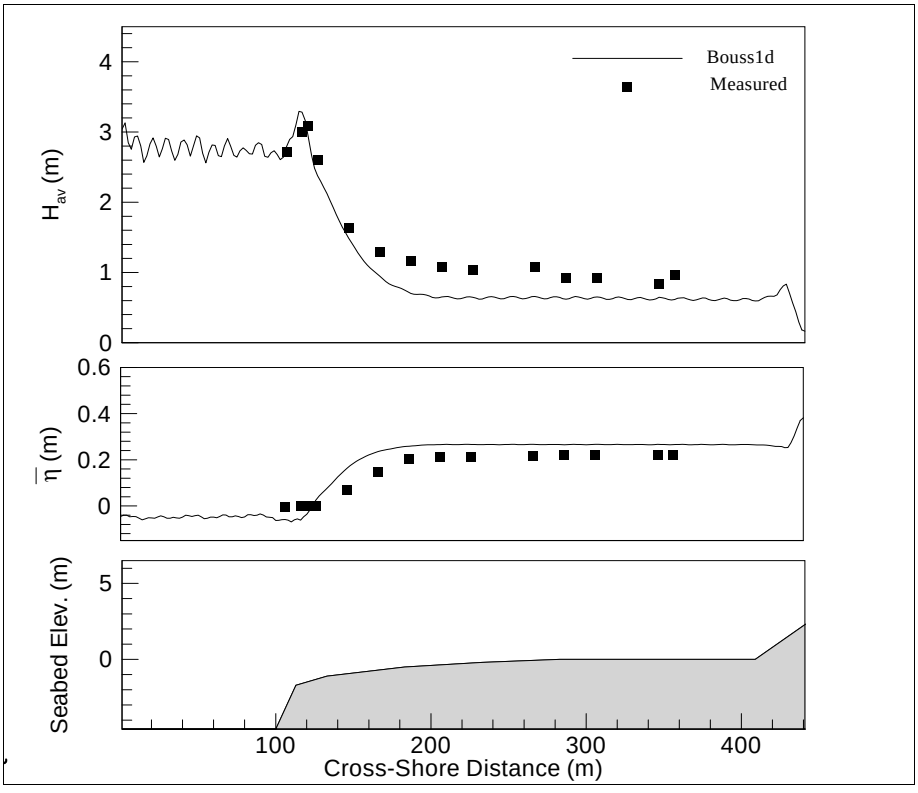

Figure A9. Test run 33 (SWL = 2.1 m, *H* = 2.84 m, *T* = 5.9 sec).

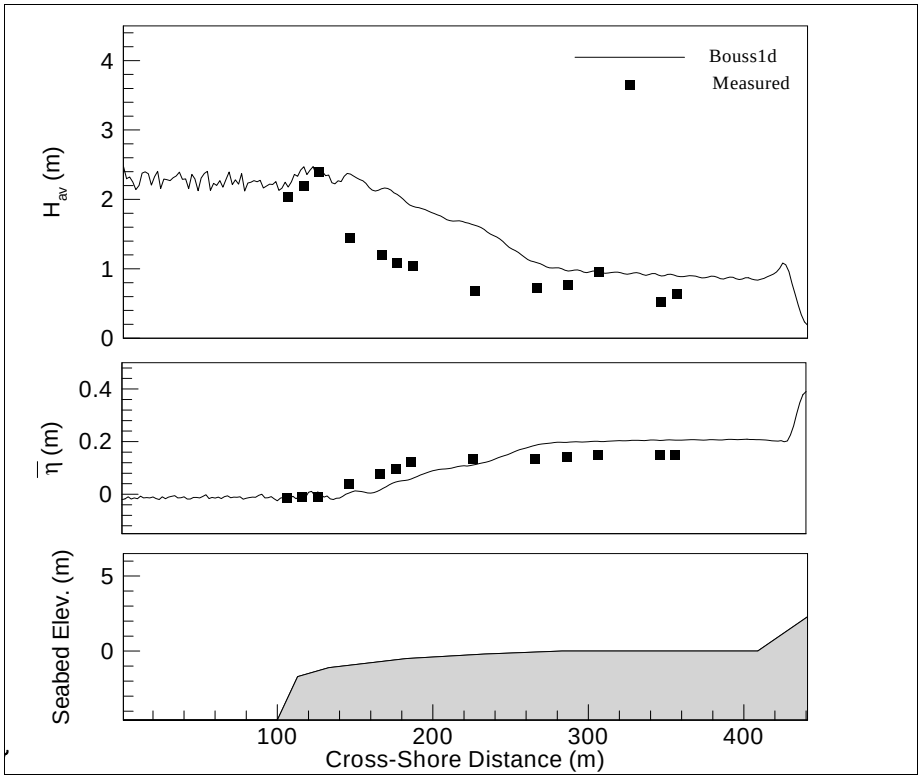

Figure A10. Test run 34 (SWL = 2.1 m, *H* = 2.11 m, *T* = 5.4 sec).

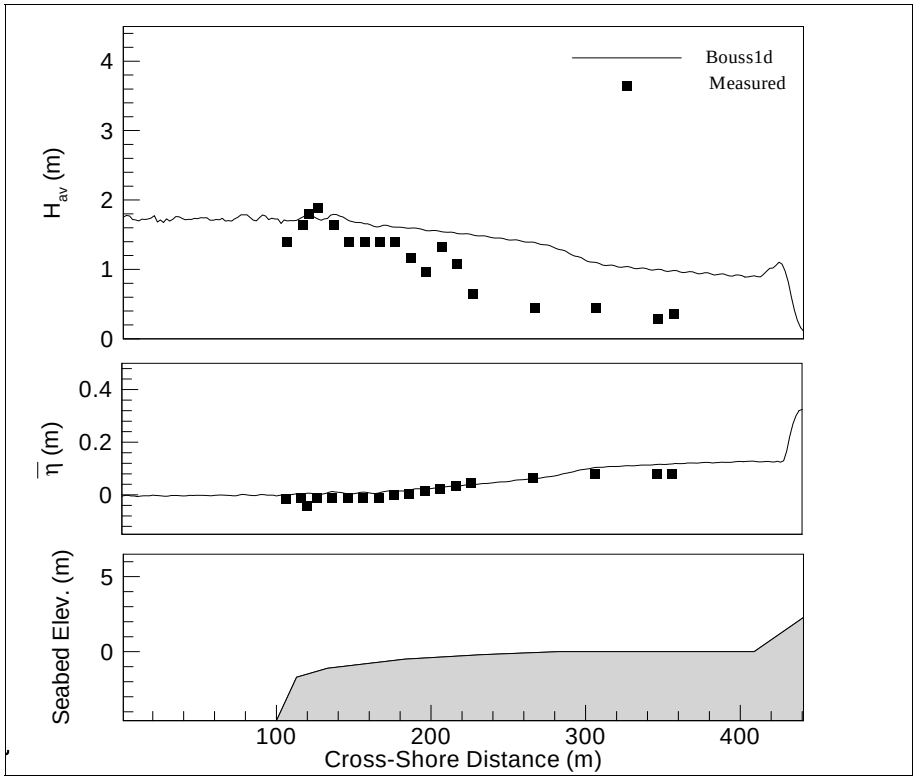

Figure A11. Test run 35 (SWL = 2.1 m, *H* = 1.6 m, *T* = 4.7 sec).

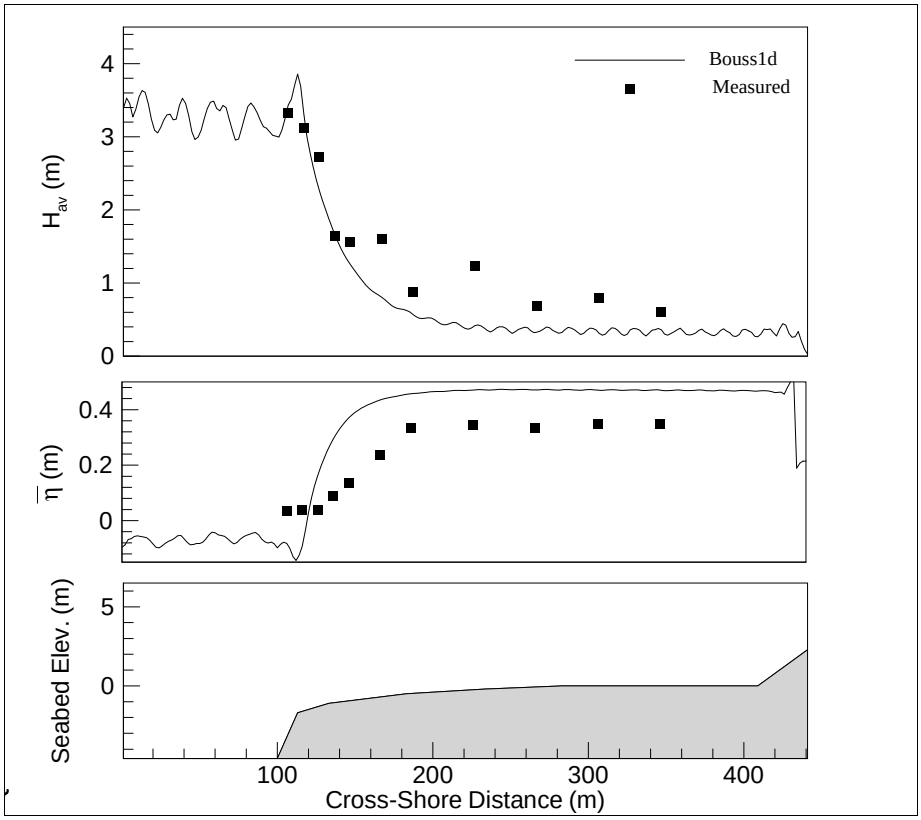

Figure A12. Test run 36 (SWL = 2.1 m, *H* = 1.01 m, *T* = 3.8 sec).

Table A1. Calculated wave heights from RBREAK2 for Hayman Island reef experiments.

Distance from toe (m)			0	20	40	60	80	100	120	140	160	180	190	200	210	220	230	240	250	260	270	280	290	300
Case	*H* (m)	*T* (sec)	Average Wave Heights (m)																					
HAY11	3.61	6.80	3.79	4.20	3.80	2.82	1.84	1.38	1.42	0.87	1.08	0.72	0.90	0.57	0.64	0.77	0.45	0.55	0.68	0.40	0.52	0.58	0.38	0.50
HAY12	3.45	6.62	3.58	3.98	2.94	2.21	1.73	1.42	1.24	0.80	0.93	0.92	0.60	0.75	0.61	0.59	0.68	0.43	0.64	0.38	0.55	0.46	0.42	0.50
HAY13	2.63	5.90	2.59	3.16	2.24	2.00	1.45	1.07	0.99	0.84	0.71	0.57	0.68	0.64	0.49	0.41	0.43	0.51	0.39	0.41	0.35	0.33	0.37	0.37
HAY14	2.19	5.41	2.14	2.69	2.23	1.34	1.37	1.22	0.99	0.84	0.73	0.58	0.48	0.41	0.38	0.39	0.40	0.41	0.40	0.38	0.38	0.33	0.28	0.28
HAY15	1.66	4.70	1.62	2.02	1.95	1.48	1.01	0.69	0.60	0.53	0.47	0.47	0.37	0.43	0.37	0.22	0.26	0.26	0.19	0.23	0.27	0.26	0.29	0.24
HAY16	1.05	3.84	1.04	1.20	1.12	0.84	0.76	0.70	0.53	0.39	0.39	0.36	0.35	0.30	0.31	0.18	0.27	0.16	0.19	0.15	0.17	0.14	0.16	0.14
HAY21	3.39	6.75	3.40	3.62	2.04	1.53	0.95	0.90	0.73	0.57	0.38	0.39	0.41	0.31	0.29	0.31	0.29	0.27	0.25	0.25	0.26	0.24	0.19	0.21
HAY22	3.35	6.66	3.36	3.46	2.18	1.56	0.86	0.66	0.52	0.53	0.47	0.36	0.36	0.33	0.28	0.29	0.28	0.24	0.25	0.25	0.23	0.21	0.20	0.21
HAY23	3.03	5.81	3.18	3.26	1.76	1.02	0.91	0.60	0.51	0.45	0.42	0.32	0.29	0.30	0.27	0.25	0.22	0.21	0.22	0.23	0.21	0.19	0.20	0.20
HAY24	2.07	5.36	2.02	2.35	1.56	1.05	0.60	0.46	0.40	0.29	0.26	0.24	0.20	0.19	0.19	0.18	0.18	0.16	0.15	0.14	0.13	0.13	0.12	0.13
HAY25	1.60	4.69	1.57	2.17	1.29	0.75	0.50	0.39	0.32	0.26	0.20	0.17	0.16	0.15	0.14	0.14	0.14	0.14	0.14	0.13	0.13	0.11	0.10	0.09
HAY26	1.02	3.80	1.03	1.28	0.82	0.54	0.36	0.26	0.23	0.17	0.14	0.11	0.11	0.10	0.10	0.09	0.09	0.09	0.08	0.08	0.07	0.07	0.07	0.06
HAY31	3.57	6.70	3.60	3.94	2.67	1.75	1.35	1.16	0.71	0.76	0.49	0.59	0.55	0.47	0.42	0.37	0.33	0.34	0.38	0.38	0.36	0.31	0.29	0.27
HAY32	3.25	6.62	3.46	4.09	2.34	1.97	1.49	0.97	0.80	0.73	0.64	0.43	0.39	0.41	0.44	0.45	0.44	0.41	0.35	0.33	0.30	0.28	0.26	0.26
HAY33	2.84	5.90	2.89	2.95	1.83	1.65	1.23	0.97	0.64	0.61	0.44	0.42	0.34	0.36	0.36	0.30	0.32	0.31	0.27	0.28	0.24	0.25	0.25	0.20
HAY34	2.11	5.40	2.04	2.67	1.73	1.32	0.91	0.73	0.62	0.41	0.40	0.30	0.27	0.28	0.26	0.26	0.24	0.19	0.17	0.17	0.17	0.17	0.18	0.18
HAY35	1.60	4.69	1.56	1.85	1.22	1.02	0.73	0.51	0.43	0.36	0.30	0.27	0.25	0.24	0.21	0.21	0.19	0.17	0.17	0.13	0.16	0.15	0.12	0.13
HAY36	1.05	3.84	1.05	1.35	1.03	0.61	0.49	0.43	0.30	0.24	0.21	0.14	0.14	0.14	0.14	0.13	0.13	0.13	0.13	0.12	0.12	0.12	0.11	0.11

Table A2. Calculated wave setups from RBREAK2 for Hayman Island reef experiments.

Distance from toe (m)			0	20	40	60	80	100	120	140	160	180	190	200	210	220	230	240	250	260	270	280	290	300
Case	*H* (m)	*T* (sec)	Setup/Setdown (m)																					
HAY11	3.61	6.80	-0.06	-0.06	0.33	0.45	0.49	0.46	0.52	0.51	0.56	0.51	0.56	0.53	0.53	0.56	0.53	0.54	0.56	0.54	0.54	0.55	0.54	0.55
HAY12	3.45	6.62	-0.06	-0.11	0.22	0.32	0.38	0.46	0.44	0.45	0.50	0.50	0.47	0.49	0.48	0.48	0.50	0.48	0.50	0.48	0.49	0.49	0.49	0.49
HAY13	2.63	5.90	-0.03	-0.16	0.07	0.20	0.24	0.21	0.24	0.25	0.25	0.26	0.26	0.26	0.26	0.25	0.26	0.26	0.26	0.26	0.26	0.26	0.26	0.26
HAY14	2.19	5.41	-0.02	-0.09	0.07	0.05	0.15	0.16	0.16	0.16	0.17	0.17	0.17	0.16	0.16	0.17	0.17	0.17	0.17	0.17	0.17	0.17	0.17	0.17
HAY15	1.66	4.70	-0.01	-0.08	-0.03	0.05	0.05	0.06	0.07	0.07	0.07	0.08	0.08	0.08	0.08	0.08	0.08	0.08	0.08	0.08	0.08	0.08	0.08	0.08
HAY16	1.05	3.84	0.00	-0.05	-0.04	-0.02	-0.01	0.00	0.00	0.01	0.01	0.01	0.01	0.01	0.01	0.01	0.01	0.01	0.01	0.01	0.01	0.01	0.01	0.01
HAY21	3.39	6.75	-0.10	0.22	0.47	0.59	0.64	0.67	0.67	0.67	0.67	0.67	0.67	0.67	0.67	0.67	0.67	0.67	0.67	0.67	0.67	0.67	0.67	0.67
HAY22	3.35	6.66	-0.10	0.21	0.49	0.61	0.60	0.63	0.64	0.65	0.66	0.65	0.66	0.66	0.65	0.66	0.66	0.65	0.65	0.66	0.66	0.65	0.66	0.66
HAY23	3.03	5.81	-0.06	0.16	0.52	0.59	0.61	0.62	0.63	0.64	0.64	0.64	0.64	0.64	0.64	0.64	0.64	0.64	0.64	0.64	0.64	0.64	0.64	0.64
HAY24	2.07	5.36	-0.03	0.04	0.19	0.26	0.27	0.28	0.28	0.29	0.29	0.29	0.29	0.29	0.29	0.29	0.29	0.29	0.29	0.29	0.29	0.29	0.29	0.29
HAY25	1.60	4.69	-0.02	-0.01	0.10	0.13	0.15	0.15	0.15	0.16	0.16	0.16	0.16	0.16	0.16	0.16	0.16	0.16	0.16	0.16	0.16	0.16	0.16	0.16
HAY26	1.02	3.80	-0.01	-0.05	0.01	0.03	0.04	0.04	0.04	0.04	0.04	0.04	0.04	0.04	0.04	0.04	0.04	0.04	0.04	0.04	0.04	0.04	0.04	0.04
HAY31	3.57	6.70	-0.09	0.01	0.45	0.50	0.54	0.60	0.59	0.60	0.60	0.61	0.61	0.61	0.61	0.61	0.61	0.61	0.61	0.61	0.61	0.61	0.61	0.61
HAY32	3.25	6.62	-0.06	0.05	0.43	0.55	0.60	0.62	0.60	0.63	0.62	0.62	0.62	0.63	0.63	0.63	0.63	0.63	0.63	0.63	0.63	0.63	0.63	0.63
HAY33	2.84	5.90	-0.05	0.00	0.25	0.40	0.42	0.44	0.43	0.44	0.44	0.44	0.44	0.44	0.45	0.44	0.45	0.45	0.45	0.45	0.45	0.45	0.45	0.45
HAY34	2.11	5.40	-0.03	-0.11	0.08	0.19	0.20	0.21	0.22	0.22	0.23	0.23	0.23	0.23	0.23	0.23	0.23	0.23	0.23	0.23	0.23	0.23	0.23	0.23
HAY35	1.60	4.69	-0.02	-0.08	0.02	0.08	0.09	0.10	0.11	0.11	0.11	0.11	0.11	0.11	0.11	0.11	0.11	0.11	0.11	0.11	0.11	0.11	0.11	0.11
HAY36	1.05	3.84	-0.01	-0.06	-0.02	0.00	0.01	0.02	0.02	0.02	0.02	0.02	0.03	0.03	0.03	0.03	0.03	0.03	0.03	0.03	0.03	0.03	0.03	0.03

Table A3. Calculated maximum runup from RBREAK2 for Hayman Island reef experiments.

Case	H (m)	T (sec)	R_{max} (m)
HAY11	3.61	6.80	0.715
HAY12	3.45	6.62	0.645
HAY13	2.63	5.90	0.371
HAY14	2.19	5.41	0.254
HAY15	1.66	4.70	0.131
HAY16	1.05	3.84	0.025
HAY21	3.39	6.75	0.783
HAY22	3.35	6.66	0.767
HAY23	3.03	5.81	0.730
HAY24	2.07	5.36	0.335
HAY25	1.60	4.69	0.184
HAY26	1.02	3.80	0.052
HAY31	3.57	6.70	0.750
HAY32	3.25	6.62	0.774
HAY33	2.84	5.90	0.554
HAY34	2.11	5.40	0.348
HAY35	1.60	4.69	0.165
HAY36	1.05	3.84	0.058

Appendix B: The Earlier Sensitivity Study

Drs. Edward F. Thompson (retired) and Donald Ward performed an unpublished sensitivity study in 2005 and 2006 concerning effects of input parameters on BOUSS-1D model results. A summary of their works is presented here, including the description of some simulations, issues pertaining to the selection of model parameters, and observations and conclusions about how model parameters affected the BOUSS-1D predictions. This earlier work is replaced by a recent comprehensive study described in Chapter 3 of this report. The preliminary findings from the earlier exploratory research study are provided here because they shed useful insight to users of the BOUSS-1D model. In particular, the roles of certain model parameters that have been investigated and their effects in model predictions may be useful to users of BOUSS-1D.

As a result of the 2005 sensitivity study, research was initiated to improve the BOUSS-1D representation of wave breaking to mimic the natural reef processes occurring over steep-slopes and highly dissipative reef environments. Results presented in Chapter 3 of this report for four reef applications have been obtained with a recent Boussinesq wave model that includes new wave breaking and wave dissipation schemes. Interested readers may refer to Demirbilek and Nwogu (2007) for a description of the new wave breaking formulas implemented in BOUSS-1D. The results and observations given in this section of the report are applicable to the 2005 version of the model, which may be compared to the Chapter 3 findings.

The model sensitivity study considered evaluation of BOUSS-1D with data from two physical model studies conducted by Seelig (1983) and Mase (1989). Details of the sensitivity study are described next.

Results for the Seelig reef experiments

The following test cases were run in this initial evaluation: 1111, 1122, 1123, 1133, 1134, and 2133. The runs were simulated at laboratory scale using Seelig's model profile. The profile was modified for case 1134 by replacing the flat offshore bottom with an offshore slope because BOUSS-1D had difficulty simulating these very high, near breaking incident waves.

Generally, individual waves in a coastal wave time series are identified by a zero-crossing analysis. That approach is not suitable for fringing reef applications because of the energetic long waves that may be superimposed on the short waves. Therefore a program was written that identifies significant peaks and troughs based on a minimum elevation difference and a minimum time difference. Threshold values used in the program were 0.25 times the time series standard deviation for elevation difference (or 0.0625 H_s) and 0.25 T_p for time difference. The subroutine was documented by Thompson (1980).

Two conclusions from the initial evaluation were:

- Mean ponding level $\bar{\eta}_{mean}$: BOUSS-1D results were similar to Seelig's data, but the standard deviation σ_x from BOUSS-1D was generally too large.
- $R_{\max}$: BOUSS-1D values are too high for 1133 and 2133, but are reasonable for other cases.

Based on these initial evaluations, a series of sensitivity tests was conducted to evaluate the influence of various model input parameters on key results, particularly σ_x and $R_{\max}$ (Table B1. In the sensitivity study, the most tests were run for test case 1133. The primary parameter investigated in the sensitivity tests was the Chezy bottom friction coefficient C_f. Default settings used for all runs (unless indicated otherwise in the table) were, in model units as: grid spacing = 0.1 m, duration = 500 sec, time step = 0.016 sec, turbulent length scale l_t = 0.012 m, minimum flooding depth = 0.0001 m, and Smagorinsky constant C_s = 0.2.

Both simulation results and corresponding physical model results from Seelig's experiments are listed in Table B1. The experimental results were extracted from figures in Seelig (1983). Physical model results are shown as a range of values for parameters which Seelig showed as scatter points from individual experimental runs. The BOUSS-1D test result, which was considered the best match to the physical model, is highlighted in Table B1, along with the corresponding physical model parameters.

Table B1. Sensitivity study results from BOUSS-1D for Seelig experiments (Tests 1133 and 2133).

Test	$\bar{\eta}_{mean}$ (m)	σ_x (m)	$\eta_{1\%}$ (m)	$\frac{(H_s)_t}{d}$	R_{max} (m)	$R_{2\%}$ (m)	Description
Seelig data	1.2-1.4	0.23-0.27	1.5-1.9	0.45	4.5-5.3		Physical model, depth over reef crest = 0.0
1133b	1.31	0.53	3.06	0.35	7.44	6.13	C_f = 20
1133c	1.27	0.54	3.09	0.40	9.02	6.94	C_f = 30, Δx = 0.05 m
1133d	1.27	0.5	2.94	0.35	7.55	4.76	C_f = 20, Δx = 0.05 m
1133e	1.27	0.64	3.35	0.46	9.76	8.84	C_f = 90
1133f	1.3	0.47	2.83	0.31	6.22	4.67	C_f = 15
1133g	1.29	0.47	2.82	0.3	6.01	4.61	C_f = 15, C_s = 0.5
1133h	1.11	0.45	2.61	????	4.9	4.33	C_f = 15, I_t = 0.24
1133i	1.29	0.42	2.5	0.31	4.78	4.51	C_f = 15, seed option(reverse digits in default)
1133j	1.09	0.44	2.41	0.29	4.8	4.72	C_f = 20, seed option, I_t = 0.24
1133k	1.29	0.47	2.71	0.36	5.87	5.84	C_f = 20, seed option
1133l	1.28	0.42	2.49	0.31	4.81	4.46	C_f = 15, seed option, Δt = 0.008 sec
1133m	1.12	0.47	2.48	0.33	5.52	5.19	C_f = 20, seed option, min flood depth = 0.001 m
1133n	1.18	0.43	2.51	0.34	5.71	5.13	C_f = 20, seed option, Δx = 0.05 m, Δt = 0.004 sec
Seelig data	0.8-1.0	0.37-0.42	1.5-1.9	0.45	5.5-6.3		Physical model, depth over reef crest = 2.0 m prototype
2133	0.89	0.62	2.76	0.37	7.5	5.79	C_f = 20
2133a	0.9	0.52	2.36	0.35	5.4	5.27	C_f = 15, seed option
2133b	0.8	0.51	2.26	0.34	5.2	4.97	C_f = 15, seed option, min flood depth = 0.001 m
2133c	0.9	0.55	2.46	0.34	5.4	5.27	Same as 2133a but SWL incr by adding 2 m in bathy file & keep input tide = 0
2133d	0.91	0.58	2.49	0.37	6.54	4.96	C_f = 20, seed option, duration = 2048, use high tide bathy file & input tide = 0
2133e	0.92	0.52	2.28	0.35	5.37	4.17	C_f = 15, seed option, duration = 2048, use high tide bathy file & input tide = 0

The sensitivity tests include trial variations of several different input parameters which could potentially help to improve the BOUSS-1D calibration for fringing reef applications. Most parameters have a fairly evident role in the tests. However, the role of the random seed is not so straightforward. This seed is the basis for “random” simulation of the incident wave time series from a JONSWAP spectrum. Initially, the random seed was planned to remain constant. However, the default seed resulted in one unusually high elevation and runup peak in many runs. The peak was considerably higher than would be expected in a short time series. It gave an unrepresentative $R_{\max}$ and distorted the values of other

parameters related to extremes. The random seed used in place of the default in some runs removed that distortion. Model developers have since revised the code and the seed is no longer a user-controlled parameter.

The following conclusions were drawn from the sensitivity runs made for the 1133 and 2133 test cases:

1. C_f = 15 provides the best match to the physical model data for both water levels tested.
2. Impact of Δx (1133b vs. 1133d): minor, except small Δx leads to lower $R_{2\%}$.
3. Impact of Δt (1133i vs. 1133l): minor.
4. Impact of random seed (1133b vs. 1133k; 1133f vs. 1133i): major impact on $\eta_{1\%}$ and $R_{\max}$ for these particular seed values.
5. Impact of l_t (1133f vs. 1133h; 1133j vs. 1133k): increasing l_t gives decreased $\overline{X}$, $\eta_{1\%}$, $R_{\max}$, and $R_{2\%}$.
6. Impact of C_s (1133f vs. 1133g): no impact.
7. Impact of minimum flooding depth (1133k vs. 1133m): increasing minimum flooding depth gives decreased $\bar{\eta}_{mean}$, $R_{\max}$, and $R_{2\%}$.
8. Impact of Courant number C_R (1133k vs. 1133n): minor.

BOUSS-1D produces reasonable estimates of $\bar{\eta}_{mean}$ and $R_{\max}$, but it overestimated σ_x and $\eta_{1\%}$ and underestimated $(H_s)_t/d$. The BOUSS-1D surface elevation time series over the reef for case 1134 reveals a striking prominence of long waves and diminished presence of wind waves in the lagoon. The leading edge of the wind wave crests is particularly distinctive in the representative physical model lagoon time series given in Seelig (1983), characterized by an exceptionally high, steep face and initial crest, which often drops quickly to a lower crest elevation on the back side and transitions more gradually down to lower, non-crest elevations. The steep, high initial crest faces in the physical model, suggesting breaking wave bores, are not present in the numerical model time series. These differences in the time series can directly account for the persistent differences between the physical model and the BOUSS-1D values of the parameters σ_x, $\eta_{1\%}$, and $(H_s)_t/d$.

An additional suite of tests was run with BOUSS-1D for the Seelig profile to verify that the above conclusions would apply for a shorter period wave condition as well (Table B2). Some of these tests were run with a duration of 2048 sec, which matches Seelig's runs, while most of the BOUSS-1D tests used a shorter duration. As previously, the BOUSS-1D test results

which were considered the best match to the physical model are highlighted in Table B2, along with the corresponding physical model parameters. Conclusions are similar to those above, although $C_f = 20$ seemed preferable to $C_f = 15$ for these shorter period cases.

Table B2. Sensitivity study results from BOUSS-1D for Seelig experiments (Tests 1123 and 2123).

Test	$\overline{X}$ (m)	σ_x (m)	$\eta_{1\%}$ (m)	$\frac{(H_s)_t}{d}$	R_{max} (m)	$R_{2\%}$ (m)	Description
Seelig data	1.2-1.3	0.24	1.5-1.8	0.32	4.0-4.3		Physical model, depth over reef crest = 0.0
1123	1.05	0.41	2.35	0.27	3.94	3.76	$C_f = 20$
1123a	1.06	0.37	2.16		3.27	3.23	$C_f = 15$
1123b	1.04	0.47	2.51	0.31	4.62	4.36	$C_f = 30$
1123c	1.05	0.38	2.06	0.27	3.89	3.59	$C_f = 20$, duration = 750 sec
1123d	1.06	0.36	2.05	0.27	3.94	3.2	$C_f = 20$, duration = 2048 sec
1123e	1.08	0.32	1.96		3.28	2.73	$C_f = 15$, duration = 2048 sec
Seelig data	0.8	0.37-0.40	1.5-1.8	0.41-0.42	4.7-5.1		Physical model, depth over reef crest = 2.0 m prototype
2123	0.77	0.43	1.85	0.3	4.29	3.46	$C_f = 20$, duration = 2048 sec
2123a	0.79	0.39	1.76	0.29	3.74	3.15	$C_f = 15$, duration = 2048 sec
2123b	0.72	0.42	1.82	0.28	4.04	3.21	$C_f = 20$, duration = 2048 sec, min flood depth = 0.001 m

Results for the Mase (1989) runup experiments

Since the comparisons with Seelig's physical model data raised some questions about the BOUSS-1D simulation of physical processes during wave transformation and breaking over a steep bottom slope and a flat fringing reef, it was worthwhile to evaluate the BOUSS-1D performance for a similar but different wave transformation scenario. Thus, BOUSS-1D was run to match several cases of Mase physical model data (Mase 1989) on wave transformation over plane slopes. For slopes of 1:30, 1:10, and 1:5, BOUSS-1D was run to match the case with the lowest peak frequency (0.4 Hz) and the highest H_s. Also, Mase experiments were repeated with two groupiness factors (*GF*). The BOUSS-1D runs matched the more highly grouped wave condition ($GF = 0.74$). The *GF* computed from the BOUSS-1D time series was 0.749, which was considered sufficiently close to that of the physical model experiments.

The analysis procedure used for comparisons with Seelig's data was also applied for the comparison with Mase's data. Since Mase reported only runup parameters, long wave parameters from the BOUSS-1D simulations cannot be compared to physical model data. Results for the 1:30 slope are given in Table B3. Results for the 1:10 slope are given in Table B4. Runs for the 1:5 slope failed before completion, suggesting that a 1:5 slope is too steep for the version of BOUSS-1D used at the time. For the 1:30 and 1:10 slopes, input parameters (mainly C_f) were varied to evaluate the ability of BOUSS-1D to simulate the physical model results. The dependence of runup parameters on C_f and the agreement between BOUSS-1D results and the physical model data are shown graphically in Figures B1 and B2.

Table B3. Sensitivity study results from BOUSS-1D for Mase experiments (1:30 slope, H_s = 4.69 cm, T_p = 2.5 sec).

Test	$\frac{R_{max}}{H_0}$	$\frac{R_{2\%}}{H_0}$	$\frac{R_{1/10}}{H_0}$	$\frac{R_{1/3}}{H_0}$	$\frac{\overline{R}}{H_0}$	Description
Mase data, GF = 0.74	1.15	1.15	1.04	0.85	0.53	Physical model, 1:30 slope
01a	1.031	1.031	0.974	0.846	0.593	C_f = 30
01b	0.776	0.776	0.724	0.632	0.43	C_f = 20
01c	1.107	1.107	1.042	0.929	0.675	C_f = 35
01d	1.403	1.145	1.048	0.875	0.582	C_f = 30, duration = 1600 sec
01e						C_f = 30 (same as 01a)
01f	1.534	1.229	1.139	0.95	0.651	C_f = 35, duration = 1600 sec
01g	1.238	1.031	0.946	0.794	0.544	C_f = 25, duration = 1600 sec
01h						C_f = 30, H_s = 0.15625 m

Table B4. Sensitivity study results from BOUSS-1D for Mase experiments (1:10 slope, H_s = 5.16 cm, T_p = 2.5 sec).

Test	$\frac{R_{max}}{H_0}$	$\frac{R_{2\%}}{H_0}$	$\frac{R_{1/10}}{H_0}$	$\frac{R_{1/3}}{H_0}$	$\frac{\overline{R}}{H_0}$	Description
Mase data, GF = 0.74	2.76	2.26	2.05	1.61	0.95	Physical model, 1:10 slope
01a	1.739	1.645	1.495	1.161	0.743	C_f = 30
01b	1.802	1.73	1.562	1.195	0.778	C_f = 40
01c	1.609	1.568	1.431	1.157	0.772	C_f = 40, Δx = 0.05 m
01d	1.92	1.813	1.62	1.216	0.782	C_f = 80
01e	1.941	1.823	1.612	1.187	0.756	C_f = 100

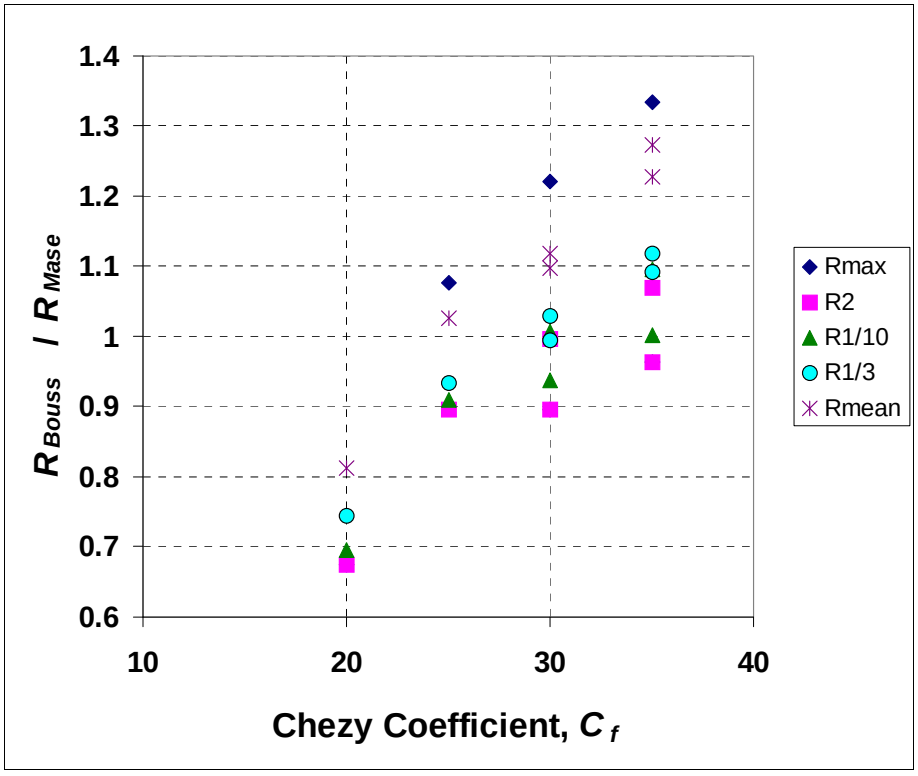

Figure B1. Comparison of BOUSS-1D runup estimates with runup data of Mase (slope = 1:30, H_s = 4.69 cm, T_p = 2.5 sec).

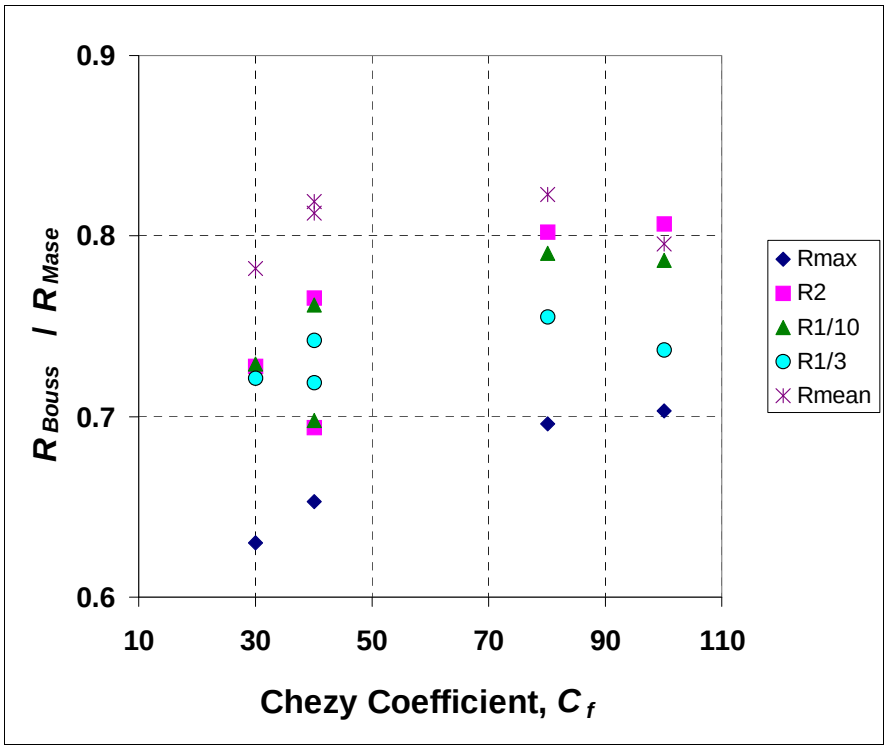

Figure B2. Comparison of BOUSS-1D runup estimates with runup data of Mase (slope = 1:10, H_s = 5.16 cm, T_p = 2.5 sec).

To gain further insight into the impact of a reef, a flat reef was inserted into the 1:30 plane slope in BOUSS-1D. In prototype units, assuming a 1:64 scale as with Seelig's experiments, the reef was approximately 196 m wide with a still-water depth over the reef of 0.13 m.

From the comparison of BOUSS-1D results to the physical model data of Mase for the 1:30 slope tests, the following conclusions were drawn:

1. With the onset of depth-induced breaking, H_{m0} decreases and local water level increases as the distance from shore decreases.
2. With the onset of depth-induced breaking, long wave energy increases as the distance from shore decreases.
3. Even very near shore (prototype depth of 1 m), incident wave period is very evident in surface elevation time series. This was not as apparent over the reef in the fringing reef tests with BOUSS-1D.
4. The BOUSS-1D simulations which best match Mase's data have $C_f = 30$ and a duration of 1,600 sec (the same duration as Mase's experiments).
5. A larger H_{m0} gives strong nearshore long wave oscillations. These simulations had a clear presence of wind wave periods in the surface elevation time series, and high runup peaks. Similar results were obtained for BOUSS-1D simulations with high waves in Seelig's lagoon.
6. Adding a flat reef to the 1:30 slope reduced runup but did not have much impact on water surface elevations over the reef.
7. For the 1:30 slope with a flat reef inserted, increasing H_{m0} to 10 m (prototype) gives higher mean water level over the reef, higher runup, much stronger surf beat and disappearance of most evidence of T_p in the surface elevation time series over the reef. As for the Seelig reef profile, the BOUSS-1D simulation with a reef fronted by a gentle 1:30 slope essentially transfers wind wave energy over the reef into long wave energy.
8. The 1:10 slope is not well-simulated with $C_f = 30$, giving runup significantly lower than the physical model data. Increasing C_f to 100, the upper limit of the present BOUSS-1D model, still results in runup below the physical model data.
9. Since very different values of C_f seem to be needed for calibration on the 1:30 and 1:10 plane slopes and since the optimum C_f for the 1:10 slope seems to be outside the range of plausible values, it appears that the representation of wave breaking in the present BOUSS-1D model is missing some important physical processes.
10. The 1:5 plane slope is too steep for BOUSS-1D to successfully simulate.

As a result of these and other tests that were performed, research was initiated to investigate and improve the BOUSS-1D representation of wave breaking and to more closely mimic many natural wave reef processes. Results for reef applications provided in Chapter 3 of this report are based on a revised BOUSS-1D model which includes three new wave breaking and wave dissipation schemes. See Demirbilek and Nwogu (2007) for a description of the new wave breaking formulas that have been implemented in BOUSS-1D/2D models for reef applications.

Appendix C: Additional Results for Seelig Reef Experiments

The first set of wave parameters and results of the wave model simulations for the Seelig reef experiments have been listed in Chapter 3. These results corresponded to the lagoon water depth and width of 0 and 150 m, respectively. Additional results are provided here for the lagoon water depth of 2 m and width of 150 m, and also for the wider lagoon width of 525 m with water depths of 0 and 2 m.

Table C1. Input wave parameters used in simulations for Seelig experiments (lagoon width = 150 m, depth = 2 m).

Test ID	H_s (m)	T_p (sec)	$H_s^2 T_p$ (m^2*sec)
201	2.51	8	50.4
202	3.91	8	122.6
203	4.48	8	160.6
204	5.04	8	203.5
205	3.26	10	106.3
206	5.29	10	279.3
207	6.48	10	420.3
208	4.41	12	233.5
209	7.17	12	616.9
210	8.61	12	889.0
211	5.07	14	359.4
212	7.49	14	785.0
213	9.90	14	1372.4
214	5.05	16	407.2
215	7.87	16	991.2
216	10.53	16	1773.8

Table C2. Input wave parameters used in simulations for Seelig experiments (lagoon width = 525 m, depth = 0 m).

Test ID	H_s (m)	T_p (sec)	$H_s^2 T_p$ (m²*sec)
301	3.75	8	112.4
302	4.07	8	132.3
303	4.71	8	177.2
304	2.12	12	54.0
305	4.61	12	254.6
306	7.24	12	629.5
307	8.21	12	808.8
308	1.75	16	48.9
309	5.29	16	448.3
310	7.89	16	995.0
311	9.32	16	1391.0
312	10.29	16	1694.5

Table C3. Input wave parameters used in simulations for Seelig experiments (lagoon width = 525 m, depth = 2 m).

Test ID	H_s (m)	T_p (sec)	$H_s^2 T_p$ (m²*-sec)
401	1.20	8	11.4
402	2.59	8	53.7
403	4.48	8	160.3
404	2.07	12	51.5
405	7.00	12	588.3
406	1.69	16	45.5
407	5.20	16	432.5
408	7.71	16	950.1
409	10.24	16	1677.4

Seelig (1983) used an absorber on the beach in his experiments for physical modeling tests conducted with wave and water levels listed in Tables C2 and C3. This prevented the measuring of the wave runup for the set of experimental parameters listed in Tables C2 and C3. Significant wave heights saved at RBREAK2 nodal points for the narrow and wide reefs are given in Tables C4 and C5, respectively. Wave setup (setdown) at the RBREAK2 nodal points for the narrow and wide reefs respectively are given in Tables C6 and C7. Table C8 gives the vertical elevation of maximum runup computed by RBREAK2.

Table C4. Calculated significant wave heights from RBREAK2 (lagoon width = 150 m, depth = 2 m).

Distance from toe (m)				0	32	64	96	128	160	192	224	256	288	320	352	368	384	400	416	432
CASE	H_s (m)	T_p (sec)	SWL (m)	Significant wave height (m)																
107	5.05	12	0	4.83	4.96	5.50	5.95	5.60	4.81	4.15	3.60	2.97	2.07	0.99	0.86	0.79	0.74	0.70	0.70	0.65
108	7.76	12	0	7.39	7.72	8.68	8.28	7.08	5.99	5.05	4.17	3.44	2.53	1.43	1.33	1.26	1.25	1.16	1.18	1.17
109	9.15	12	0	8.71	9.16	10.24	9.15	7.58	6.40	5.30	4.40	3.65	2.85	1.72	1.50	1.50	1.43	1.34	1.32	1.39
113	5.36	16	0	5.09	5.50	6.11	6.60	6.71	6.64	6.06	5.40	4.78	3.31	1.72	1.38	1.31	1.22	1.20	1.14	1.16
114	8.23	16	0	7.81	8.52	9.71	10.04	9.43	8.57	7.46	6.52	5.54	4.02	2.30	1.89	1.89	1.75	1.67	1.71	1.77
115	10.55	16	0	10.08	11.07	12.68	12.03	10.85	9.61	8.26	7.14	6.11	4.63	2.91	2.47	2.21	2.17	2.20	2.24	2.37
208	4.41	12	2	4.19	4.24	4.74	5.09	5.18	4.76	4.38	3.92	3.30	2.62	1.60	1.24	1.19	1.14	1.06	1.02	0.97
209	7.17	12	2	6.82	7.00	7.90	8.02	7.17	6.27	5.38	4.63	3.97	3.07	1.93	1.66	1.58	1.50	1.42	1.35	1.30
210	8.61	12	2	8.15	8.44	9.48	9.13	7.96	6.89	5.83	4.93	4.17	3.29	2.14	1.89	1.79	1.75	1.57	1.47	1.52
214	5.04	16	2	4.78	5.18	5.72	6.00	6.35	6.44	6.09	5.73	5.24	4.24	2.60	2.15	1.95	1.86	1.79	1.66	1.59
215	7.87	16	2	7.49	8.20	9.11	9.57	9.48	8.83	7.96	7.18	6.28	5.01	3.17	2.64	2.47	2.36	2.20	2.04	2.07
216	10.53	16	2	10.07	11.01	12.39	12.44	11.68	10.23	9.14	8.06	6.98	5.75	3.70	3.22	3.05	2.85	2.69	2.64	2.58

Table C5. Calculated significant wave heights from RBREAK2 (lagoon width = 525 m, depth = 0 m).

Distance from toe, m			0	32	64	96	128	160	192	224	256	288	320	352	384	416	448	480	512
CASE	H_s (m)	T_p (sec)	Significant wave heights (m)																
305	4.61	12	4.40	4.52	4.99	5.36	5.10	4.56	3.94	3.37	2.78	1.86	0.88	0.79	0.74	0.73	0.66	0.63	0.59
306	7.24	12	6.92	7.18	7.97	7.75	6.69	5.51	4.77	3.87	3.24	2.36	1.28	1.18	1.11	1.06	1.02	0.93	0.83
307	8.21	12	7.84	8.19	9.06	8.44	7.06	5.89	5.02	4.06	3.40	2.50	1.49	1.38	1.29	1.22	1.17	1.02	0.90
309	5.29	16	5.04	5.42	6.02	6.44	6.57	6.52	5.97	5.34	4.63	3.16	1.64	1.40	1.24	1.15	1.05	1.06	0.99
310	7.88	16	7.49	8.13	9.22	9.59	8.97	8.32	7.07	6.20	5.31	3.61	2.23	2.02	1.82	1.66	1.53	1.56	1.39
312	10.29	16	9.79	10.73	12.10	11.69	10.37	9.36	8.06	6.85	5.75	4.40	2.84	2.48	2.25	2.07	2.11	2.00	1.80
404	2.07	12	1.98	2.00	2.18	2.28	2.39	2.50	2.54	2.47	2.26	1.94	1.19	0.93	0.84	0.74	0.67	0.61	0.56
405	7.00	12	6.69	6.90	7.62	7.76	7.03	5.93	5.28	4.44	3.75	2.91	1.90	1.58	1.43	1.30	1.21	1.15	1.11
407	5.20	16	4.92	5.33	5.84	6.10	6.47	6.52	6.12	5.70	5.11	4.13	2.55	2.14	1.93	1.70	1.61	1.52	1.41
408	7.71	16	7.32	7.97	8.77	9.24	9.18	8.53	7.66	7.10	6.11	4.74	3.14	2.63	2.36	2.12	1.95	1.90	1.72
409	10.24	16	9.75	10.68	11.90	11.89	11.21	9.94	8.75	7.74	6.76	5.47	3.66	3.08	2.78	2.71	2.49	2.27	2.08

(Continued)

Table C5. (Concluded).

Distance from toe, m			544	576	608	640	672	704	736	768	800	544	576	608
CASE	H_s (m)	T_p (sec)	Significant wave heights (m)											
305	4.61	12	0.59	0.58	0.58	0.61	0.53	0.52	0.58	0.50	0.47	0.59	0.58	0.58
306	7.24	12	0.90	0.86	0.88	0.79	0.71	0.64	0.76	0.64	0.62	0.90	0.86	0.88
307	8.21	12	0.97	0.98	1.04	0.89	0.79	0.79	0.79	0.88	0.79	0.97	0.98	1.04
309	5.29	16	0.91	0.83	0.88	0.95	0.84	0.79	0.74	0.73	0.84	0.91	0.83	0.88
310	7.88	16	1.28	1.09	1.31	1.32	1.21	1.16	1.04	1.04	1.18	1.28	1.09	1.31
312	10.29	16	1.63	1.70	1.66	1.64	1.73	1.48	1.40	1.38	1.73	1.63	1.70	1.66
404	2.07	12	0.53	0.51	0.50	0.45	0.42	0.43	0.40	0.39	0.38	0.53	0.51	0.50
405	7.00	12	1.09	1.09	1.04	0.97	1.00	0.94	0.97	0.90	0.90	1.09	1.09	1.04
407	5.20	16	1.30	1.26	1.22	1.15	1.13	1.08	1.03	0.95	1.03	1.30	1.26	1.22
408	7.71	16	1.62	1.65	1.74	1.61	1.48	1.40	1.35	1.31	1.43	1.62	1.65	1.74
409	10.24	16	2.03	2.21	2.12	2.14	1.96	1.89	1.77	1.73	1.98	2.03	2.21	2.12

Table C6. Calculated setup from RBREAK2 (lagoon width = 150 m, depth = 2 m).

Distance from toe, m				0	32	64	96	128	160	192	224	256	288	320	352	368	384	400	416
CASE	H_s (m)	T_p (sec)	SWL (m)	Setup/Setdown (m)															
107	5.05	12	0	-0.08	-0.09	-0.13	-0.16	-0.10	-0.06	-0.03	0.03	0.09	0.23	0.62	0.62	0.63	0.63	0.63	0.63
108	7.76	12	0	-0.16	-0.19	-0.25	-0.23	-0.12	0.02	0.11	0.17	0.25	0.41	0.86	0.88	0.88	0.89	0.89	0.89
109	9.15	12	0	-0.22	-0.27	-0.33	-0.24	-0.09	0.06	0.18	0.25	0.35	0.52	0.99	1.02	1.03	1.02	1.03	1.03
113	5.36	16	0	-0.08	-0.10	-0.13	-0.17	-0.17	-0.14	-0.09	-0.03	0.09	0.34	1.05	1.08	1.08	1.09	1.09	1.09
114	8.23	16	0	-0.18	-0.21	-0.27	-0.31	-0.21	-0.09	0.01	0.15	0.30	0.66	1.40	1.46	1.46	1.46	1.47	1.48
115	10.55	16	0	-0.29	-0.34	-0.43	-0.37	-0.19	-0.03	0.16	0.33	0.51	0.92	1.68	1.76	1.77	1.78	1.78	1.79
208	4.41	12	2	-0.05	-0.04	-0.05	-0.06	-0.05	-0.03	0.00	0.08	0.11	0.20	0.28	0.37	0.37	0.37	0.37	0.38
209	7.17	12	2	-0.13	-0.13	-0.16	-0.15	-0.08	0.01	0.07	0.16	0.24	0.35	0.48	0.57	0.57	0.58	0.58	0.59
210	8.61	12	2	-0.19	-0.20	-0.23	-0.19	-0.07	0.04	0.14	0.23	0.32	0.44	0.58	0.69	0.69	0.70	0.70	0.70
214	5.04	16	2	-0.06	-0.06	-0.07	-0.09	-0.08	-0.07	-0.04	0.03	0.08	0.22	0.53	0.65	0.66	0.66	0.67	0.67
215	7.87	16	2	-0.15	-0.16	-0.19	-0.22	-0.18	-0.08	0.00	0.13	0.22	0.46	0.85	0.99	1.01	1.02	1.03	1.03
216	10.53	16	2	-0.27	-0.29	-0.35	-0.35	-0.22	-0.04	0.13	0.27	0.42	0.69	1.15	1.32	1.33	1.35	1.36	1.36

Table C7. Calculated setup from RBREAK2 (lagoon width = 525 m, depth = 0 m).

Distance from toe, m			0	32	64	96	128	160	192	224	256	288	320	352	384	416	448	480	512
CASE	H_s (m)	T_p (sec)	Setup/setdown (m)																
305	4.61	12	-0.07	-0.10	-0.14	-0.12	-0.09	-0.06	-0.03	0.00	0.05	0.17	0.61	0.55	0.56	0.56	0.56	0.56	0.56
306	7.24	12	-0.15	-0.20	-0.25	-0.20	-0.11	0.00	0.08	0.11	0.20	0.34	0.83	0.79	0.80	0.80	0.80	0.79	0.79
307	8.21	12	-0.19	-0.24	-0.31	-0.21	-0.10	0.03	0.13	0.17	0.26	0.41	0.92	0.89	0.89	0.89	0.89	0.89	0.89
309	5.29	16	-0.09	-0.12	-0.16	-0.15	-0.15	-0.13	-0.08	-0.05	0.06	0.32	1.07	1.04	1.05	1.06	1.06	1.06	1.06
310	7.88	16	-0.18	-0.22	-0.29	-0.28	-0.20	-0.09	-0.01	0.10	0.24	0.58	1.38	1.39	1.40	1.41	1.41	1.41	1.41
312	10.29	16	-0.29	-0.35	-0.45	-0.36	-0.19	-0.03	0.15	0.29	0.46	0.84	1.68	1.71	1.72	1.73	1.74	1.74	1.74
404	2.07	12	-0.02	-0.03	-0.04	0.00	0.00	-0.01	0.00	-0.02	-0.01	0.02	0.09	0.11	0.11	0.11	0.11	0.11	0.12
405	7.00	12	-0.13	-0.16	-0.19	-0.15	-0.08	-0.02	0.05	0.09	0.16	0.26	0.42	0.47	0.47	0.48	0.48	0.48	0.49
407	5.20	16	-0.07	-0.09	-0.12	-0.10	-0.10	-0.08	-0.06	-0.04	0.03	0.16	0.50	0.58	0.59	0.60	0.61	0.62	0.62
408	7.71	16	-0.15	-0.18	-0.23	-0.22	-0.19	-0.10	-0.03	0.07	0.16	0.36	0.79	0.89	0.90	0.91	0.93	0.94	0.94
409	10.24	16	-0.26	-0.30	-0.38	-0.35	-0.23	-0.05	0.09	0.19	0.32	0.60	1.08	1.19	1.21	1.23	1.24	1.26	1.26

(Continued)

Table C7. (Concluded).

Distance from toe, m			544	576	608	640	672	704	736	768	800
CASE	H_s (m)	T_p (sec)	Setup/setdown (m)								
305	4.61	12	0.56	0.56	0.56	0.56	0.56	0.56	0.56	0.56	0.57
306	7.24	12	0.79	0.79	0.79	0.79	0.79	0.79	0.80	0.80	0.81
307	8.21	12	0.89	0.89	0.89	0.89	0.89	0.89	0.89	0.89	0.90
309	5.29	16	1.06	1.06	1.06	1.06	1.06	1.06	1.06	1.06	1.07
310	7.88	16	1.41	1.41	1.42	1.42	1.42	1.42	1.42	1.42	1.43
312	10.29	16	1.74	1.74	1.75	1.75	1.75	1.75	1.75	1.75	1.77
404	2.07	12	0.12	0.12	0.12	0.12	0.12	0.12	0.12	0.12	0.11
405	7.00	12	0.49	0.49	0.49	0.49	0.49	0.49	0.49	0.49	0.49
407	5.20	16	0.63	0.63	0.63	0.64	0.64	0.64	0.64	0.64	0.64
408	7.71	16	0.95	0.95	0.95	0.96	0.96	0.96	0.96	0.97	0.96
409	10.24	16	1.26	1.27	1.28	1.28	1.29	1.29	1.29	1.29	1.30

Table C8. Calculated maximum runup computed by RBREAK2 for Seelig test cases.

Case	H_s (m)	T_p (sec)	SWL (m)	R_{max} (m)
107	5.05	12	0.00	2.38
108	7.76	12	0.00	3.82
109	9.15	12	0.00	4.55
113	5.36	16	0.00	3.89
114	8.23	16	0.00	5.52
115	10.55	16	0.00	6.93
208	4.41	12	2.00	2.57
209	7.17	12	2.00	4.03
210	8.61	12	2.00	4.83
214	5.04	16	2.00	4.06
215	7.87	16	2.00	5.81
216	10.53	16	2.00	7.44
305	4.61	12	0.00	1.79
306	7.24	12	0.00	2.45
307	8.21	12	0.00	2.73
309	5.29	16	0.00	2.60
310	7.88	16	0.00	3.63
312	10.29	16	0.00	4.57
404	2.07	12	2.00	1.09
405	7.00	12	2.00	2.53
407	5.20	16	2.00	2.93
408	7.71	16	2.00	4.00
409	10.24	16	2.00	5.21

The sensitivity of the WAV1D model results using the ABJB07 breaking formulation is depicted in Figure C1. This is illustrated for the measured and computed wave setup and maximum wave runup for the Seelig reef experiments. Results for two values of the wave breaking intensity factor (B = 1.0 and 1.3) are provided. As can be seen from Figure C1, the WAV1D model estimates for wave setup show a stronger dependence on the wave intensity factor as compared to the maximum wave runup. Model results provided in Chapter 5 for four laboratory experiments were all based on the wave intensity factor B = 1.0.

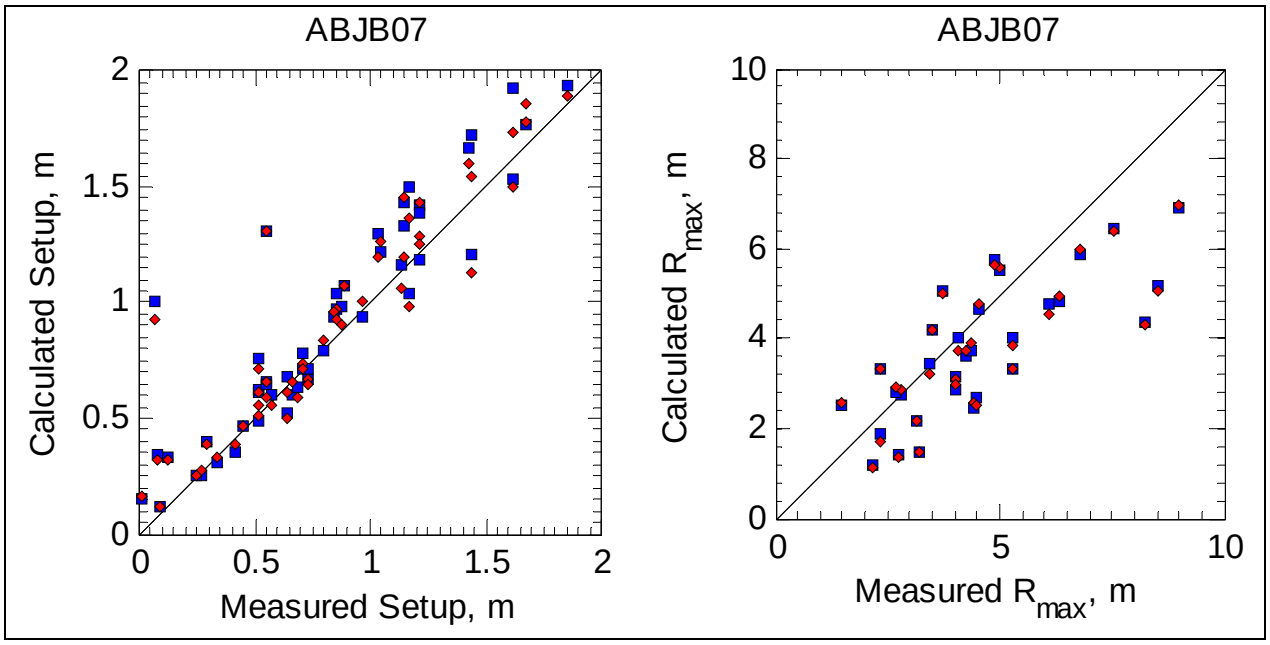

Figure C1. Comparison of measured and computed wave setup and maximum runup for Seelig's reef experiments using ABJB07 with B = 1.0 (blue squares) and B = 1.3 (red diamonds)

Appendix D: Additional Results for CHL Reef Experiments

Chapters 3, 4, and 5 of this report provided results from three wave model simulations for the CHL reef experiments. Because the CHL reef experiments have not been published previously, additional results are provided here for the remaining test conditions.

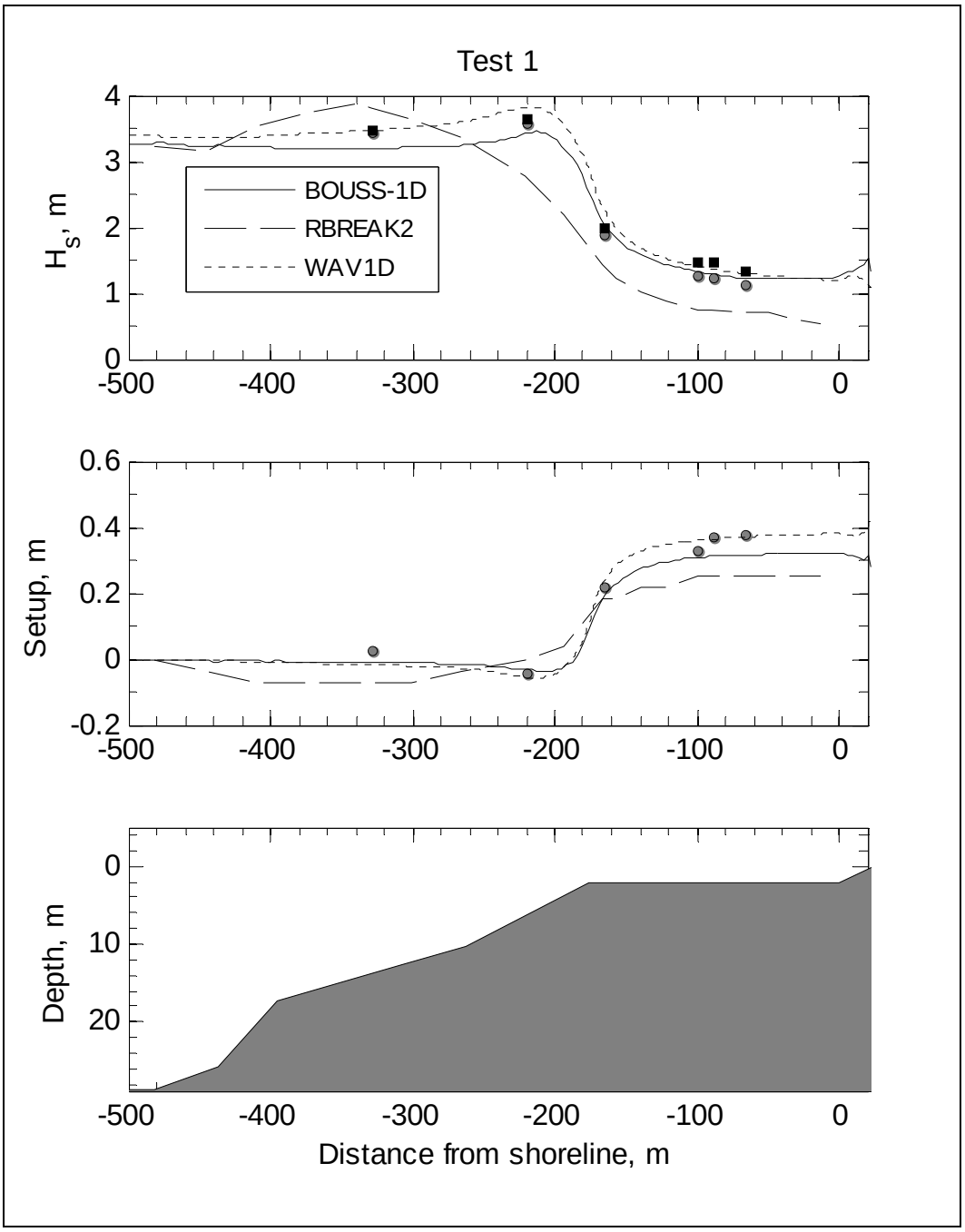

Figure D1. Comparison of three wave model results with data for Test 1 of CHL experiments.

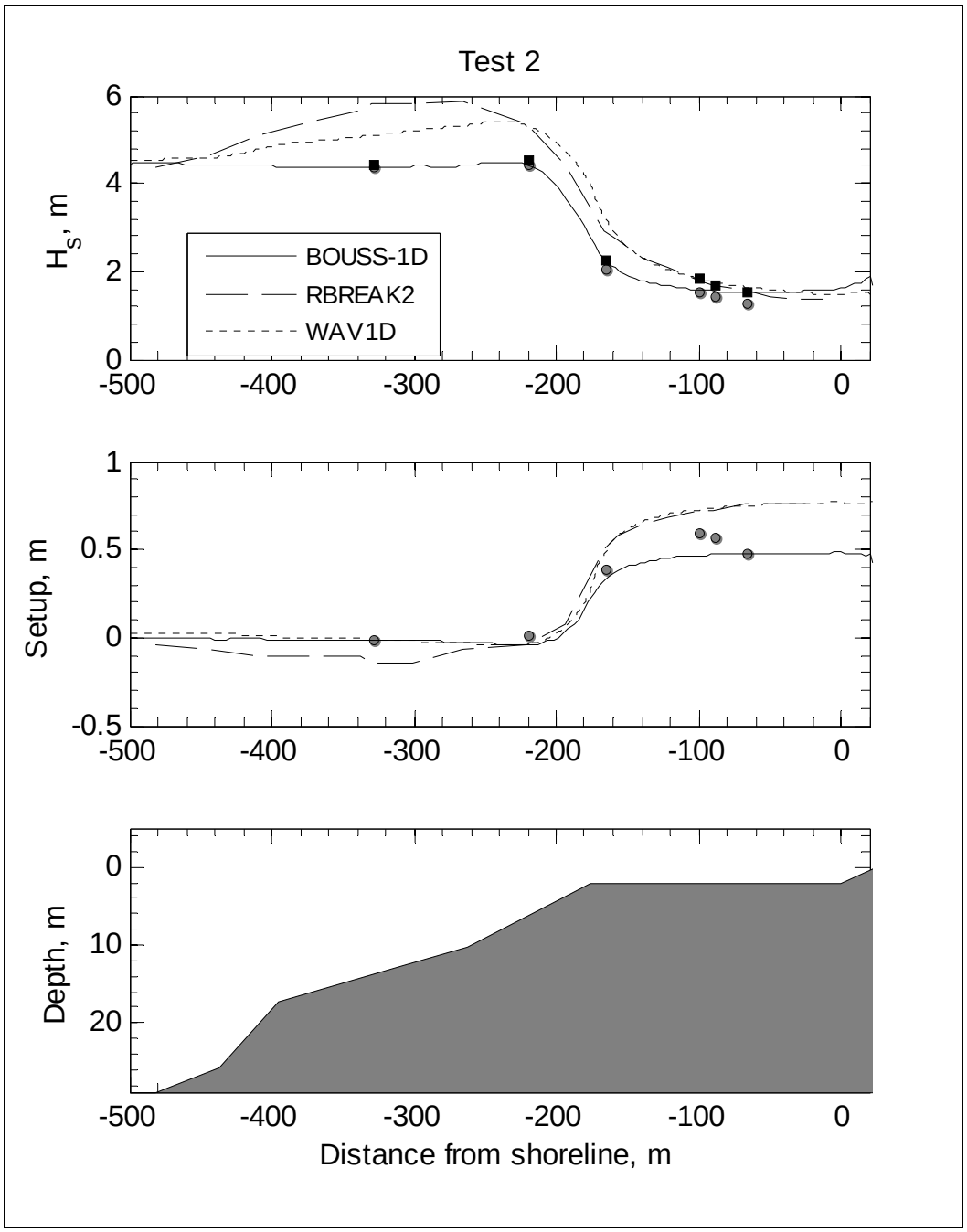

Figure D2. Comparison of three wave model results with data for Test 2 of CHL experiments.

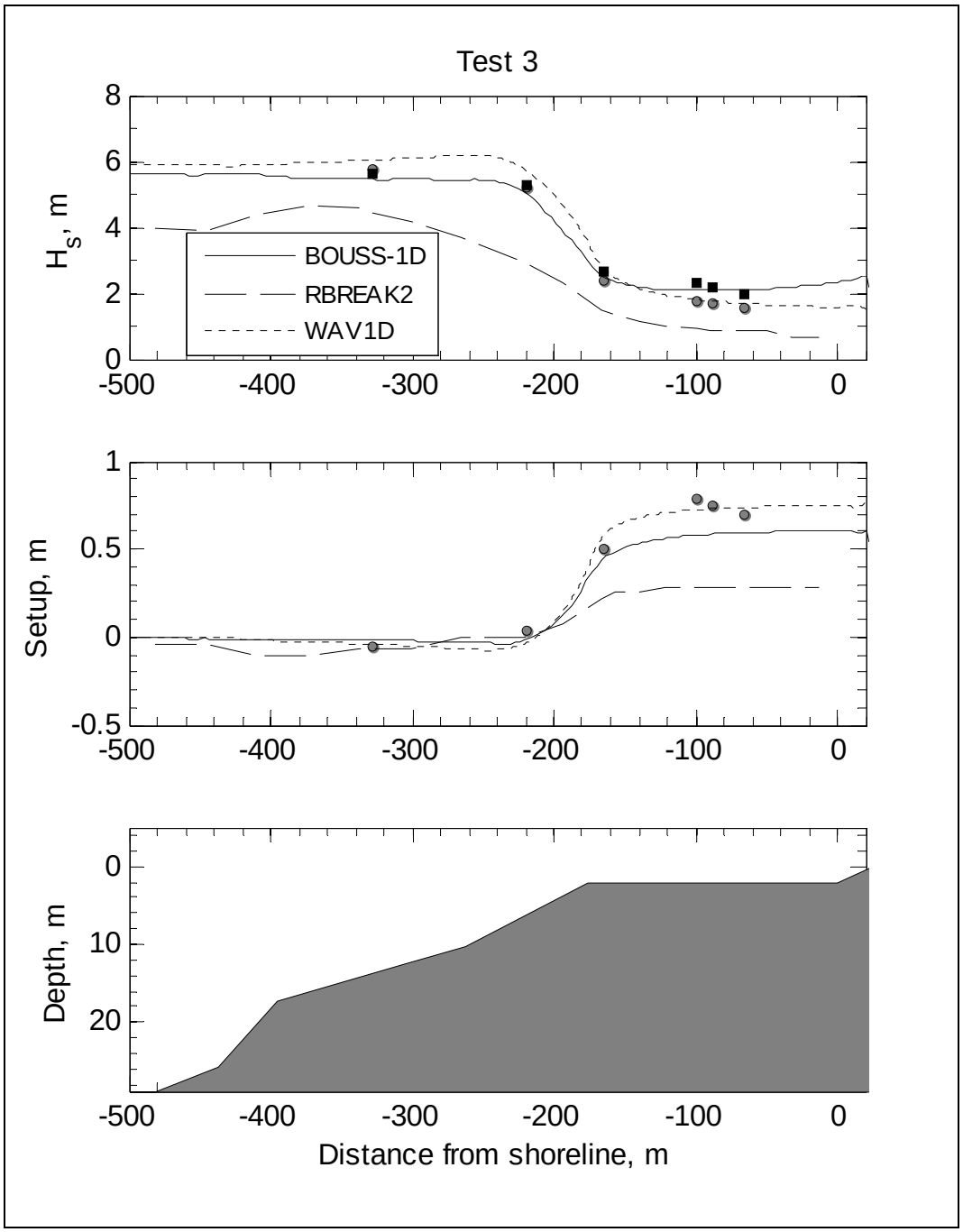

Figure D3. Comparison of three wave model results with data for Test 3 of CHL experiments.

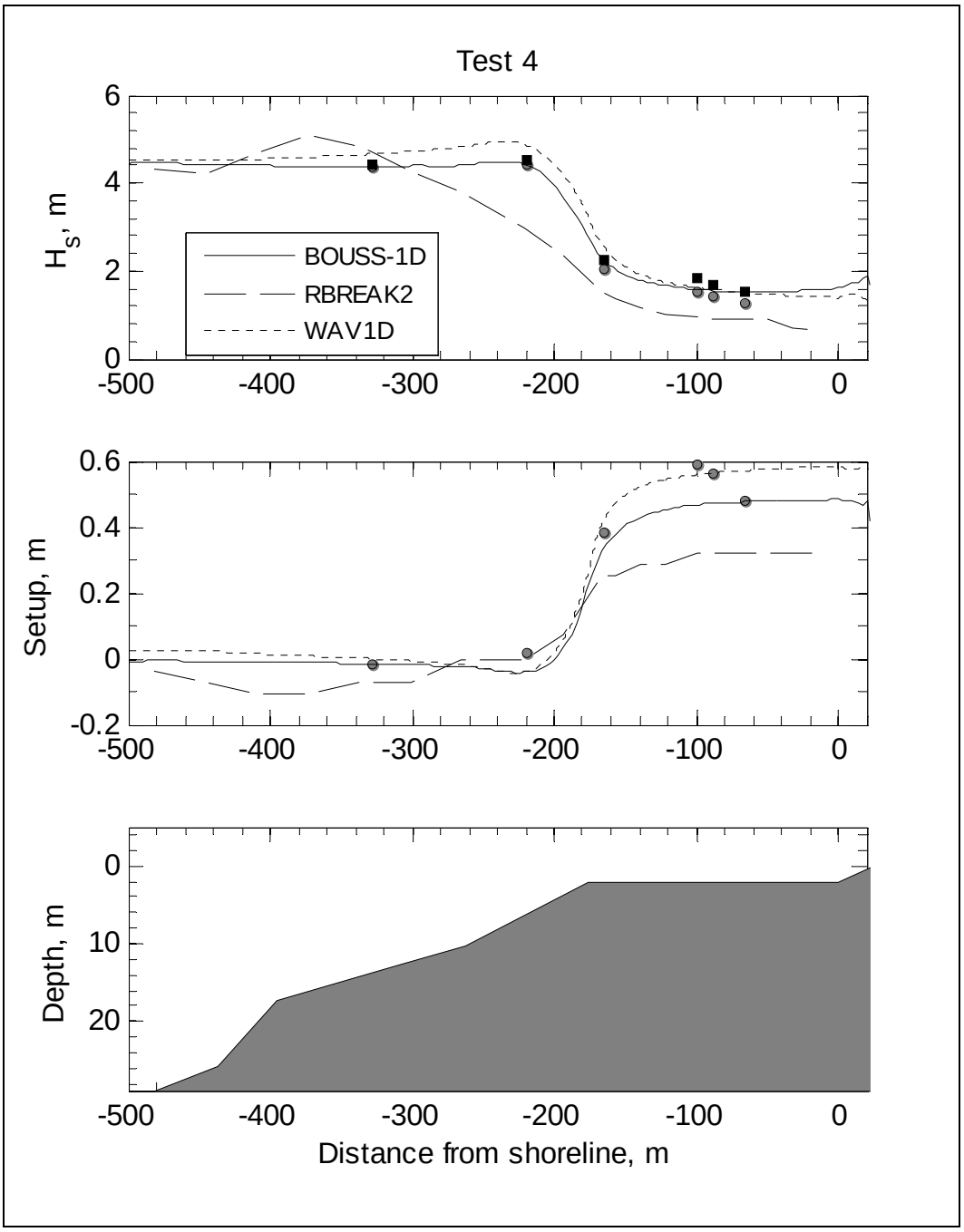

Figure D4. Comparison of three wave model results with data for Test 4 of CHL experiments.

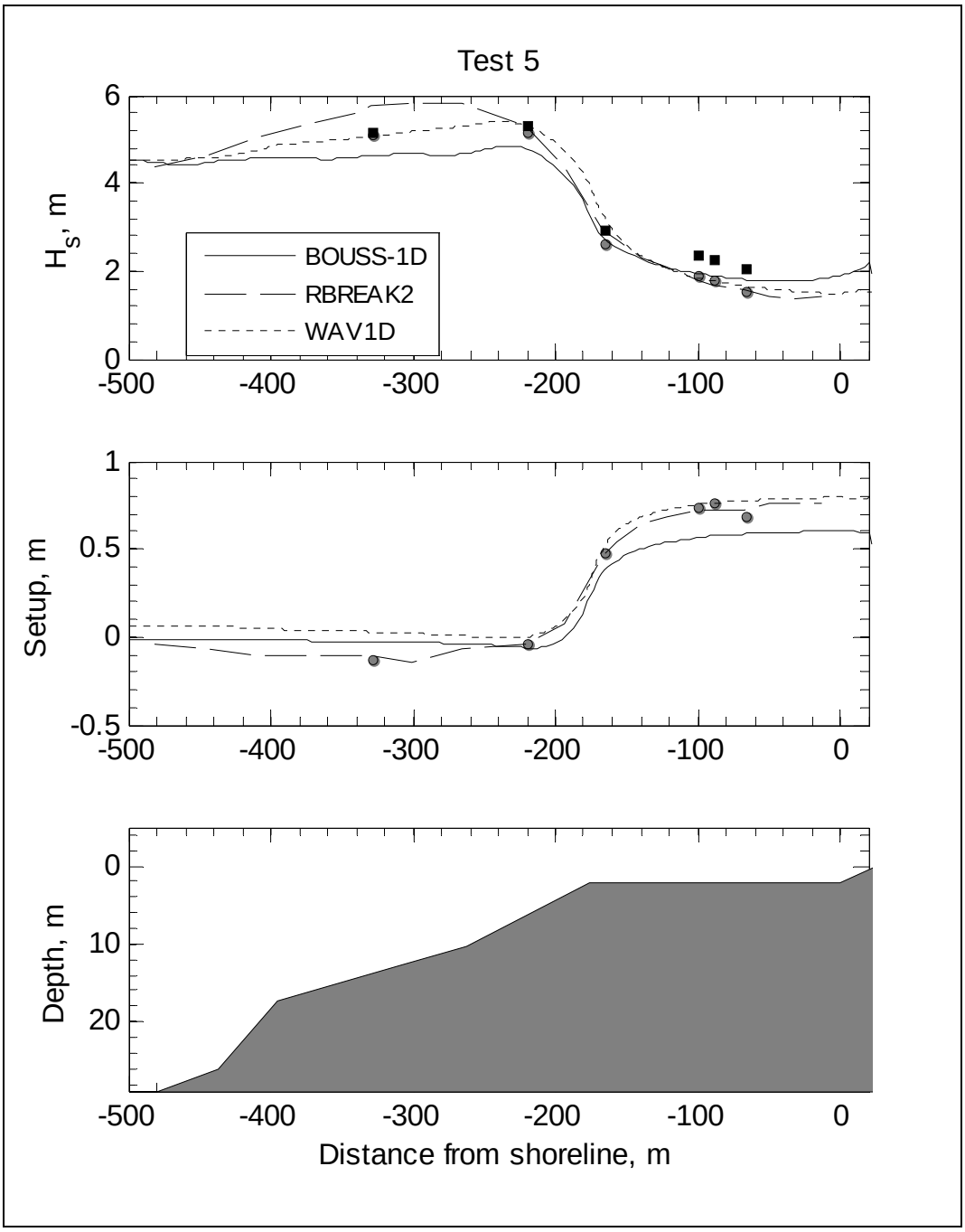

Figure D5. Comparison of three wave model results with data for Test 5 of CHL experiments.

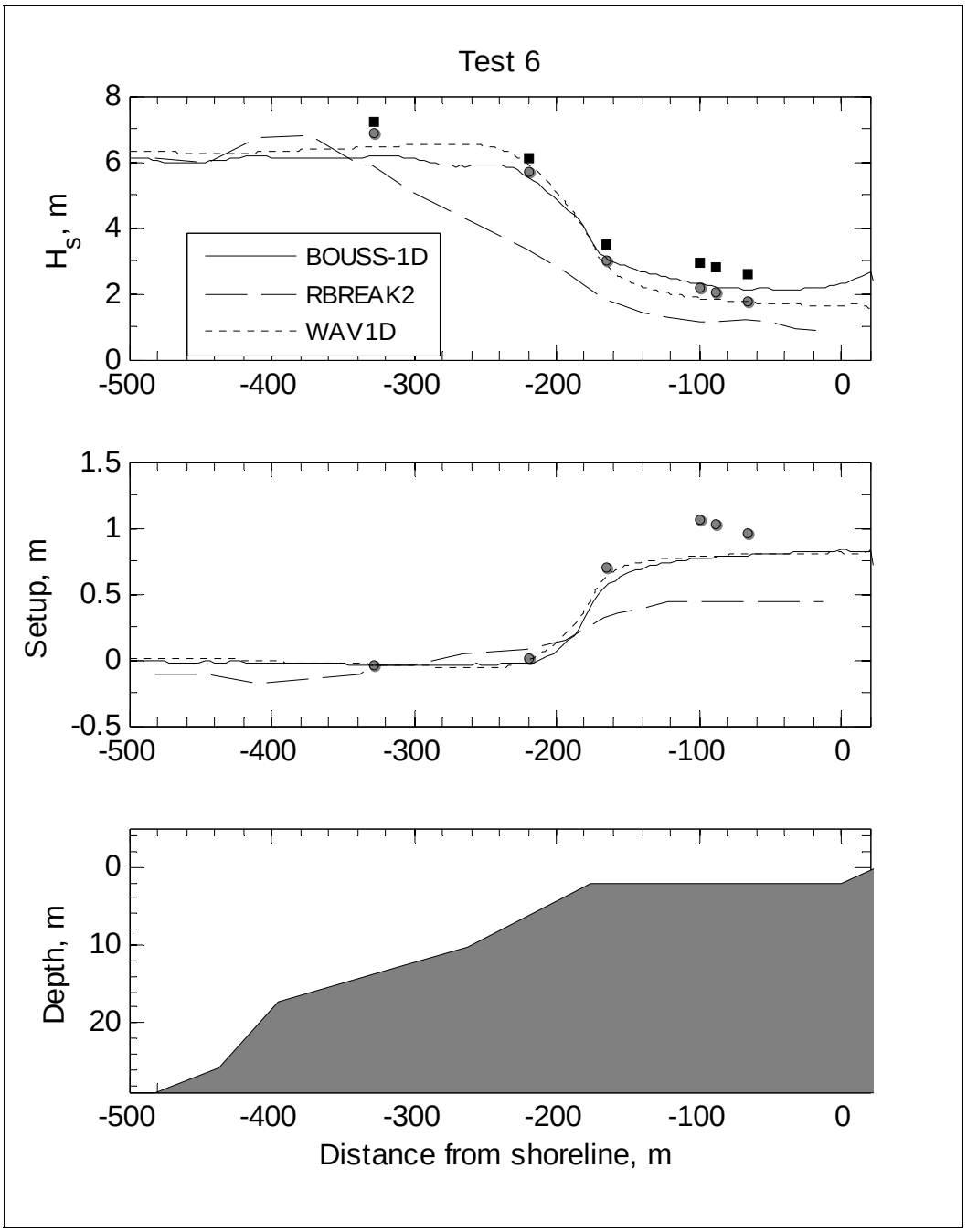

Figure D6. Comparison of three wave model results with data for Test 6 of CHL experiments.

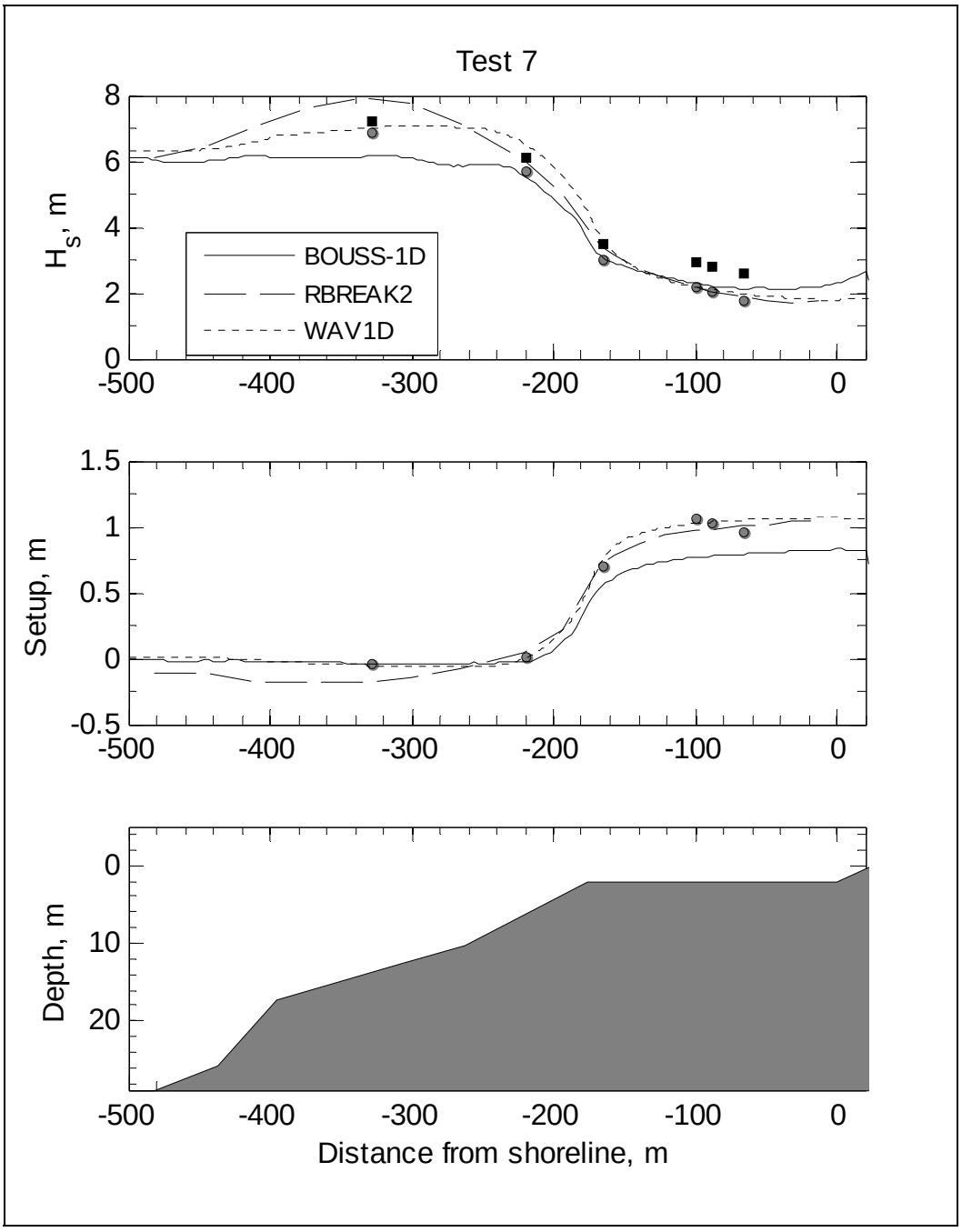

Figure D7. Comparison of three wave model results with data for Test 7 of CHL experiments.

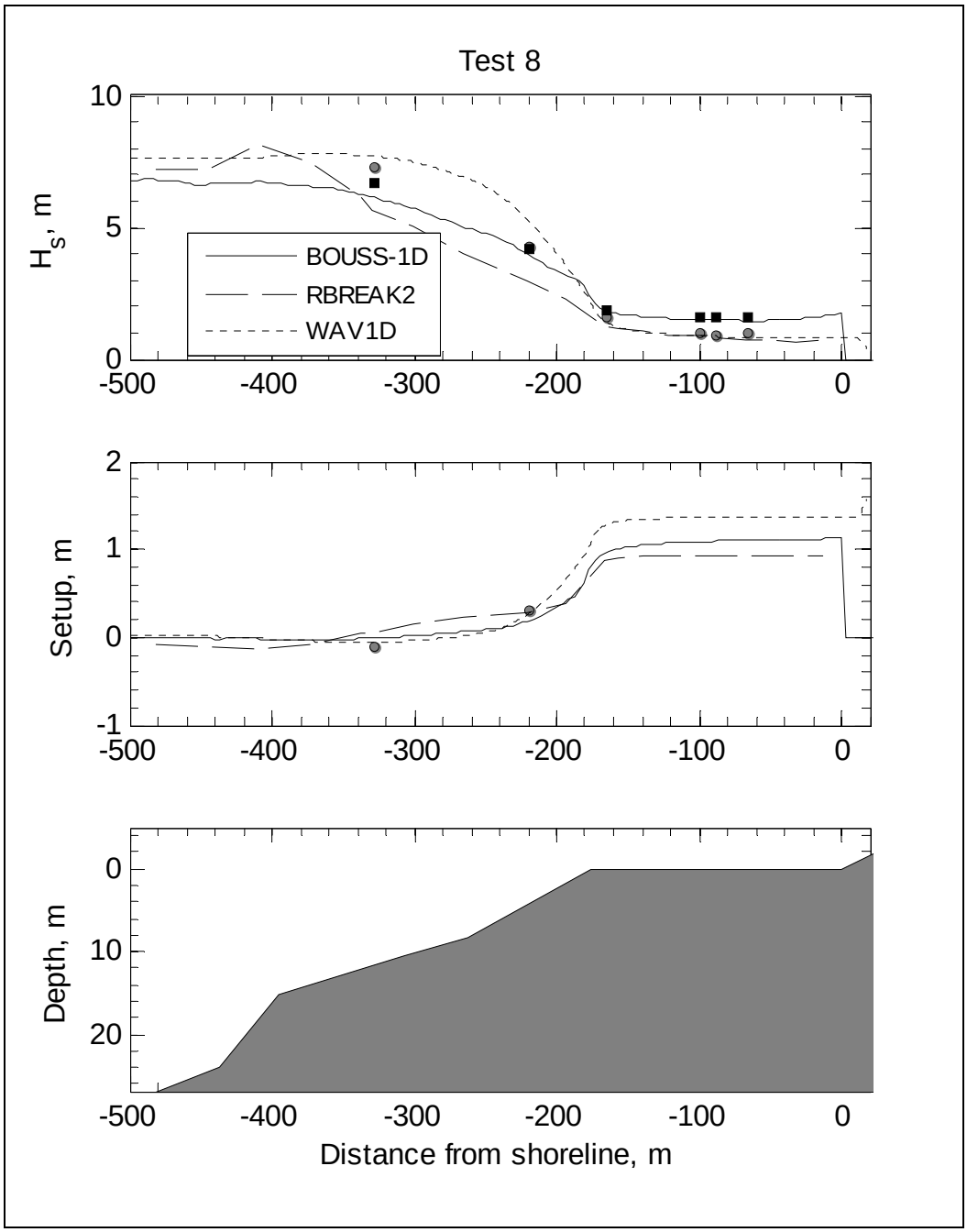

Figure D8. Comparison of three wave model results with data for Test 8 of CHL experiments.

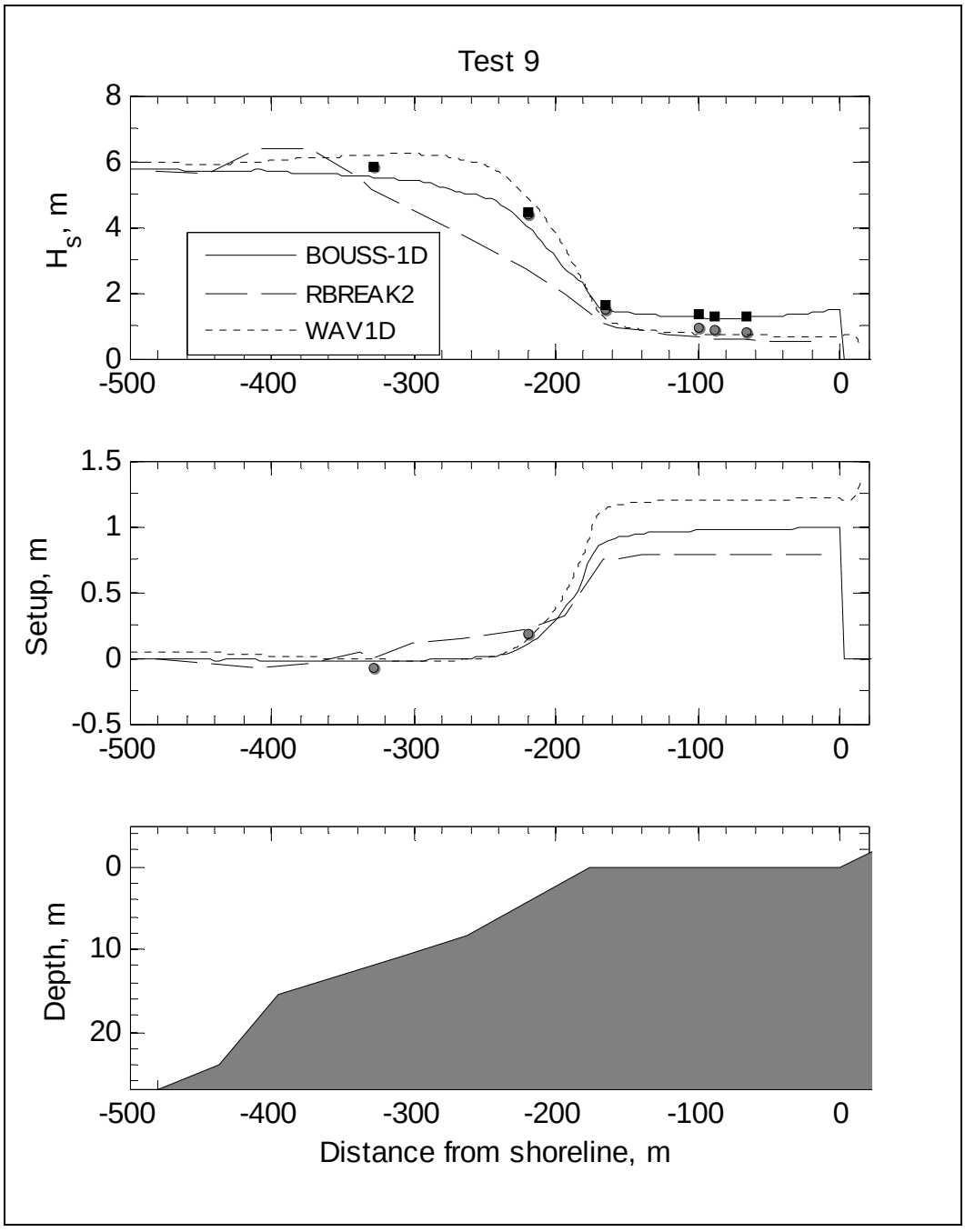

Figure D9. Comparison of three wave model results with data for Test 9 of CHL experiments.

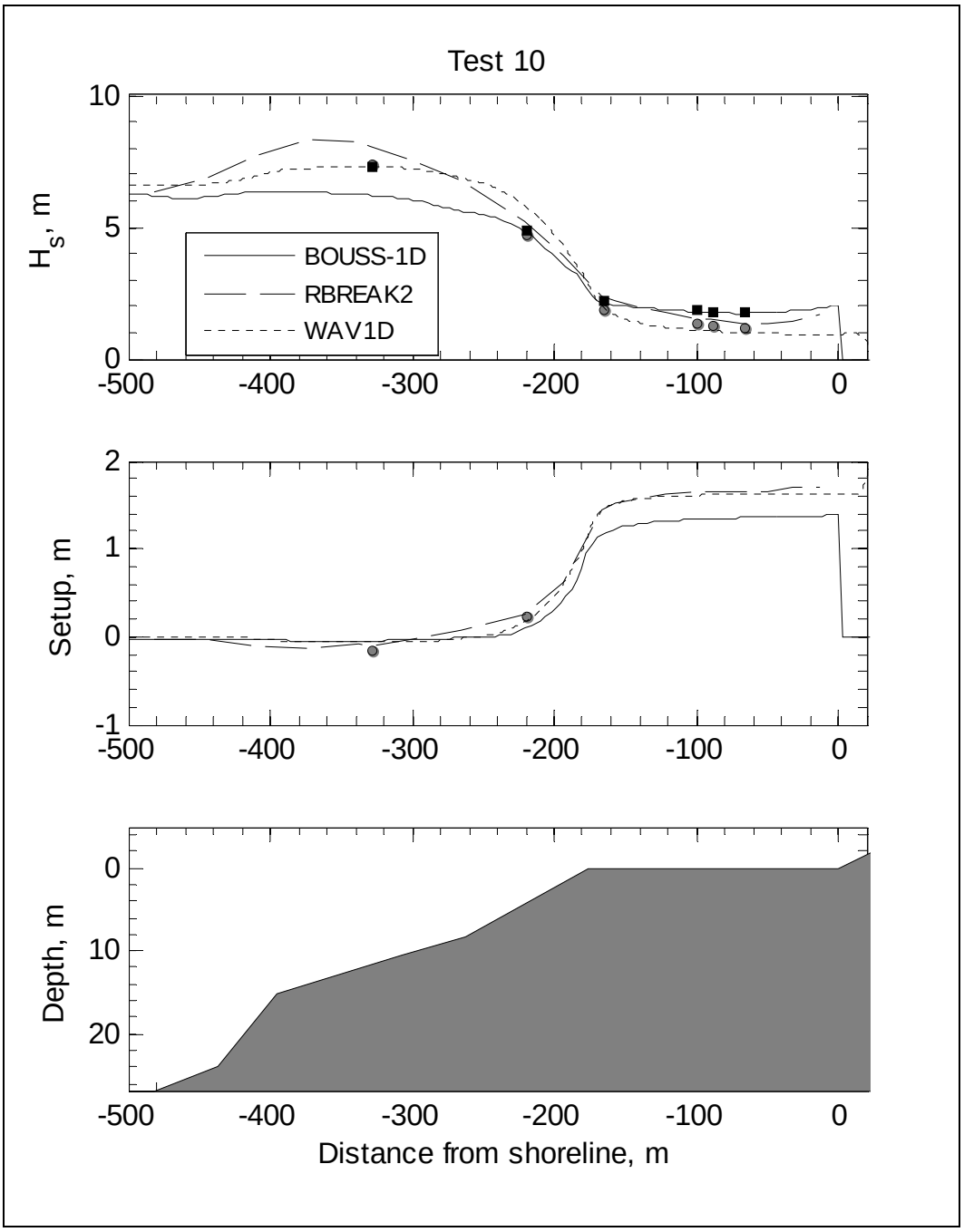

Figure D10. Comparison of three wave model results with data for Test 10 of CHL experiments.

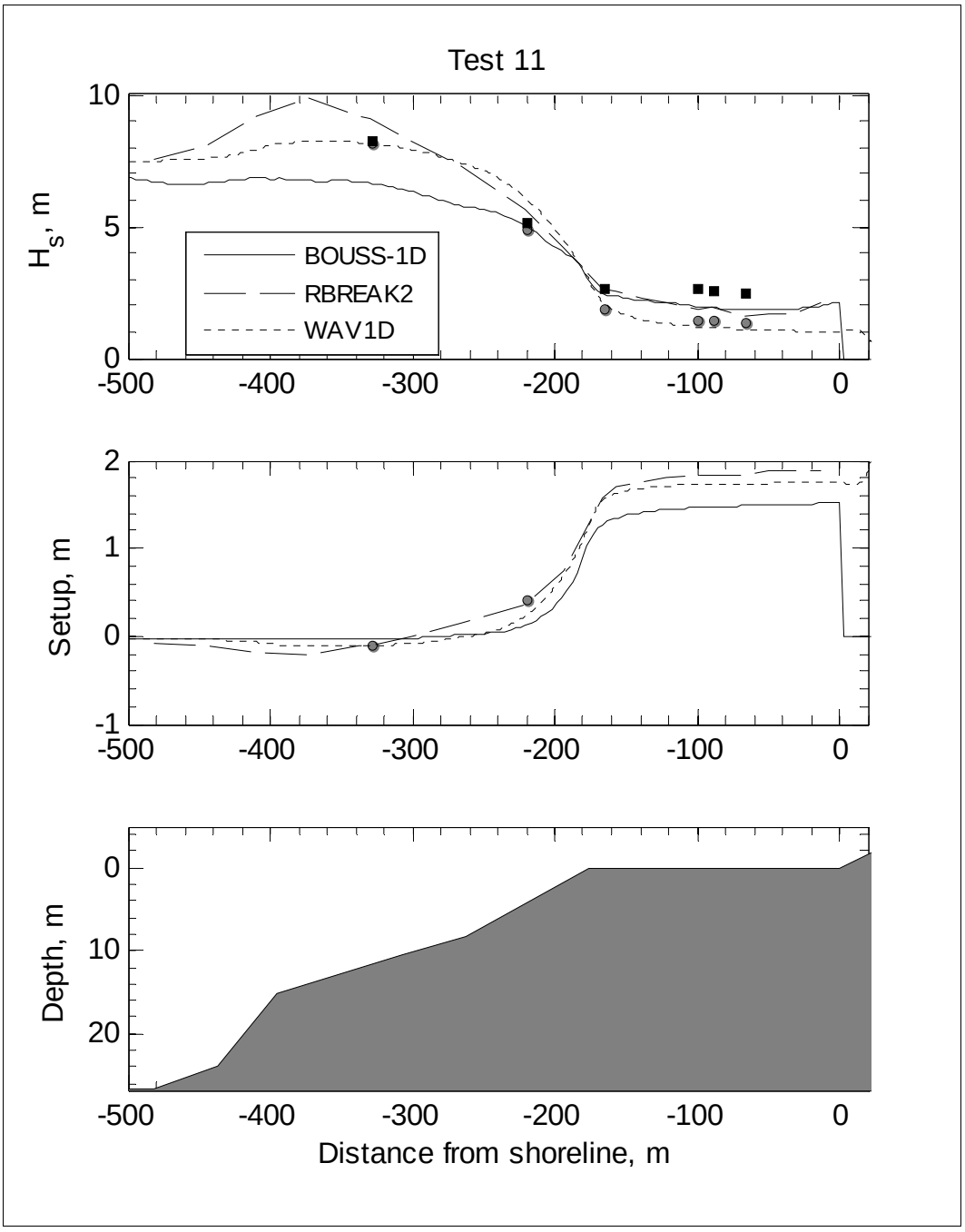

Figure D11. Comparison of three wave model results with data for Test 11 of CHL experiments.

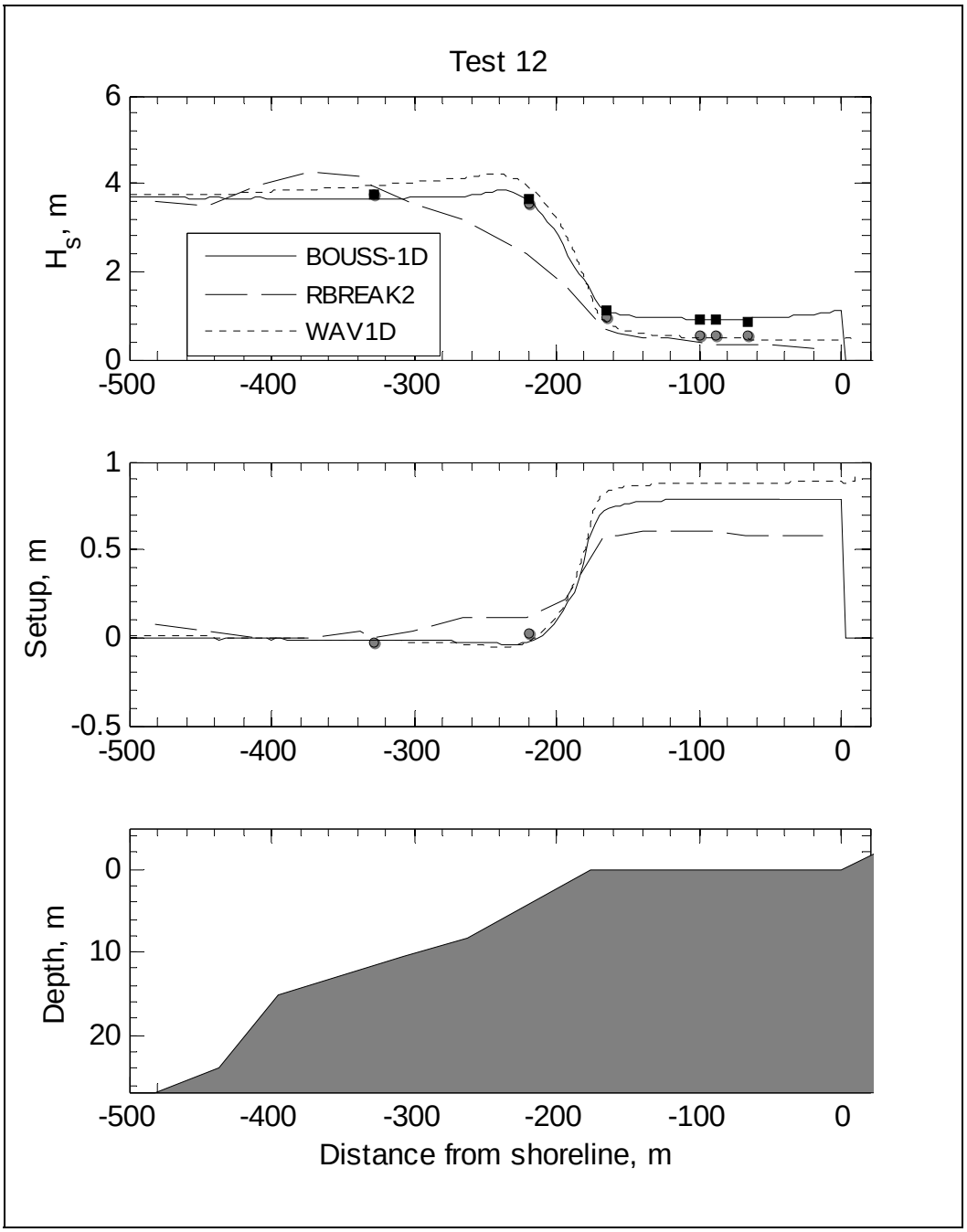

Figure D12. Comparison of three wave model results with data for Test 12 of CHL experiments.

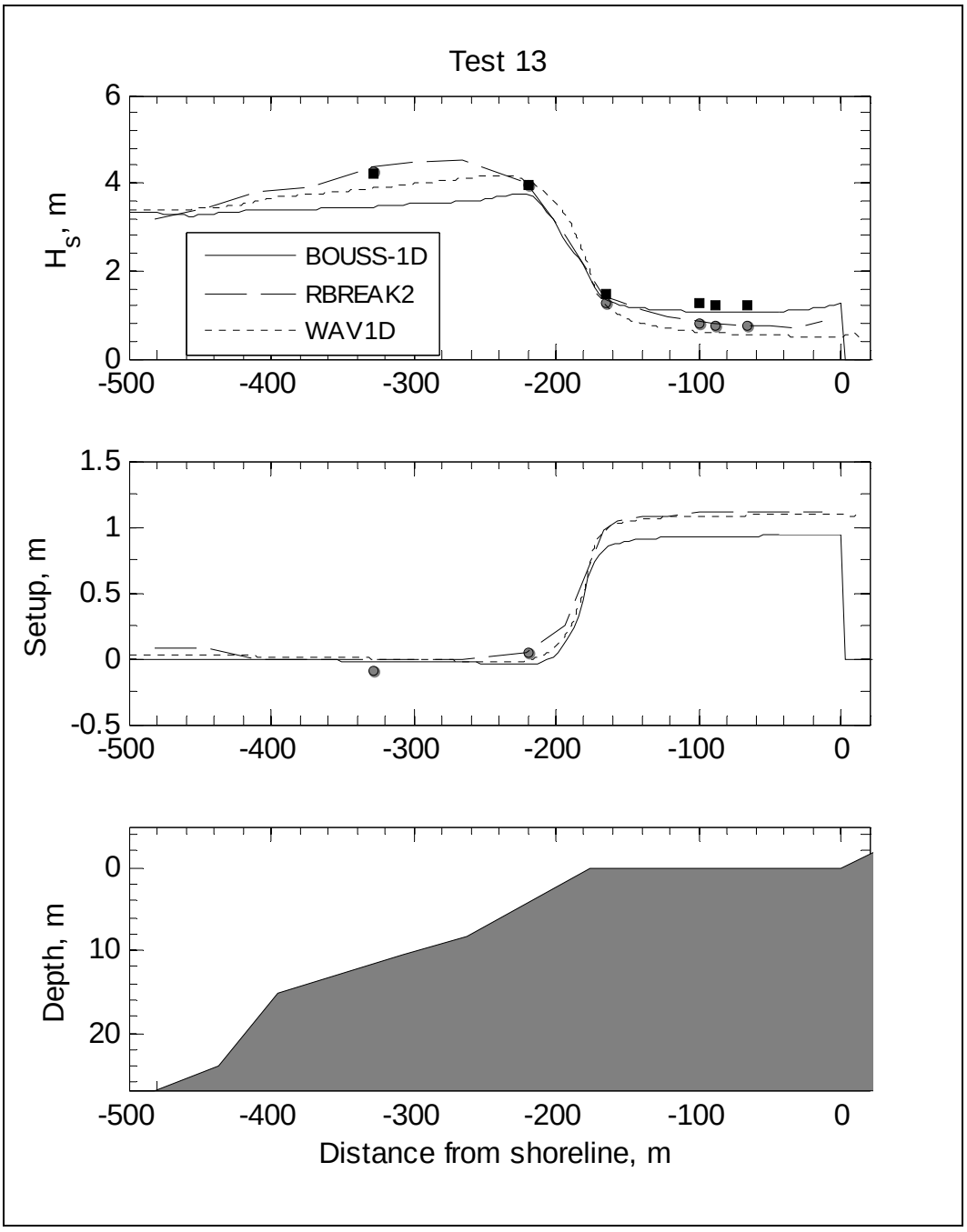

Figure D13. Comparison of three wave model results with data for Test 13 of CHL experiments.

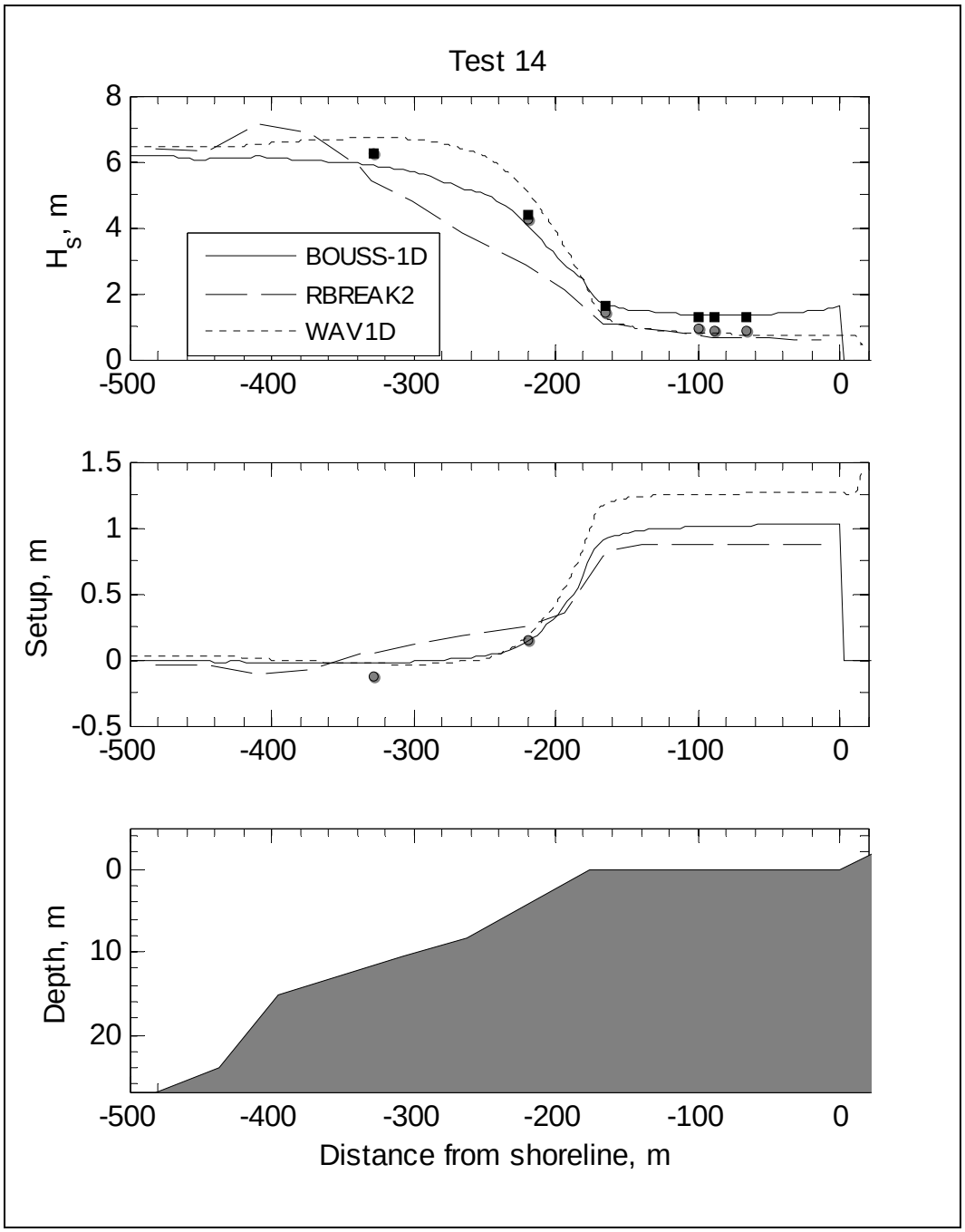

Figure D14. Comparison of three wave model results with data for Test 14 of CHL experiments.

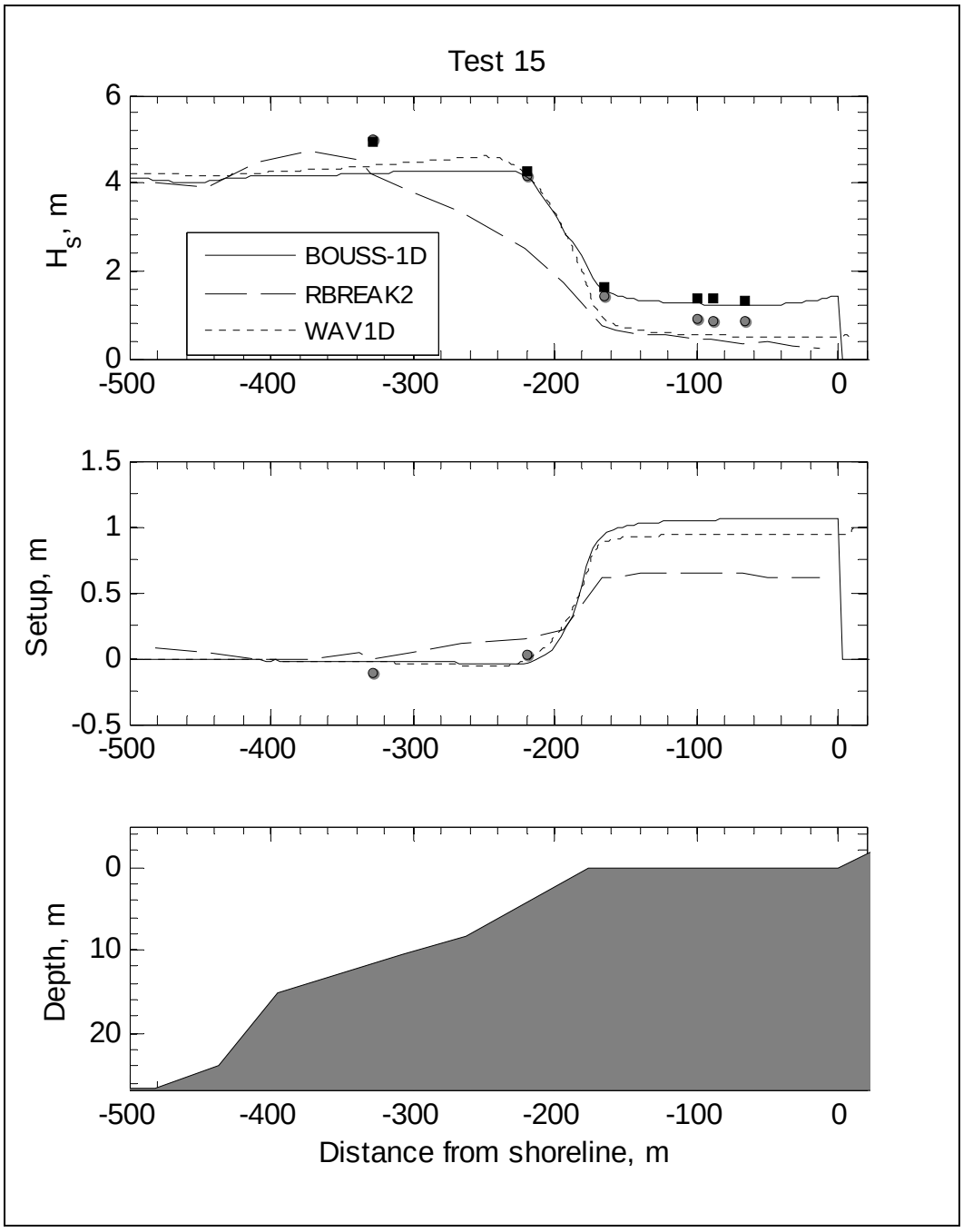

Figure D15. Comparison of three wave model results with data for Test 15 of CHL experiments.

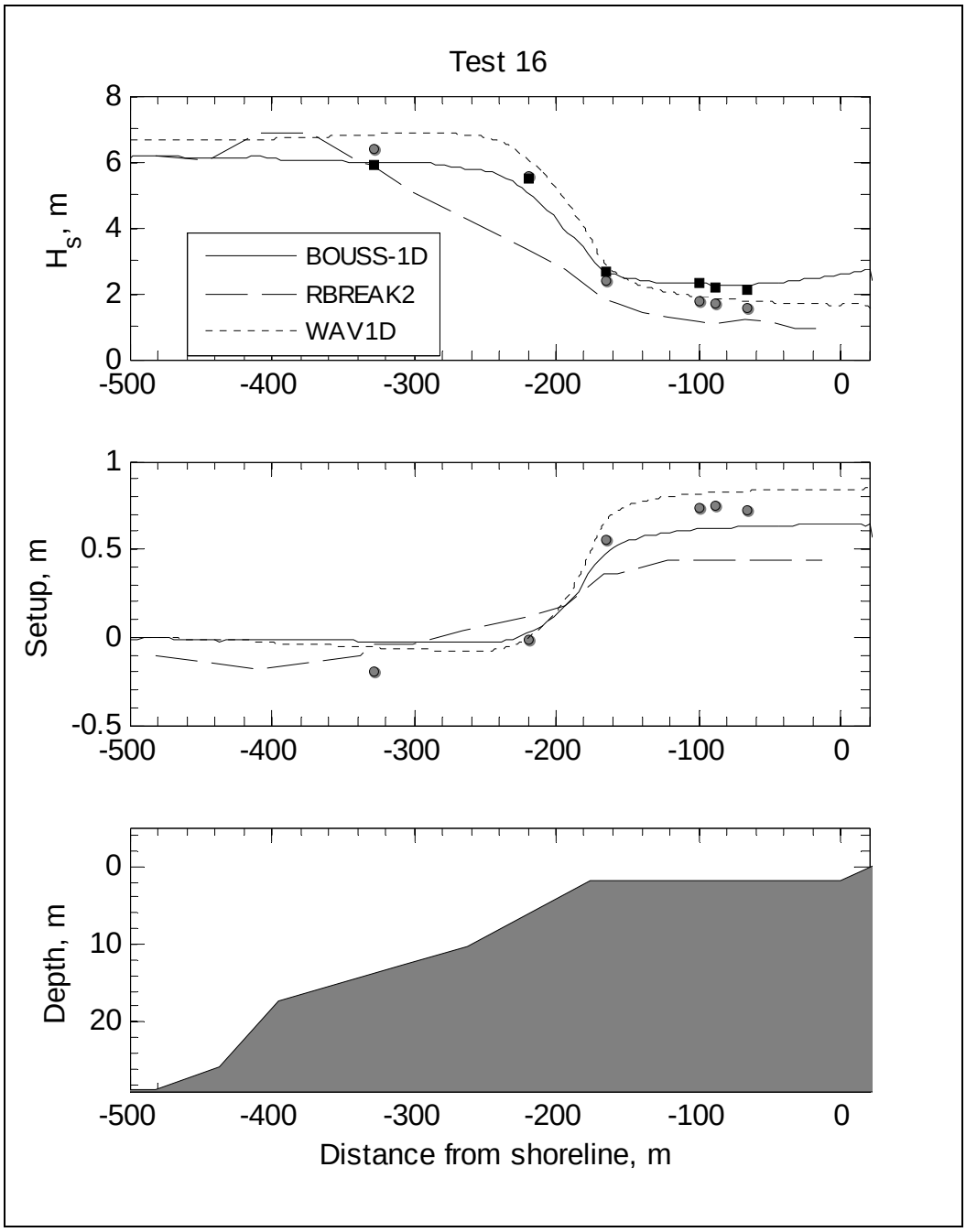

Figure D16. Comparison of three wave model results with data for Test 16 of CHL experiments.

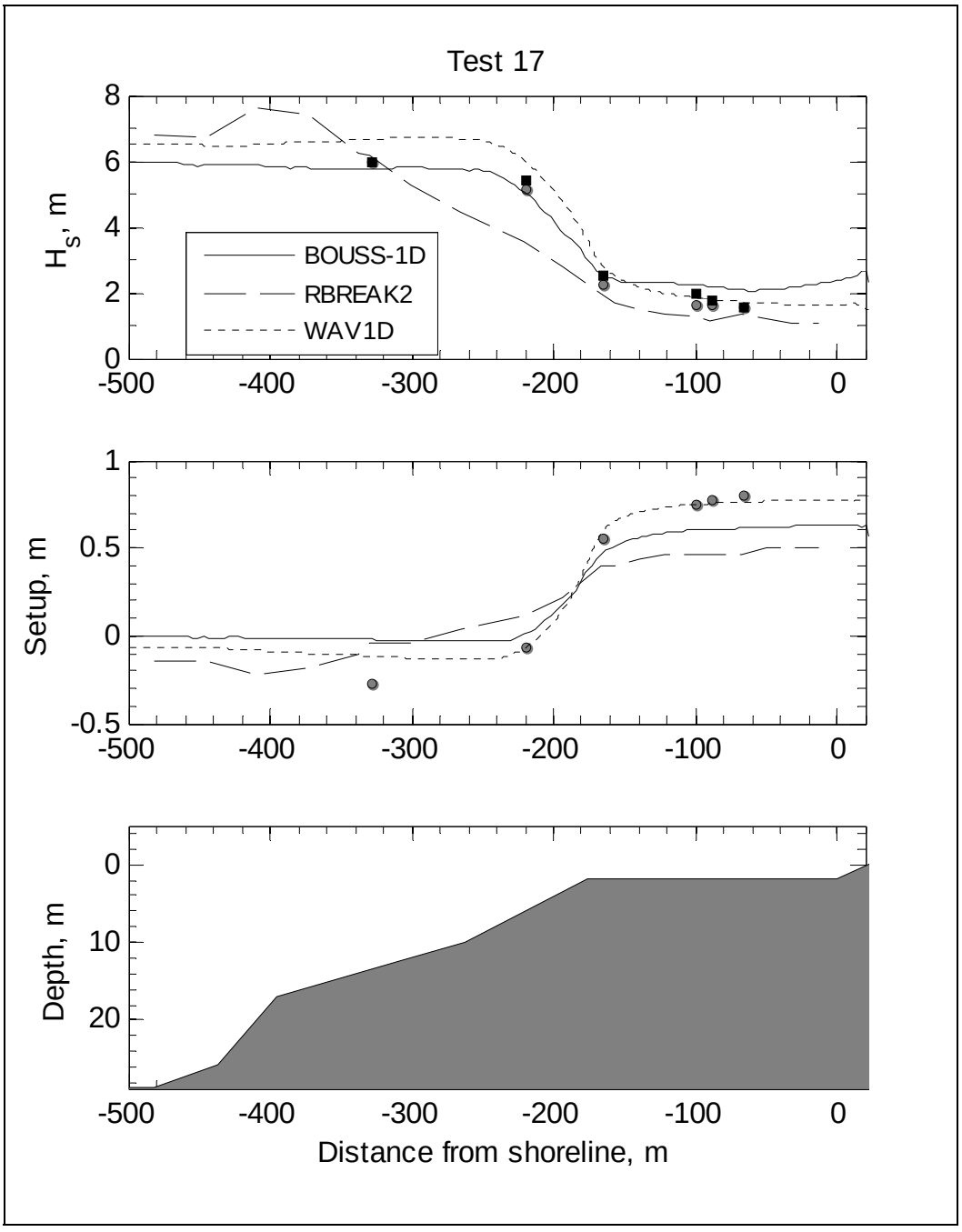

Figure D17. Comparison of three wave model results with data for Test 17 of CHL experiments.

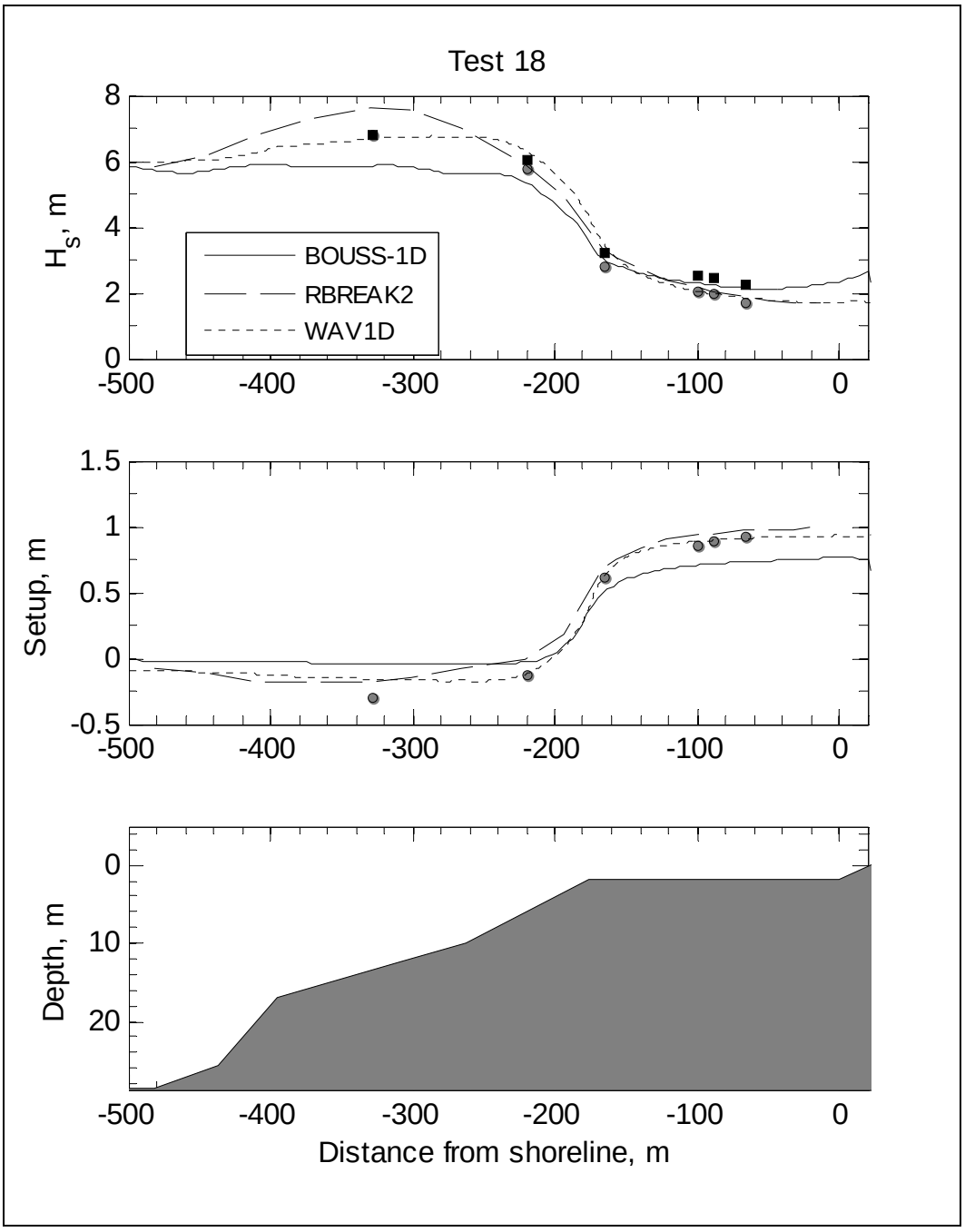

Figure D18. Comparison of three wave model results with data for Test 18 of CHL experiments.

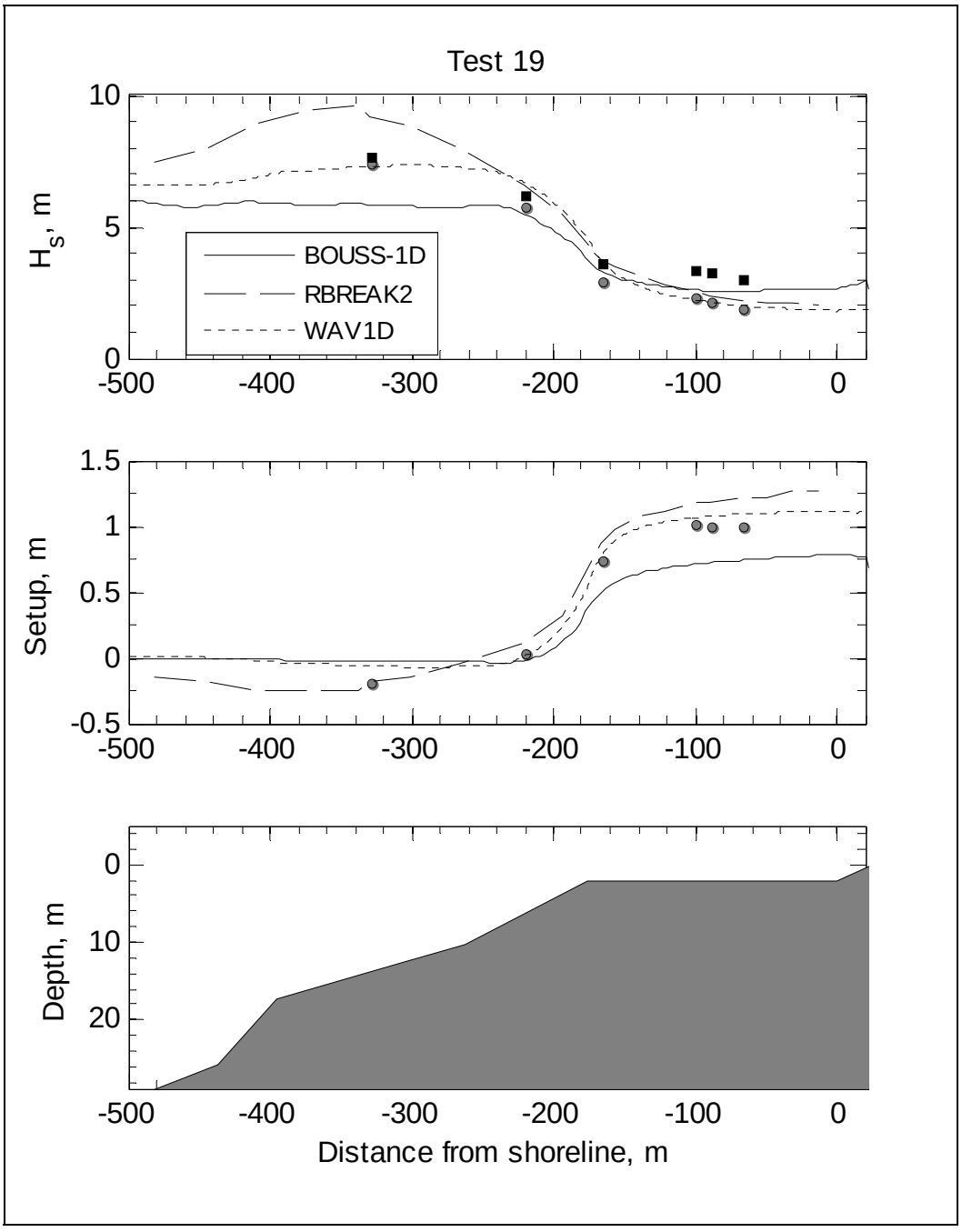

Figure D19. Comparison of three wave model results with data for Test 19 of CHL experiments.

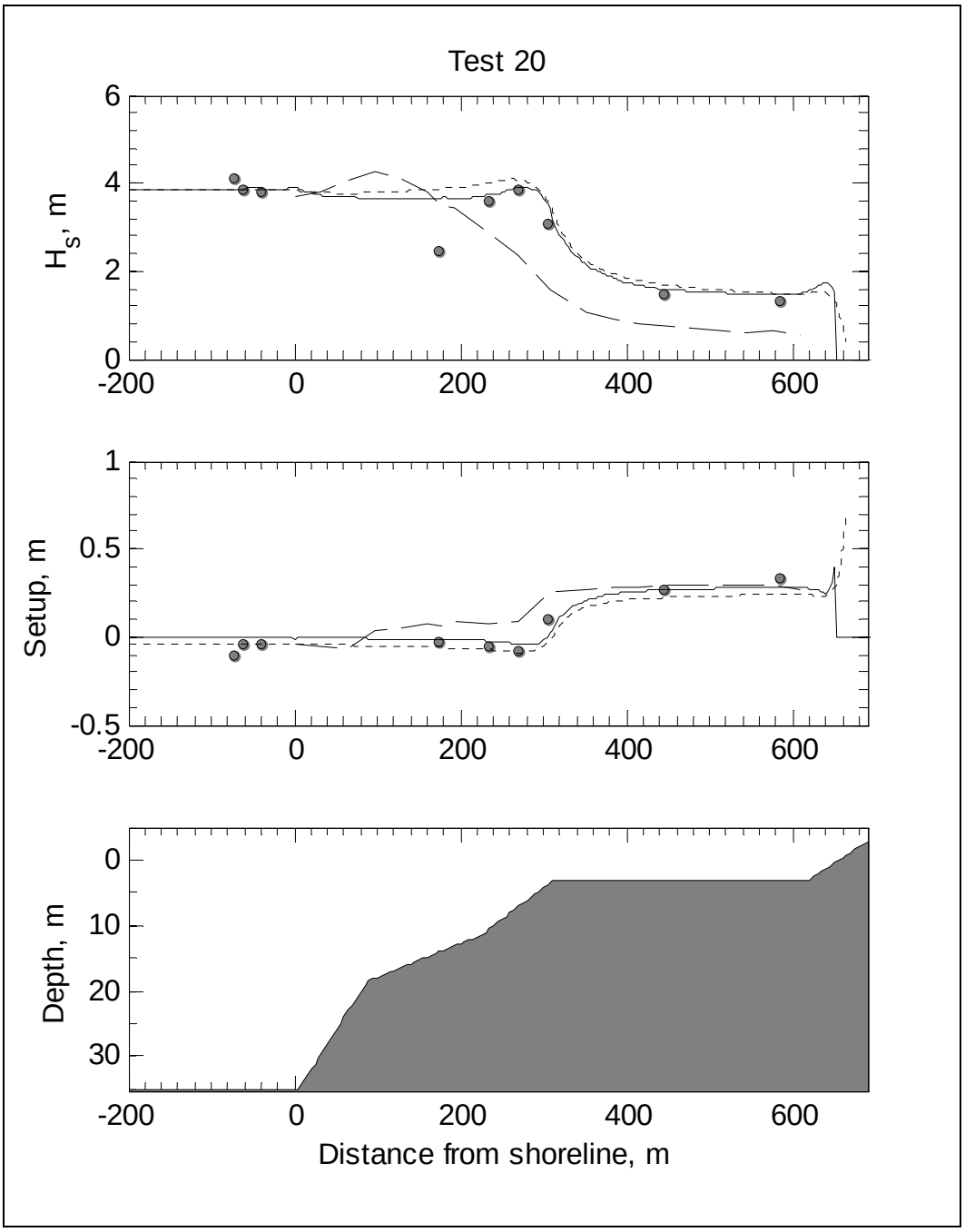

Figure D20. Comparison of three wave model results with data for Test 20 of CHL experiments.

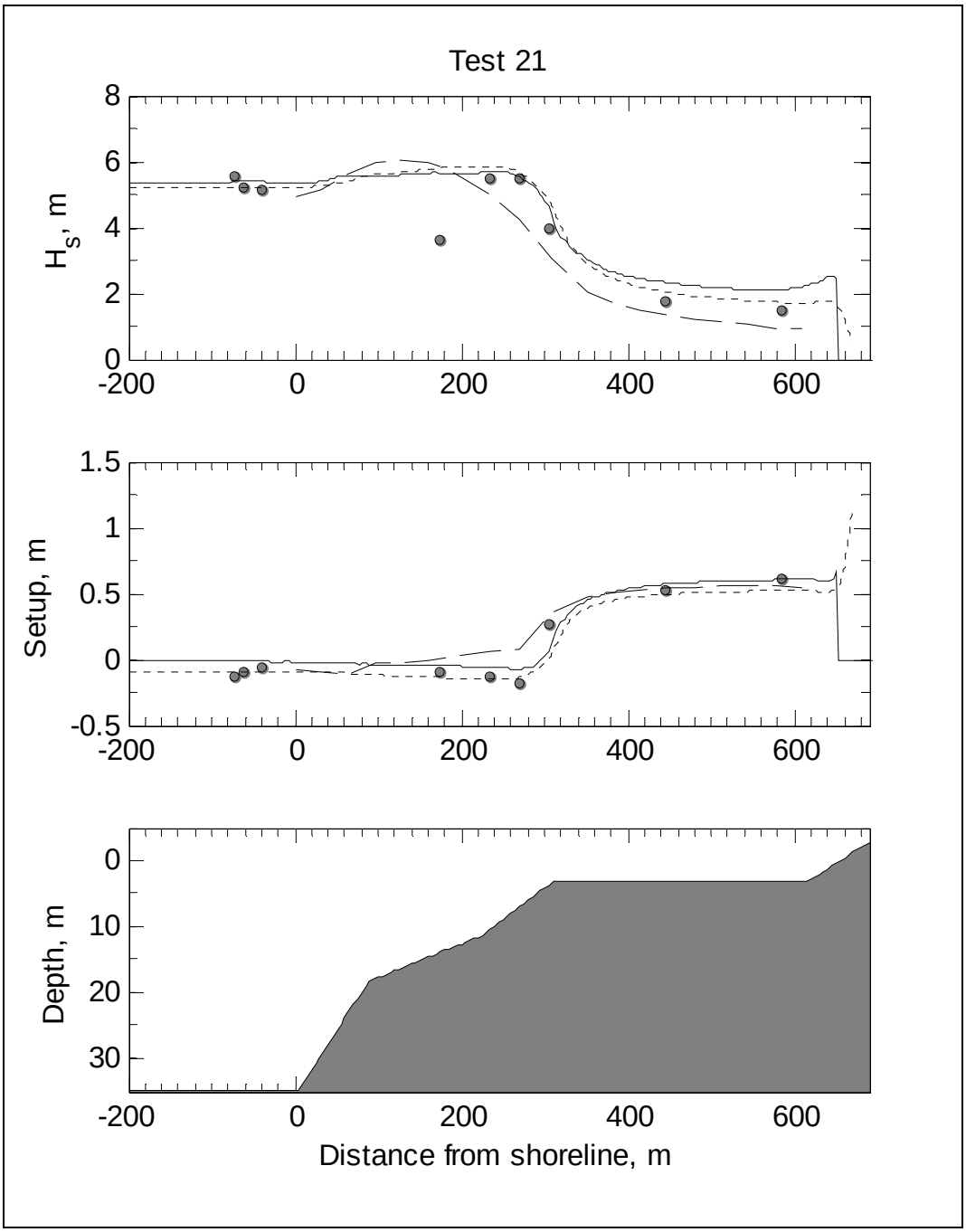

Figure D21. Comparison of three wave model results with data for Test 21 of CHL experiments.

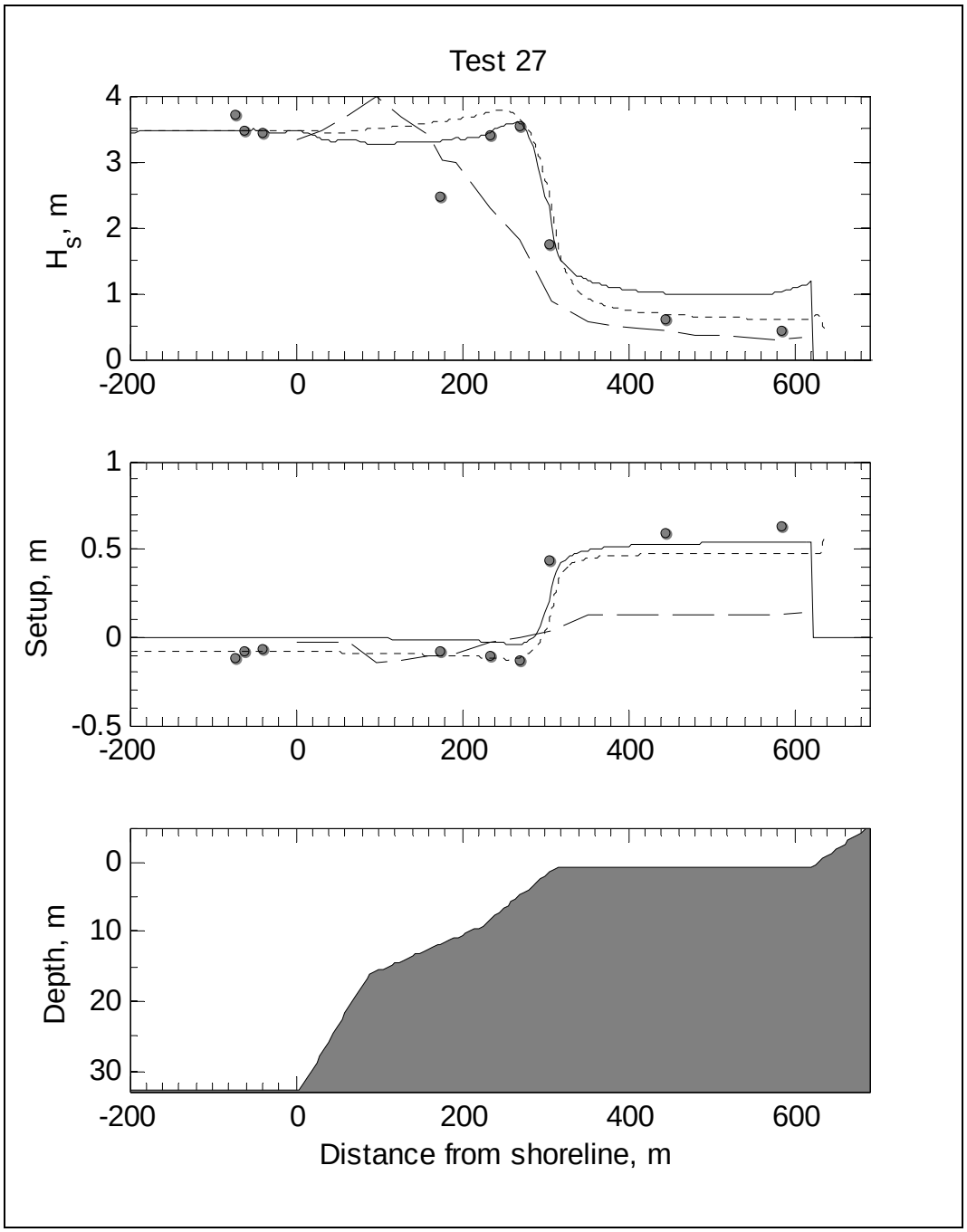

Figure D22. Comparison of three wave model results with data for Test 27 of CHL experiments.

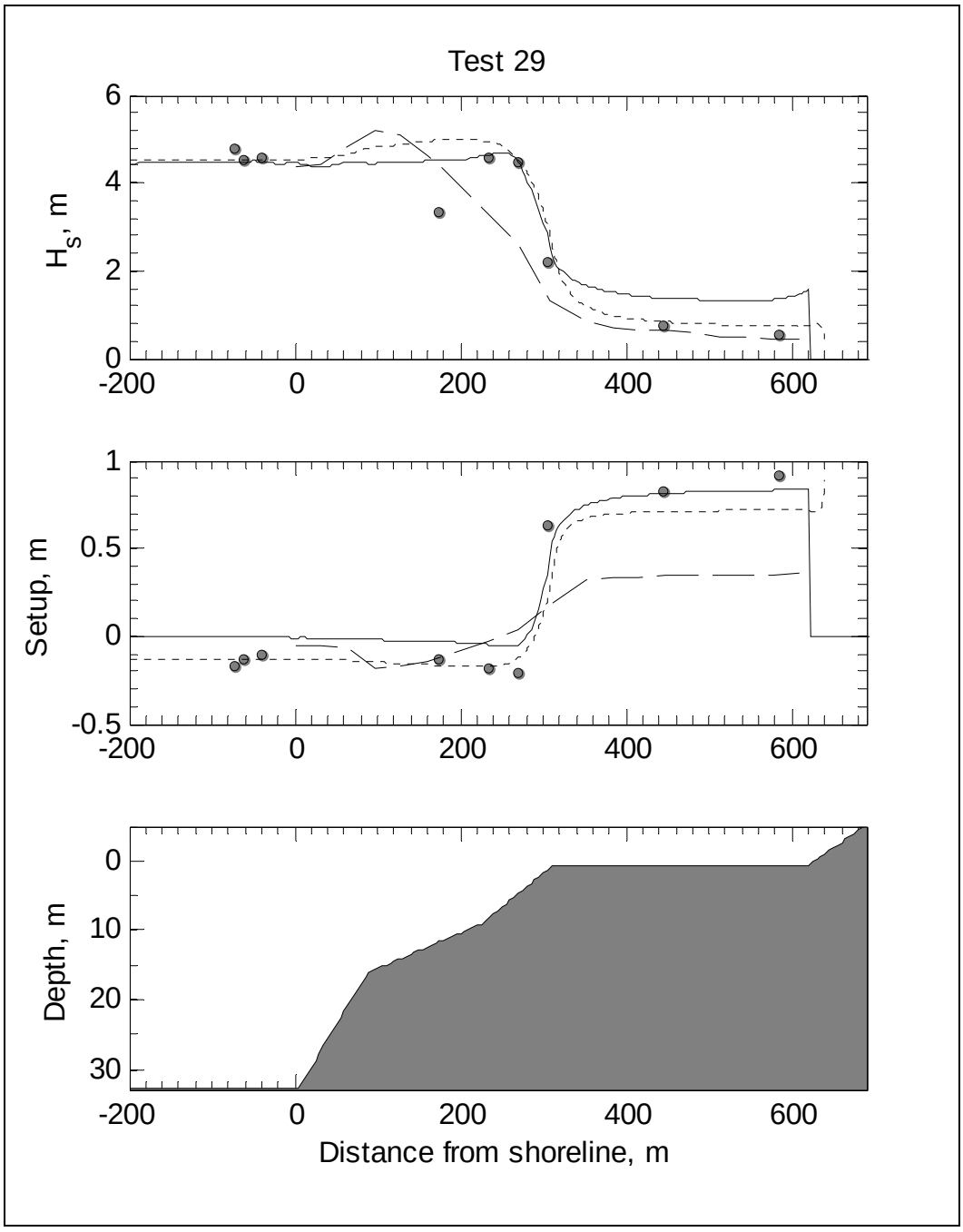

Figure D23. Comparison of three wave model results with data for Test 29 of CHL experiments.

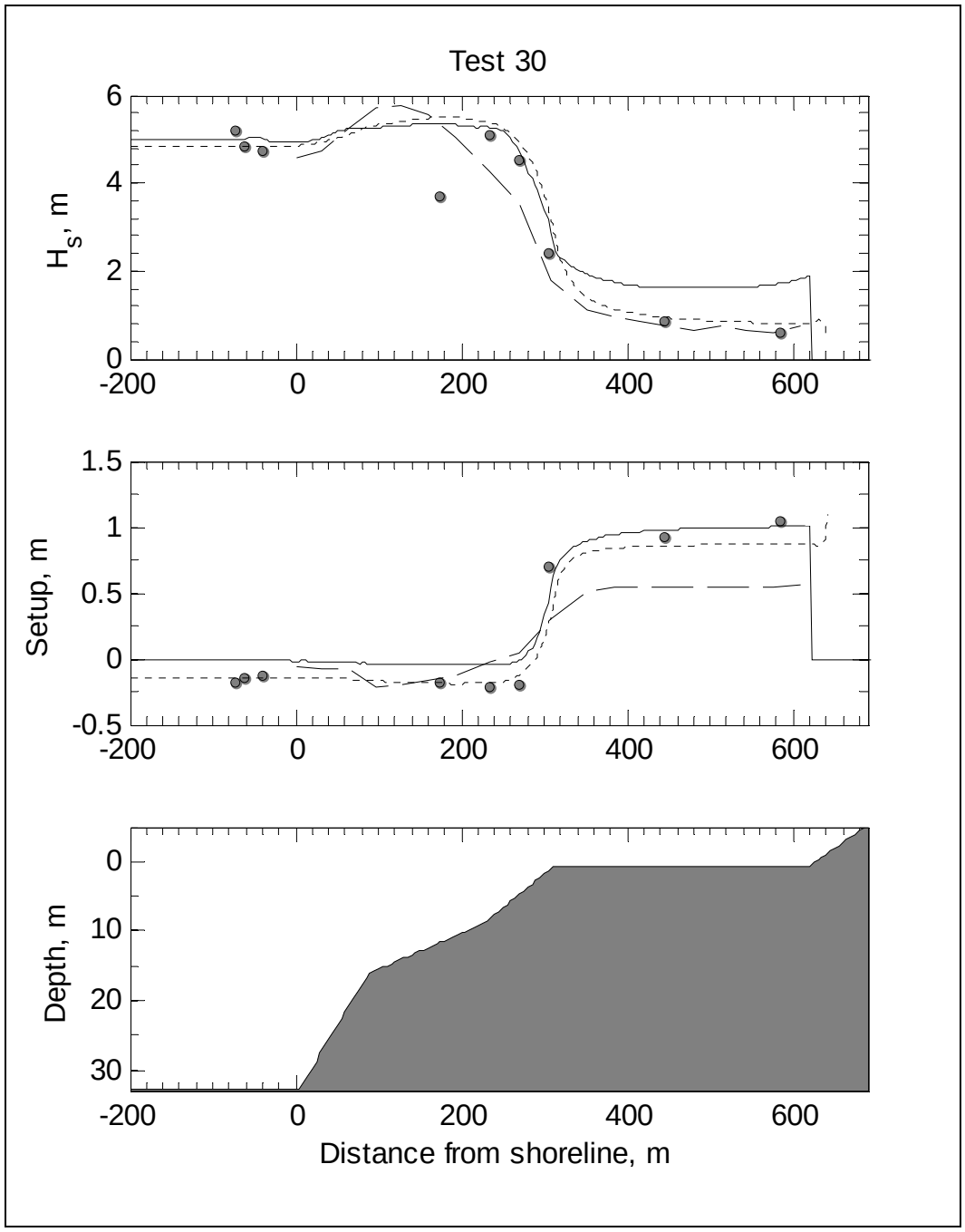

Figure D24. Comparison of three wave model results with data for Test 30 of CHL experiments.

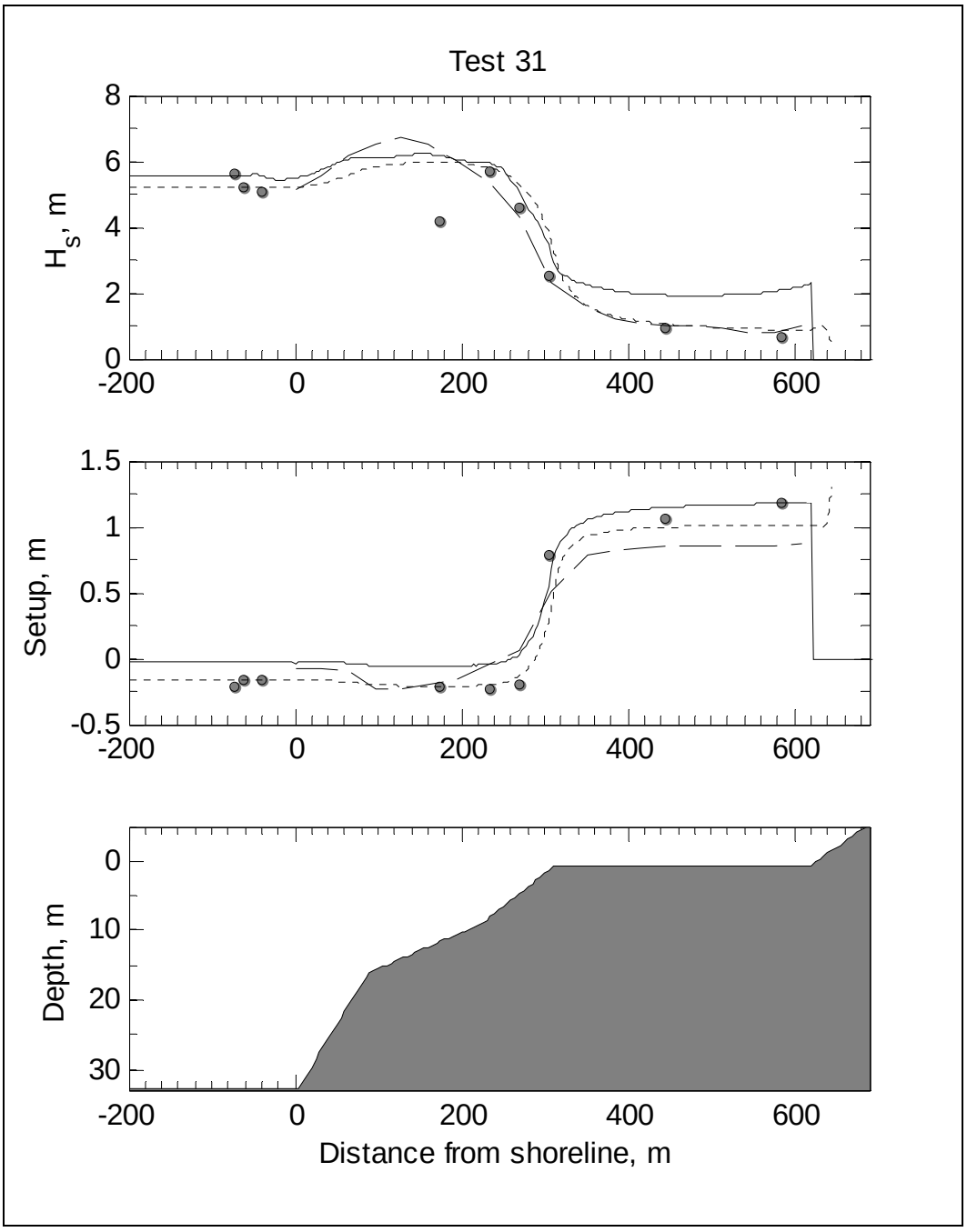

Figure D25. Comparison of three wave model results with data for Test 31 of CHL experiments.

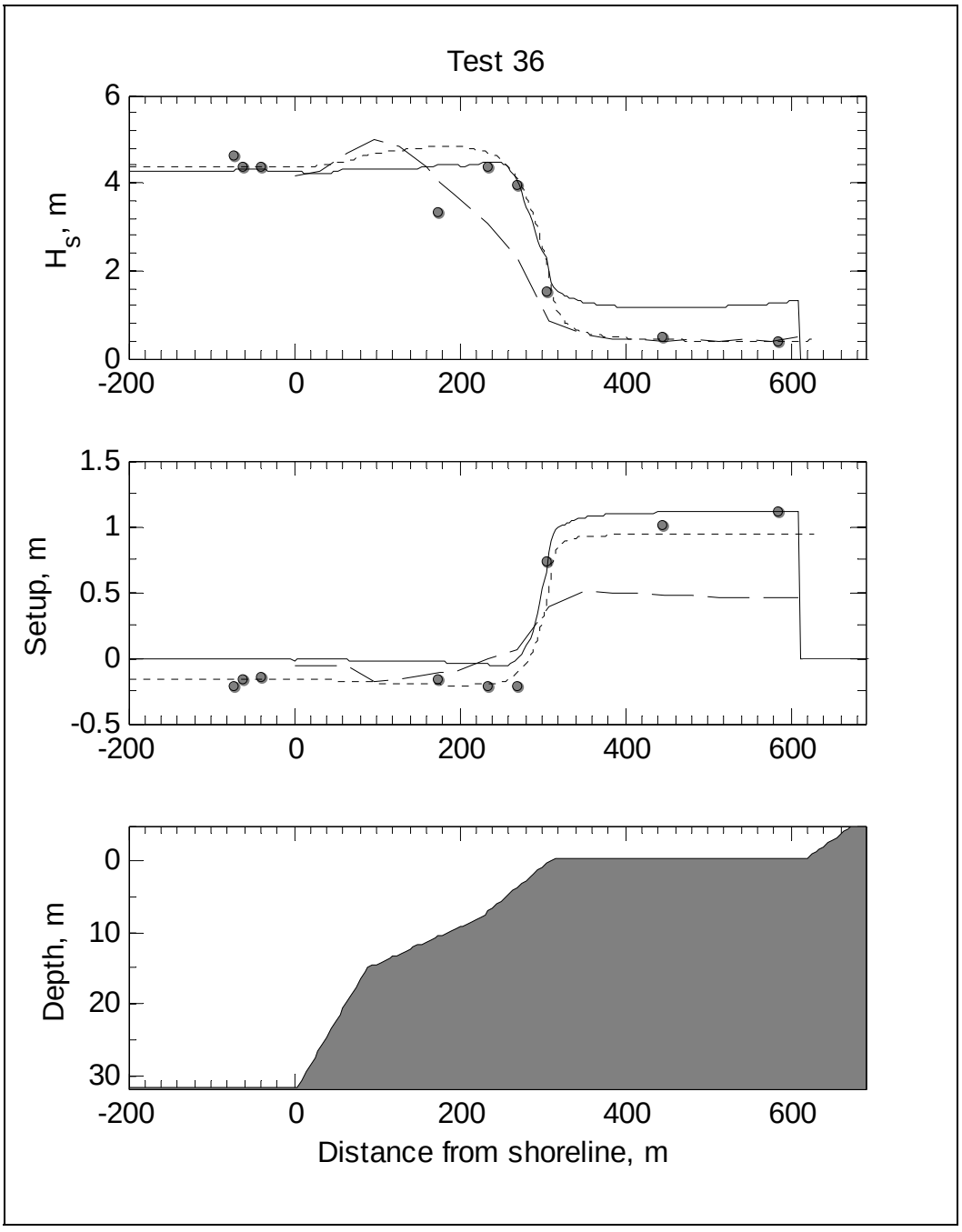

Figure D26. Comparison of three wave model results with data for Test 36 of CHL experiments.

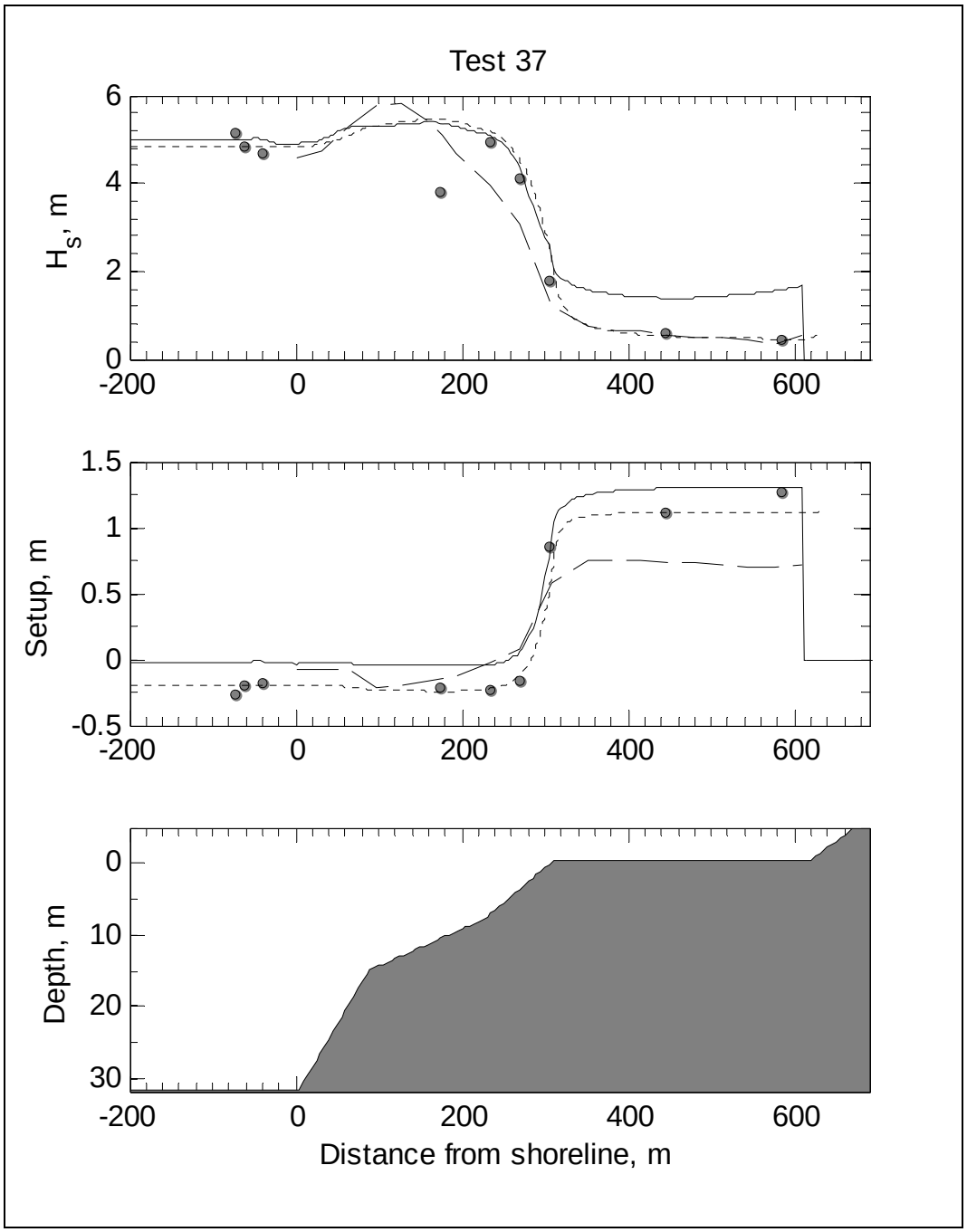

Figure D27. Comparison of three wave model results with data for Test 37 of CHL experiments.

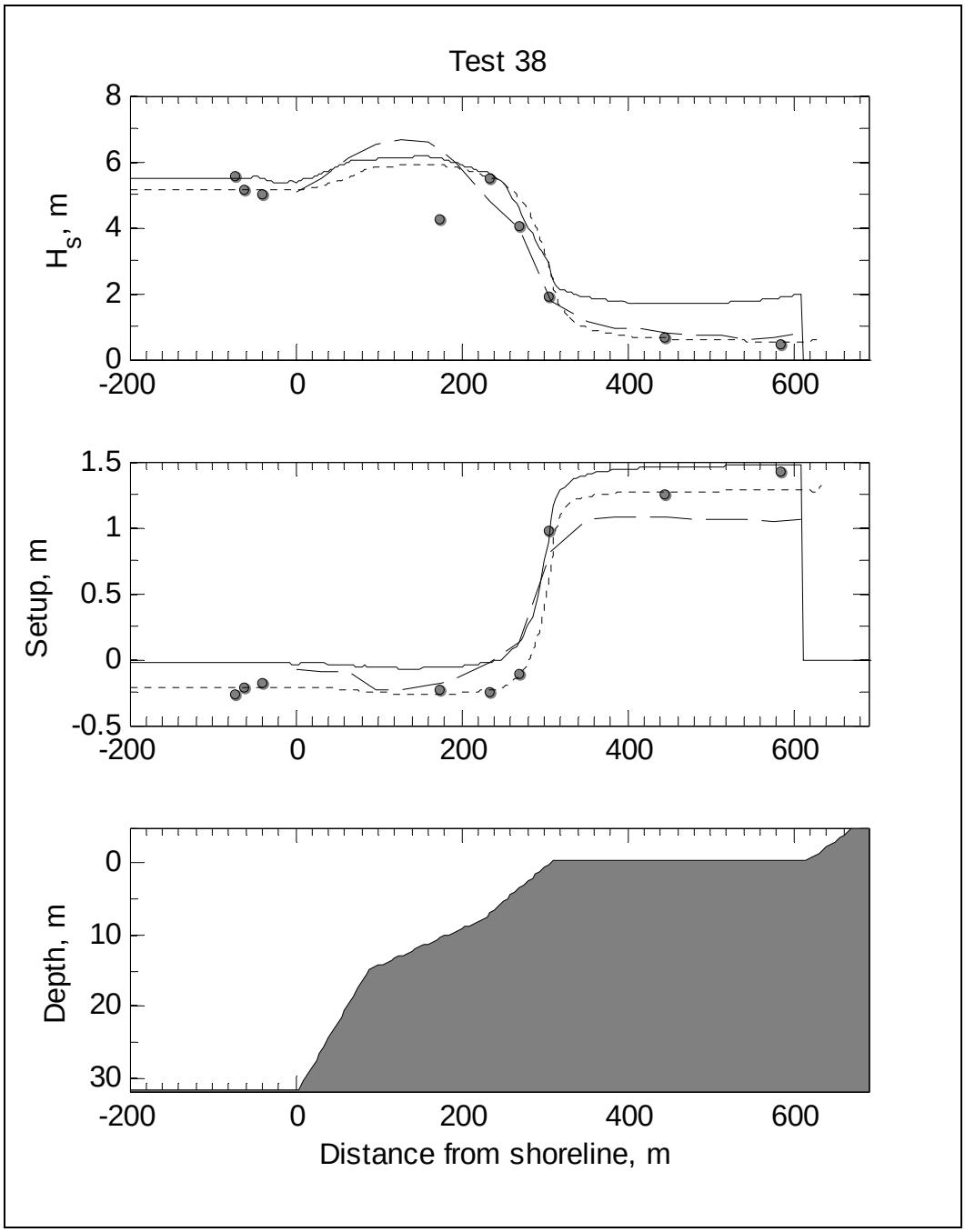

Figure D28. Comparison of three wave model results with data for Test 38 of CHL experiments.

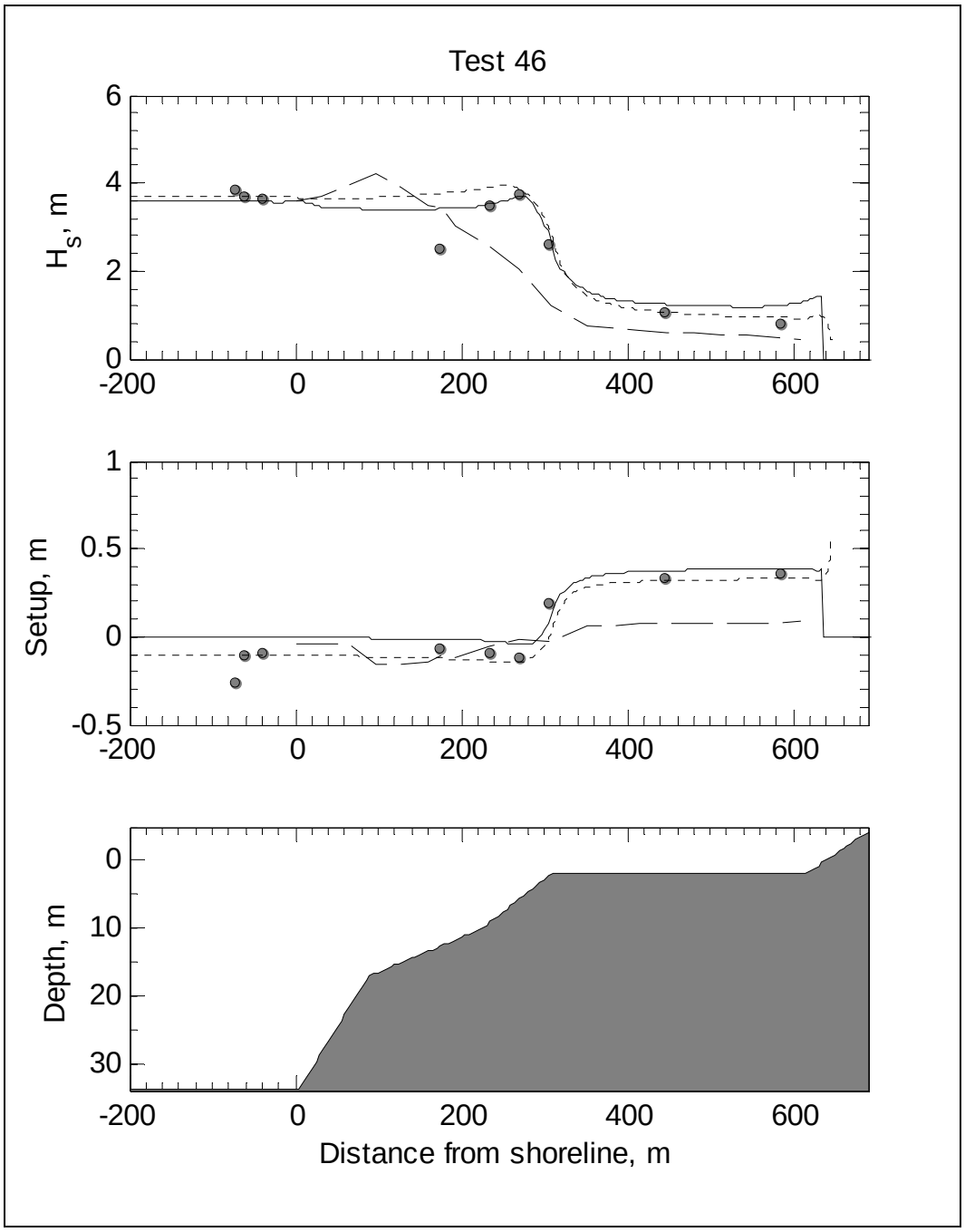

Figure D29. Comparison of three wave model results with data for Test 46 of CHL experiments.

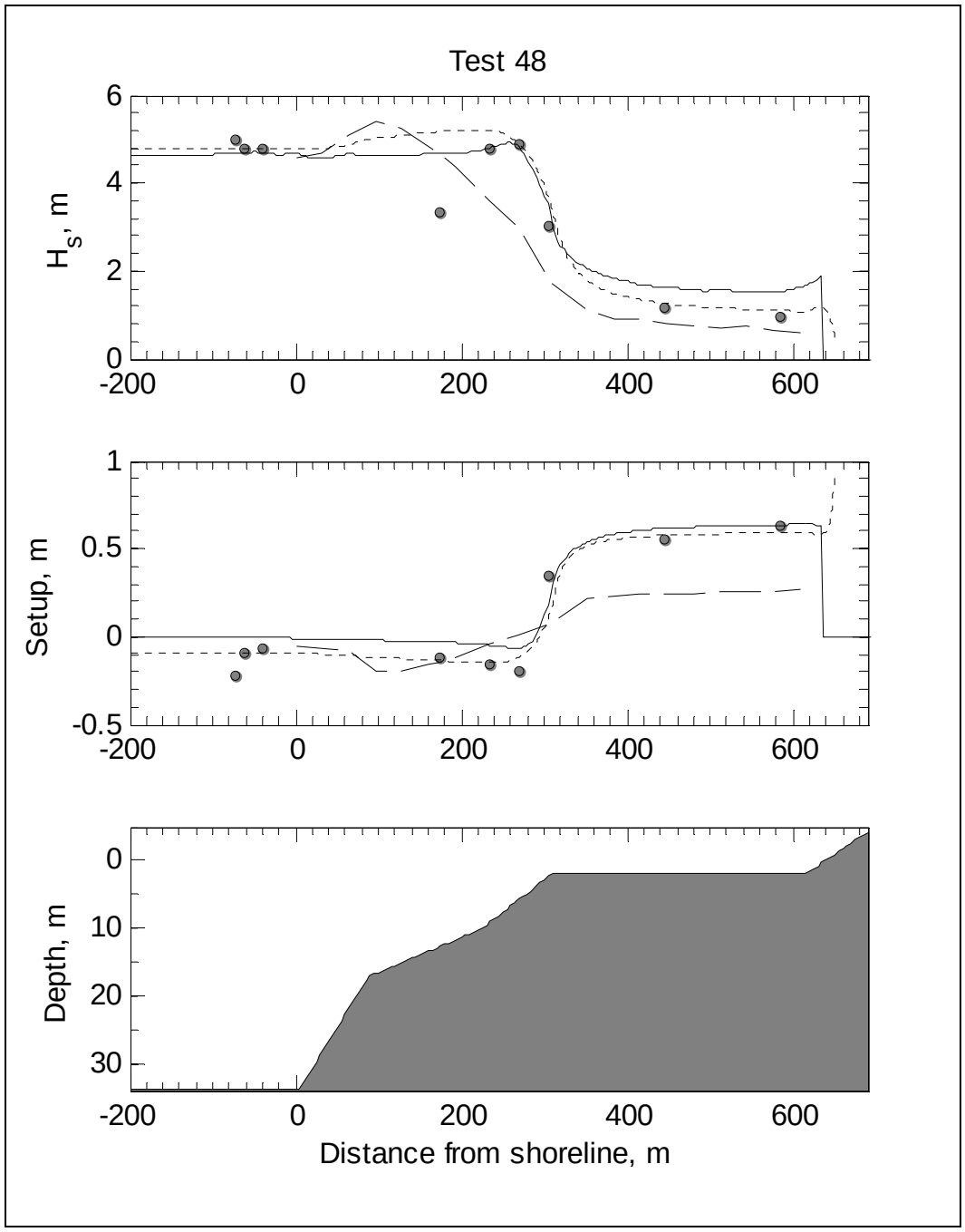

Figure D30. Comparison of three wave model results with data for Test 48 of CHL experiments.

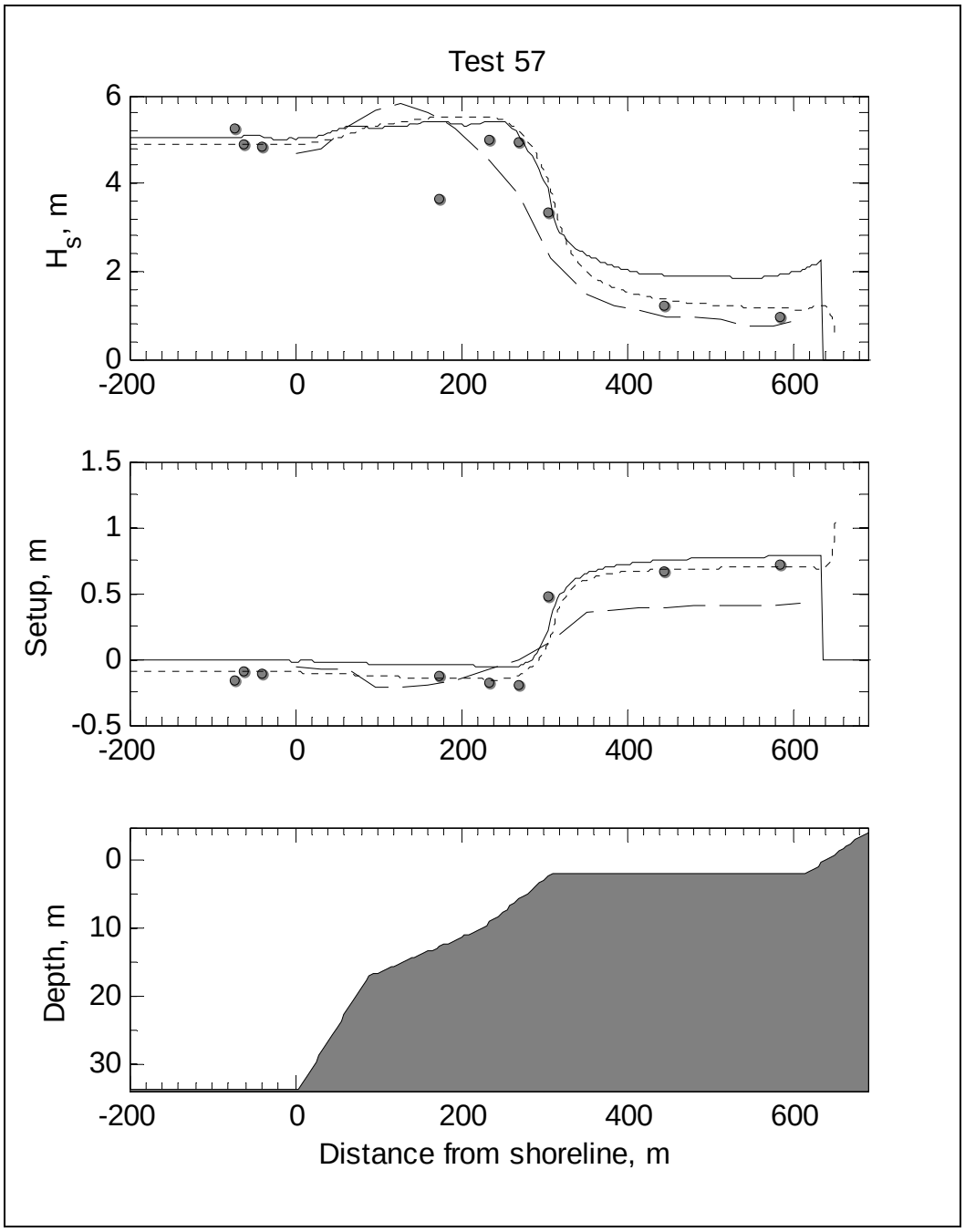

Figure D31. Comparison of three wave model results with data for Test 57 of CHL experiments.

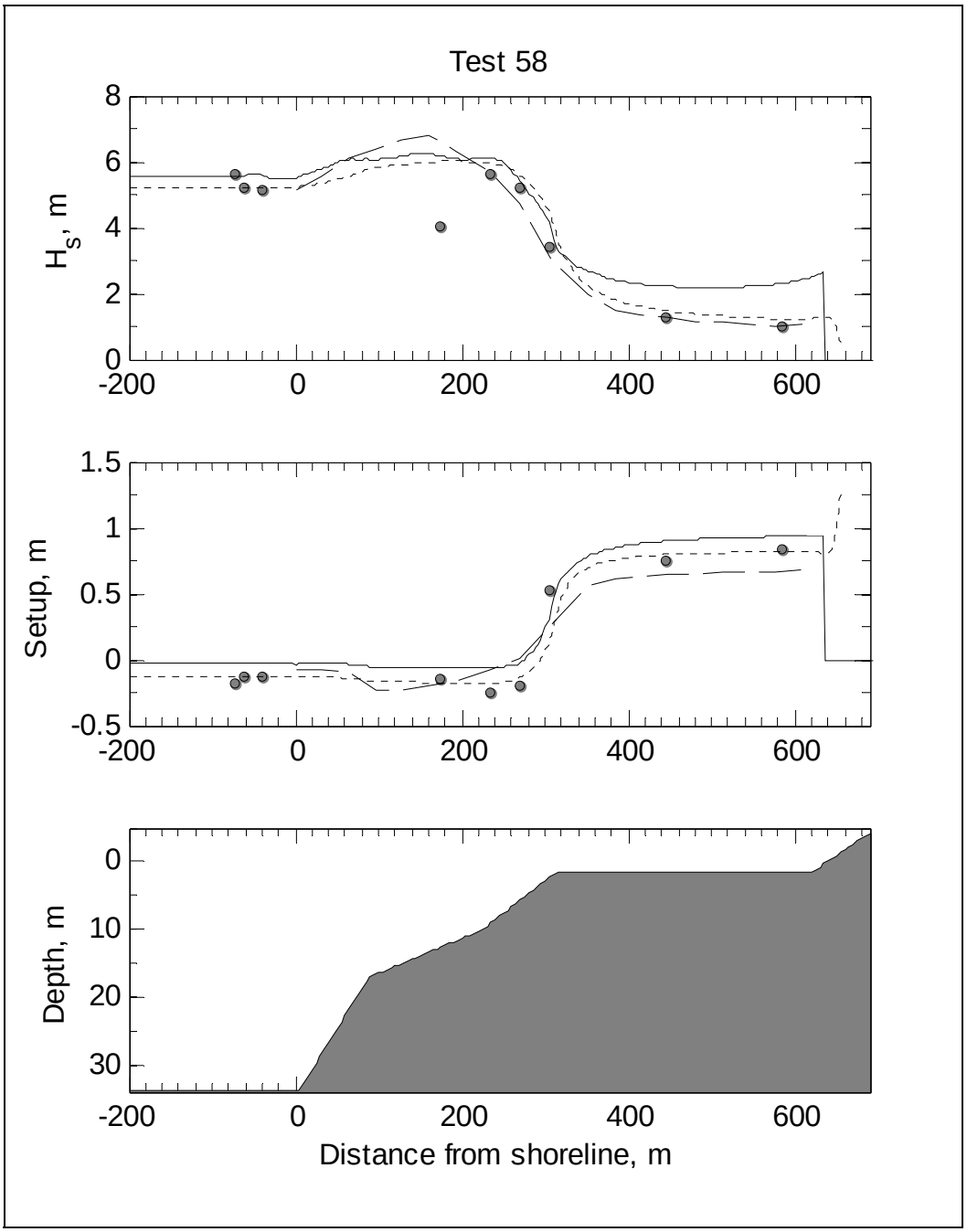

Figure D32. Comparison of three wave model results with data for Test 58 of CHL experiments.

Table D1. Calculated wave height estimates from RBREAK2 for CHL experiments.

Distance from toe, m			0	36	72	108	144	152.1	180	216	261	288	315	324	342	360	381.6	392.4	414	432	450	468
CASE	H_s (m)	T_p (m)	Significant wave heights,(m)																			
Guam01	3.38	10.02	3.25	3.16	3.52	3.75	3.89	3.81	3.63	3.36	2.78	2.20	1.45	1.22	1.01	0.87	0.77	0.74	0.72	0.71	0.62	0.55
Guam02	4.56	15.00	4.38	4.64	5.06	5.39	5.69	5.80	5.82	5.85	5.31	4.41	2.91	2.70	2.30	2.08	1.80	1.70	1.58	1.44	1.36	1.38
Guam03	4.17	10.02	5.41	5.30	5.99	6.26	5.56	5.50	4.78	4.13	3.20	2.54	1.67	1.60	1.32	1.18	1.08	1.02	1.11	1.04	0.83	0.82
Guam04	4.50	10.02	4.32	4.20	4.69	5.07	4.85	4.72	4.29	3.82	2.98	2.37	1.55	1.37	1.18	1.00	0.93	0.88	0.91	0.89	0.73	0.66
Guam05	4.53	15.00	4.35	4.60	5.02	5.34	5.63	5.77	5.78	5.81	5.30	4.40	2.91	2.69	2.29	2.08	1.78	1.69	1.57	1.43	1.36	1.39
Guam06	6.34	10.02	6.08	5.97	6.74	6.81	5.88	5.86	5.04	4.28	3.33	2.67	1.83	1.67	1.44	1.27	1.14	1.10	1.18	1.13	0.95	0.88
Guam07	6.34	15.00	6.09	6.43	7.10	7.65	7.88	7.89	7.75	7.17	6.03	5.02	3.43	3.15	2.74	2.46	2.18	2.03	1.91	1.75	1.70	1.76
Guam08	7.56	10.02	7.22	7.21	8.18	7.43	6.17	5.70	5.08	4.02	2.96	2.28	1.22	1.17	1.09	0.94	0.88	0.81	0.76	0.71	0.69	0.70
Guam09	5.98	10.02	5.71	5.64	6.42	6.40	5.52	5.15	4.51	3.73	2.73	1.95	1.03	0.89	0.82	0.75	0.67	0.62	0.56	0.49	0.52	0.49
Guam10	6.73	15.00	6.37	6.82	7.70	8.27	8.23	8.02	7.56	6.79	5.25	3.89	2.39	2.22	1.98	1.75	1.51	1.47	1.37	1.38	1.39	1.64
Guam11	7.96	15.00	7.53	8.04	9.19	9.82	9.14	9.06	8.25	7.29	5.67	4.17	2.60	2.52	2.26	2.09	1.86	1.90	1.62	1.66	1.69	2.10
Guam12	3.74	10.02	3.58	3.50	3.95	4.25	4.17	3.95	3.55	3.16	2.39	1.65	0.67	0.60	0.52	0.46	0.40	0.37	0.33	0.33	0.27	0.22
Guam13	3.38	15.00	3.22	3.47	3.79	3.90	4.28	4.40	4.48	4.54	3.99	2.84	1.44	1.30	1.12	0.95	0.84	0.79	0.74	0.75	0.69	0.85
Guam14	6.66	10.02	6.36	6.32	7.15	6.89	5.83	5.38	4.78	3.83	2.85	2.13	1.09	1.04	0.94	0.84	0.74	0.69	0.66	0.64	0.62	0.57
Guam15	4.18	10.02	3.99	3.91	4.45	4.72	4.52	4.21	3.78	3.31	2.47	1.71	0.75	0.66	0.55	0.54	0.43	0.44	0.35	0.38	0.30	0.27
Guam16	6.44	10.02	6.17	6.06	6.88	6.88	5.93	5.90	5.07	4.30	3.36	2.70	1.84	1.65	1.45	1.27	1.15	1.09	1.17	1.12	0.94	0.89
Guam17	7.09	10.02	6.79	6.68	7.61	7.39	6.22	6.20	5.28	4.43	3.54	2.79	1.95	1.69	1.50	1.37	1.25	1.17	1.35	1.23	1.07	1.05
Guam18	6.05	15.00	5.82	6.14	6.75	7.28	7.56	7.62	7.51	6.97	5.89	4.94	3.34	3.07	2.71	2.40	2.15	2.03	1.85	1.73	1.64	1.71
Guam19	7.81	15.00	7.46	7.95	8.95	9.42	9.56	9.16	8.83	7.95	6.59	5.44	3.72	3.45	3.13	2.78	2.55	2.38	2.21	2.10	2.09	2.03

Table D2. Calculated wave setup estimates from RBREAK2 for CHL experiments.

Distance from toe, m			0	36	72	108	144	152.1	180	216	261	288	315	324	342	360	381.6	392.4	414	432	450	468
CASE	H_s (m)	T_p (m)	Setup/Setdown (m)																			
Guam01	3.38	10.02	-0.02	-0.04	-0.07	-0.07	-0.06	-0.06	-0.05	-0.03	-0.01	0.04	0.17	0.20	0.22	0.23	0.24	0.24	0.24	0.25	0.25	0.25
Guam02	4.56	15.00	-0.05	-0.06	-0.11	-0.11	-0.11	-0.13	-0.13	-0.08	-0.05	0.06	0.49	0.56	0.64	0.68	0.71	0.72	0.74	0.75	0.76	0.77
Guam03	4.17	10.02	-0.07	-0.10	-0.15	-0.13	-0.09	-0.06	-0.05	0.00	0.06	0.12	0.30	0.33	0.36	0.37	0.38	0.39	0.39	0.39	0.39	0.39
Guam04	4.50	10.02	-0.04	-0.06	-0.11	-0.10	-0.08	-0.06	-0.06	-0.01	0.02	0.07	0.24	0.26	0.29	0.30	0.31	0.31	0.32	0.32	0.32	0.32
Guam05	4.53	15.00	-0.04	-0.06	-0.11	-0.11	-0.11	-0.13	-0.13	-0.08	-0.05	0.06	0.48	0.56	0.63	0.67	0.70	0.71	0.73	0.74	0.75	0.76
Guam06	6.34	10.02	-0.10	-0.12	-0.17	-0.15	-0.10	-0.05	-0.04	0.02	0.09	0.16	0.34	0.37	0.40	0.42	0.43	0.43	0.44	0.44	0.44	0.44
Guam07	6.34	15.00	-0.10	-0.12	-0.18	-0.19	-0.19	-0.17	-0.15	-0.08	0.03	0.21	0.71	0.79	0.88	0.93	0.97	0.98	1.00	1.02	1.03	1.04
Guam08	7.56	10.02	-0.06	-0.09	-0.15	-0.07	0.05	0.04	0.14	0.21	0.29	0.41	0.87	0.90	0.93	0.94	0.95	0.95	0.95	0.95	0.95	0.95
Guam09	5.98	10.02	0.00	-0.02	-0.08	-0.05	0.03	0.01	0.09	0.14	0.21	0.33	0.74	0.77	0.79	0.80	0.80	0.80	0.80	0.80	0.80	0.80
Guam10	6.73	15.00	-0.02	-0.04	-0.12	-0.15	-0.09	-0.10	-0.02	0.09	0.24	0.63	1.45	1.52	1.59	1.63	1.65	1.66	1.67	1.67	1.68	1.69
Guam11	7.96	15.00	-0.08	-0.10	-0.18	-0.22	-0.10	-0.10	0.02	0.15	0.36	0.77	1.60	1.68	1.76	1.80	1.83	1.84	1.85	1.86	1.86	1.88
Guam12	3.74	10.02	0.07	0.05	0.00	0.01	0.03	0.02	0.05	0.09	0.12	0.21	0.56	0.58	0.60	0.60	0.60	0.59	0.59	0.59	0.59	0.59
Guam13	3.38	15.00	0.08	0.06	0.01	0.01	0.00	0.01	0.01	0.01	0.05	0.24	0.98	1.03	1.08	1.10	1.11	1.11	1.11	1.12	1.12	1.12
Guam14	6.66	10.02	-0.02	-0.05	-0.11	-0.06	0.04	0.02	0.11	0.17	0.24	0.37	0.80	0.83	0.85	0.86	0.86	0.86	0.86	0.86	0.86	0.87
Guam15	4.18	10.02	0.06	0.04	-0.01	-0.01	0.03	0.01	0.05	0.10	0.13	0.23	0.60	0.62	0.64	0.64	0.64	0.64	0.63	0.63	0.63	0.63
Guam16	6.44	10.02	-0.10	-0.13	-0.18	-0.15	-0.10	-0.05	-0.04	0.02	0.09	0.16	0.35	0.37	0.41	0.42	0.43	0.43	0.44	0.44	0.45	0.45
Guam17	7.09	10.02	-0.13	-0.15	-0.21	-0.17	-0.10	-0.04	-0.02	0.04	0.12	0.20	0.38	0.41	0.45	0.46	0.47	0.48	0.49	0.49	0.49	0.49
Guam18	6.05	15.00	-0.09	-0.11	-0.16	-0.17	-0.18	-0.16	-0.16	-0.08	0.01	0.18	0.68	0.75	0.84	0.89	0.93	0.94	0.96	0.97	0.98	0.99
Guam19	7.81	15.00	-0.16	-0.17	-0.25	-0.26	-0.24	-0.19	-0.14	-0.03	0.11	0.34	0.88	0.97	1.08	1.13	1.18	1.19	1.21	1.23	1.24	1.25

Table D3. Calculated maximum wave runup estimates from RBREAK2 for CHL experiments.

CASE	H_s (m)	T_p (m)	SWL (m)	R_{max} (m)
Guam01	3.38	10.02	2.00	1.65
Guam02	4.56	15.00	2.00	3.05
Guam03	4.17	10.02	2.00	1.65
Guam04	4.50	10.02	2.00	2.02
Guam05	4.53	15.00	2.00	4.41
Guam06	6.34	10.02	2.00	2.02
Guam07	6.34	15.00	2.00	4.77
Guam08	7.56	10.02	0.00	2.08
Guam09	5.98	10.02	0.00	2.17
Guam10	6.73	15.00	0.00	4.39
Guam11	7.96	15.00	0.00	5.12
Guam12	3.74	10.02	0.00	0.95
Guam13	3.38	15.00	0.00	2.41
Guam14	6.66	10.02	0.00	1.79
Guam15	4.18	10.02	0.00	1.11
Guam16	6.44	10.02	2.00	2.65
Guam17	7.09	10.02	2.00	2.87
Guam18	6.05	15.00	2.00	4.59
Guam19	7.81	15.00	2.00	5.68

Appendix E: Additional Results for UM Reef Experiments

Wave modeling results for the UM reef experiments have been provided in Chapters 3, 4, and 5 of this report. Additional RBREAK2 results are provided here that show spatial variation of the calculated significant wave height, wave setup and maximum runup.

Table E1. Calculated wave height estimates from RBREAK2 for UM experiments.

Distance from toe (m)			0	40	80	120	160	200	220	240	294	336	386	440	480	520	560	600	640	680	720	760
CASE	H_s (m)	T_p (m)	Significant Wave Heights (m)																			
Test 20	3.90	10	3.70	3.81	4.08	4.28	4.11	3.81	3.49	3.46	2.87	2.34	1.56	1.04	0.89	0.79	0.74	0.69	0.65	0.60	0.62	0.56
Test 17	4.99	12	4.75	4.83	5.28	5.61	5.52	5.14	4.90	4.58	3.97	3.39	2.42	1.48	1.27	1.16	1.00	0.94	0.93	0.93	0.77	0.76
Test 21	5.25	14	4.94	5.12	5.64	5.96	6.05	5.97	5.82	5.59	4.99	4.24	3.07	2.04	1.69	1.47	1.34	1.22	1.13	1.06	0.96	0.92
Test 18	5.44	16	5.20	5.59	6.05	6.36	6.66	6.77	6.64	6.56	6.00	5.16	3.78	2.52	2.16	1.93	1.68	1.51	1.44	1.31	1.20	1.23
Test i46	3.78	10	3.57	3.71	3.97	4.21	3.92	3.50	3.42	3.03	2.57	2.05	1.19	0.77	0.68	0.65	0.57	0.57	0.53	0.52	0.50	0.43
Test 48	4.80	12	4.58	4.67	5.12	5.41	5.27	4.84	4.64	4.38	3.61	3.00	1.75	1.09	0.90	0.90	0.79	0.75	0.69	0.74	0.62	0.61
Test 57	4.93	14	4.66	4.80	5.32	5.64	5.81	5.61	5.44	5.23	4.52	3.75	2.30	1.46	1.19	1.09	0.95	0.96	0.93	0.76	0.75	0.89
Test 58	5.44	16	5.15	5.57	6.11	6.41	6.69	6.78	6.59	6.30	5.70	4.71	2.98	1.96	1.52	1.36	1.30	1.15	1.16	1.04	0.98	1.05
Test 27	3.52	10	3.33	3.46	3.71	3.98	3.69	3.40	3.01	2.98	2.30	1.82	0.88	0.57	0.49	0.46	0.43	0.36	0.35	0.33	0.29	0.33
Test 29	4.54	12	4.35	4.42	4.86	5.18	5.09	4.62	4.38	4.04	3.30	2.62	1.31	0.86	0.70	0.65	0.62	0.57	0.50	0.47	0.44	0.44
Test 30	4.86	14	4.59	4.76	5.26	5.70	5.79	5.54	5.31	5.02	4.28	3.55	1.79	1.09	0.95	0.83	0.77	0.67	0.75	0.63	0.58	0.74
Test 31	5.44	16	5.17	5.55	6.14	6.50	6.70	6.55	6.24	6.02	5.32	4.31	2.34	1.52	1.22	1.05	1.00	1.01	0.95	0.78	0.81	1.00
Test 36	4.35	12	4.15	4.26	4.68	5.00	4.85	4.37	4.02	3.74	3.05	2.30	0.87	0.56	0.44	0.42	0.37	0.43	0.38	0.43	0.39	0.48
Test 37	4.86	14	4.59	4.75	5.29	5.77	5.80	5.39	5.09	4.70	3.96	3.08	1.24	0.77	0.65	0.63	0.56	0.49	0.50	0.44	0.35	0.52
Test 38	5.38	16	5.08	5.47	6.08	6.51	6.63	6.57	6.31	5.96	4.83	3.95	1.75	1.13	0.93	0.92	0.76	0.70	0.73	0.61	0.68	0.77

Table E2. Calculated wave setup estimates from RBREAK2 for UM experiments.

Distance from toe, m			0	40	80	120	160	200	220	240	294	336	386	440	480	520	560	600	640	680	720	760
CASE	H_s (m)	T_p (m)	Setup/Setdown (m)																			
Test 20	3.90	10	-0.04	-0.05	-0.07	0.03	0.05	0.07	0.06	0.09	0.07	0.09	0.25	0.27	0.28	0.29	0.29	0.29	0.29	0.29	0.29	0.27
Test 17	4.99	12	-0.07	-0.08	-0.10	0.00	0.01	0.03	0.05	0.06	0.07	0.11	0.32	0.39	0.41	0.42	0.43	0.43	0.43	0.44	0.44	0.42
Test 21	5.25	14	-0.08	-0.09	-0.11	-0.02	-0.02	0.00	0.01	0.02	0.05	0.08	0.36	0.48	0.51	0.53	0.54	0.55	0.55	0.56	0.56	0.54
Test 18	5.44	16	-0.07	-0.09	-0.11	-0.02	-0.02	-0.02	-0.01	0.00	0.02	0.07	0.39	0.59	0.65	0.67	0.69	0.70	0.71	0.71	0.72	0.70
Test 46	3.78	10	-0.04	-0.04	-0.04	-0.16	-0.15	-0.14	-0.11	-0.11	-0.05	-0.02	-0.03	0.06	0.07	0.07	0.07	0.07	0.07	0.07	0.07	0.09
Test 48	4.80	12	-0.06	-0.07	-0.07	-0.20	-0.19	-0.16	-0.14	-0.12	-0.04	0.01	0.07	0.22	0.23	0.24	0.25	0.25	0.25	0.25	0.25	0.27
Test 57	4.93	14	-0.07	-0.07	-0.08	-0.21	-0.22	-0.20	-0.18	-0.16	-0.08	0.00	0.14	0.35	0.38	0.39	0.39	0.40	0.40	0.40	0.40	0.42
Test 58	5.44	16	-0.08	-0.08	-0.09	-0.23	-0.23	-0.20	-0.19	-0.17	-0.08	0.00	0.27	0.56	0.61	0.63	0.64	0.65	0.66	0.66	0.66	0.68
Test 27	3.52	10	-0.03	-0.03	-0.03	-0.14	-0.13	-0.11	-0.11	-0.09	-0.03	0.00	0.04	0.12	0.13	0.13	0.13	0.13	0.13	0.13	0.13	0.14
Test 29	4.54	12	-0.06	-0.06	-0.06	-0.19	-0.17	-0.14	-0.11	-0.10	-0.02	0.04	0.18	0.32	0.33	0.34	0.34	0.34	0.34	0.34	0.34	0.36
Test 30	4.86	14	-0.07	-0.07	-0.08	-0.21	-0.20	-0.17	-0.15	-0.12	-0.03	0.05	0.31	0.52	0.54	0.54	0.55	0.55	0.55	0.55	0.55	0.56
Test 31	5.44	16	-0.08	-0.09	-0.09	-0.23	-0.23	-0.21	-0.18	-0.16	-0.04	0.06	0.50	0.79	0.82	0.84	0.85	0.85	0.86	0.86	0.86	0.88
Test 36	4.35	12	-0.05	-0.06	-0.06	-0.19	-0.16	-0.13	-0.11	-0.11	-0.01	0.06	0.39	0.50	0.50	0.49	0.48	0.47	0.46	0.46	0.45	0.45
Test 37	4.86	14	-0.07	-0.07	-0.09	-0.21	-0.19	-0.16	-0.14	-0.13	-0.03	0.08	0.58	0.74	0.75	0.74	0.73	0.72	0.71	0.71	0.70	0.71
Test 38	5.38	16	-0.08	-0.09	-0.10	-0.24	-0.23	-0.20	-0.18	-0.14	-0.03	0.13	0.81	1.06	1.07	1.08	1.07	1.07	1.06	1.05	1.05	1.06

Table E3. Calculated maximum wave runup estimates from RBREAK2 for UM experiments.

CASE	H_s (m)	T_p (sec)	R_{max} (m)
Test 20	3.90	10	1.70
Test 17	4.99	12	2.45
Test 21	5.25	14	2.81
Test 18	5.44	16	3.48
Test 46	3.78	10	1.16
Test 48	4.80	12	1.72
Test 57	4.93	14	2.09
Test 58	5.44	16	2.85
Test 27	3.52	10	0.74
Test 29	4.54	12	1.19
Test 30	4.86	14	1.80
Test 31	5.44	16	2.69
Test 36	4.35	12	3.60
Test 37	4.86	14	2.70
Test 38	5.38	16	2.20

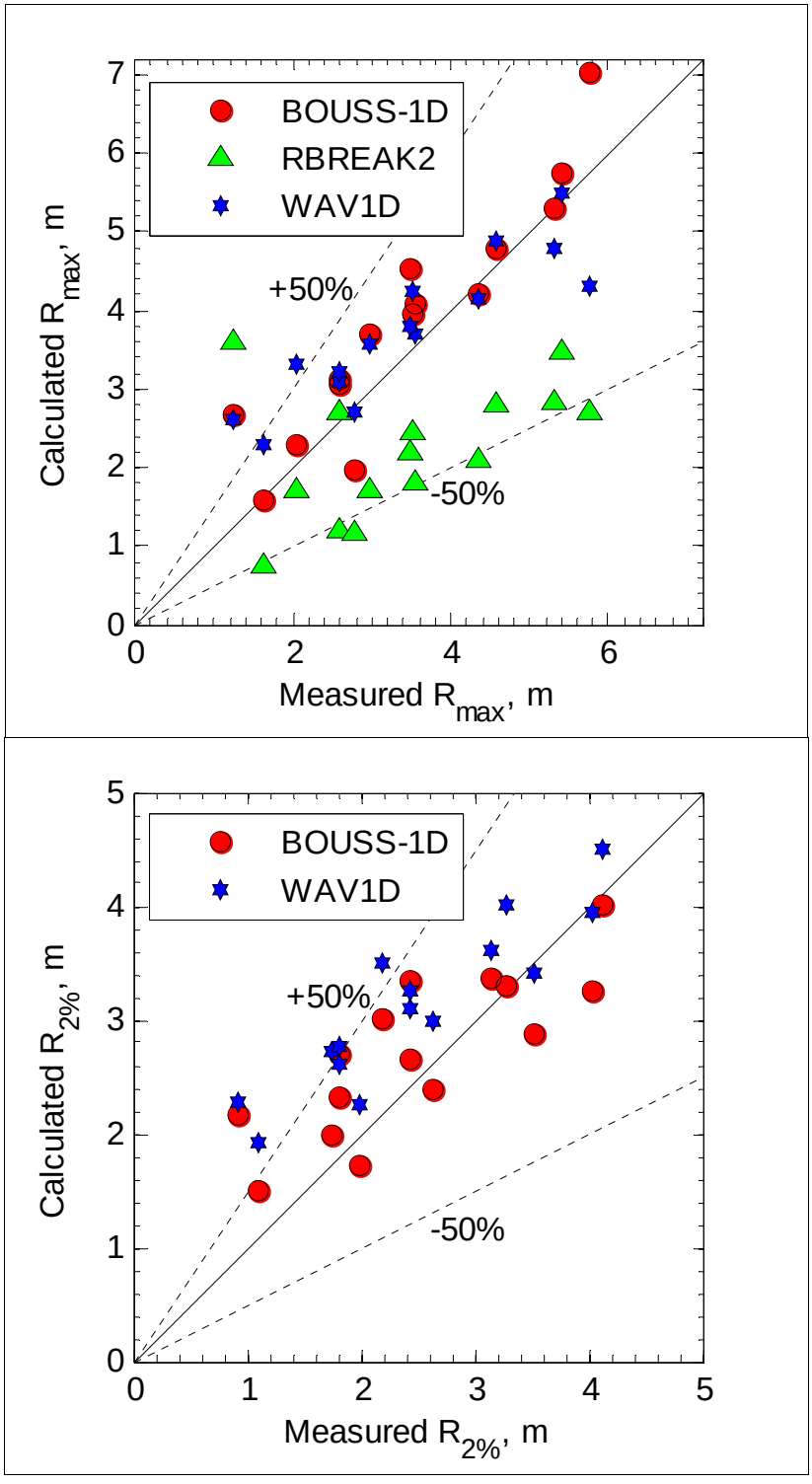

Figure E1. Comparison of calculated and measured maximum and 2-percent runup from BOUSS-1D and WAV1D for UM experiments.

REPORT DOCUMENTATION PAGE

Form Approved
OMB No. 0704-0188

1. REPORT DATE *(DD-MM-YYYY)*	2. REPORT TYPE	3. DATES COVERED *(From - To)*
January 2009	Final report	

4. TITLE AND SUBTITLE

Wave Transformation Over Reefs: Evaluation of One-Dimensional Numerical Models

5a. CONTRACT NUMBER

5b. GRANT NUMBER

5c. PROGRAM ELEMENT NUMBER

6. AUTHOR(S)

Zeki Demirbilek, Okey G. Nwogu, Donald L. Ward, and Alejandro Sánchez

5d. PROJECT NUMBER

5e. TASK NUMBER

5f. WORK UNIT NUMBER

7. PERFORMING ORGANIZATION NAME(S) AND ADDRESS(ES)

U.S. Army Engineer Research and Development Center
Coastal and Hydraulics Laboratory
3909 Halls Ferry Road
Vicksburg, MS 39180-6199

8. PERFORMING ORGANIZATION REPORT NUMBER

ERDC/CHL TR-09-1

9. SPONSORING / MONITORING AGENCY NAME(S) AND ADDRESS(ES)

Headquarters, U.S. Army Corps of Engineers
Washington, DC 20314-1000

10. SPONSOR/MONITOR'S ACRONYM(S)

11. SPONSOR/MONITOR'S REPORT NUMBER(S)

12. DISTRIBUTION / AVAILABILITY STATEMENT

Approved for public release; distribution is unlimited.

13. SUPPLEMENTARY NOTES

14. ABSTRACT

Three one-dimensional (1D) numerical wave models are evaluated for wave transformation over reefs and estimates of wave setup, runup, and ponding levels in an island setting where the beach is fronted by fringing reef and lagoons. The numerical models are based on different governing equations. BOUSS-1D and RBREAK2 are phase-resolving models that respectively solve the time-dependent Boussinesq and shallow water equations. WAV1D solves the 1D wave-averaged energy conservation equation.

Laboratory data obtained from four physical modeling studies conducted by Seelig (1983), Gourlay (1994), Thompson (2005), and Demirbilek and Nwogu (2007) are used in the evaluation of numerical models. The numerical models produced reasonable correlation with the data. Overall BOUSS-1D representation of wave breaking and wave dissipation were realistic and compared well to data. The model's estimates are sensitive to values of input bottom friction and turbulence length scale coefficients. RBREAK2 is robust because it does not attempt to explicitly represent the wave breaking processes. However, the model is highly dissipative when applied to wide fringing reefs and is only applicable when the runup beach is reasonably close to the predominant wave breaking location. The model predictions were also found to be less sensitive to values of friction factor. The correlation with one of the data sets was good, but not as good for two other data sets. WAV1D is the simplest model evaluated in this study. This model is appropriate for preliminary and feasibility level estimates.

15. SUBJECT TERMS

Boussinesq equation
Energy conservation equation
Fringing reefs and lagoons
Numerical wave modeling
Wave breaking
Wave-current interactions
Wave transformation
Wave-wave interactions

16. SECURITY CLASSIFICATION OF:			17. LIMITATION OF ABSTRACT	18. NUMBER OF PAGES	19a. NAME OF RESPONSIBLE PERSON
a. REPORT	b. ABSTRACT	c. THIS PAGE			19b. TELEPHONE NUMBER *(include area code)*
UNCLASSIFIED	UNCLASSIFIED	UNCLASSIFIED		207	